SOME ASPECTS OF MANGANESE AND IRON CHEMISTRY WITH POLYDENTATE LIGANDS

Ph.D. THESIS

by

SWEETY RATHI

DEPARTMENT OF CHEMISTRY
INDIAN INSTITUTE OF TECHNOLOGY ROORKEE
ROORKEE – 247 667 (INDIA)
DECEMBER, 2015

SOME ASPECTS OF MANGANESE AND IRON CHEMISTRY WITH POLYDENTATE LIGANDS

A THESIS

*Submitted in partial fulfilment of the
requirements for the award of the degree*

of

DOCTOR OF PHILOSOPHY

in

CHEMISTRY

by

SWEETY RATHI

**DEPARTMENT OF CHEMISTRY
INDIAN INSTITUTE OF TECHNOLOGY ROORKEE
ROORKEE – 247 667 (INDIA)
DECEMBER, 2015**

INDIAN INSTITUTE OF TECHNOLOGY ROORKEE
ROORKEE

CANDIDATE'S DECLARATION

I hereby certify that the work which is being presented in the thesis, entitled **"SOME ASPECTS OF MANGANESE AND IRON CHEMISTRY WITH POLYDENTATE LIGANDS"** in partial fulfilment of the requirements for the award of the Degree of Doctor of Philosophy and submitted in the Department of Chemistry of the Indian Institute of Technology Roorkee, Roorkee is an authentic record of my own work carried out during a period from December, 2010 to December, 2015 under the supervision of Dr. Kaushik Ghosh, Associate Professor, Department of Chemistry, Indian Institute of Technology Roorkee, Roorkee.

The matter presented in the thesis has not been submitted by me for the award of any other degree of this or any other Institute.

(SWEETY RATHI)

This is to certify that the above statement made by the candidate is correct to the best of my knowledge.

(Kaushik Ghosh)
Supervisor

Date:

Dedicated
To
My Parents

ABSTRACT

Coordination chemistry is an important branch of chemistry which deals with study of compounds formed between metal ions and ligands (neutral or negatively charged). Inorganic chemistry has several branches and bioinorganic chemistry is one of them. Bioinorganic chemistry describes the mutual relationship between inorganic chemistry and biochemistry. This basically deals with the role of inorganic substances such as metal ions, composite ions, coordination compounds or inorganic molecules inside the living organism. Role of bioinorganic chemistry is to understand all the possible interactions between these inorganic substances and the biological tissues. These interactions can only be studied with the knowledge of coordination chemistry where metal ions bind with the ligands which could be the side chain of amino acid or any other biomolecule. Hence bioinorganic chemistry goes hand in hand with the coordination chemistry. These understandings could be further utilized for the advancement of several fields such as medicinal chemistry, biochemistry, environmental chemistry, chemistry of catalysis and metallopharmaceutical research. Transition metals have been a part of active site in various enzymes due to several bases such as stability in variety of geometries, multiple coordination site, stability in variety of oxidation state and capability of stabilizing intermediates in several processes. A significant aim of bioinorganic chemistry is to design small inorganic coordination complexes which have similar structural features and also function in a manner similar to their natural ones. The synthetic approach mainly deals with the active site and its coordination environment. Manganese and iron both the metals are found in the active site of native enzymes but these molecules as such cannot be utilized as pharmaceutical agents. These metals have been used widely for structural, functional or structural−functional mimicking of these metal enzymes. In this regard complexes which are cheap, low molecular weight, less toxic and having good

solubility in water are highly demanding. Moreover, manganese and iron complexes have been utilized for various medicinal applications. In continuation of the importance of these metals, design and synthesis of fluorescent probes selective and sensitive for monitoring heavy and transition metal ions is a demanding and promising area of research because of the prominent impact of metal ions in environment and biology. A remarkable development of small fluorescent molecule with selectivity towards metal ions has been dragged attention of researchers. These studies are found to be helpful to understand transport and localization as well as physiological and pathological effect of metal ions in the cell. Due to high sensitivity, rapid response and simplicity, fluorescence has attracted much attention for the detection of several chemical analytes in solution. Iron is an important transition metal found in biology exhibiting crucial roles in several catalytic and enzymatic reactions and its imbalance can cause harmful effects hemochromatosis, cancer etc. Hence detection of iron and its concentration as well as localizations are extremely important for the treatment of such diseases.

The thesis entitled "**Some Aspects of Manganese and Iron Chemistry with Polydentate Ligands**" is divided into seven chapters. In present studies, we have designed novel bidentate and tridentate ligands having meridional geometry. Synthesized ligands were further subjected to characterization and data supports the proper synthesis of ligands. The ligands used in present investigation have been depicted in the Fig. 1.

CH3PhimpH   R$_1$- H, R$_2$-CH$_3$
OCH3PhimpH   R$_1$- H, R$_2$-OCH$_3$
tBuPhimpH   R$_1$=R$_2$-3,5 di-tert-butyl
NO2PhimpH   R$_1$- H, R$_2$-NO$_2$

Fig.1 Ligands utilized for the present studies.

These ligands were utilized to synthesize mononuclear manganese and iron complexes. Complexes of manganese and iron were also characterized using various spectroscopic techniques. The representative complexes were subjected to X–ray crystallography to justify the molecular structure. Redox activities of all the complexes were optimized using electrochemical studies.

First chapter presents an introduction to coordination chemistry of manganese and iron. In this chapter background of the present work along with literature review are described. The chemical systems reported in this thesis are deeply introduced in this chapter. The various chemical methods and equipments used are comprehensively summarized.

In **chapter two**, tridentate ligands ^{OCH3}PhimpH, ^{CH3}PhimpH, ^{tBu}PhimpH and ^{NO2}PhimpH have been synthesized and characterized. The designed tridentate ligands having N_2O donors upon deprotonation bind to iron(III) resulting in a series of novel iron complexes. All the complexes were characterized by elemental analysis, IR and UV–visible spectral studies. Spectroscopic data, magnetic moment and conductivity measurement clearly expressed the formation of $[Fe(^{OCH3}Phimp)_2](ClO_4)$ (**1**), $[Fe(^{CH3}Phimp)_2](ClO_4)$ (**2**), $[Fe(^{tBu}Phimp)_2](ClO_4)$ (**3**) and $[Fe(^{NO2}Phimp)_2](ClO_4)$ (**4**) complexes. Molecular structure of complex **1** was determined by single crystal X–ray diffraction study. A distorted octahedral geometry was observed having FeN_4O_2 coordination sphere. Molecular structure studies interpret tridentate meridional coordination of ligand around iron(III) metal centre. Electrochemical studies were also investigated for synthesized complexes. Theoretical calculation using DFT was also performed to optimize the geometrical and structural parameters. TD–DFT was also optimized to observe the electronic properties and data obtained was found to be consistent with that of experimentally obtained values. Complexes **1**, **2**, **3** and **4** utilized to optimize oxidation of *o*–aminophenol in methanol. Complexes were found to be efficient in the oxidation of *o*–aminophenol. Kinetic experiments were also explored to gain better insight into the oxidation process. Representative complex exhibited nuclease as well as protease activities in absence of external agents. Complex was found to cleave the DNA and protein *via* self activated mechanism.

Chapter three tridentate ligands ^{OCH3}PhimpH, ^{CH3}PhimpH, and ^{tBu}PhimpH having N_2O donors coordinates to manganese(III) after deprotonation affording a series of mononuclear manganese complexes. All the complexes were characterized by elemental analysis, IR and UV–visible spectral studies. Magnetic moments and conductivity measurements suggested the

formulation of [Mn(^{OCH3}Phimp)$_2$]ClO$_4$ (**5**), [Mn(^{CH3}Phimp)$_2$]ClO$_4$ (**6**) and [Mn(^{tBu}Phimp)$_2$]ClO$_4$ (**7**) manganese complexes respectively. Molecular structure of **7** was determined by X–ray crystallography and structural features were also explored. Cyclic voltammetric studies were also monitored for all the complexes in the series. DFT calculations were also monitored for representative metal complex to optimize geometrical and structural parameters. TD–DFT studies explained the electronic properties and are in good agreement with those of experimentally obtained. The phenoxyl radical complexes were generated at room temperature in CH$_3$CN solution by adding [(NH$_4$)$_2$[Ce^{IV}(NO$_3$)$_6$] and were characterized by UV–visible spectral studies. The phenoxyl radical complex generated at room temperature exhibited nuclease as well as protease activity with *pBR322* DNA without any external agent.

In **chapter four**, two novel ligands H–N$_3$L (1–phenyl–1–(pyridine–2–ylmethyl)–2–(pyridine–2–ylmethylene)hydrazine) and Me–N$_3$L (1–phenyl–2–(1–(pyridin–2–yl)ethylidene)–1–(pyridin–2–ylmethyl)hydrazine) have been designed and synthesized. These ligands have been characterized using various spectroscopic techniques such as UV–visible, IR, GC–MS and NMR spectral studies. Synthesized ligands have been utilized to prepare mononuclear complexes of manganese. A series of manganese complexes [Mn(H–N$_3$L)Cl$_2$] (**8**), [Mn(H–N$_3$L)$_2$](ClO$_4$)$_2$ (**9**), Mn(Me–N$_3$L)Cl$_2$ (**10**) and [Mn(Me–N$_3$L)$_2$](ClO$_4$)$_2$ (**11**) were synthesized and characterized by spectroscopic techniques. Molecular structure of complex **10**.CH$_3$COCH$_3$ was determined by single crystal X–ray diffraction technique. Molecular structures interpret distorted octahedral geometry and tridentate meridional coordination of ligand around manganese. Redox properties were also explored for the synthesized metal complexes. Theoretical calculations were also performed using complex **10** and the geometrical and structural parameters were also

investigated. TD–DFT calculations justify the electronic properties obtained from the experimentally obtained values. The complexes **8**, **9**, **10** and **11** were employed to catalyze the dismutation of superoxide using xanthine–xanthine oxidase–nitroblue tetrazolium assay and obtained good IC_{50} values. DNA interaction studies were also monitored using all complexes. Nuclease as well as protease activity exhibited in presence of oxidising agent for the representative complex.

In **chapter five**, tridentate ligands H–N_3L (1–phenyl–1–(pyridine–2–ylmethyl)–2–(pyridine–2–ylmethylene)hydrazine) and Me–N_3L (1–phenyl–2–(1–(pyridin–2–yl)ethylidene)–1–(pyridin–2–ylmethyl)hydrazine) have been utilized to synthesized mononuclear iron complexes. Complexes [H–Fe(N_3L)Cl_3] (**12**) [H–Fe(N_3L)$_2$](ClO_4)$_2$ (**13**) [Fe(Me–N_3L)Cl_3] (**14**) and [Fe(Me–N_3L)$_2$](ClO_4)$_2$ (**15**) have been synthesized and characterized using elemental analysis, IR, UV–visible and ESI–MS spectral studies. Magnetic moment and conductivity measurements also supported the formulated structures of the complexes. NMR spectral studies were also performed for complexes **13** and **15** due to the presence of low spin Fe(II) metal centre. Structural and geometrical aspects were monitored using DFT calculations. TD–DFT calculations were also performed to optimize the electronic properties and found to be in good agreement with the experiment one. Electrochemical studies were also investigated for all the complexes in the series. Due to the stability in buffer these complexes were subjected to the DNA interaction studies. DNA binding studies were monitored using UV–visible, fluorescence and CD spectral studies. These studies indicated that all the complexes bind well with the DNA. Nuclease activity was also monitored for the representative complexes and exhibited oxidative DNA nuclease in presence of oxidizing agent (H_2O_2).

In **chapter six**, a naphthylamine based probe NED1 (N–(2–aminoethyl)naphthalen–1–amine) was utilized for the detection of Hg(II), Fe(II), Fe(III) in mixed aqueous media via fluorescence quenching. These sensitive metal ions bind with the probe by forming a 1:1 complex. Time resolved fluorescence and quantum yield of probe NED1 in absence as well as in presence of metal ions were investigated. Extent of binding of probe with sensitive metal ions was calculated. Sensitivity of the probe in presence of other metal ions was examined using competitive binding studies. Probe NED1 displayed sensitivity towards Hg(II) during *in vitro* as well as *in vivo* studies. This multianalyte probe demands biological applications in cell imaging and in logic gates.

Chapter seven presents the synthesis a novel fluorescent probe NED2 (2–((2–(naphthalen–1–ylamino)ethylimino)methyl)phenol) has been synthesized *via* a simple one step synthetic procedure and characterized by various spectroscopic methods. Photo–physical properties of NED2 have been investigated to study the sensing of metal ions in methanolic solution. Probe NED2 was found to be highly selective for iron over tested metal ions. Probe NED2 selectively detected iron in both +2 and +3 oxidation states giving rise to yellow–brown and purple color respectively. The naked eye detection of iron is useful for the discrimination of +2 and +3 oxidation state while fluorescence studies concludes selective and specific sensitivity towards Fe(III). Probe NED2 was found to be highly sensitive and selective towards Fe(III) during fluorimetric detection. Binding stoichiometry was found to be 1:1 for Fe(III) and probe NED2. DFT calculation provided that the decrease in the energy gap between HOMO and LUMO is probably responsible for the quenching of fluorescence. Logic gates application of the probe NED2 was also explored.

The material, reagents synthetic procedure and experimental details for complexes will be described in the respective chapters.

The thesis concludes with a few suggestions for further work.

LIST OF PUBLICATIONS

Journal Publications

1. Kaushik Ghosh, Nidhi Tyagi, Pramod Kumar, **Sweety Rathi**, Udai P. Singh "Efficient nuclease activity of dinuclear iron(III) complex with ligand having carboxamido nitrogen donors" *Inorg. Chem. Commun.* **2012**, *20*, 167-171.

2. Kaushik Ghosh, **Sweety Rathi**, Ritu Kushwaha "Sensing of Fe(III) ion via turn–on fluorescence by fluorescence probes derived from 1-naphthylamine" *Tetrahedron Lett.,* **2013**, *54*, 6460–6463.

3. Kaushik Ghosh, **Sweety Rathi** "A novel probe for selective colorimetric sensing of Fe(II) and Fe(III) and specific fluorometric sensing of Fe(III): DFT calculation and logic gate application" *RSC Adv.,* **2014**, *4*, 48516–48521.

4. S. G. Leonardi, Davide Aloisio, Nicola Donato, **Sweety Rathi**, Kaushik Ghosh, Giovanni Neri "Electrochemical sensing of ascorbic acid by a novel manganese(III) complex" *Mater. Lett.,* **2014**, *133*, 232–235.

5. Kaushik Ghosh, **Sweety Rathi**, Pankaj Gupta, Priya Vashisth, Vikas Pruthi "A simple fluorescent probe derived from naphthylamine for selective detection of Hg^{II}, Fe^{II} and Fe^{III} ions in mixed aqueous media: Applications in living cells and logic gates" *Eur. J. Inorg. Chem.*, **2015**, 311-317.

6. Kaushik Ghosh, Nidhi Tyagi, Hemant Kumar, **Sweety Rathi** "DNA interaction, SOD, peroxidase and nuclease activity studies of iron complex having ligand with carboxamido nitrogen donors" *Spectrochim. Acta A,* **2015**, *146*, 292-296.

7. Kaushik Ghosh, **Sweety Rathi**, Deepshikha Arora **"**Fluorescence spectral investigation on interaction fluorescent probes with Bovine Serum Albumin (BSA)**"** *J. Lumin.,* **2015** (Manuscript under revision).

8. **Sweety Rathi**, Ankur Maji, Ovender Singh, Kaushik Ghosh, "Mononuclear iron complexes derived from tridentate ligands: Synthesis, characterization, DFT calculations and DNA interaction studies"*J. Indian Chem. Soc.*, **2015** (Animesh Chakravorty special issue) (Manuscript under revision).

9. Kaushik Ghosh, **Sweety Rathi**, Ankur Maji, U. P. Singh "Synthesis and reactivity studies on new iron(III) complexes derived from tridentate ligands having N_2O donors: *o*-aminophenol oxidation, nuclease and protease activity" (Manuscript under preparation).

10. Kaushik Ghosh, **Sweety Rathi**, Ankur Maji, U. P. Singh "Manganese(III) complexes derived from ligand having N_2O donors: Generation of phenoxyl radical species, nuclease and protease activity" (Manuscript under preparation).

11. Kaushik Ghosh, **Sweety Rathi**, Ankur Maji, U. P. Singh "Synthesis and characterization

of mononuclear manganese complexes derived from tridentate ligand having N_3 donors: Superoxide dismutase, DNA interaction and protease activity" (Manuscript under preparation).

Conference/ Workshop

12. Fifth BRNS-AEACI winter school (SAC-5) on analytical chemistry, December 3-10, 2012.
13. International workshop on chemical evolution and origin of life March, 21-23, 2013.
14. Symposium on modern trends in inorganic chemistry-XV (MTIC-XV), December 13-16, 2013 (Poster presentation).
15. Indo-French symposium on functional metal-organics: Applications in materials and catalysis, February 24-26, 2014 (Poster presentation).

ACKNOWLEDGEMENTS

LIST OF TABLES

LIST OF FIGURES

solution for 6 h

incubation at 25 °C. (a) **8** and **10** (b) **9** and **11** with CT–DNA and its interaction with complexes spectra recorded in 5% dimethylformamide

metal ions (10 eq)

TABLE OF CONTENTS

Chapter-1

General Introduction and Reactivity of Manganese and Iron Complexes: Chemical System and Physical Methods

1.1. Abstract

In this chapter, background of the present work along with literature review has been described. The chemical systems reported in this thesis are deeply introduced in this chapter. The various chemical methods and equipments used are comprehensively summarized.

1.2. Introduction

Coordination chemistry is an important branch of chemistry which deals with the study of compounds formed between metal ions and ligands (neutral or negatively charged).[1] Inorganic chemistry has several branches and bioinorganic chemistry is one of them. Bioinorganic chemistry describes the mutual relationship between inorganic chemistry and biochemistry. This basically deals with the role of inorganic substances such as metal ions, composite ions, coordination compounds or inorganic molecules inside the living organism. Role of bioinorganic chemistry is to understand all the possible interactions between these inorganic substances and the biological tissues. These interactions can only be studied with the knowledge of coordination chemistry where metal ions bind with the ligands. These could be the side chain of amino acids or any other biomolecule.[2] Hence bioinorganic chemistry goes hand in hand with the coordination chemistry. These understandings could be further utilized for the advancement of several fields such as medicinal chemistry, biochemistry, environmental chemistry, chemistry of catalysis and metallopharmaceutical research.[3,4]

1.3. Coordination chemistry in biology

Metal ions such as alkali, alkaline earth metals and transition metals have evolved during life processes and found in living organism. In living organism some metals bind with the ligands more efficiently as compare to others. These preferential bindings have been suggested by Irving–Williams series for divalent transition metals for a ligand.[5] On the other hand, some ligands preferentially bind with a particular metal. These trends can be explained in terms of hard and soft acid–base interactions. Hard and soft acids and bases (HSAB) principle is basically implied to understand the way of coordination of

ligand with the metal ion. HSAB principle states that "hard acids prefer to react with hard bases, and soft acids react with soft bases".[6,7]

1.3.1. Metal ions

In biological function there are some deciding factors which control the properties of metal ions in biological system such as:

(i) Metal site and protein environment which regulates the reactivity at metal site.

(ii) Stereochemistry at metal site and ligand coordination to metal center.

Metals are important in biological system due to their redox and coordination properties. These metals can bind with the ligands following ionic or covalent mode of coordination. Hence metals can be classified into two categories according to the strength of metal ions to form complexes with the ligands.

1.3.1.1. Ionic (hard, class A) group

This involves metals having small ionic radii and/or high oxidation states such as groups 1 and 2 and the left hand side transition metals (preferentially in higher oxidation state). These metals generally form stable complexes with nitrogen and oxygen donors (amines, ketones, water).

1.3.1.2. Covalent (soft, class B) group

This includes metals with large ionic radii, high polarizablity such as transition metals in lower oxidation states (metal carbonyls). These sorts of metals form stable complexes with the ligands SCN^-, CN^- etc.

1.3.2. Ligands

Ligands also behave in the similar fashion. A particular type of ligand prefers to bind with a certain kind of metal ion only. Hence ligands can also be categorized into two classes on the basis of donor sites and polarizability.

1.3.2.1. Ionic (hard) group

Preferentially those ligands which are small, highly electronegative and not highly polarisable such as oxygen donor group (carboxylate, alcohol) fall in this class.

1.3.2.2. Covalent (soft) group

Ligands which are more polarizable, less electronegative and larger in size are the members of this class of group. Mainly ligands having sulphur (thioethers, thiolates) or phosphorus donor atoms belong to this category. Nitrogen donor ligands such as imidazole are considered as intermediates.

Hence it can be summarized that ionic metals preferentially bind with ionic ligands and covalent metal ions preferentially bind with covalent ligands. Some of the examples of hard and soft acid–bases have been listed into Table 1.1.

Table 1.1 Hard and soft acid–bases[6,7]

Metal ions (acids)	Ligands (bases)
<u>Hard acids</u>	**<u>Hard bases</u>**
H^+, Li^+, Na^+, K^+, Be^{+2}, Mg^{+2}, Ca^{+2}, Al^{+3}, Cr^{+3}, Mn^{+2}, Fe^{+3}	NH_3, N_2H_4, H_2O, OH^-, NO_3^-, ClO_4^-, CO_3^{2-}, SO_4^{2-}, F^-, Cl^-
<u>Borderline (intermediate) acids</u>	**<u>Borderline (intermediate) bases</u>**
Fe^{+2}, Co^{+2}, Ni^{+2}, Cu^{+2}, Zn^{+2}, Pb^{+2}	$C_6H_5NH_2$, C_5H_5N, Br^-, NO_2^-, SO_3^{2-}, N_2
<u>Soft acids</u>	**<u>Soft bases</u>**
Pd^{+2}, Pt^{+2}, Cu^+, Ag^+	H^-, CN^-, SCN^-, I^-, CN^-, C_2H_4, CO, C_6H_6

1.3.3. Nature of metal ions

Selection of metal by an enzyme can be classified on the basis of several origins such as availability of metal ion at the place and time of origin of that enzyme. On the other hand, the role of metal enzyme in a particular activity also helps in the selection process of metal ion. A redox inactive metal (zinc) can be preferred in those enzymes which requires metal ion for coordination only and activate the substrate due to its Lewis acidity. Alternatively, if metal is involved in variable oxidation state during catalytic cycle then redox active metal is required for the same. Redox active metals play crucial role in several electron transfer reactions.[8,9] Oxidation state, donor atoms in ligands and geometry of ligands are the other deciding factors to perform a specific function in an enzyme.

1.3.4. Biological significance of transition metal ions

Transition metals have been a part of active site in various enzymes due to several origins such as stability in variety of geometries, multiple coordination site, stability in

variety of oxidation state and capability of stabilizing intermediates in numerous processes. Metalloproteins and cofactors consume transition metals to maintain the optimum concentration inside living organism.[10–13] The optimum concentration range is very narrow and hence both the deficiency as well as excess could be dangerous for the organism.[14] These transition metals can impart crucial role in several processes such as electron transfer, charge carriers, storage and transport as given in Table 1.2 (Fig. 1.1).

Metals and biology: Classification according to function

Transport and storage protein   Enzymes   Aproteic system   Metals in medicine

Electron transport | Storage Transport Structural agents | Coordination of O_2 | Photoredox | Transport of metals | Therapeutics interaction with nucleic acids | Diagnosis

Cytochromes (Fe) Ferritin (Fe)
Iron-sulfur (Fe)   Transferrin (Fe)
Blue copper (Cu) Ceruloplasmin (Cu)

Hemoglobin (Fe)
Myoglobin (Fe)
Hemocyanin (Cu)

Chlorophyll (Mg) Siderophores (Fe)
Photosystem II   Metallochaperons
(Mg,Mn)

Apoptosis (Mn,Zn)
Diabetes (V)   IRM(Gd)
Alzheimer
(Zn,Fe,,Al)
Anticancer (Pt, Ru)

Hydrolases | Oxidoreductases | Isomerases and synthetases

Carboxypeptidase (Zn)
Aminpeptidase (Mg, Mn, Cu)
Phosphatases (Mg, Zn,Cu, Fe)

Oxidase (Fe, Cu, Mo)
Peroxidase (Fe, Mn, V)
Dehydrogenases (Fe, Cu, Mo, Ni, Zn)
Hydrolases (Fe, Cu, Mo)
Oxygenases (Fe)
Superoxide dismutase (Cu, Zn, Fe, Ni)
Nitrogenase (Fe, Mo)
Hydrogenases (Fe, Ni)

Vitamin B_{12} (Co)

Fig. 1.1 Metal ions involved in biology and their functions

Table 1.2 Functions performed by a number of transition metals in biology

Metal	Function
Vanadium	Nitrogen fixation, oxygenation, halogenation (haloperoxidases), ATPase inhibition
Chromium	Carbohydrate utilization
Manganese	Photosynthesis, oxidase, superoxide dismutase, dehydrogenase
Iron	Oxygenation, deoxygenation, dioxygen transport and storage, electron transfer, nitrogen fixation, superoxide dismutase
Cobalt	Oxidase, alkyl group transfer
Nickel	Hydrogenase, hydrolase, dehydrogenase, urease
Copper	Oxidase, dioxygen transport, electron transfer, oxygenation, superoxide dismutase
Zinc	Structure, hydrolase, oxidoreductase, transferase, ligase, lipase
Molebednum	Nitrogen fixation, oxidoreductases, oxotransfer
Tungsten	Dehydrogenase

1.3.5. Ligands in biological systems

Ligands are equally important as that of metal ions due to their ability to alter the redox properties. Ligands also facilitate stabilization of multiple oxidation states, lability and stability of complexes. In living organism, there are several ligands which could bind with the metal ions to perform specific functions. These ligands can be classified into two classes.

1.3.5.1. Natural ligands or biological ligands

Ligands which are found in biological systems[15] and have ability to coordinate with metals are known as natural ligands such as

(a) Peptides and proteins: These can behave as a ligand into two ways:

(i) Deprotonated amide nitrogen or carbonyl oxygen from the peptide chain acting as ligand (nitrile hydratase).[16]
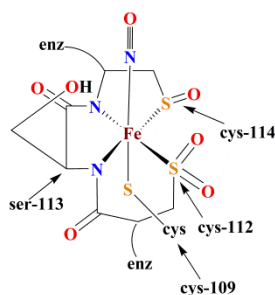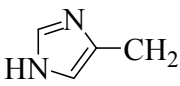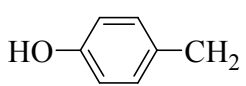
Fig. 1.2 Synthetic model of nitrile hydratase

(ii) Amino acid side chains such as imidazole (histidine), carboxylate (aspartic acid) etc acting as ligand (Table 1.3).

Table 1.3 List of amino acid residue as a ligand and their preferred metal ions

Residue	Substituents	Metals
Histidine	(imidazole structure) $-CH_2$	Zn, Fe, Cu
Cysteine	$-CH_2SH$	Zn, Fe, Cu
Methionine	$-CH_2CH_2SCH_3$	Fe, Cu
Glutamic acid	$-CH_2CH_2COOH$	Ca, Zn, Fe
Aspartic acid	$-CH_2COOH$	Ca, Zn, Fe
Tyrosine	$HO-$ (benzene ring) $-CH_2$	Ca, Zn, Fe, Mn
Serine	$-CH_2OH$	Ca
Asparagine	$-CH_2CONH_2$	Ca
Glutamine	$-CH_2CH_2CONH_2$	Fe
Threonine	$-CH(OH)CH_3$	Ca

(b) Cofactors and prosthetic groups: Flavin adenine dinucleotide (FAD), tetrapyrole, pterin (Fig. 1.3) respectively.
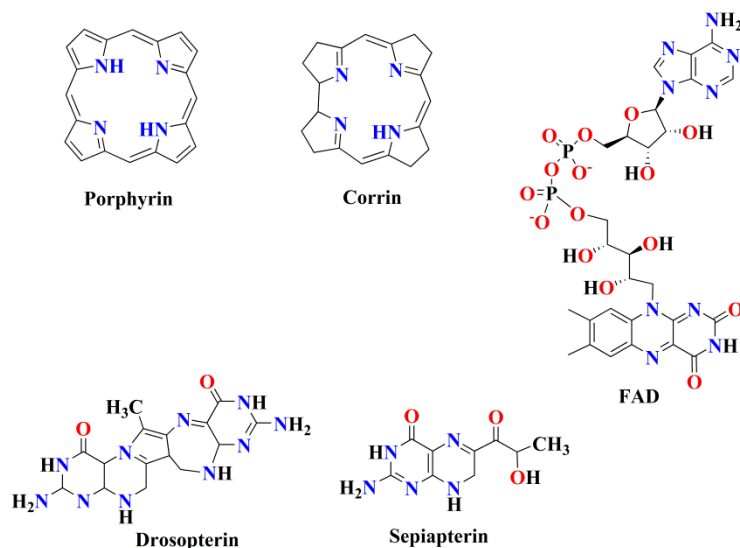
Fig. 1.3 Cofactors and prosthetic groups

(c) Small molecules: Oxygen, water.

(d) Nucleic acids: Nitrogenous bases of nucleic acid (guanine).

1.3.5.2. Non−biological ligands

These are the molecules which are not found inside the body but taken from outside the body and behave as ligands.

(a) Drugs: Ligands found in drugs.

(b) Small toxic ligands: CO, NO, CN^-, F^-, H_2S.

1.4. Bioinorganic coordination chemistry

A significant aim of bioinorganic chemistry is to design small inorganic coordination complexes which have similar structural features and also functions in a manner similar to their natural ones. The synthetic approach mainly deals with the active

site and its coordination environment. Existence of transition metals in the active site of various metalloenzymes has been described previously. This work deals with the manganese and iron chemistry therefore the enzymes having these metals will be the main area of concern. Hence in this context of present thesis, the details of the roles of manganese and iron have been described below.

1.5. Manganese: General chemistry

Manganese (*symbol* Mn) is the third most abundant transition metal in Earth's crust and the eighth most abundant crustal metal overall. In terms of abundance of transition metals manganese is considerable less abundant than iron. In periodic table this metal positioned in 4th period and 7th group having electronic configuration [Ar] $3d^5 4s^2$. It has only one naturally occurring isotope. Manganese is more electropositive metal ion as compared to its neighbor in the periodic table. Oxidation states of manganese have been observed from $-$III to VII but on the basis of geochemical distribution of manganese in hydrosphere, lithosphere and atmosphere mainly Mn(II), Mn(III) and Mn(IV) were involved. Out of these metal oxidation state Mn(II) is most stable one. Spin pairing in manganese (II) complexes can be achieved using ligands such as cyanide. $[Mn(CN)_6]^{3-}$ is low$-$spin octahedral complex of manganese. Almost all Mn(III) complexes are high$-$spin and have octahedral geometry. Mn(IV) is found in photosystem II which is a water oxidising enzyme. Mn(VII) behaves as an extremely strong oxidising agent. These oxidation states behave as Lewis acids and exhibit a preferential coordination for the oxygen donors.[17]

1.5.1. Biological role of manganese

Manganese is found to be an essential element in living beings and plays key role in various important functions such as photosystem II and disposal of harmful radicals (such as superoxide dismutase). A healthy human adult contain 10–20 mg of manganese. In biological system manganese may have oxidation state II, III, IV and possibly V. In many proteins containing manganese, preferentially manganese is having II oxidation state with high–spin and no coordination geometry preference. Strength of complexes is weak as compared to other transition metal ions found in biological system excluding Ca(II) and Mg(II) ions. Due to the similar ionic radius Mn(II) can substitute Zn(II) and Fe(II) in protein. The one of the crucial role of manganese in nature is in photosynthesis (Fig. 1.4).[18,19]
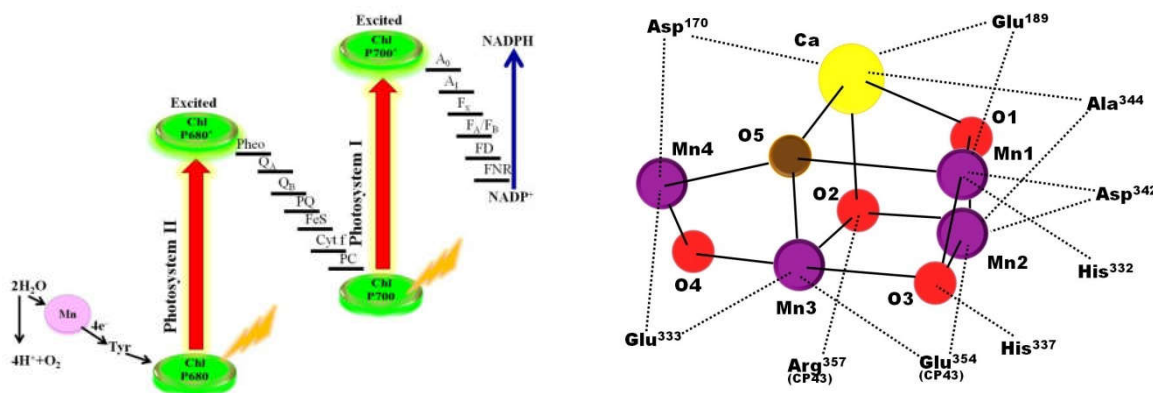
Fig. 1.4 Manganese in oxygen evolving complex in photosystem II[20]

Manganese is found in the active site of various enzymes and imparts crucial properties to achieve specific functions. Table 1.4 depicts enzyme containing manganese in the active site and functions performed by them.

Table 1.4 List of enzymes containing manganese in active site and their functions

Enzymes	Functions	Type
Manganese superoxide dismutase (Mn–SOD)[21]	Dismutation of superoxide radicals	Mononuclear
Manganese peroxidase (Mn–P)[22]	Convert peroxide to water using H^+	Mononuclear
Manganese dioxygenase[23]	Incorporating two atoms of oxygen	Mononuclear
3–Deoxy–D–arabino–heptulosonate–7–phosphate synthetase (DAHPS)[24]	Responsible for synthesis of aromatic compounds in microorganism and plants	Mononuclear
2–C–methyl–D–erythritol 2,4–cyclodiphosphate synthase (MECDP)[25]	Part of isoprenoid biosynthesis in many plants and bacteria	Mononuclear
Inorganic phosphatase[26]	Catalyze the hydrolysis of $P_2O_7^{4-}$ to phosphate	Mononuclear
Isopentenyl diphosphate isomerase[27]	Catalyze the isomerisation of isopentenyl diphosphate to dimethylallyl diphosphate	Mononuclear
Manganese lipoxygenase (Mn–LO)[28]	Catalyze dioxygenation of polyunsaturated fatty acids in lipids	Mononuclear
Oxalate oxidase[29,30]	Convert oxalate to CO_2 and H_2O_2	Mononuclear
Oxalate decarboxylase[31]	Convert oxalate to formate and CO_2	Mononuclear
Manganese ribonucleotide reductase[32]	Catalyzes the formation of deoxyribo–nucleotides from ribonucleotides	Dinuclear
Arginases[33]	Catalyze the hydrolysis of L–arginine to L–ornithine and urea	Dinuclear
Manganese catalase[34]	Detoxification of hydrogen peroxide	Dinuclear

Amino peptidase[35]	Catalyze the hydrolysis of the amino end of polypeptides and protein	Dinuclear
Isomerases[36]	Catalyze the interconversion of D−glucose and D−fructose	Dinuclear
Transferases[37]	Catalyze the transfer of nucleotide sugar residue to a hydroxyl group on target protein, lipid or carbohydrate	Dinuclear
Glutamine synthetase[38]	Catalyze the conversion of L−glutamate, ATP and ammonia into L−glutamine, ADP and PO_4^{3-}	Dinuclear
Phosphoglycerate mutase[39]	Catalyze the inter−conversion of 3−phosphoglycerate and 2 phosphor−glycerate	Dinuclear
Oxygen evolving complex (OEC) or (PSII)[40]	Carry out the four electron oxidation of water to dioxygen	Tetranuclear

1.6. Iron: General chemistry

Iron is a distinctive metal present around and inside us having electron configuration $[Ar]3d^6 4s^2$. It is a member of 4th period and 8th group in the modern periodic table. This metal has been a part of man's material progress since prehistoric times. It is found to be the fourth most abundant element (after oxygen, silicon and aluminium) and the second most abundant metal in Earth's crust. Iron has four naturally occurring isotopes. Iron can have oxidation state −II to VI, although two most stable oxidation states are II and III. Iron (III) complexes may be low or high−spin and generally have octahedral geometry. One important aspect to be considered in the iron chemistry is the effect of ligand on oxidation and spin state of iron as shown in Fig. 1.5.
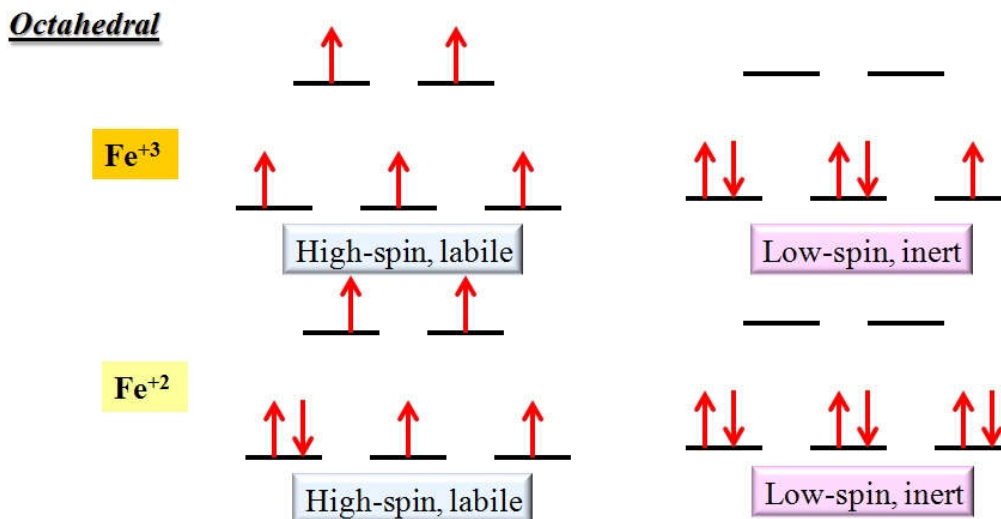
Fig. 1.5 Effect of ligand environment on the oxidation state and spin state of iron

Ligand strength and the environment around metal centre have a tendency to modulate the redox property of the iron. A complex will be labile if it is having a weak field ligand and will form preferentially high−spin complexes and vice versa. Presence of large, bulky ligands as in metalloproteins can cause a tetrahedral environment, in which iron prefers to form high−spin complexes in both the oxidation state.[19] Iron has been found an important metal in various catalytic processes due to its biological relevance and abundance in nature.[41–43]

1.6.1. Biological role of iron

Being vital to plant as well as animal, iron imparts valuable role in biology. The adult human body contains about 4 g of iron out of which only 1 g of iron per day is absorbed while about 3 g are in the form of haemoglobin. Iron is important in several aspects such as dioxygen transport (Fig. 1.6), storage, electron transfer, nitrogen fixation, superoxide dismutation.[20,44]
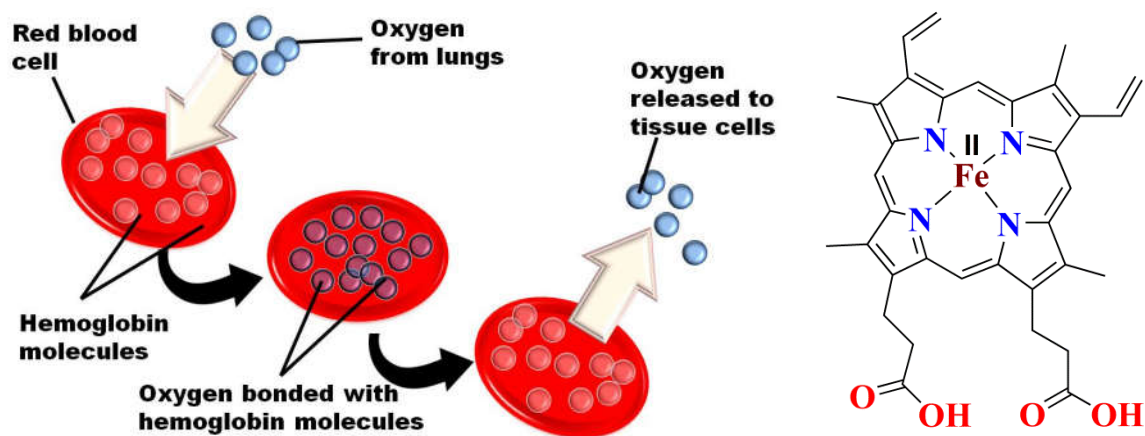
Fig. 1.6 Oxygen transport process

Iron is preferred over other transition metal due to some characteristic features present in iron, less or not at all present in the other transition metals which are as followed:

(a) Abundant and ubiquitous in nature.

(b) Ease of swapping between the oxidation states II and III and can reach up to IV and V in some processes.

(c) Change of spin state in the presence of ligand environment and strength.

(d) Flexibility towards donor atom in a ligand, coordination and geometry.

Iron containing protein can be classified depending on its prosthetic group as depicted in Table 1.5.

Table 1.5 Iron containing protein and their sites

Iron containing protein					
Heme protein	**Protein**	Hemoglobin	Myoglobin	Cytochrome oxidase	Cytochrome P450
	Fe atom	4	1	2	1
	Site	RBC	Muscle	Mitochondria	ER, Mitochondria
Non−heme protein	**Protein**	Aconitase	Transferrin	Lactoferrin	Ferritin
	Fe atom	2	2	2	4000
	Site	TCA cycle	Plasma	Milk	Tissue
Iron−sulfur proteins	**Protein**	Complex III FeS	Xanthine oxidase	Succinate DH	Adrenodoxin
	Fe atom	2	8	4	2
	Site	Mitochondria	Liver	Mitochondria	Mitochondria

One of the interesting family of enzymes containing iron is cytochrome which are the members of heme proteins (Table 1.5).[45–48] These are monooxygenase enzyme containing type b heme protein which catalyzes a variety of oxo transfer reactions such as hydroxylation, epoxidation, amine and sulphide oxidation.[48–50]

1.7. Applications of manganese and iron complexes

In metalloenzymes presence of metal and environment of ligand around metal centre exhibit unique properties to perform special functions such as catalysis and electron transfer.[51–53] To mimic these enzymes, there is a need to synthesize some inorganic coordination complexes. These complexes should possess similar structural and spectroscopic features along with similar functions, as of their natural counterparts.

Synthesized model inorganic complexes could be helpful to understand native enzymes by changing ligand environment, coordination geometry, metal ion etc. In this regard, a wide range of metalloenzymes have been synthesized to perform specific functions.

1.7.1. Structural–functional modeling of metalloenzymes

Herein, the goal is to understand the contribution of manganese and iron complexes in the field of bioinorganic chemistry. These manganese and iron complexes could have been structural, functional and/or structural and functional model of enzymes. Herein some enzymes have been described which are of great significance in manganese and iron chemistry recently. These enzymes have been utilized either for structural or functional modelling using manganese and iron complexes.

1.7.1.1. Superoxide dismutase (SOD) enzymes

Superoxide radical is reactive oxygen species (ROS) produced during cellular processes or some environmental conditions such as interaction of UV radiation with biomolecules, enzymatic activities in phagocytic cells (neutrophils and macrophages) or as a by–product of cellular respiration. ROS such as hydrogen peroxide, hydroxyl radicals and peroxynitrites are also formed through superoxide ions.[54] These reactive oxygen species initiates damaging and uncontrollable reactions in cells leading damage to DNA and other cell components.[55,56] These uncontrolled production of ROS and damage caused by them is responsible for many diseases such as atherosclerosis, rheumatoid arthritis, autoimmune disease, Parkinson's disease, Huntington's disease and Alzheimer's disease.[56,57] Superoxide radicals can act as signalling agent, a safe intermediate which decomposes immediately or a toxic species. In body its level is regulated by two enzymes superoxide reductase(SOR) and superoxide dismutase(SOD) (Scheme 1.1).[58]

Rective oxygen species production and removal
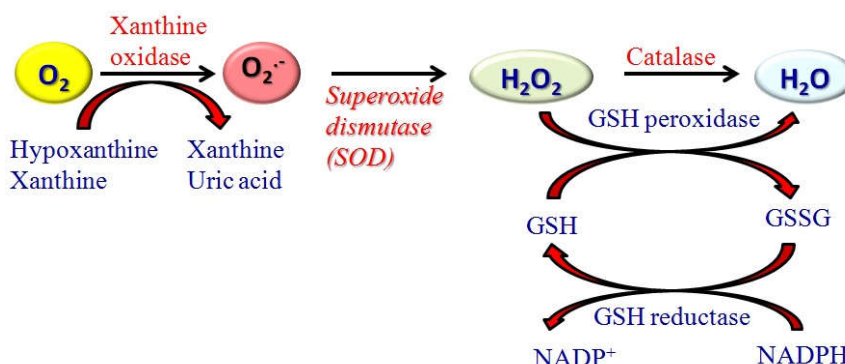
Scheme 1.1 Superoxide dismutase: Production and dismutation of reactive oxygen species (plasma reduced glutathione (GSH), GSSG–oxidised glutathione or glutathione disulfide)

Both the metalloenzymes are redox active and control the concentration of superoxide radicals. The equations shown below represent the difference in the functions of two enzymes.

$$O_2^{\cdot-} + 2H^+ + e^- \xrightarrow{\text{SOR}} H_2O_2 \qquad \text{Metal: Fe}$$

$$2O_2^{\cdot-} + 2H^+ \xrightarrow{\text{SOD}} H_2O_2 + O_2 \qquad \text{Metal: Ni, Fe, Mn and Cu-Zn}$$
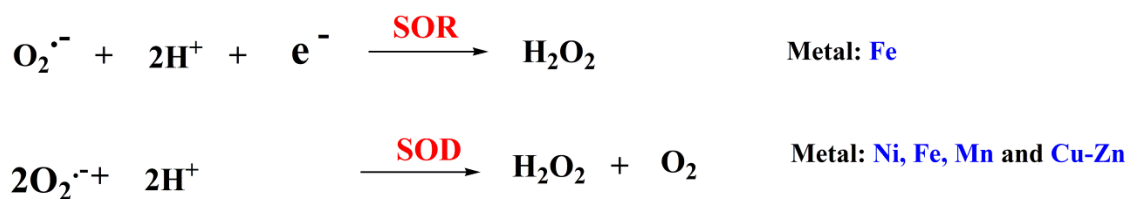
Superoxide dismutase enzymes were first discovered by Irwin Fridovich and Joe McCord.[59] This enzyme is responsible for the regulation of antioxidant–oxidant balance in many organisms.[60] On the basis of metal ion present, this metalloenzyme has been categorized into four types: Ni–SOD,[61] Mn–SOD,[3] Fe–SOD,[62] and Cu/Zn–SOD.[55] Ni–SOD was found in cytosol of s*treptomyces* and *cyanobacteria*,[61] as well as in a few

green algae.[63,64] Mn–SOD was discovered in the cytosol of *archaea*,[65,66] bacteria[67] and eukaryotic cells typically contain Mn–SOD in the mitochondrial matrix. Fe–SOD is found in bacterial cytosol enzyme.[67] In eukaryotic cells, Cu/Zn–SOD is primarily found in cytosol but also found in the mitochondrial membrane space and nucleus.[68]

Mn–SOD and Fe–SOD enzymes both have subunit of size about 22 kDa and have substantial sequence similarity.[69] Two residues are considered as distinguishing Mn–SOD from Fe–SODs which are residue 77 *(E. coli* numbering) is glycine in Mn–SODs and glutamine in Fe–SODs and residue 146 is alanine in all Fe–SODs, and either glutamine or histidine in Mn–SODs.[21]
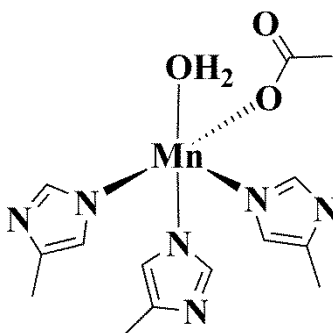
Fig. 1.7 Active site structure of human mitochondrial Mn–SOD

Metal ion is located deep within hydrophobic pocket in the protein formed by two subunits. Manganese coordination geometry is distorted trigonal bipyramidal with two histidine ligands and the aspartate donor in the equatorial plane and axial histidine and a water or OH^- group in axial position (Fig. 1.7).

Catalytic mechanism have been shown in Scheme 1.2 which involves change in oxidation state of metal ion between II and III.[70] In the beginning metal is found in

oxidized state where axial ligand is hydroxide. On arrival of superoxide anion metal centre expands its coordination number (trigonal bipyramidal to octahedral) and metal itself got reduced to Mn(II) on protonation of the −OH group and finally release of a dioxygen molecule occurs. Another superoxide anion binds to this reduced Mn(II) centre, which oxidizes to transfer its proton with the production of hydroperoxo species. Finally, H_2O_2 release subsequently upon protonation of the manganese (III)−hydroperoxo intermediate.
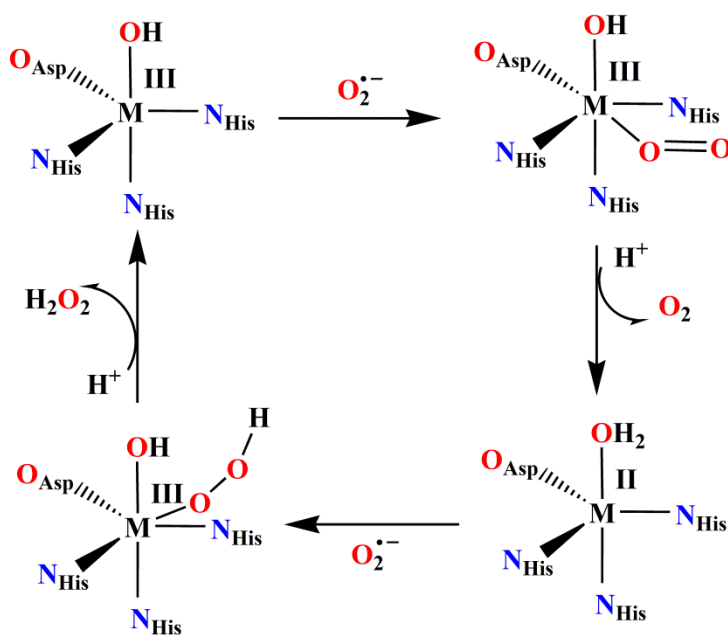
Scheme 1.2 Schematic representation of mechanism of superoxide dismutase enzyme

Manganese and iron complexes as SOD mimic

Manganese and iron both the metals are found in the active site of native enzyme[69,71–73] but these molecules as such cannot be utilized as pharmaceutical agents.[74] These metals have been used widely for structural, functional or structural−functional

mimicking of these metal enzymes. In this regard complexes which are cheap, low molecular weight, less toxic and having good solubility in water are highly demanding.

Manganese complexes have been displayed SOD activity and used to cure oxidative stress. Several manganese complexes have been synthesized in this regard using ligands as shown in Fig. 1.8. Remarkable work in this area has been done by several groups. Ivanovic–Burmazovic and co–workers have synthesized seven–coordinated manganese complexes $[Mn(L)(H_2O)_2]^{2+}$, L represents an equatorial pentadentate macrocyclic ligand with five nitrogen donor atoms. SOD activities of these complexes were monitored and these complexes found to be potent superoxide dismutase (SOD) mimics. They have also indicted probable use of the synthesized complexes as potential human therapeutics to cure diseases caused by the overproduction of superoxide.[75] In continuation of these works, Burmazovic and co–workers have utilized Stopped–flow measurements combined with time–resolved UV–visible spectroscopy for the spectral analysis of superoxide decay. This group have performed the comparative study of catalytic activity of putative manganese SOD (superoxide dismutase) mimics known in the literature.[76] Recently Kose and co–workers have synthesized manganese(II) complexes utilizing pentadentate ligand derived from Schiff's base which exhibited excellent SOD (IC$_{50}$~1μM) activity.[77] Similarly Signorella and co–workers synthesized manganese(III) complex using unsymmetrical hexadentate ligand 1–[N–(2–pyridylmethyl),N–(2–hydroxybenzyl)amino]–3–[N′–(2–hydroxybenzyl),N′–(4–methylbenzyl)amino]propan–2–ol having N_3O_3 donor which exhibited SOD activity having good IC$_{50}$ value (1.26 μM). This complexes was found to be efficient in disproportionation of H_2O_2 and superoxide ion.[78] Scorpiand–like ligands are also an

important class of ligands. Clares *et. al.* have utilized these macrocyclic ligands to prepare manganese(II) complexes and monitored *in vitro* and *in vivo* activities. *In vitro* activity was performed following the McCord–Fridovich method. Manganese complexes were subjected to monitor the antioxidant behavior of these compounds on bacteria, yeast and fish embryos.[79]
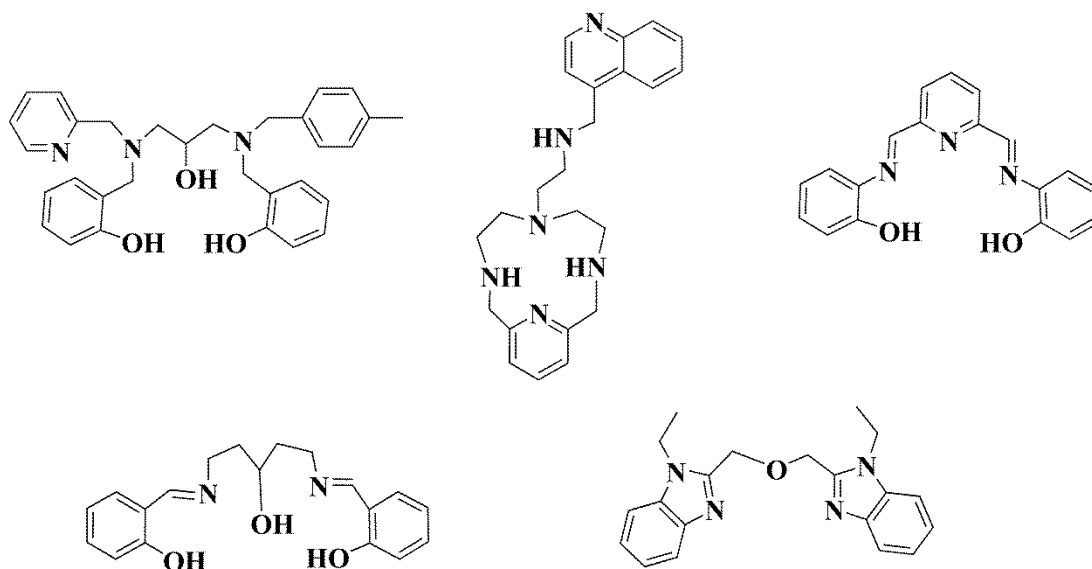
Fig. 1.8 Ligands utilized for the synthesis of complexes as SOD mimic

Studies on, SOD activities have been an interesting area to explore and a lot of work has been done in this regard.[48,80–93] Most of the SOD mimic molecules are manganese complexes as mentioned above and they have been found successful in *in vitro* as well as *in vivo* studies such as EUK–134. EUK–134 has been found a potent antioxidant in rat kidneys and limbic systems.[94,95] Investigation of the literature illustrated that manganese(II) as well as manganese(III) complexes could be used as superoxide scavenger molecules.

EUK-8   **EUK-134**
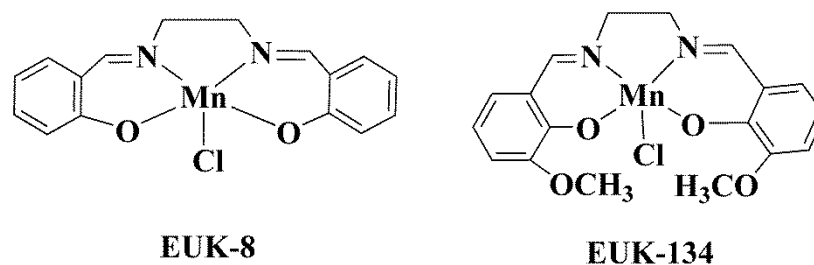
Fig. 1.9 Manganese complexes as potent SOD mimic

Iron complexes have also been studied as SOD mimic although they can produce hydroxyl radical on reacting with H_2O_2 which could be fatal. The advantage of iron complex over manganese is that these complexes are kinetically and thermodynamically more stable.[96] Recently, Hitomi and co–workers reported iron complexes $[Fe^{III}(dpaq^R)Cl]Cl$ having different electron donating and withdrawing substituent in ligand framework and these complexes served as pure SOD mimic without any peroxidase activity. Iron complexes were found to be more effective SOD mimic as compare to iron salen complexes. Introduction of electron donating group in ligand frame showed enhancement in the SOD activity.[97] Pap and co–workers reported hexa–coordinated iron(III) complexes utilizing isoindoline derived ligands. The SOD activities of complexes were evaluated using indirect method and NBT assay. Synthesized complex exhibited good correlation between the redox potential and SOD activity. SOD like activity exhibited that the rate determining step is the reduction of the metal center.[98] Ivanovic–Burmazovic and co–workers have synthesized seven–coordinated iron and manganese complexes $[Fe^{III}(dapsox)(H_2O)_2]ClO_4.H_2O$, $[Fe^{II}(H_2dapsox)(H_2O)_2](NO_3)_2,H_2O$ and $[Mn^{II}(H_2dapsox)(CH_3OH)(H_2O)](ClO_4)_2(H_2O)$ using acyclic and rigid pentadentate $H_2dapsox$ ligand $[H_2dapsox=2,6–$ diacetylpyridinebis(semioxamazide)]. Superoxide dismutase activities of these complexes

were studied spectrophotometrically, electrochemically, and using a submillisecond mixing UV–visible stopped–flow techniques. The IC_{50} values were found to be in the millimolar (mM) range and proved to be effective SOD mimic.[99] In this regard, several iron complexes were synthesized and there SOD activities were optimized.[97,99–106]

1.7.1.2. Catechol dioxygenases (CDO)

Dioxygen–activating enzymes are very important for several catalytic reactions.[107–114] Catechol dioxygenase enzymes play crucial role during degradation of aromatic compounds in soil bacteria usually using *cis*–diol catechol as a substrate.[115] On the basis of site of cleavage these can be further categorized into two classes: Intradiol catechol dioxygenase and extradiol catechol dioxygenase[116] as shown in Scheme 1.3.
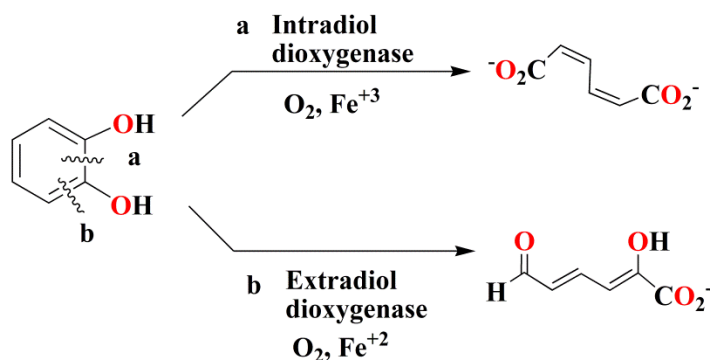
Scheme 1.3 Oxidative cleavage of catechol using (a) intradiol dioxygenase to give *cis,cis*muconic acid product; (b) extradiol dioxygenase to give 2–hydroxymuconate semialdehyde product

Crystallographic studies were found to be helpful to understand the reason behind different cleavage products. It was found out that intradiol catechol dioxygenase contains iron(III) centre having two tyrosine and two histidine residue[117] while in extradiol

catechol dioxygenase two histidine and one glutamic acid was coordinated to iron(II) centre in square pyramidal geometry (Fig. 1.10).[118–121]

Hence modelling of these enzymes have appeared as an interesting area to explore.[121,122]

Intradiol Catechol Dioxygenase   **Extradiol Catechol Dioxygenase**
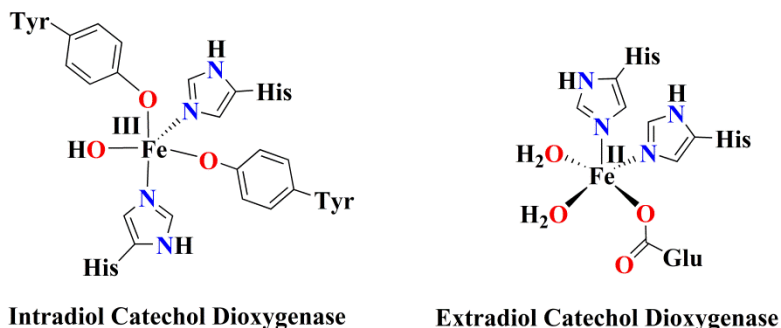
Intradiol	**Extradiol**
✓ Cleave C–C double bond between phenolic hydroxyl group	✓ Cleave C–C double bond adjacent to phenolic hydroxyl group
✓ Fe(III) as a cofactor	✓ Fe(II) as a cofactor
✓ Trigonal bipyramidal geometry	✓ Square pyramidal geometry
✓ e.g. 3,4 PCD and 1,2 CTD	✓ e.g. 4,5 PCD and 2,3 CTD

Fig. 1.10 Active site structures of catechol dioxygenase enzymes

Manganese and iron complexes as catechol dioxygenase mimic

Pioneer work has been done by several research groups to exploit the chemistry of these enzymes. Most of the work has been done using iron complexes but manganese catechol dioxygenase have also been characterized.[123] Reddig *et. al.* have synthesized mononuclear manganese complexes [Mn(L$_1$)(tcc)], [Mn(L$_2$)(tcc)]. H$_2$O. 0.5CH$_3$OH, [Mn(L$_3$)(tcc)]. CH$_2$Cl$_2$, [Mn(L$_4$)(tcc)]. 1.5CH$_2$Cl$_2$, [Mn(L$_5$)(tcc)] and (HN(C$_2$H$_5$)$_3$)[Mn(L$_6$)(tcc)]. CH$_2$Cl$_2$ using tetradentate ligands HL$_1$ (2–[(bis(pyridin–2–

ylmethyl)amino)methyl]phenol), HL_2 (2–[[(((6–methylpyridin–2–yl)methyl)(pyridin–2–ylmethyl)amino]methyl] phenol), HL_3 (2–[[(((6–methylpyridin–2–yl)methyl)(pyridin–2–ylmethyl)amino]methyl]–4–nitrophenol), HL_4 (2–[(bis(pyridin–2–ylmethyl)amino)methyl]–4–bromophenol), HL_5 (2–[(bis(pyridin–2–ylmethyl)amino)methyl]–6–methoxyphenol) and H_2L_6 ([(bis(2–hydroxy–5–nitrobenzyl))(pyridin–2–ylmethyl)]amine) respectively and monitored effect of electron donating and withdrawing group on the enzymatic activity. These complexes were found as structural manganese analogous for substituted forms of iron–containing intradiol cleaving catechol dioxygenases. Hence complexes exhibited structural mimicking of the active site of manganese substituted catechol dioxygenases.[124]

Bugg and co–workers explained the reaction mechanism involved during the catalytic process. They have synthesized an iron complex using tridentate ligand 1,4,7–triazacyclononane (TACN) and a proton donor. Complex was found to be an extradiol mimic and the effect of Fe(II) and Fe(III) on extradiol catechol cleavage was also optimized. Both the oxidation states was found to be active to the cleavage but promising results were obtained for Fe(II) which is the oxidation state found in native enzyme. Effect of electron donating group was also optimized in the substrate.[125] Bugg and co–workers further proposed the mechanism as well as reaction intermediate involved during the catalytic process.[126–129] In continuation of advancement to this enzymatic chemistry, Que and co–workers also suggested role of iron centre, type and environment of the ligand around metal centre.[130–133] Palani and co–workers synthesized iron complexes derived from tridentate N_3 ligands pyrazol–1–ylmethyl(pyrid–2–ylmethyl)amine (L1), 3,5–dimethylpyrazol–1–ylmethyl(pyrid–2–ylmethyl)amine (L2),

3–iso–propylpyrazol–1–ylmethyl(pyrid–2–ylmethyl)amine (L3) and (1–methyl–1H–imidazol–2–ylmethyl)pyrid–2–ylmethylamine (L4) and also synthesized adduct of iron(III) [Fe(L)(DBC)(CH$_3$OH)] using 3,5–di–*tert*–butylcatecholate (DBC^{2-}) where ligand tridentate substituted monophenolate L such as 2–((N–benzylpyrid–2–ylmethylamino)methyl)phenol (H(L1)), 2–((N–benzylpyrid–2–ylmethylamino)–methyl)–4,6–dimethylphenol (H(L2)), 2–((N–benzylpyrid–2–ylmethylamino)methyl)–4,6–di–tert–butylphenol (H(L3)) and 2–((N–benzylpyrid–2–ylmethylamino) methyl)–4–nitrophenol (H(L4)) and also optimized their activity as dioxygenase model. All these complexes exhibited the functional mimicing of the native enzyme.[134,135] They have explored effect of Lewis acidity of iron,[136] effects of ligand basicity, steric hindrance on the cleavage activity.[136–145] In this regard, Paine and co–workers also synthesized iron complex [(L)$_3$Fe$_3$(DBC)$_3$] where L is 1–(2–pyridylmethyl)pyrrolidine–2–carboxylate a proline based flexible tridentate facial NNO donor ligand and the complex was found to be selective towards functional modelling of extradiol cleavage activity. Cleavage products resulted into an equal amount of extra and intradiol cleavage products without any auto–oxidation product.[146] Several iron complexes have been synthesized and found as potent applicant for the catechol dioxygenase activity.[136,147,148]

1.7.1.3. *o*–aminophenol dioxygenase (APD)

During microbial degradation of aromatic compound ring cleavage is a crucial step. Dioxygenases are responsible for such reaction in aerobic bacteria using aromatic ring with cis–diol as a substrate.[149] 2–aminophenol shows analogy to catechols as amino and hydroxyl group have comparable size and similar effects on electrophilic aromatic substitution. In continuation of this, a new ring cleaving enzyme *o*–aminophenol

1,6–dioxygenase has been discovered which converts *o*–aminophenol to 2–aminomuconic acid semialdehyde.[150] The process starts during growth of *Pseudomonas pseudoalcaligenes* JS45 on nitrobenzene where reduction of nitrobenzene to hydroxylaminobenzene and then rearrangement to 2–aminophenol occurs.[151] A schematic presentation has been shown in Scheme 1.4.
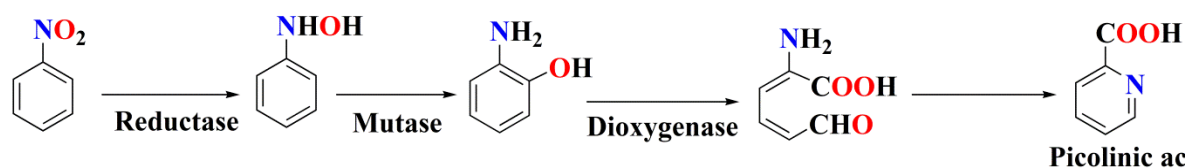
Scheme 1.4 Formation of ring cleavage product picolinic acid during degradation of nitrobenzene in *P. pseudoalcaligenes*

Manganese and iron complexes as *o*–aminophenol dioxygenase mimic

Iron complexes have been utilized for the mimicking of 2–aminophenol dioxygenase enzyme. Fiedler and co–workers synthesized iron containing complexes having similar structural and electronic features as that of native enzyme.[152] Paine and co–workers have synthesized non heme iron(II) complexes using tetradentate nitrogen donor ligand 6–Me$_3$–TPA = tris(6–methyl–2–pyridylmethyl)amine and 4–*t*Bu–HAP = monoanionic 2– amino–4–tert–butylphenolate. In this work, they have utilized these complexes for dioxygen reactivity and found out that complexes behaves as a functional model for APD (2–aminophenol–1,6–dioxygenase) and 3–hydroxyanthranilate–3,4–dioxygenase (HAD) enzymes.[153,154] Paine and co–workers also elucidated effect of supporting ligands on the reactivity of iron(II)–aminophenolate

complexes towards molecular oxygen.[155] In continuation of these studies, Paine and co−workers also exploited tridentate ligand to explore the modelling of APD.[156]

1.7.1.4. *o*−aminophenol oxidase

Enzyme phenoxazinone synthase is naturally isolated from bacterium *Streptomyces antibioticus* and catalyzes the oxidative coupling of two molecules of a substituted *o*−aminophenol to phenoxazinone chromophore in the final step during biosynthesis of the antineoplastic agent, acinomycin D.[157] General reaction can be summarized as in Scheme 1.5.
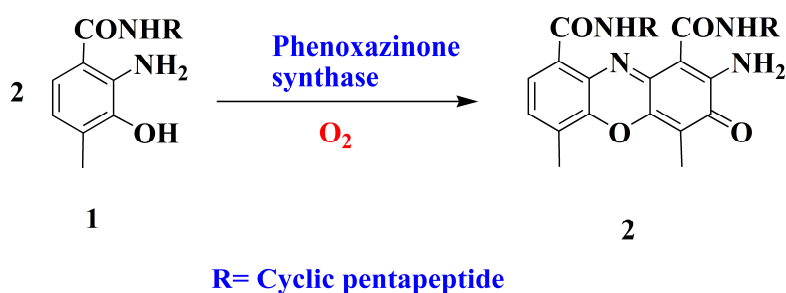
Scheme 1.5 oxidation of *o*−aminophenol in presence of oxygen

Later on, according to the extensive study on chemistry of the phenoxazinone chromophore, four pathways were proposed for the oxidation of *o*−aminophenol to 2−aminophenoxazinone for the enzymatic reaction (Scheme 1.6).[158,159]
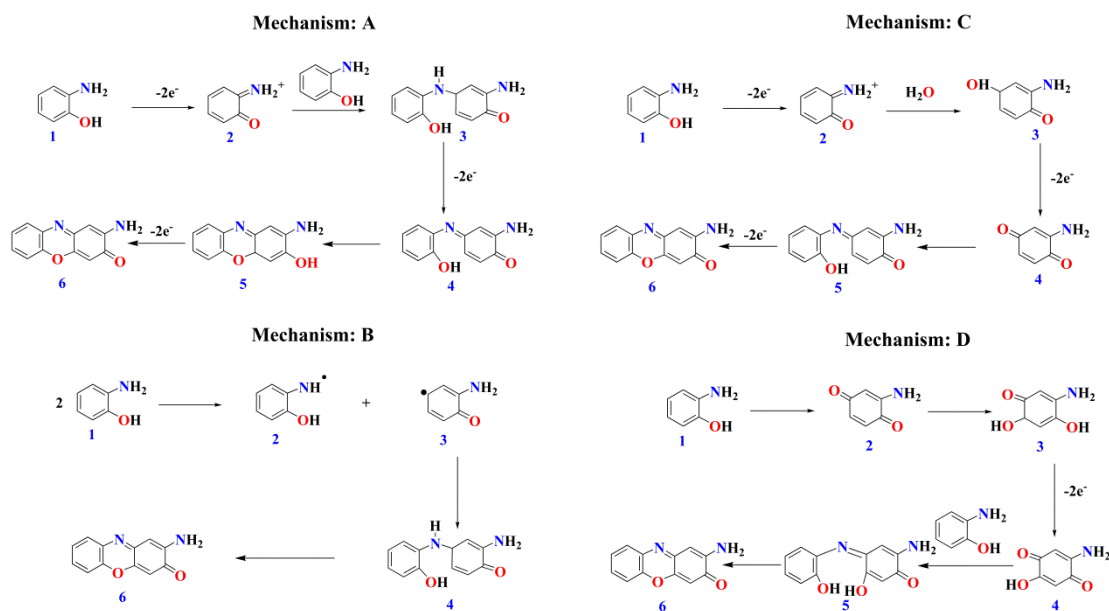
Scheme 1.6 Proposed mechanism for the formation of 2−aminophenoxazinone

Manganese and iron complexes as *o*−aminophenol oxidase mimic

Manganese complexes exhibiting oxidation of *o*−aminophenol have been reported. Simandi and co−workers reported a dioximatomanganese(II) complex $[Mn_2(HL)_2](BPh_4)_2$ having ligand $[HON=C(CH_3)C(CH_3)=NCH_2CH_2]_2NH$ as H_2L. On dissolution of this complex in methanol a monomeric species $[Mn(HL)]^+$ is produced which oxidizes *o*−aminophenol. Hence species generated behave as a functional model for phenoxazinone synthase.[160] Speier and co−workers prepared mononuclear manganese(II) complex $[Mn(6'Me_2indH)(H_2O)_2(CH_3CN)](ClO_4)_2$ and monitored the oxidation of *o*−aminophenol. Complex was found to be effective in oxidizing oxidation of *o*−aminophenol and followed a first order kinetcis.[161] Recently, Panja have reported manganese complexes $[Mn(L^1)Cl_2]$. 2MeOH and $[Mn(L^2)Cl_2]$ complexes derived from tetradentate ligands and evaluated oxidation of *o*−aminophenol. Both the complexes were found to be effective in the oxidation of *o*−aminophenol.[162] Iron complexes are also

equally important for such catalytic activities. Mathur and co−workers utilized ligands N,N′−Bis(2−methylbenzimidazolyl) pyridinediamide [GBPA=L1] and N−picolylated−N,N′−Bis(2−methylbenzimidazolyl)hexandiamide [PicGBHA=L2] for the synthesis of iron complexes and optimize the oxidation of o−aminophenol. Kinetic studies were also explored and effect of $E_{1/2}$ on the catalytic activity was also studied.[163] Kaizer and co−workers synthesized series of iron complexes derived from 1,3−bis(5−methyl−2−thiazolylimino)isoindoline ligand and these complexes were found to be a suitable catalyst for the oxidation of o−aminophenol. They have also proposed mechanism depending on the oxidant (i) a metal based oxidation for dioxygen (ii) a hydroxyl radical mediated process. Kinetic studies were also performed for the complexes.[164] In continuation of these studies several iron complexes were synthesized and found to be potent catalyst for the oxidation of o−aminophenol.[110,165,166]

1.7.1.5. Galactose and glyoxal oxidase (GAO and GLX)

Function of the metal in the active site of enzymes such as galactose oxidase, amine oxidases, ribonucleotide reductase and cytochrome c−oxidase is to coordinate O_2 in their reduced forms and then generation of a metal−bound, activated oxygen species through the proper redox chemistry. Galactose oxidase is an enzyme having transition metal at centre along with the tyrosine residue which catalyzes the two−electron oxidation of primary alcohols.[167–169] Galactose oxidase although displays an unpredictably low specificity for the primary alcohol but completely regioselective. This enzyme does not utilize secondary alcohols as a substrate.[170]

Free radical catalysis has become an emerging field of free radical enzymology.[171–173] Galactose oxidase (GAO) is the member of a family of enzymes known as

radical–copper oxidases along with the fungal enzyme, glyoxal oxidase (GLX).[174–176] This enzyme is a physiological partner of lignin peroxidase[177,178] and manganese peroxidase.[179] Galactose oxidase utilizes primary alcohol as a substrate and converts it to aldehyde while the glyoxal oxidase converts aldehyde to carboxylic acid. Both the processes involve two electron oxidation and the overall reactions of GAO and GLX are described below in Scheme 1.7.[173,180]

$$\text{GAO:} \quad RCH_2OH \ + \ O_2 \ \longrightarrow \ RCHO \ + \ H_2O_2$$

$$\text{GLX:} \quad RCHO \ + \ O_2 \ \longrightarrow \ RCOOH + \ H_2O_2$$
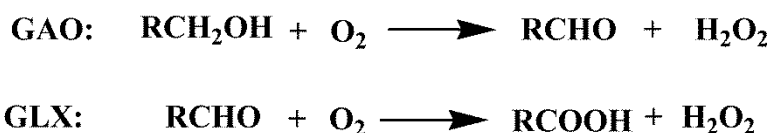
Scheme 1.7 Reaction catalyzed by galactose oxidase and glyoxal oxidase

Galactose oxidase[171,181] is an oxidation–reduction catalyst exploiting an unusual free radical coupled copper in its active site.[171,182] This consists two distinct one–electron acceptors, Cu(II) metal center and a stable protein free radical. Primary structure of amino acid sequence of glyoxal oxidase and galactose oxidase has no homology but these two enzymes show similarities in active site structure and chemistry.[178,179] Active site of the galactose oxidase enzyme consists a mononuclear copper ion having square pyramidal coordination geometry (Fig. 1.11) in which copper ion is coordinated to a tyrosinate residue (Tyr272), two histidine residues (His496 and His581) along with a water molecule (pH 7.0) or acetate (pH 4.5) in the equatorial plane. Apical position was occupied by tyrosinate residue (Tyr495) at a distance of 2.65 Å from copper centre.[171,179] An exceptional characteristic of this active site represents the alteration of the tyrosinate residue located in the equatorial plane by a covalent linkage to the sulphur of adjacent

cysteine residue.[172,183] During catalytic cycle mononuclear copper ion accommodate three forms as fully oxidized, fully reduced and an inactive form. Fully oxidized form contains copper(II) antiferromagnetically coupled to a tyrosyl radical and is catalytically active . The fully reduced copper(I) centre have three coordinated Tyr272, His496 and His581 and separated Tyr495 and solvent, this form is also catalytically active form.[184]
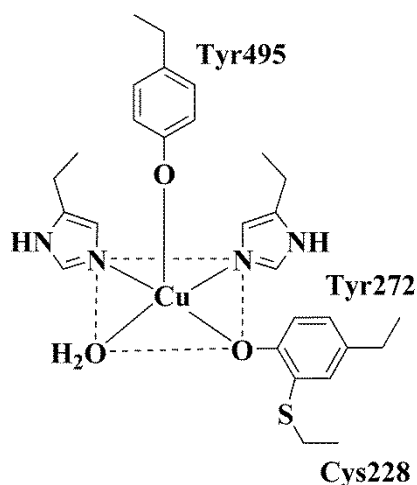
Fig. 1.11 Active site structure of galactose oxidase

The redox potential range required for the conversion of GAO and GLX to the active form has been determined by spectrochemical titration as + 0.45 V and 0.66 V (*vs* NHE) respectively.[171,172] Galactose oxidase enzyme involves one electron transfer processes, single electron transfer (SET), hydrogen atom transfer (HAT) and proton transfer (PT)) during its catalytic cycle and the mechanism has been shown in Scheme 1.8.[172]
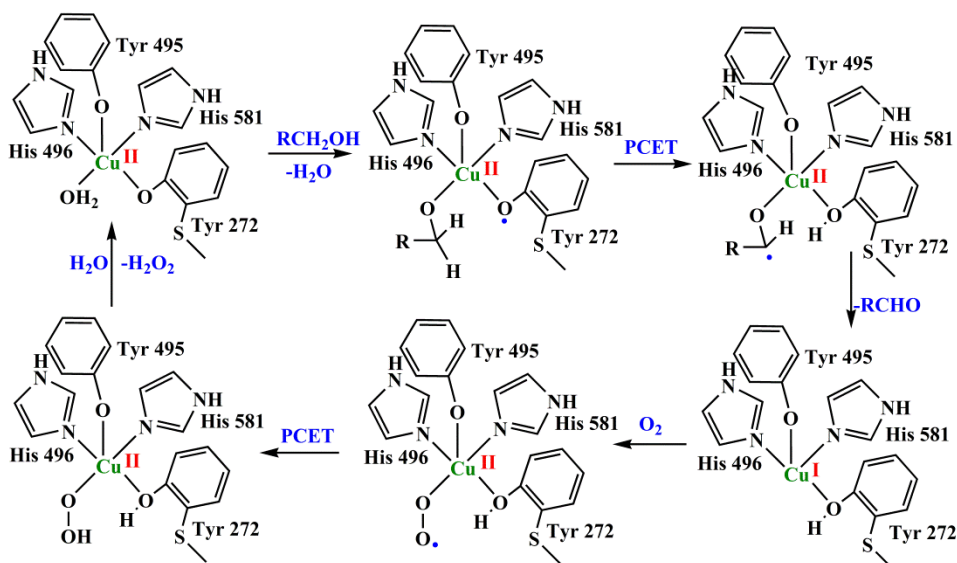
Scheme 1.8 Conversion of primary alcohol to aldehyde *via* galactose oxidase enzyme

Proton coupled electron transfer (PCET) is an overall process which include both proton as well as electron transfer.[185] Transfer of proton and electron could follow a single kinetic step using concerted proton–electron transfer (CPET). A process where transfer of proton and electron occurs simultaneously from donor to acceptor is termed as hydrogen atom transfer. This is a limiting case of PCET. Due to the presence of phenoxyl radical acceptor in the active site of enzyme, hydrogen atom transfer is thought to be a probable process followed rather than a more generalized sequential PCET process.[171]

Manganese and iron complexes as galactose oxidase/glyoxal oxidase mimic

Oxidation chemistry is very important in case of iron and manganese.[186] Syntheses of coordination compounds containing non–innocent ligands have been considered of interest in various fields of inorganic chemistry such as coordination chemistry[187] and bioinorganic chemistry.[188] Phenoxyl radical chemistry of transition metals was unexplored due to the facts that phenoxyl radicals are transient species and metal–oxygen

bond in phenoxyl radical complexes was weaker due to the decreased π–donating properties in phenoxyl radical complexes as compare to ionic phenolates complexes. Advancement in the field of radical complexes increased now a days and researchers are more interested to explore the chemistry of these radical containing metal complexes towards catalysis in various organic substrates. To enhance the stability of radical in ligand, ortho and para substitutions with the electron donating group have been proved a good alternative. Some of the ligands which are capable of generating phenoxyl radical have been shown in Fig. 1.12. One electron oxidation of a phenolato containing transition metal complex can be either metal or ligand centred in nature.[189]
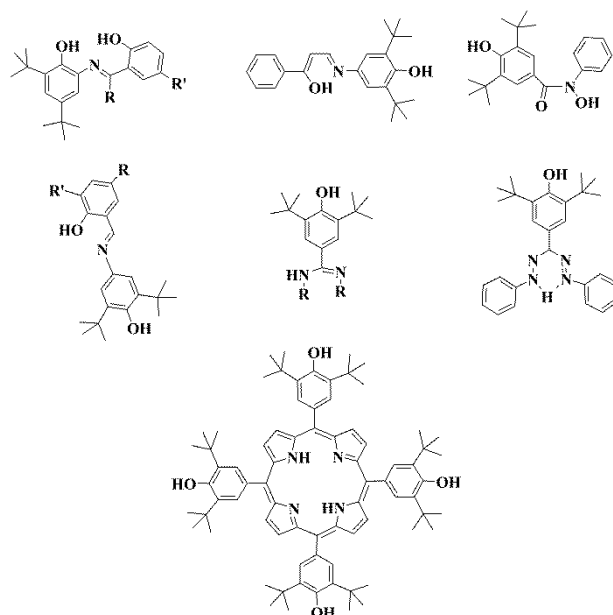
Fig. 1.12 Ligands containing oxidizable pendant phenols utilized for the synthesis of metal complexes for oxidation reaction

Phenoxyl containing manganese complexes are more complicated due to the accessibility of metal as well as ligand centre electron transfer process in normal potential range.[190,191] These sort of ligand can stabilize manganese in Mn(II), Mn(III) and even

Mn(IV) oxidation states. Wieghardt and co–workers synthesized a series of complexes including manganese(III) using tetradentate monoanionic macrocyclic ligand. Electronic, resonance Raman and EPR spectra were utilized to assure the presence of radical complexes. Complexes generated stable phenoxyl radicals in the solution using electrochemical oxidation process.[192] Fujii and co–worker reported mixed–valence ligand radicals of manganese(III) salen complexes.[193] They tried to explore the active species which are transiently generated from chiral manganese(III) salen complexes and found excellent catalyst towards asymmetric oxidation.[194] Iron complexes of phenolato containing complexes are also gaining importance. Mendes and co–workers synthesized diazocyclebis(di*tert*butylphenol) ligands having phenolato arm and their corresponding iron complexes. They have established the generation of phenoxyl radical using electrochemical as well as UV–visible studies. During studies they explored the effect of Lewis acidity on the oxidation behavior.[195] Saberikia and co–workers also synthesized a tetradentate ligand having two phenolato arm [6,6'(((((tetrahydrofuran2yl)methyl)azanediyl)bis(methylene))bis(2,4dichlorophenol)] (H_2L^{THF}) and its corresponding iron(III) complex. They have found out electrochemical oxidations were ligand–centered on the other hand, reductions were metal–centered related to Fe^{III}/Fe^{II} couple.[196] Verani *et. al.* synthesized a five coordinated iron(III) complex using phenolato containing ligand with N_2O_3 donor atoms. In nature the phenolate/phenoxyl couple is coordinated to metal ion in pentacoordinated fashion, which could be responsible for the observed redox flexibility. Process of phenoxyl radical generation was studied and first oxidation was found to be ligand centered in nature.[197] Verani *et. al.* studied the redox and electronic behavior of iron high–spin $3d^5$ ions in

five−coordinate ligand fields and provided major insight into bioinspired redox cycling using experimental and theoretical studies.[198] In continuation of contribution towards radical chemistry Verani and co−workers have studied the effect of ligand rigidity and ring substitution on the structural and electronic properties of iron complexes with tridentate ligands.[199]

1.7.2. Interaction with biomolecules

1.7.2.1. DNA interaction studies

DNA is a nucleotide having genetic information which makes it a molecule of great significance. Activation or inhibition of DNA function is necessary to cure or control certain diseases. Hence interaction of DNA with the small molecules is important and a fascinating area to explore.[200−202] Synthesis of therapeutic agent which can cleave DNA specifically and selectively is a demanding area.[3,203] Metal complexes may interact with the DNA from electrostatic interactions with the anionic phosphate backbone to soft nucleophilic interactions with the purine heterocycles. Metal interaction can be classified in two cegories: DNA binding and DNA cleavage (nuclease). These two further sub−classified according to their mode of interaction and action. Binding of DNA can be categorized into two classes.

1.7.2.1.1. Non−covalent binding

Non−covalent interaction arises due to the interaction of the molecule with DNA through hydrogen bonding, electrostatic forces, Van−der Waal forces, hydrophobic interactions, intercalation and electric field of the DNA.[3] Depending on the mode of interactions non−covalent interactions can be further classified in three categories. These interactions depend on the charge, shape and planarity of the complexes.

1.7.2.1.1.1. External or electrostatic interaction

This involves interactions between positive charge of metal ion with the negatively charged phosphate backbone and interactions with the electron donor groups of the bases. Main forces of interaction are electrostatic and includes the charge of the molecule, ligand hydrophobicity and total size of the ions.[204,205]

1.7.2.1.1.2. Groove or surface interaction

Double helix structure of B–DNA has nearly 10 base pairs per turn which consist of two grooves of different width: Major groove (22 Å) and minor groove (12 Å). These grooves may also serve as site of interaction with the small molecules.[3] It is found that small molecules prefer to bind with B–DNA *via* minor groove, on the other hand, DNA binding proteins or gene–targeted oligonucleotides interact at major groove.[205]

1.7.2.1.1.3. Intercalation

Intercalation starts with the binding of molecule as a major groove binder.[206] Extended planar aromatic ring system and chemical nature which can slot between base pairs is an essential criterion to intercalation. Process starts with the access of intercalating ligand through the major groove leading to this ligand behave as a new base pair.[3,206] Upon binding deoxyribose–phosphate backbone unwinds and stabilized by interactions such as π–π stacking interactions, dipole–dipole interactions or hydrogen bonding with the planar aromatic moiety. DNA intercalators were found to be effective in treating cancer cells. DNA intercalators could be organic molecules (berberine, ethidium bromide, proflavine, daunomycin, doxorubicin, and thalidomide)[207] or metal complexes (platinum complexes).[208]

1.7.2.1.2. Covalent binding

This mode of binding is completely irreversible and leads to inhibition of cell process. This process results into the complete cell death. It involves interaction between soft metal ion and nucleophilic site of nitrogenous base.[209] The probable site of coordination could be N−7 position of gauanine and adenine, N−3 position of cytosine, deprotonated N−3 position on thymine and uracil.[3,210,211] The well known example is *cis–*platin (cisdiamminedichloroplatinum) an anticancer drug which interacts with N7 positions of guanine (Scheme 1.9).[212–214]
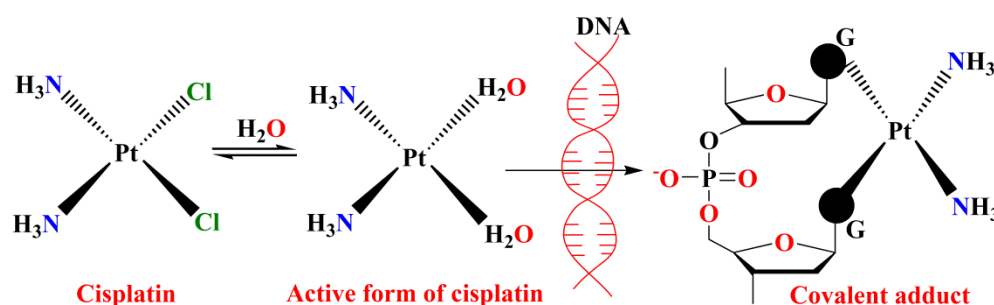
Scheme 1.9 Mode of covalent binding of cis−platin with DNA

However these platinum based drugs have some drawbacks which restrict its application such as poor solubility, acquired drug resistance and need for intravenous administration.[202] Hard metals prefer to interact with oxygen atom of phosphate group.[215,216]

1.7.2.3. DNA cleavage or nuclease

Cleavage of DNA is an important process in all living beings. Nucleases are the enzymes which catalyze and repair DNA strands. One of the examples of such enzyme is restriction endonuclease which is responsible for the cleavage of foreign DNA during

38

viral infection.[217,218] Basically cleavage can be categorized into three forms: (i) Oxidative cleavage (ii) Hydrolytic cleavage (iii) Photolytic cleavage. A brief discussion on these cleavages is as followed:

1.7.2.3.1. Oxidative cleavage or nuclease

Oxidative cleavage basically involves oxidation of either sugar moiety[219] or the nucleobases[220] by some reactive intermediates produced such as hydroxyl radical (HO˙), superoxide anion (O_2^-), hydrogen peroxide (H_2O_2) and singlet oxygen ($^1O_2$).
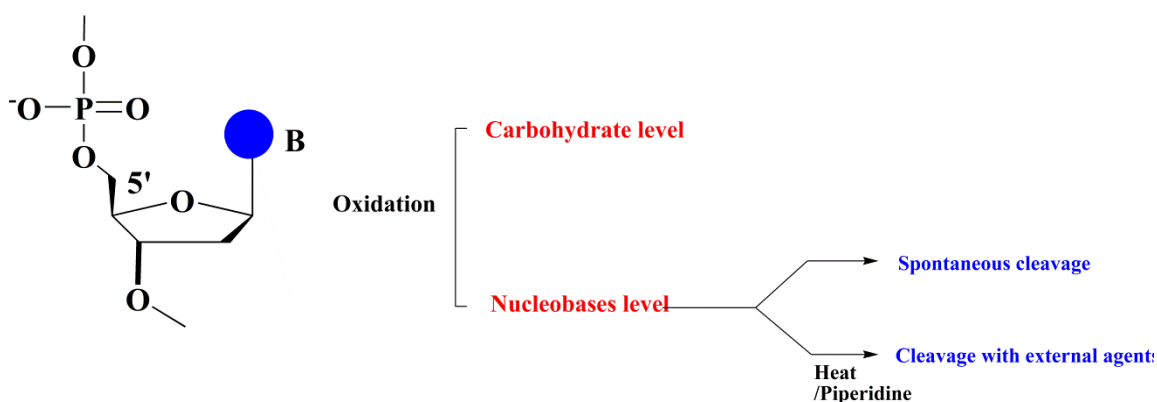
Scheme 1.10 Types of oxidative cleavage of DNA

Mode of action of oxidative cleavage follow three pathways: Hydrogen abstraction, addition and electron transfer.[221] Besides reactive oxygen intermediates, metal bound intermediate can also follow this pathway as in iron bleomycin. Bleomycin (BLM) is an antitumor drug and one of the most effective natural compound for oxidation of DNA. Umezawa and co−workers were first to isolate BLM in form of copper complex from *Streptomyces verticillus*.[222] BLM is capable of inducing both single and double strand breaks in DNA in the presence of both a metal ion in a low oxidation state (e.g. Fe(II) or Cu(I)) and dioxygen (Fig. 1.13).
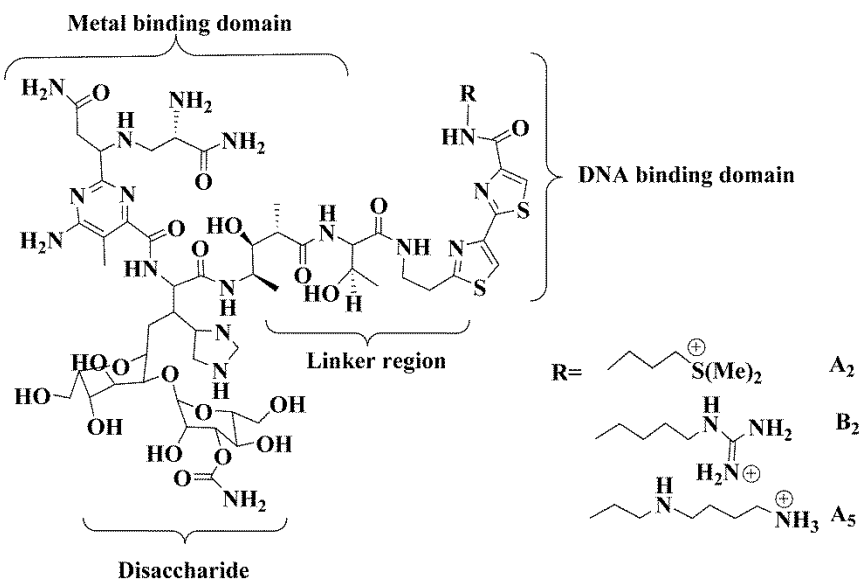
Fig. 1.13 Structure of bleomycin (BLM)

Redox chemistry of iron bleomycin is widely studied[223] and catalytic cycle proposed for the mechanism is shown in the Scheme 1.11.[224–227]
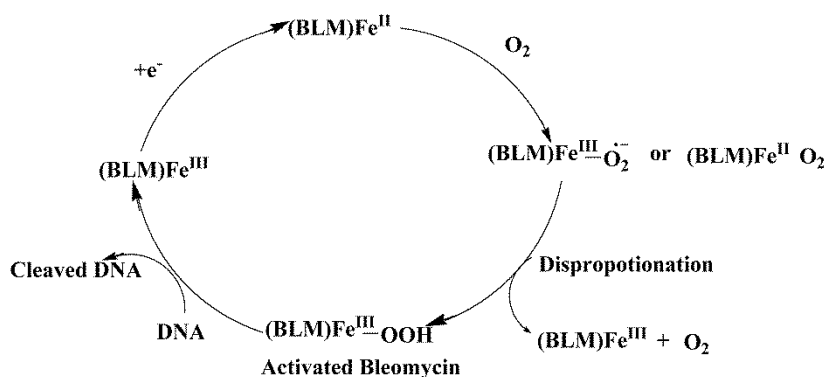
Scheme 1.11 Proposed catalytic cycle of iron bleomycin for DNA cleavage

1.7.2.3.2. Hydrolytic cleavage

Stability of phosphodiester bond in DNA under ambient condition is very high (half–life ten to billions of years).[228,229] Metal ions behave as Lewis acid during

hydrolysis reactions and activate phosphate group to nucleophilic attack.[230,231] The widely accepted mechanism of DNA hydrolysis is as shown in scheme 1.12.[232–234]
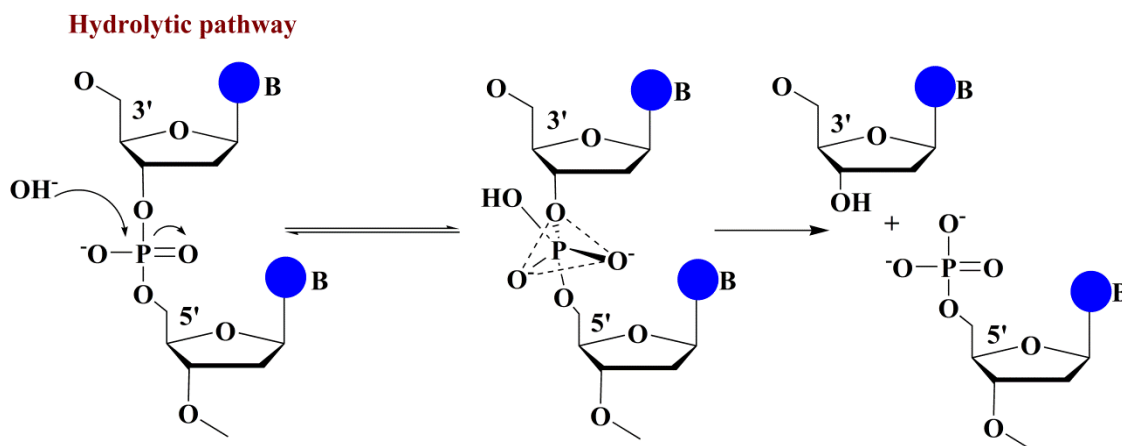
Scheme 1.12 Proposed mechanism for DNA hydrolysis

1.7.2.3.3. Photolytic cleavage

Photolytic cleavage can be proceed through UV induced DNA damage or cleavage due to reactive oxygen species. These reactive oxygen species are generated due to organic compounds of metal complexes.[220,235–237]
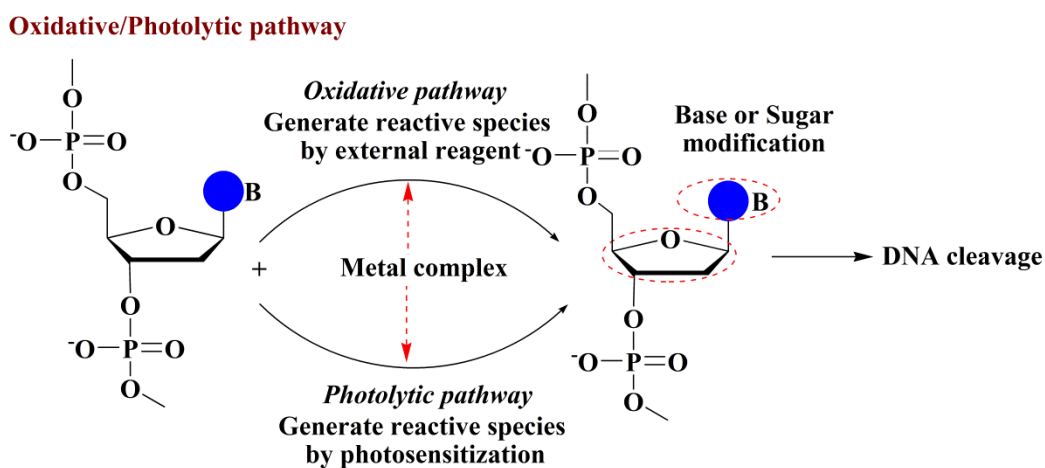
Scheme 1.13 Mode of nuclease *via* oxidative and photolytic pathway

Manganese and iron complexes interacting with DNA

Thamilarasan and co−workers synthesized metal complexes of $Mn(bpy)_2(N_3)_2$, $Co(bpy)_2(N_3)_2 \cdot 3H_2O$ and $Zn_2(bpy)_2(N_3)_4$ [bpy= 2,2bipyridine] and monitored the interaction studies with the DNA. These complexes bind with CT−DNA in an intercalative mode for manganese and cobalt while zinc complexes interacted *via* groove binding mode. Further they have optimized nuclease activity and found out that complexes of manganese and cobalt followed oxidative mechanism while in case of zinc complexes hydrolytic cleavage was found.[238] Zhu and co−workers have synthesized manganese complexes using 1,8−naphthalene dicarboxylic and 1,10−phenanthroline and complexes cleaved DNA following oxidative cleavage.[239] Manganese complexes have been synthesized using ligand N,N,N',N'−2,6−bis(((2−(dimethylamino)ethyl)(pyridin−2−ylmethyl)amino)methyl)−4−methoxyphenol by Tao and co−workers complexes were found to be capable of promoting DNA cleavage through an oxidative pathway *via* hydroxyl radical, singlet oxygen or singlet oxygen−like species.[240] Zampakou and co−workers synthesized manganese complexes derived from quinolone antibacterial drug oxolinic acid (Hoxo). These complexes were subjected to DNA interaction studies. Intercalative mode of DNA was found to be the probable mode of nuclease.[241] In continuation of these studies Macias *et. al.* synthesized manganese complexes using ligand sulfonamides derived from 8−aminoquinoline. These complexes followed oxidative cleavage of DNA.[242]

Neves and co−workers synthesized an iron complex tris−{[1,2,5]−thiadiazolo−[3,4−f]−[1,10]−phenanthrolineiron(II)}hexafluorophosphate and studied the DNA interaction studies. Results showed cleavage of DNA through

photolytic cleavage.[243] Bal–Demirci and co–workers have synthesized iron complex derived from thiosemicarbazone. Complex was found to be interactive with DNA through the nitrogenous base adenine.[244] Hadadzadeh *et. al.* synthesized mononuclear iron complex using ligand tppz (2,3,5,6tetra(2pyridyl)pyrazine). These complexes interact well with CT–DNA and also cleaved the DNA through the singlet oxygen radical species.[245] In continuation of work, Parveen and co–workers synthesized iron complex derived from valine and monitored its nuclease activity. Complex was found to be cleaving the plasmid using hydrolytic pathway.[246] Due to effective physical and chemical application of Schiff base derived metal complexes, these complexes have been used for various biological applications. Iron complexes derived from tridentate o–hydroxynaphthaldehyde and L–alanine (nal), L–phenylalanine (nphal), L–aspartic acid (nas) and L–arginine (nar) have been synthesized. These complexes interacted with DNA through intercalative mode.[247] Cowan *et. al.* synthesized metal complexes using chelating ligands and subjected them for the nuclease activity. Complexes cleaved the DNA *via* reactive oxygen species.[248] Chiral ligand L1=(R/S)(±)1naphthylN(pyridine2ylmethylene)ethanamine, L2= (R/S)(±)2naphthylN(pyridine2ylmethylene)ethanamine have been utilized to synthesize iron complexes. Gu and co–workers suggested the groove binding mode of interaction with DNA.[249]

Chakravarty and co–workers explored the structure–activity relationship in a series ternary iron(III) complexes with modified dipyridophenazine ligands and these complexes were found to be efficient in DNA cleavage *via* photolytically.[250] Chakravarty and co–workers have synthesized iron(III) benzhydroxamate complex of dipicolylamine

ligand having a pendant pyrenyl moiety and their cleavge property was optimized towards plasmid DNA[251] and also explored the cytotoxicity activity.[252] They have utilized iron complexes for nuclease[253] these complexes exhibited photocytotoxicity in visible light.[254]

1.7.2.2. Protein cleavage or protease

Proteases are the enzymes which are responsible for the cleavage of highly stable peptide bonds. These enzymes can hydrolyze the peptide linkage in protein. Depending on the site of cleavage protease can be categorized in two classes:

(a) Exopeptidases: Cleave the peptide bonds nearby to the termini of the peptide chain such as aminopeptidases and carboxypeptidase A.

(b) Endopeptidases: Cleave peptide bond irrespective of its position in the peptide chain such as trypsin, pepsin and chymotrypsin.

Several physiological disorders such as muscular dystrophy, amyotrophic lateral sclerosis, respiratory distress syndrome, progeria, rheumatoid arthritis, alzheimer's disease and Werner's syndrome[255–257] are consequence of accumulation of oxidised protein due to some reactive oxygen species. Hence detection of these accumulated proteins are very important to study.

Manganese and iron complexes as artificial protease

Chakravarty and co–workers have reported three oxo–bridged diiron(III) complexes [$Fe_2(\mu–O)(L–his)_2(B)_2$]–$ClO_4)_2$ derived from L–histidine and heterocyclic bases. One of the complex was found to be efficient to cleave the bovine serum albumin (BSA) protein in Tris–HCl/NaCl buffer medium *via* OH radical pathway.[258,259] Smith *et. al.* have reported mixed valence iron dinuclear complex using ligand H_2L1 =

2–{[[3–[((bis–(pyridin–2–ylmethyl)amino)methyl)–2–hydroxy–5–methylbenzyl](pyridin–2–ylmethyl)amino]methyl]phenol} which was found to be an efficient artificial protease.[255]

1.7.3. Metal complexes in medicine

Role of inorganic chemistry in the field of medicine can be categorized into two forms, first the drug which acts on metal in free form or bound to metal and second is metal based drug where central metal imparts the important action. In pharmaceuticals, metal based drug are found to be of great interest. Advancement in the field of bioinorganic chemistry lead to parallel growth in medicinal chemistry using biological as well as non–biological metals.[147,260–266] These inorganic metal complexes are made up of either element essential for life such as iron in anaemia or some toxic metal such as platinum in cancer treatment. Inorganic complex have been found as chemotherapeutic agent such as anticancer agent (cis[$Pt(NH_3)_2Cl_2$]),[267] metal–mediated antibiotics (bleomycin), magnetic resonance imaging (MRI) agent (gadolinium compounds), antibacterials, antivirals, antiparasitics, and radiosensitizing agents. In this regard organometallic complexes are also found to be excellent cure for cancer, HIV and malaria.[268] Several nitric oxide (NO) donors have been proved cytotoxic to tumor cells leading to apoptosis during *in vitro* studies.[269,270] Metal complexes have also been utilized as an alternative for the treatment of cancer.[271–274] Various metals have been utilized for the medicinal studies as shown in Fig. 1.14 and Table 1.6.
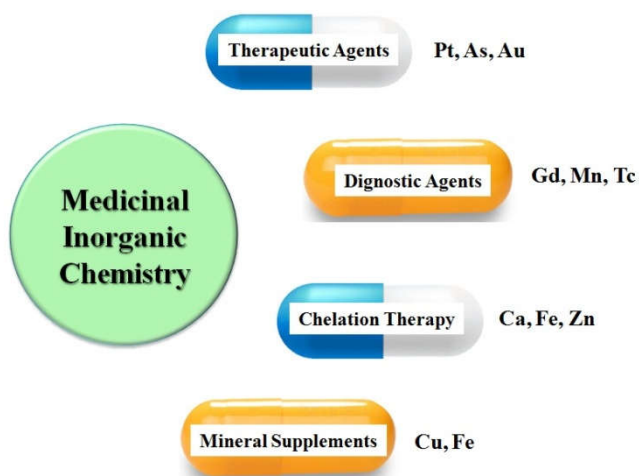
Fig. 1.14 Metals involved in medicinal inorganic chemistry

Table 1.6 List of metal and their therapeutic applications

Metal	Applications
Chromium	Dietary (trace mineral) supplement
Manganese	MRI contrast agent
Iron	MRI contrast agent, dietary supplement
Cobalt	Treatment and diagnosis of pernicious anemia, dietary supplement
Nickel	Dietary (trace mineral) supplement
Copper	Treatment for Menke's disease, Cu PET – radioimaging, intrauterine contraception
Zinc	Treatment of eczema, dietary supplement

Manganese and iron complexes acting as medicine

Chelation therapy in medicine is generally considered as using chelating agents to remove toxic heavy metals from the body (Fig. 1.15). In body tissue, these chelates bind

with the toxic metal and form a complex which is released in the blood. In kidney these chelate filtered out and then excreted through the urine.
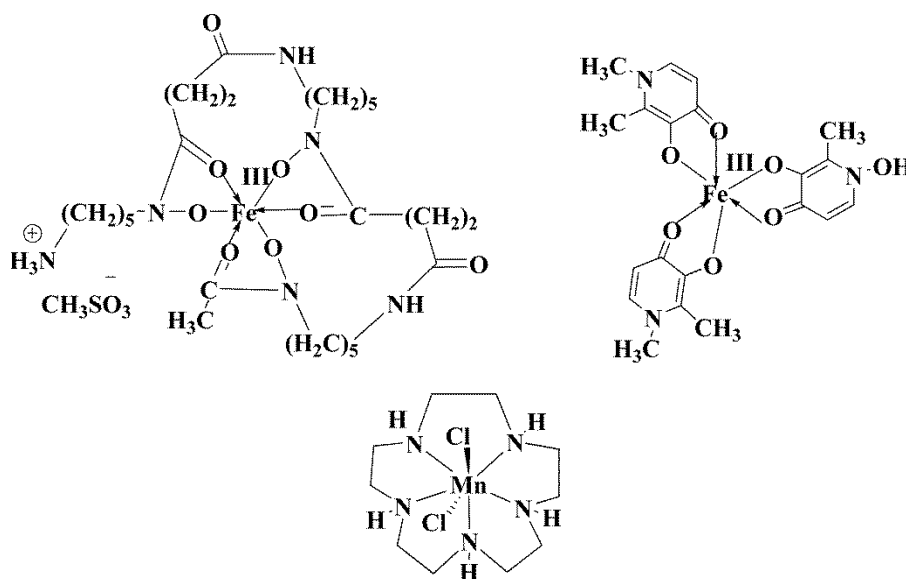
Fig. 1.15 Examples of some of the metal chelating system

Manganese and iron complexes have been utilized for various medicinal applications.[275] Manganese complexes are also gaining importance in medicine. In this regard, Mascharak and co−workers used manganese complexes for delivery of carbon mono-oxide into the tissues, which is used as a signaling molecule in mammalian physiology.[276,277] Mandal and co−workers monitored antitumour activities of manganese (III) salen complexes.[275,278]

Sodium nitroprusside, $Na_2[Fe(CN)_5NO]$ widely used to induce hypotension during surgery.[279,280] Mascharak and co−workers have synthesized iron nitrosyl complexes which release NO on illumination of light and could be utilized in photodynamic therapy.[281–283] Mandal and co−workers explained iron salophen complexes in

leukemia.[270,278,284] Due to the paramagnetic nature of manganese(II) and iron(III) metal complexes have been utilized for MRI studies.[285–303]

1.7.4. *In silico* studies

Theoretical studies of transition metal complexes and reactions performed by these complexes are gaining importance these days.[304–307] These studies help to understand various parameters such as geometries, bonding nature and reaction behavior. Density functional theory (DFT) calculations basically give information about bond distance, bond angle and nature of HOMO−LUMO orbital in metal complexes whether ligand centered or metal centered. Time dependent (TD) DFT calculations give knowledge of spectroscopic properties, energy level, transition probability and also gives rise to the theoretical spectra.

In silico studies using manganese and iron complexes

Manganese complexes have been utilized for several catalytic applications experimentally. Hence these complexes have been an important tool for the theoretical chemist to better understand a particular system. In this regard, lot of work have been performed using theoretical calculations. Romain and co−workers have synthesized mononuclear manganese complex utilizing tolylterpy = 4'(4methylphenyl)2,2':6',2"terpyridine) ligand manganese metal ion was in the unusual III oxidation state stabilzed exclusively by neutral nitrogen donor ligands. This complex was further subjected to theoretical studies to explain geometry and magnetic properties.[308] Ruiz *et. al.* studied the magnetic properties of a new family of single−molecule magnet having nickel and manganese complexes using theoretical methods based on density functional theory (DFT).[309] Wieghardt *et. al.* utilized

complexes $[M(bpy)_3]^n$ and $[M(tpy)_2]^m$ (M=Mn, Tc, Re; n=2+, 1+, 0, 1 −; m = 2+, 1+, 0) for the electronic, magnetic and X−ray structural studies. Molecular and electronic structures further supported by broken symmetry (BS) density functional theoretical calculations.[310] In continuation of the theoretical calculation studies Zheng and co−workers utilized manganese nitrosyl complexes synthesized by Merkle and co−workers.[311] These complexes release NO on exposure to light and may serve a potent NO delivery agent in photodynamic therapy (PDT). Zheng and co−workers performed systematic theoretical study on the mechanism of dissociation of NO from manganese nitrosyls and studies supported the use of complexes in PDT.[312] Manganese complexes were also utilized for better insight into the chemistry involved during various spectroscopic properties.[313–316]

Iron complexes have been attracted the interest of theoretical chemist and great work has been done in this concern. Nam *et. al.* compared the reactivity of manganese(IV) and iron(IV) oxo complexes containing pentadentate N4Py ligand in chemical oxidation reaction. Hydrogen atom transfer (HAT) and oxygen atom transfer (OAT) reactions were compared and iron (IV) oxo complexes were found to be more effective.[317] To and coworkers utilized $[Fe^{III}(L1)Cl_2]^+$ complexes synthesized by macrocyclic ligand L1=N,N'dimethyl2,11diaza[3,3](2,6)pyridinophane for water oxidation reactions and DFT calculations supported the generation of an Fe(V)=O species responsible for formation of O–O bond in water oxidation.[318] Several other iron complexes were used to study reactions theoretically to support the experimental facts.[319–325]

1.8. Sensing of iron metal ion

Design and synthesis of fluorescent probes selective and sensitive for monitoring heavy and transition metal ions is a demanding and promising area of research due to the prominent impact of metal ions in environment and biology.[326–329] A remarkable development of small fluorescent molecule with selectivity towards metal ions has been dragged attention of researchers.[237,330] These studies are found to be helpful to understand transport and localization as well as physiological and pathological effect of metal ions in the cell.[331] Due to high sensitivity, rapid response and simplicity, fluorescence has attracted much attention for the detection of several chemical analytes in solution.[332] Iron is an important transition metal found in biology exhibiting crucial roles in several catalytic and enzymatic reaction and its imbalance can cause harmful effects hemochromatosis, cancer etc.[3,333,334] Hence detection of iron and its concentration as well as localizations are extremely important for the treatment of such diseases. Most common oxidation states of iron are Fe(II) and Fe(III) which are important for ordinary and related chemistry.[1] Naked eye detection for metal ions is important for qualitative identification as well as quantitative detection. Hence simple and easy to use colorimetric probes are highly demanding for metal ion sensing.[335] Different colorimetric as well as fluorimetric probes have been reported for iron sensing.[336–344] Probes which could work in aqueous media and at physiological pH are also highly demanding for living cell applications.[345–347]

1.9. Outline of present investigation

In present studies, we have designed bidentate and tridentate ligands having meridional geometry. All the ligands were characterized by IR, UV−visible, GS−MS and

NMR spectral studies and data obtained supported the synthesis of desired ligands. These tridentate ligands ^{OCH3}PhimpH, ^{CH3}PhimpH, ^{NO2}PhimpH, ^{tBu}PhimpH, H−N$_3$L and Me−N$_3$L were utilized to synthesize mononuclear manganese and iron complexes respectively. On the other hand, ligands NED1 and NED2 were utilized for the sensing of metal ions in solution. Ligands used in present investigation have been depicted in Fig. 1.16. All the complexes of manganese and iron were also characterized using various spectroscopic techniques such as IR, UV−visible, conductivity measurements and ESI−MS spectral studies. Magnetic moment studies were also performed for all the complexes. The representative complexes were subjected to X−ray crystallography to justify the molecular structure. Redox behavior of all the complexes were investigated using electrochemical studies. Iron complexes [Fe(^{OCH3}Phimp)$_2$](ClO$_4$) (**1**), [Fe(^{CH3}Phimp)$_2$](ClO$_4$) (**2**), [Fe(^{tBu}Phimp)$_2$](ClO$_4$) (**3**) and [Fe(^{NO2}Phimp)$_2$](ClO$_4$) (**4**) were used for the oxidation of *o*−aminophenol oxidation and kinetic studies were also performed using these complexes. Due to the presence of ligand having redox active nature [Fe(^{tBu}Phimp)$_2$](ClO$_4$) complex was used to study the nuclease as well as protease activity. Similarly manganese complexes [Mn(^{OCH3}Phimp)$_2$]ClO$_4$ (**5**), [Mn(^{CH3}Phimp)$_2$]ClO$_4$ (**6**) and [Mn(^{tBu}Phimp)$_2$]ClO$_4$ (**7**) derived from N$_2$O donor were used to study the phenoxyl radical generation using absorption spectral studies. Complex [Mn(^{tBu}Phimp)$_2$]ClO$_4$ (**7**) was also utilized for nuclease and protease activity. Manganese complexes Mn(H−N$_3$L)Cl$_2$ (**8**), [Mn(H−N$_3$L)$_2$](ClO$_4$)$_2$ (**9**), Mn(Me−N$_3$L)Cl$_2$ (**10**) and [Mn(Me−N$_3$L)$_2$](ClO$_4$)$_2$ (**11**) derived from tridentate ligand having N$_3$ donor were employed for DNA binding studies. Complex Mn(Me−N$_3$L)Cl$_2$ also exhibited nuclease as well as protease activity in presence of oxidizing agent. Iron complexes Fe(H−N$_3$L)Cl$_3$

(**12**), [Fe(H−N$_3$L)$_2$](ClO$_4$)$_2$ (**13**), Fe(Me−N$_3$L)Cl$_3$ (**14**) and [Fe(Me−N$_3$L)$_2$](ClO$_4$)$_2$ (**15**) of

ligands having 3N donors were synthesized and subjected to DNA binding studies.

Complex Fe(H−N$_3$L)Cl$_3$ (**12**) exhibited nuclease activity in presence of oxidizing agent.

Ligand NED1 was used to study the sensing of mercury and iron metal ion in mixed

aqueous media and application of these results were studied in the field of logic gates and

living cells. Ligand NED2 was synthesized and used to sense iron in presence of other

served metal ions in methanol solutions. Results obtained during the studies were used in

the field of logic gate applications.

1.9.1. Ligands and their descriptions

Tridentate ligands with different coordinating donor atoms have been synthesized

in present studies and have been represented in the Fig. 1.16. These ligands were

coordinated to the metal centre in a meridional fashion.
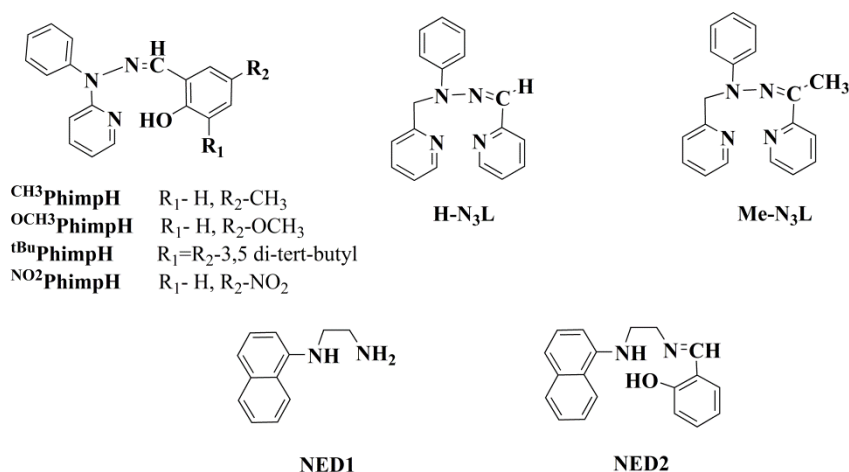
Fig. 1.16 Ligands with abbreviations utilized for the present work

1.9.2. Description of starting materials

Manganese and iron complexes were prepared using the above mentioned ligands. On the basis of HSAB principle suitable metal salts were selected to prepare iron and manganese complexes. In case of manganese complexes $MnCl_2 \cdot 4H_2O$, $Mn(ClO_4)_2 \cdot 6H_2O$, $Mn(CH_3COO)_3 \cdot 2H_2O$ were used as starting materials, on the other hand $NEt_4[FeCl_4]$, $Fe(ClO_4)_2 \cdot xH_2O$, anhydrous $FeCl_3$ and $Fe(ClO_4)_3 \cdot xH_2O$ were utilized to prepare iron complexes. Synthesized complexes were then subjected to the various characterization techniques to ensure the synthesis of the desired complexes.

1.9.3. Description of activity studies

1.9.3.1. *o*–aminophenol oxidation and kinetics

Oxidation of *o*–aminophenol (OAP) in presence of catalytic amount of iron complexes were performed under aerobic atmosphere in methanol at ambient temperature. The change in absorbance at 430 nm ($\varepsilon=24 \times 10^3 \, M^{-1} cm^{-1}$) a characteristic of 2–aminophenoxazin–3–one formed, was optimized as a function of time to follow the reaction kinetics.

1.9.3.2. Mimicking of galactose oxidase: Generation of phenoxyl radical complexes

To mimic galactose oxidase and glyoxal oxidase enzymes, phenoxyl radical was generated using phenolato containing metal complexes. Phenoxyl radical species were generated *in situ* by adding adequate amount of $[(NH_4)_2[Ce^{IV}(NO_3)_6]$ (CAN) into CH_3CN solutions at low temperature. *In situ* generation of phenoxyl radical was confirmed by color change along with the characteristic peaks in UV–visible spectra.

1.9.3.3. Superoxide dismutase activity

SOD activity was first explained by Fridovich and McCord using cytochrome c assay.[16,45] Xanthine/xanthine oxidase system was used to produce superoxide ions.[348] In this assay reduction of nitro blue tetrazolium (NBT) by superoxide was monitored spectrophotometrically. In this study, xanthine/xanthine oxidase was used to generate superoxide radicals and indicator NBT was added. NBT produced a blue formazan dye after reduction with superoxide ions which shows characteristics absorbance at λ_{max} 560 nm. IC_{50} values were calculated. IC_{50} value for SOD activity can be summarized as the concentration of a particular tested compound for 50% inhibition of NBT reduction by superoxide ions. The mode of action is shown in Scheme 1.14.
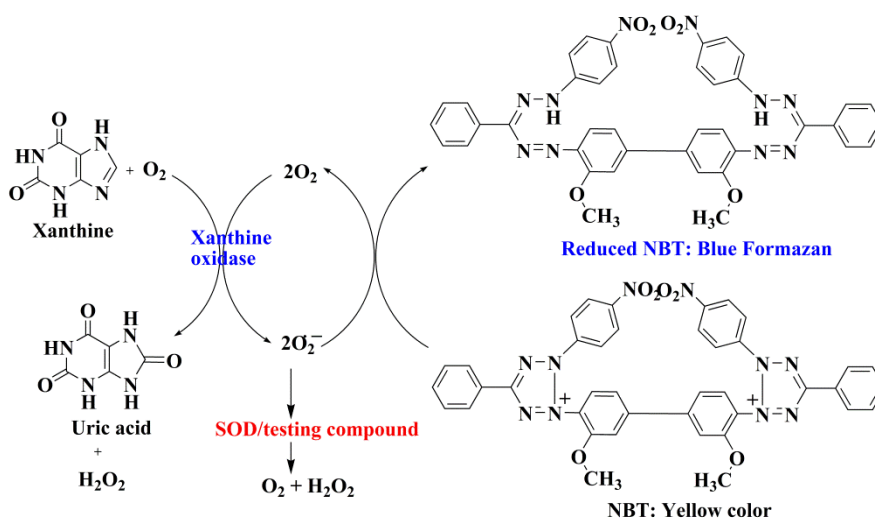
Scheme 1.14 Schematic representation of SOD activity determination by NBT assay

1.9.3.4. DNA interaction studies

DNA binding studies monitored using absorbance, fluorescence quenching and circular dichroism spectral studies. All the binding experiments performed in 0.1 M phosphate buffer (pH = 7.2). Initially stability of complexes monitored in the phosphate

buffer (pH = 7.2) for a specified time. DNA binding experiments were performed in 0.1 M phosphate buffer (pH 7.2) using a solution of calf thymus (CT) DNA. UV–visible absorbance studies at 260 and 280 nm (A_{260}/A_{280}) indicating a ratio of 1.8 shows that CT–DNA is sufficiently protein free.[349] Concentration of DNA solution was monitored at 260 nm using absorbance and the extinction coefficient ε_{260} was taken 6600 cm^{-1}.[350]

Absorbance titration experiments were carried out using a fixed amount of complex concentration and varying the CTDNA concentration in 0.1 M phosphate buffer (pH 7.2). Extent of binding was observed by calculating the binding constant K_b using a plot of [DNA]/($\varepsilon_a - \varepsilon_f$) *vs.* [DNA] using equation given below:

$$[DNA]/(\varepsilon_a - \varepsilon_f) = [DNA]/(\varepsilon_b - \varepsilon_f) + [K_b(\varepsilon_a - \varepsilon_b)]^{-1}$$

where [DNA] is the concentration of DNA in base pairs. The apparent absorption coefficients ε_a, ε_f and ε_b correspond to A_{obs}/[Complex], extinction coefficient of the free complex and extinction coefficient of complexes in the fully bound form respectively. The mode of binding of metal complexes with CT–DNA determined by value of the binding constant (K_b) and change observed in absorption spectra. The order of binding constant K_b of metal complexes is groove or surface binder < intercalator < metalloinsertor.[174]

Fluorescence spectral studies were also performed to confirm the predicted mode and extent of binding using ethidium bromide (EB) displacement assay. EB is not fluorescent in free form and emits intense fluorescence in presence of DNA due to its strong intercalation between the DNA base pairs. This enhanced fluorescence can be quenched by the addition of the complexes which has a tendency to interact with the EB–DNA. This will cause a reduction in the emission intensity indicating the competitive

binding with EB and metal complexes. Fluorescence quenching experiments were carried out by the successive addition of complexes to the fixed amount of DNA containing 5 µM EB in 0.1 M phosphate buffer (pH 7.2). Wavelength of excitation used during experiment was 250 nm and emissions were observed in the range of 500–700 nm. Stern–Volmer quenching constants[351] were calculated using the given equation.

$$I_0/I = 1 + K_{sv}Q$$

Where I_0 and I are the fluorescence intensities in the absence and presence of complex and Q is the concentration of quencher (metal complex). K_{sv} is a linear Stern–Volmer constant and given as the ratio of slope to intercept in the plot of I_0/I versus Q. Binding mode of complexes determine by the order of Stern–Volmer constant (K_{sv}), groove or surface binder < intercalator < metalloinsertor.

Circular dichroism (CD) spectroscopic technique is useful in monitoring the conformational change observed in DNA during interaction studies in solution. The CD spectrum of CT–DNA exhibits one positive band at 278 nm due to base stacking and one negative band at 246 nm due to helicity and recorded in the range of 225–300 nm. CD spectra of CT–DNA in absence and presence of the metal complexes were monitored with 0.1 cm pathlength cuvette after incubation of 10 min at 25 °C. The concentration of the complexes and CT–DNA were 50 and 200 µM respectively. The mode of interaction was explained by the change and shifting in molar ellipticity of positive and negative bands. Conformation of DNA remains same if there is no shift in wavelength of positive and negative bands.[352]

1.9.3.5. Nuclease activity

The cleavage of plasmid DNA was examined by the change of supercoiled (SC) DNA to nicked circular (NC) and linear circular (LC) form having different size. Linear form of DNA is produced when both strands of the DNA are cleaved opposite to each other and a single cut in DNA leads to the formation of NC form. Migration of these three forms differs as a function of the applied voltage, buffer concentration, agarose concentration and the amount of super helical twists in DNA. The order of migration is supercoiled >> linear > nicked, in most of the plasmids. After completion of electrophoresis, gel is stained with ethidium bromide and visualized through Gel–Doc instrument. The intensities of the individual bands were compared to determine the relative amounts of supercoiled, nicked and linear form.

Cleavage of plasmid DNA was performed using agarose gel electrophoresis in trisboric acid EDTA (TBE) buffer. Supercoiled *pBR322* DNA was incubated with complexes in 0.1 M phosphate buffer (pH = 7.2) for few hours at 37 °C. The oxidative DNA cleavage by the complexes were studied in presence of H_2O_2 (50–400 μM, oxidizing agent). After incubation loading buffer is added (25% bromophenol blue and 30% glycerol). The agarose gel (0.8%) containing 0.4 μg/mL of ethidium bromide was prepared and electrophoresis of DNA cleavage products were performed. Gel was run at 60 V for 2 h in tris–boric acid–EDTA (TBE) buffer and bands were identified by placing the stained gel under an illuminated UV lamp. Fragments were photographed by using Gel–doc system.

1.9.3.6. Protein cleavage activity

Protein cleavage experiments were carried out by incubating BSA with test compounds varying in the range of concentrations 10−100 μM in 10% DMF using 0.1 M phosphate buffer (pH = 7.2). Samples were incubated at 50 °C for 20 h. After incubation, an aliquot was mixed with loading buffer (100 mM Tris−HCl (pH 6.8), 4% (w/v) sodium dodecyl sulphate (SDS), 20% (v/v) glycerol and 0.2% (w/v) bromophenol blue) and protein solutions were then denatured by heating (85 °C) for 3 min. Incubated protein samples were then subjected to a discontinuous SDS−PAGE (having 2% acrylamide for the stacking gel and 10% acrylamide for the separation gel) in a Genei vertical gel electrophoresis apparatus. The electrophoresis was performed at 70 V for stacking gel and 100 V for separation gel. Coomassie Brilliant Blue R−250 solution was used for staining the gels which were subsequently destained with a water/methanol/acetic acid (1:5:4) mixture for 3 h. The gels, after destaining, were scanned with gel−documentation system and images were reproduced without further processing.

1.10. Survey of contents in the present thesis

Aim of the present thesis work was to design the molecules of the interest, validation of the synthesis using analytical and spectroscopic techniques. Finally, performances of the synthesized ligands and/or complexes were monitored in different fields such as catalysis, DNA and protein interactions and metal ion sensing.

In **chapter 2,** tridentate ligands ^{OCH3}PhimpH, ^{CH3}PhimpH, ^{tBu}PhimpH and ^{NO2}PhimpH have been synthesized and characterized. Designed tridentate ligands having N$_2$O donors upon deprotonation bind to iron(III) resulting in a series of novel iron complexes. All the complexes were characterized by elemental analysis, IR and UV−

visible spectral studies. Spectroscopic data, magnetic moments and conductivity measurement clearly expressed the formation of $[Fe(^{OCH3}Phimp)_2](ClO_4)$ (**1**), $[Fe(^{CH3}Phimp)_2](ClO_4)$ (**2**), $[Fe(^{tBu}Phimp)_2](ClO_4)$ (**3**) and $[Fe(^{NO2}Phimp)_2](ClO_4)$ (**4**) complexes. Molecular structure of complex **1** was determined by single crystal X–ray diffraction study. A distorted octahedral geometry was observed having FeN_4O_2 coordination sphere. Molecular structure studies interpret tridentate meridional coordination of ligand around iron(III) metal centre. Electrochemical studies were also investigated for synthesized complexes. Theoretical calculations (DFT) were also performed to optimize the geometrical and structural parameters. TD–DFT calculations were optimized to observe the electronic properties and data obtained was found to be consistent with experimentally obtained values. Complexes **1**, **2**, **3** and **4** were utilized to optimize oxidation of *o*–aminophenol in methanol. Complexes were found to be efficient in the oxidation of *o*–aminophenol. Kinetic experiments were also explored to gain better insight into the oxidation process. Representative complex exhibited nuclease as well as protease activities in absence of external agents. DPPH assay was used to estimate the antioxidant activity. Complex **3** cleaved DNA and protein *via* self–activated mechanism.

In **Chapter 3** a series of manganese(III) complexes derived from tridentate ligands $^{OCH3}PhimpH$, $^{CH3}PhimpH$, $^{tBu}PhimpH$ and $^{NO2}PhimpH$ have been synthesized. All the complexes were characterized by elemental analysis, IR and UV–visible spectral studies. Magnetic moments and conductivity measurements suggested the formulation of $[Mn(^{OCH3}Phimp)_2]ClO_4$ (**5**), $[Mn(^{CH3}Phimp)_2]ClO_4$ (**6**) and $[Mn(^{tBu}Phimp)_2]ClO_4$ (**7**) manganese complexes respectively. Molecular structure of **7** was determined by X–ray crystallography and structural features were also explored. Cyclic voltammetric studies

were investigated for all the complexes in the series. DFT calculations were monitored for representative metal complex to optimize geometrical and structural parameters. TD–DFT studies explained the electronic properties and are in good agreement with experimental data. Phenoxyl radical complexes were generated at room temperature in CH_3CN solutions by adding $[(NH_4)_2[Ce^{IV}(NO_3)_6]$ (CAN) and were characterized by UV–visible spectral studies. Phenoxyl radical complex generated at room temperature exhibited nuclease as well as protease activity with *pBR322* DNA without any external agent.

In **Chapter 4** ligands H–N_3L (1–phenyl–1–(pyridine–2–ylmethyl)–2–(pyridine–2–ylmethylene)hydrazine) and Me–N_3L (1–phenyl–2–(1–(pyridin–2–yl)ethylidene)–1–(pyridin–2–ylmethyl)hydrazine) have been designed and synthesized. These ligands have been characterized using various spectroscopic techniques such as UV–visible, IR, GC–MS and NMR spectral studies. Synthesized ligands have been utilized to prepare mononuclear complexes of manganese. A series of manganese complexes Mn(H–N_3L)Cl$_2$ (**8**), [Mn(H–N_3L)$_2$](ClO$_4$)$_2$ (**9**), Mn(Me–N_3L)Cl$_2$ (**10**) and [Mn(Me–N_3L)$_2$](ClO$_4$)$_2$ (**11**) were synthesized and characterized by spectroscopic techniques. Molecular structure of complex **10.CH$_3$COCH$_3$** was determined by single crystal X–ray diffraction technique. Molecular structures interpret square pyramidal geometry and tridentate meridional coordination of ligand around manganese. Redox properties were monitored for the synthesized metal complexes. Theoretical calculations were performed using complex **10** and geometrical and structural parameters were investigated. TD–DFT calculations justify the electronic properties obtained from the experimentally obtained values. Complexes **8**, **9**, **10** and **11** were employed to catalyze

the dismutation of superoxide using xanthine–xanthine oxidase–nitroblue tetrazolium (NBT) assay and obtained good IC_{50} values. DNA interaction studies were also monitored using all complexes. Complexes bind well with the DNA *via* partially intercalative pathway. Nuclease as well as protease activity performed in presence of oxidizing agent for the representative complex.

Chapter 5 includes tridentate ligands H–N_3L (1–phenyl–1–(pyridine–2–ylmethyl)–2–(pyridine–2–ylmethylene)hydrazine) and Me–N_3L (1–phenyl–2–(1–(pyridin–2–yl)ethylidene)–1–(pyridin–2–ylmethyl)hydrazine). Synthesized ligands have been utilized to synthesize mononuclear iron complexes. Complexes Fe(H–N_3L)Cl_3 (**12**), [Fe(H–N_3L)$_2$]$(ClO_4)_2$ (**13**), Fe(Me–N_3L)Cl_3 (**14**), and [Fe(Me–N_3L)$_2$]$(ClO_4)_2$ (**15**) have been synthesized and characterized using elemental analysis, IR, UV–visible and ESI–MS spectral studies. Magnetic moments and conductivity measurements supported the formulated structures of the complexes. NMR spectral studies were also performed for complexes **13** and **15** due to the presence of low–spin iron(II) metal centre. Structural and geometrical aspects were monitored using DFT calculations. TD–DFT calculations were performed to optimize the electronic properties and found to be in good agreement with the experimental data. Electrochemical studies were also investigated for all the complexes in series. Due to the stability in buffer these complexes were subjected to the DNA interaction studies. DNA binding studies were monitored using absorption, fluorescence and CD spectral studies. These studies indicated that all the complexes bind well with the DNA. Nuclease activity was monitored for the representative complexes and exhibited oxidative nuclease in presence of oxidizing agent (H_2O_2).

Chapter 6 explores the use of naphthylamine–based probe NED1 (N–(2–aminoethyl)naphthalen–1–amine) was utilized for the detection of Hg(II), Fe(II), Fe(III) in mixed–aqueous media *via* fluorescence quenching. These sensitive metal ions bind with the probe by forming a 1:1 complex. Time–resolved fluorescence and quantum yield of probe NED1 in absence as well as in presence of metal ions were investigated. Extents of binding of probe with sensitive metal ions were calculated. Sensitivity of the probe in presence of other metal ions was examined using competitive binding studies. Probe NED1 displayed sensitivity towards Hg(II) during *in vitro* as well as *in vivo* studies. This multianalyte probe demands biological applications in cell imaging and in logic gates.

Chapter 7 comprises synthesis of a novel fluorescent probe NED2 (2–((2–(naphthalen–1–ylamino)ethylimino)methyl)phenol) and NED2 was characterized by various spectroscopic methods. Photo– physical properties of NED2 have been investigated to study the sensing of metal ions in methanolic solution. Probe NED2 was found to be highly selective for iron over tested metal ions. Probe NED2 selectively detected iron in both II and III oxidation states giving rise to yellow–brown and purple color respectively. Naked eye detection of iron is useful for the discrimination of II and III oxidation state while fluorescence studies conclude selective and specific sensitivity towards Fe(III). Probe was found to be highly sensitive and selective towards Fe(III) during fluorimetric detection. Binding stoichiometry was found to be 1:1 for Fe(III) and probe NED2. DFT calculations provided that decrease in the energy gap between HOMO and LUMO is probably responsible for quenching of fluorescence. Logic gates application of the probe NED2 was also explored.

1.11. Measurements

1.11.1. Elemental analysis

C, H and N content analyses of the sample were determined using Elemenlar Vario EL III elemental analyser which utilizes thermal conductivity data for gas (CO_2, H_2O, N_2) analysis.

1.11.2. Infrared spectroscopy

IR spectra were acquired with KBr pellets with Thermo Nikolet Nexus FTIR spectrometer, using 16 scans and were reported in cm^{-1}.

1.11.3. Mass spectrometry

GC–MS was performed using PerkinElmer CLARUS 500 GC–Mass spectrometer; ESI–MS spectrometry was performed with micROTOFQ II 10328.

1.11.4. NMR spectroscopy

^{1}H and ^{13}C–NMR were recorded on Bruker AVANCE, 500 MHz and Jeol Delta 400 MHz spectrometer, chemical shift for ^{1}H–NMR spectra are related to internal standard Me_4Si for all residual protium in the deutrated solvents.

1.11.5. Conductometer

Molar conductivities were calculated in DMF at 10^3 M at 25 °C with a Systronics 304 conductometer.

1.11.6. Magnetic moment

Magnetic susceptibilities measurements were performed at room temperature with Cryogenic Limited Vibrating Sample Magnetometer model 155, using nickel as a standard.

1.11.7. UV−visible spectrophotometer

Electronic absorption spectra were recorded in different solvents such as dichloromethane, methanol, water, dimethylformamide (DMF) or dimethylsulfoxide (DMSO) solvents using an Evolution 600, Thermo Scientific UV−visible spectrophotometer in the range of 200−800 nm. A similar pair of quartz cell of path length 1 cm was used for the studies.

1.11.8. Fluorescence spectrophotometer

Emission quenching titrations were monitored on Varian fluorescence spectrophotometer. Solution preparations are same as that of electronic spectra.

1.11.9. Lifetime measurements

Time−resolved fluorescence lifetime measurements in nanoseconds were recorded in 1 cm quartz cell on a Horiba Jobin Yvon "FluoroCube Fluorescence Lifetime System".

1.11.10. Cyclic voltammetry

Electrochemical analyses were carried out using a CHI600C electroanalyzer in solvents such as DMF, dichloromethane and acetonitrile. All experiments were performed at ambient temperature and solutions were thoroughly degassed with nitrogen prior to beginning as well as during measurement, nitrogen atmosphere were maintained. A conventional three electrode arrangement consisting of platinum wire as auxiliary electrode, glassy carbon as working electrode and Ag(s)/AgCl electrode as reference electrode was used. These measurements were performed in presence of 0.1 M tetrabutylammonium perchlorate (TBAP) as the supporting electrolyte, using complexes concentration 10^{-3} M. $E_{1/2}$ value for ferrocene/ferrocenium couple *vs* Ag/AgCl was found under the similar experimental conditions.

1.11.11. X−ray structure determinations

The X−ray data collection and processing for complexes were performed on Bruker Kappa Apex−II CCD diffractometer using graphite monochromated Mo−Kα radiation (λ = 0.71070 Å). Crystal structures were solved using direct methods. Structure solution, refinement and data output were carried out with the SHELXTL program.[177,178] All non hydrogen atoms were refined anisotropically. Hydrogen atoms were placed in geometrically calculated positions and refined using a riding model. Images were created with the help of DIAMOND.[177]

R_1, wR_2 and goodness of fit (GOF) are given by following equations respectively,

$$R_1 = \Sigma \left|\left| F_o \right| - \left| F_c \right|\right| / \Sigma F_o \left| \right. \qquad \text{eq. 1}$$

$$wR_2 = [\Sigma[w(Fo^2 - Fc^2)^2]/\Sigma[w(F_o^2)^2]]^{1/2} \qquad \text{eq. 2}$$

$$^a GOF = [\Sigma[w(F_o^2 - F_c^2)^2]/M - N)]^{1/2} \qquad \text{eq. 3}$$

Where, M = number of reflections, N = number of parameters refined

Specific details for each compound will be given in the concern chapter.

1.11.12. Circular dichroism

Circular dichroism spectra of DNA were attained using a Chirascan circular dichroism spectrometer operating at 25 °C. The region between 220 and 320 nm was examined in 1 mm path length cuvette with 10 min incubation time for each sample in different solvents such as dimethylformamide.

1.11.13. Gel documentation

Sub−Cell GT agarose gel electrophoresis systems (BIO−RAD) was used for nuclease study. DNA fragments were monitored by keeping the gel under an illuminated

UV lamp and photographed with gel documentation system (BIO RAD). Protein gel electrophoresis was done by Mini–protean electrophoresis system BIO–RAD.

1.11.14. Chemicals and solvents

All the chemicals and solvents used were of analytical grade and most of these were used as obtained. The purification steps where required were performed by using standard methods.[353]

Chapter-2

Synthesis and Reactivity Studies on New Iron(III) Complexes Derived from N_2O Donor: o–Aminophenol Oxidation, Nuclease and Protease Activity

2.1. Abstract

Tridentate ligands ^{OCH3}PhimpH, ^{CH3}PhimpH, ^{tBu}PhimpH and ^{NO2}PhimpH have been synthesized and characterized. Designed ligands having N_2O donors on deprotonation coordinate to iron(III) resulting in a series of novel iron complexes. All the complexes were characterized by elemental analysis, IR and UV–visible spectral studies. Magnetic moments and conductivity measurements suggest the formulation of [Fe(^{OCH3}Phimp)$_2$](ClO$_4$) (**1**), [Fe(^{CH3}Phimp)$_2$](ClO$_4$) (**2**), [Fe(^{tBu}Phimp)$_2$](ClO$_4$) (**3**) and [Fe(^{NO2}Phimp)$_2$](ClO$_4$) (**4**) complexes respectively. Molecular structure of complex **1** was determined by single crystal X–ray diffraction study. Electrochemical studies were also performed in non–aqueous solutions. Theoretical calculations (DFT and TD–DFT) were performed to optimize the geometrical and structural parameters. Complexes **1**, **2**, **3** and **4** utilized to optimize oxidation of *o*–aminophenol in methanol. Kinetic experiments were also explored to gain better insight into the oxidation process. Representative complex **1** exhibited nuclease as well as protease activities in absence of external agent.

2.2. Introduction

Synthetic nucleases derived from metal complexes are of interest due to their applications in nucleic acid research. These complexes have been utilized as foot−printing agents, site specific cleaving agents or in medicine.[354] In this regard, cis−platin and iron−bleomycins are widely used metal based anticancer drugs.[214,223,355−358] For last few decades, platinum based drugs have been widely used for antitumor activity. Anti−cancer platinum based drugs also includes carboplatin, nedaplatin and oxaliplatin.[359] Although due to high toxicity and side effects, their applications are limited.[360,361] Metal complexes have dragged attention due to the similar mode of action as performed by natural nuclease.[362] Hence synthesis of artificial nuclease has been emerges as a challenging and demanding area. DNA cleavage using metal complexes could follow oxidative,[363] hydrolytic,[364] and/or photolytic pathways.[365,366] Depending on the mode of cleavage, these pathways require an external agent such as light, oxidizing or reducing agents. Oxidative pathway is preferred over photolytic and hydrolytic pathway due to the limitation such as effectiveness of the light penetration and the dark toxicity in photo−activated DNA cleavage and low cleaving efficiency in metal hydrolases.[367,368] Hence most of the studies on artificial chemical nuclease are those which shows oxidative cleavage.[369] Although oxidative cleavage requires external agent to cleave the DNA which limits its application in living cells. Hence a great interest has been developed to prepare complexes which are capable to cleave DNA without any external agent.[370]There are few reports on metal complexes acting as self−activated nuclease.[268,371−380] In continuation of interaction of metal complexes with the biomolecules it has been found out that metal have been playing crucial role in several biological catalyst.[19] Carboxypeptidase A is an enzyme having zinc metal in the active site imparts crucial role in the protease activity. Hence biology suggests the role of small metal complexes could be valuable for cleaving the highly stable peptide bond. In this regard

redox active ligand played crucial role to the protease activity.[381] Transition metal complexes have also been utilized for the structural and functional modelling of metalloenzymes. Role of radical in metalloenzymes is an interesting area of research.[170] Metalloenzymes such as galactose oxidase[182,382,383] and ribonucleotide reductase[384] containing phenoxyl radical have gained much attention in the recent past. It was observed that radical species performed key roles during the catalytic cycle and developed a new area of free–radical enzymology. Oxygen activation using transition metal complexes have been studied and involve mimicking of several metalloenzymes.[385–387]

Enzyme phenoxazinone synthase naturally present in the bacterium *Streptomyces antibioticus*.[157] Phenoxazinone synthase[158,388] is a type II copper containing oxidase enzyme which catalyzes oxidative coupling of substituted *o*–aminophenol to the phenoxazinone chromophore in the last step of biosynthesis of the acinomycin D (Scheme 1.5, chapter 1). Actinomycin D, a naturally found antineoplastic agent, is used to cure certain cancer.[389–391] Several complexes containing metal such as cobalt,[392–394] copper,[395] manganese[160–162] and iron[166] have been utilized to mimic this enzyme. In this work we have utilized iron complexes as a functional model of phenoxazinone synthase which involve oxygen activation. To the best of our knowledge so far, these are the only iron complexes exhibiting artificial self–activating oxidative nuclease, protease and *o*–aminophenol oxidase.

CH3PhimpH   R₁- H, R₂-CH₃
OCH3PhimpH   R₁- H, R₂-OCH₃
tBuPhimpH   R₁=R₂-3,5 di-tert-butyl
NO2PhimpH   R₁- H, R₂-NO₂
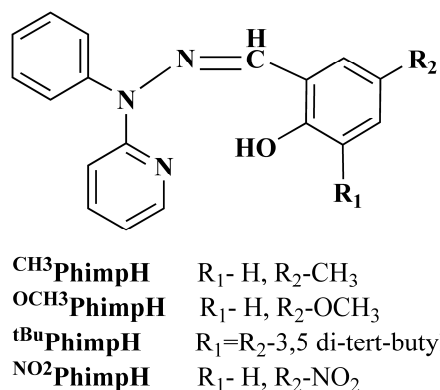
Fig. 2.1 Tridentate ligands with abbreviations used in the present work

Herein, we have synthesized[396] meridional tridentate ligands (Fig. 2.1) having one phenolato donor along with pyridine and imine moeities. These ligands have been utilized to prepare mononuclear bis complexes of iron(III) [Fe(OCH3Phimp)₂](ClO₄), (**1**), [Fe(CH3Phimp)₂](ClO₄), (**2**), [Fe(tBuPhimp)₂](ClO₄), (**3**) and [Fe(NO2Phimp)₂](ClO₄), (**4**) which have been described in the present chapter. X–ray crystallography has been utilized to determine the molecular structure of representative complex **1**. Electrochemical studies were also performed to investigate the redox behavior of ligands as well as complexes. This work presents a new approach to designing of iron complexes which are capable of self–activating nuclease as well as protease activity along with o–aminophenol oxidation.

2.3. Results and discussion

2.3.1. Synthesis and characterization of ligands

Ligands were synthesized by condensation of equivalent molar ratio of 2–(1–phenylhydrazinyl)pyridine (1.00 mmol)[170,397] with corresponding aldehydes (1.00 mmol) in methanol. The reaction mixture was stirred at room temperature for 4 h. A yellow precipitate was filtered, washed with small amount of methanol and then dried in vacuo. tBuPhimpH was synthesized by published procedure and characterization data established the proper synthesis

of ligand.[398] Scheme 2.1 provides an overview on synthetic route for the preparations of the ligands used in present studies.
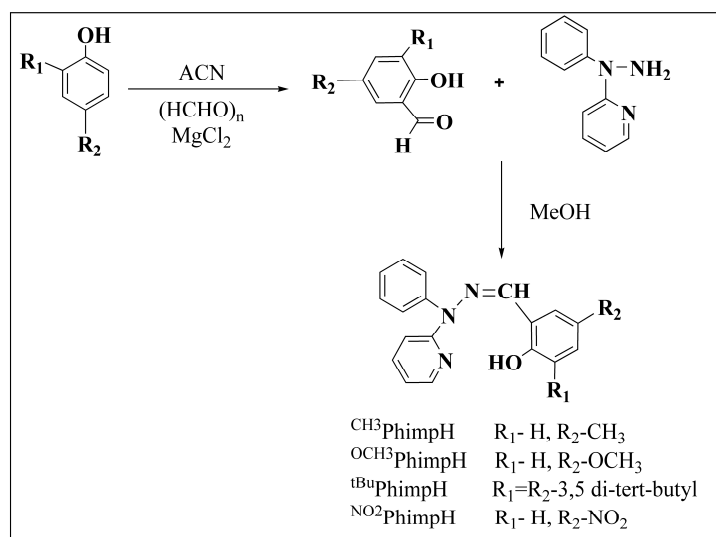
Scheme 2.1 Schematic representation of synthesis of ligands

Synthesized ligands were subjected to various characterization techniques and the preliminary data of physical analysis have been deposited in Table 2.1.

Table 2.1 Physical analysis data of ligands

Ligand	Empirical formula	Formula weight (g/mol)	Yield (%)	Color	Analysis found (Calc%)		
					% C	% H	% N
OCH3PhimpH	$C_{19}H_{17}N_3O_2$	319	63	off–white	70.98 (71.46)	4.89 (5.37)	13.43 (13.16)
CH3PhimpH	$C_{19}H_{17}N_3O$	303	60	off–white	75.87 (75.23)	5.00 (5.65)	12.53 (13.85)
NO2PhimpH	$C_{18}H_{14}N_4O_3$	334	52	yellow	65.47 (64.66)	4.50 (4.22)	16.52 (16.76)

2.3.1.1. IR spectral studies

During IR−spectral studies, free meridional tridentate ligands showed characteristic band for azomethine group $\nu_{-HC=N}$ in the range of 1580−1590 cm^{-1} (Table 2.2).

2.3.1.2. Electronic absorption spectral studies

Electronic spectra of ligands ^{OCH3}PhimpH, ^{CH3}PhimpH, ^{tBu}PhimpH and ^{NO2}PhimpH exhibited bands in range 230−390 nm (Fig. 2.2). In UV−visible, bands at lower energy around 300 nm were assigned n−π* in nature and high energy band near are 230 nm as π−π* transition.[399,400] Band observed around 320 nm is found to be due to the presence of −C=N moiety[199] as depicted in Table 2.2.

Table 2.2 Characteristic IR and UV−visible data of ligands

Ligand	Characteristic IR data (cm^{-1})^a		UV−visible data (λ_{max}/nm, ε/M^{-1}cm^{-1})^b
	ν_{-O-H}	$\nu_{-CH=N}$	
^{OCH3}PhimpH	3426	1586	356 (38,000), 318 (38,340), 230 (39,680)
^{CH3}PhimpH	3404	1589	393 (4,410), 363 (7,880), 320 (9,110), 246 (6,590)
^{NO2}PhimpH	3448	1587	345 (14,150), 320 (11,690), 300 (10,900), 246 (3,410)

^{a}Using KBr pellets, ^{b}Solvent: Dichloromethane
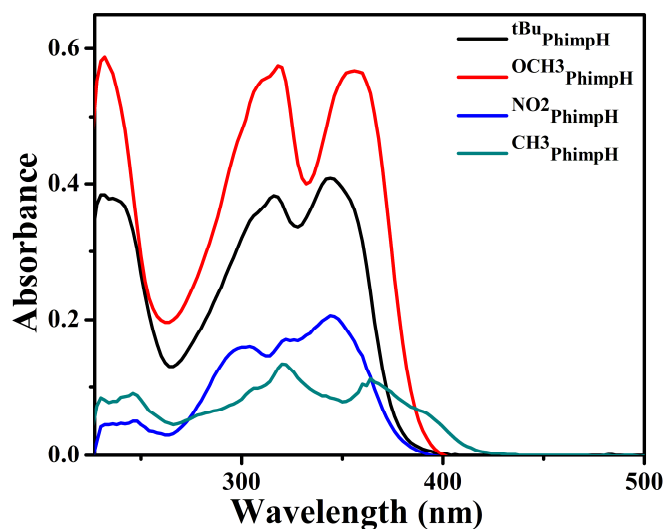
Fig. 2.2 Electronic absorption spectra of ligands in dichloromethane solutions

2.3.1.3. ESI−MS spectral studies

All the ligands were characterized by electrospray ionization mass spectral (ESI-MS) studies using acetonitrile as a solvent and data were collected in positive ion mode. In all the ligands well defined peaks were observed corresponding to m/z=(M+H)$^+$ and (M+Na)$^+$. Ligand ^{OCH3}PhimpH exhibited peak at 320.1321, 342.1134, 358.0879 corresponding to (M+H)$^+$, (M+Na)$^+$, (M+K)$^+$ respectively as shown in Fig. 2.3.
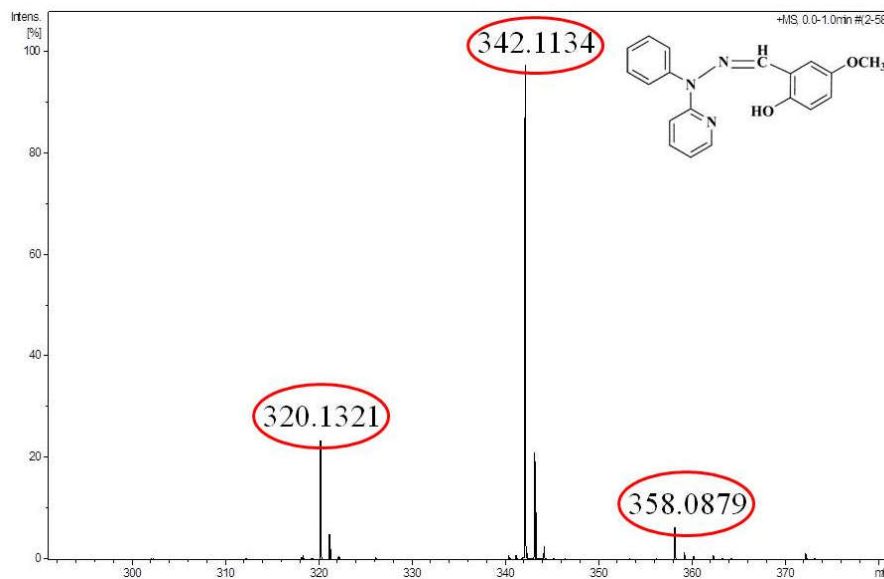
Fig. 2.3 ESI–MS spectrum of ^{OCH3}PhimpH in acetonitrile under positive ion mode

^{CH3}PhimpH exhibited peak at m/z value of 304.4157, 326.4093 corresponding to (M+H)$^+$, (M+Na)$^+$respectively (Fig. 2.4).
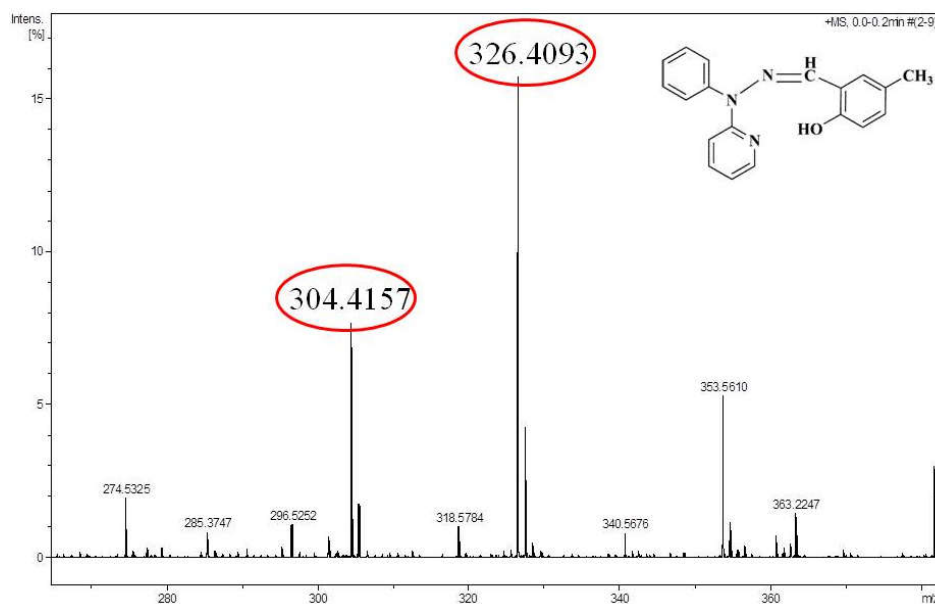
Fig. 2.4 ESI–MS spectrum of ^{CH3}PhimpH in acetonitrile under positive ion mode

^{NO2}PhimpH demonstrated only one peak at m/z value of 335.1126 corresponding to $(M+H)^{+}$ as shown in Fig. 2.5.
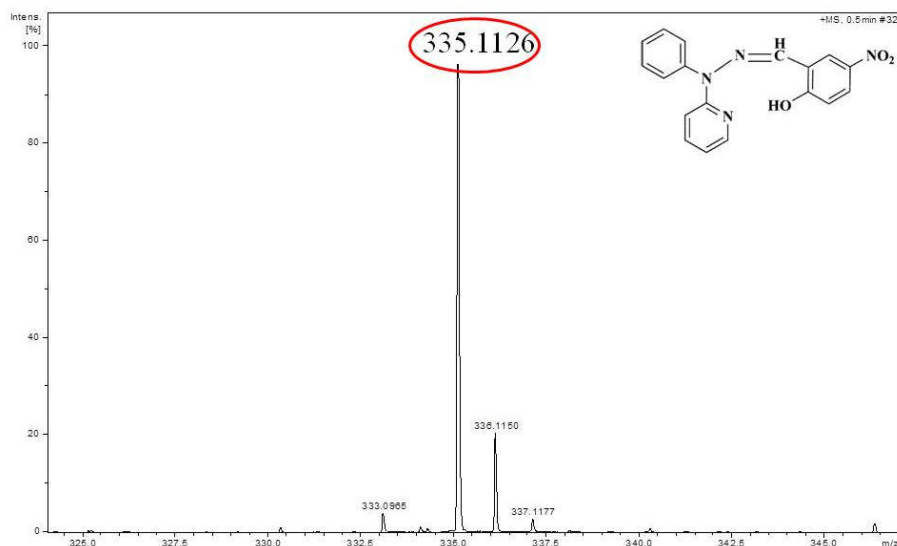
Fig. 2.5 ESI–MS spectrum of ^{NO2}PhimpH in acetonitrile under positive ion mode

2.3.1.4 NMR spectral studies

^{1}H and ^{13}C–NMR spectral studies of all the ligands were performed in CDCl$_3$. The characteristic peaks for all ligands are outlined in Table 2.3 and 2.4 respectively.

Table 2.3 ^{1}H–NMR data of ligands in CDCl$_3$

Ligand	–OH	Aromatic–H	–CH$_3$	–CH=N
^{OCH3}PhimpH	11.29 (1H)	8.27(1H), 7.67–7.51(4H), 7.35(1H), 7.32–7.28(2H), 6.96(2H), 6.84(2H)	3.71 (3H)	6.50 (1H)
^{CH3}PhimpH	11.47 (1H)	8.25 (1H), 7.57 (4H), 7.31(4H), 7.00 (2H), 6.91 (1H)	1.25 (3H)	6.81 (1H)
^{NO2}PhimpH	8.40 (1H)	8.10 (1H), 7.96 (1H), 7.72–7.65(2H), 7.63–7.51(2H), 7.38 (1H), 7.34–7.29(2H), 7.08(1H), 6.93 (1H), 6.69 (1H)	–	5.30 (1H)

¹³C–NMR spectral data has been assigned in the Table 2.4.

Table 2.4 ¹³C–NMR data of ligands in CDCl$_3$

Ligand	¹³C–NMR data
^{OCH3}PhimpH	156.73, 152.52, 151.58, 148.40, 140.87, 137.93, 137.65, 130.93, 130.00, 129.32, 118.78, 117.51, 116.84, 116.73, 114.05, 108.92, 55.93.
^{CH3}PhimpH	156.78, 155.17, 148.34, 141.51, 137.99, 137.67, 130.99, 130.94, 130.42, 130.06, 129.32, 128.35, 118.49, 116.62, 116.59, 108.87, 20.42.
^{NO2}PhimpH	163.03, 138.04, 131.34, 130.07, 129.69, 125.70, 125.50, 119.02, 117.61, 117.47, 109.16

2.3.2. Synthesis and characterization of metal complexes

To the deprotonated ligand a methanolic solution of Fe(ClO$_4$)$_3$.xH$_2$O was added dropwise in a ratio of 2:1 which resulted the formation of complexes. The synthetic routes of complexes **1**, **2**, **3** and **4** have been summarized in Scheme 2.2.

^{OCH3}PhimpH	R$_1$- H, R$_2$-OCH$_3$	**1**	[Fe(^{OCH3}Phimp)$_2$]ClO$_4$
^{CH3}PhimpH	R$_1$- H, R$_2$-CH$_3$	**2**	[Fe(^{CH3}Phimp)$_2$]ClO$_4$
^{tBu}PhimpH	R$_1$=R$_2$-3,5 di-tert-butyl	**3**	[Fe(^{tBu}Phimp)$_2$]ClO$_4$
^{NO2}PhimpH	R$_1$- H, R$_2$-OCH$_3$	**4**	[Fe(^{NO2}Phimp)$_2$]ClO$_4$
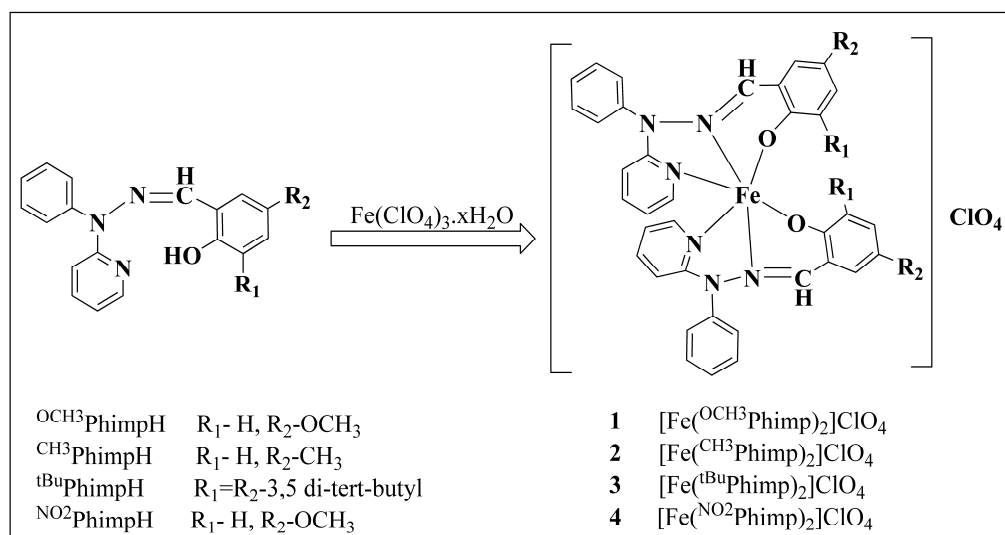
Scheme 2.2 Schematic representation of iron complex synthesis

2.3.2.1. IR spectral studies

Coordination of the nitrogen to the metal centre give rise to shift in strong and sharp band due to azomethine $v_{-HC=N}$ in the range 1605–1615 cm^{-1}.(JIB NT mam) A significant shift (~20 cm^{-1}) in stretching frequencies for $v_{-HC=N}$ clearly indicated the ligation of azomethine nitrogen (−HC=N−) to metal centre. IR bands near 1090 cm^{-1} together with a band at 623 cm^{-1} were found in all iron(III) complexes and clearly indicated presence of non−coordinated perchlorate ions.[401] The experimental values of IR data for all complexes are given in Table 2.5.

Table 2.5 Data for IR and conductivity studies of complexes

Complex	IR data (cm^{-1})^a			Conductivity data $(\Omega^{-1}cm^2mol^{-1})^b$
	v_{O-H}	$v_{-HC=N}$	$v_{ClO4}-$	
1	3437	1610	1092, 622	65 (1:1)
2	3446	1611	1092, 622	60 (1:1)
3	3447	1612	1094, 622	63 (1:1)
4	3450	1606	1098, 623	58 (1:1)

^{a}Using KBr pellets, ^{b}Solvent: dimethylformamide

2.3.2.2. Electronic absorption spectral studies

To observe the mutual influence of metal and ligand coordination, electronic absorption studies were performed for the complexes (Fig. 2.6). In UV−visible, bands at lower energy around 300 nm were assigned n−π* in nature and high energy band near 230 nm as π−π* transitions.[199,402] Absorption bands observed in the region near 400 nm is assigned as ligand to metal charge transfer (LMCT) transitions from the p_π orbital of the phenolate oxygen to $d_{\sigma*}$ orbital of high−spin iron(III) centre. The lowest energy absorptions band in the region near 500

nm is probably due to charge–transfer transition between phenolate $(p_\pi) \rightarrow$ iron(III) $(d_{\pi*})$ orbitals[403–405] as depicted in Table 2.6.

Table 2.6 Electronic spectral data of iron complexes

Complex	UV–visible data (λ_{max}/nm, ε/M^{-1}cm^{-1})[a]
1	504 (900), 396 (5,870), 365 (8,490), 310 (17,250), 237 (22,880)
2	557 (900), 493 (940), 374 (9,430), 314 (23,540), 242 (25,340)
3	560 (1,540), 483 (1,480), 375 (9,420), 314 (23,540), 244 (22,880)
4	545 (440), 350 (15,300), 300 (16,750), 237 (13,270)

[a]UV–visible data in methanol
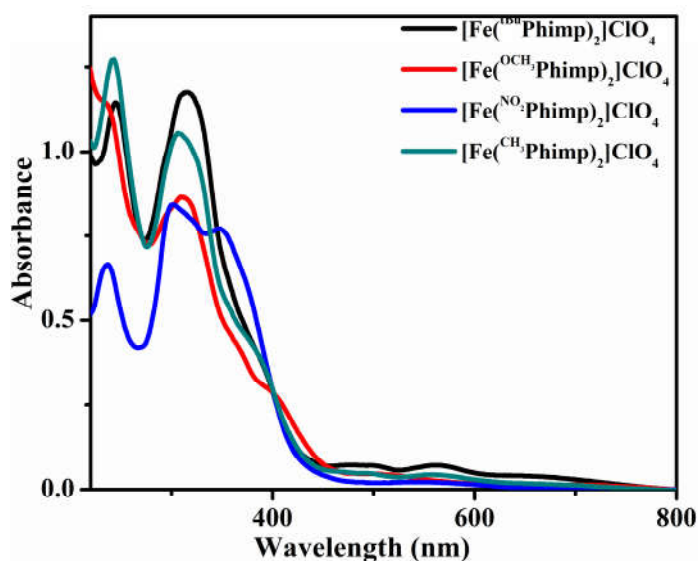
Fig. 2.6 UV–visible absorption spectra of iron(III) complexes in methanol

2.3.2.3. Conductivity studies

Experimental data for molar conductivity have been summarized in Table 2.5. The molar conductivity measurements were performed in DMF at ca. 10^{-3} M. Values obtained for complexes **1**, **2**, **3** and **4** were found to be 65, 60, 63 and 58 Ω^{-1}cm^{2}mol^{-1} respectively These

values were found to be consistent with the uni–univalent (1:1) electrolytic behavior of complexes in solutions.[406]

2.3.2.4. Magnetic moment studies

The magnetic moment of complexes **1**, **2**, **3** and **4** were 3.88, 2.91, 5.14 and 3.34 BM at 303 K respectively. These complexes have higher value as compared to low–spin iron(III) centre but lower values as compared to high–spin iron(III) centre. It has been already reported that the N_4O_2 donor set produces an overall ligand field which is closer to the crossover point. This is related as in $[N_6]$ porphyrin adducts.[407,408] This spin crossover phenomena in iron(III) has been extensively studied.[409–415]

2.3.2.5. ESI–MS spectral studies

For confirmation of structure of iron(III) complexes ESI–MS spectral studies were performed. All the complexes showed characteristic peak $[M–ClO_4]^+$ in positive ion mode. Structure of complex **1** was established using X–ray crystallography. ESI–MS spectra of complex **2** displayed peak at 660.1968 corresponding to $[M–ClO_4]^+$ in acetonitrile as shown in Fig. 2.7.
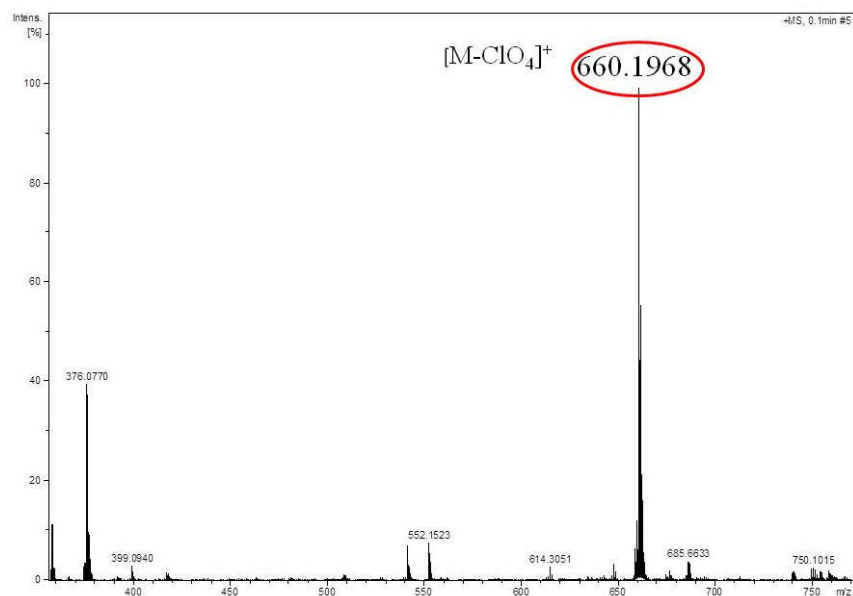
Fig. 2.7 ESI–MS spectrum of **2** in acetonitrile solution under positive ion mode

Similarly complex **3** exhibiting peak corresponding to $[M-ClO_4]^+$ at 855.4185 in acetonitrile solution (Fig. 2.8).
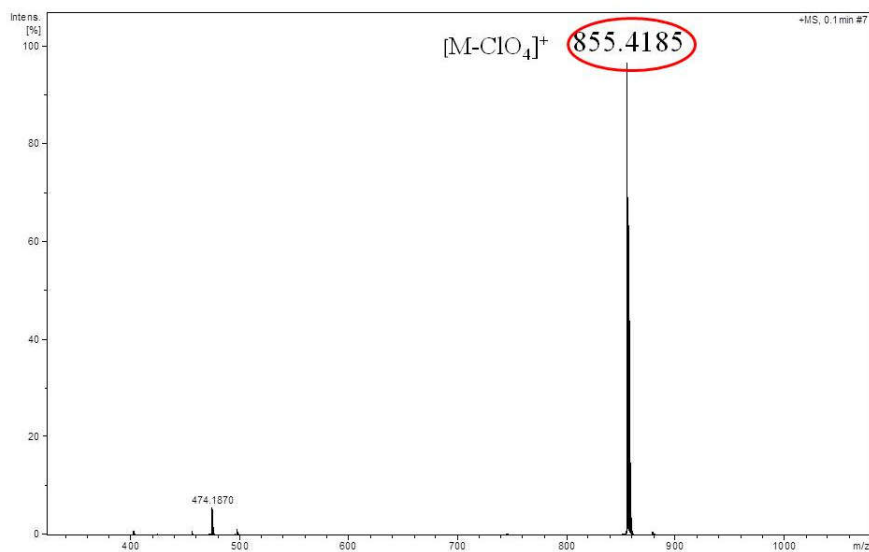
Fig. 2.8 ESI–MS spectrum of **3** in acetonitrile solution under positive ion mode

ESI–MS spectra of complex **4** exhibiting peak at 722.1378 $(M–ClO_4)^+$ in acetonitrile solution also supports the predicted structure of the complex (Fig. 2.9).
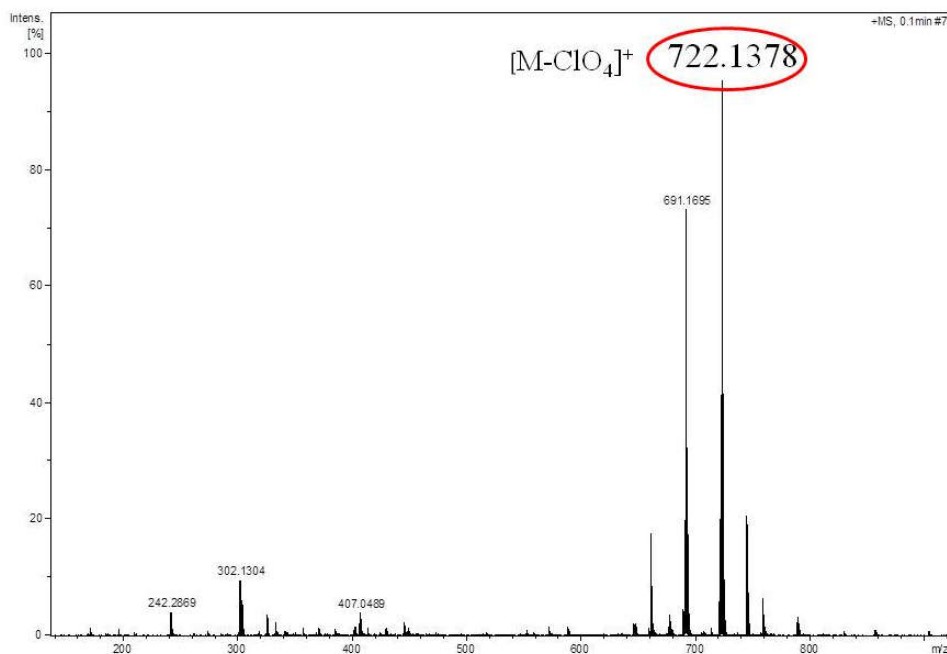
Fig. 2.9 ESI–MS spectrum of **4** in acetonitrile solution under positive ion mode

2.3.3. Molecular structure of complex 1

Crystal structure of complex **1** was obtained by single crystal X–ray diffraction technique. Crystals of diffraction quality were obtained in dichloromethane–methanol (1:1 v/v) solvent system. ORTEP diagram of complex has been shown in Fig. 2.10 exhibiting meridional coordination of ligand around metal centre. Complex **1** crystallized in the monoclinic *P*21 space group. Selected bond lengths, bond angles and crystallographic data are listed in Table 2.7 and Table 2.13.

Structure analysis of complex **1** confirms hexa–coordinated distorted octahedral geometry surrounded by four nitrogen atoms (two pyridine, two imine) and two phenolato donors to iron(III) center. All the chelate rings formed stable either five or six–membered rings.
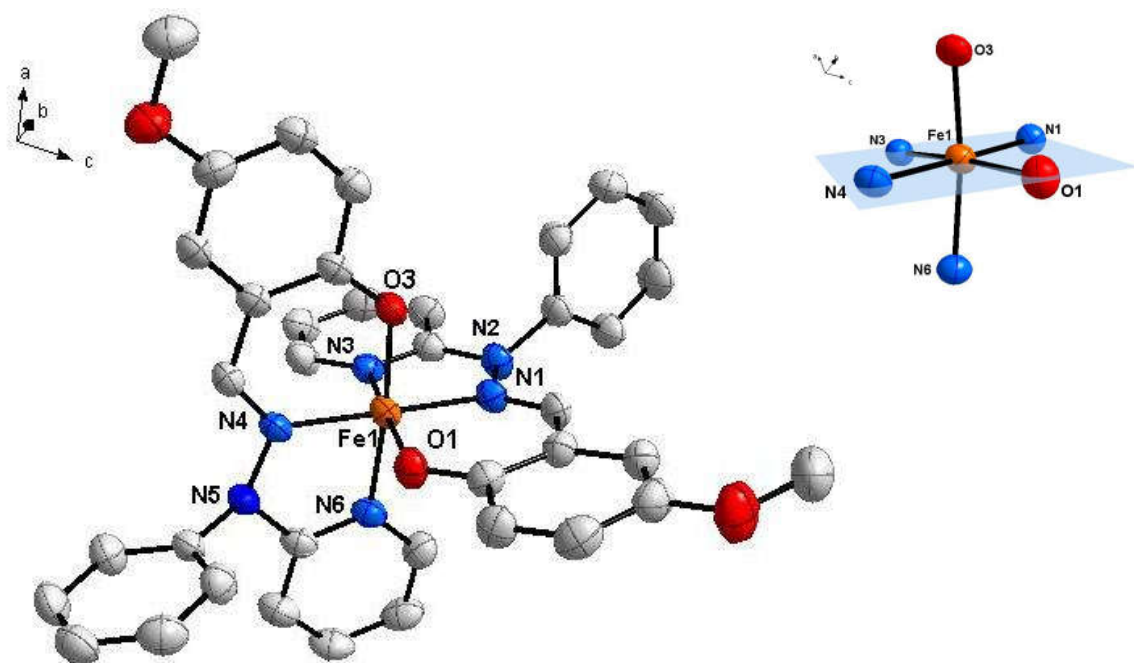
Fig. 2.10 Thermal ellipsoid diagram of the crystal structure of **1** showing the atom numbering scheme and thermal ellipsoids (50% probability level). Hydrogen atoms are omitted for clarity

In a distorted octahedral geometry two phenolato moiety coordinated to the metal centre in a cis manner at an angle O(3)–Fe1–O(1) of 96.984°. Trans atoms N(4)–Fe1–N(1), O(3)–Fe1–N(6) and N(3)–Fe1–O(1) exhibited an angle of 179.036°, 173.169° and 173.049° respectively. The phenolic bond distances Fe1–O1 and Fe1–O3 were found to be 1.8533 Å, 1.856 Å respectively. The bond distance between C26–N4 (1.28 Å) is in good agreement as reported for imine bond.[199] Average bond distances for Fe–N_{py} (1.96Å), Fe–N_{im} (1.91Å) and Fe–O_{ph} (1.85Å) are consistent with reported iron(III) metal complexes.[416] Observed distances

81

between Fe−O were shorter than the average Fe−O bond distances (1.98 Å) indicating a stronger overlap between phenolato and iron(III) metal centre.[138,417]

Table 2.7 Selected bond lengths (Å) and bond angles (°) of complex **1**

Bond lengths (Å)		Bond angles (°)	
Fe1−N1	1.9143(20)	N(1)−Fe1−O(1)	94.118(86)
		N(1)−Fe1−N(6)	99.117(92)
Fe1−N3	1.9699(22)	N(3)−Fe1−O(1)	173.049(89)
		N(3)−Fe1−O(3)	88.644(89)
		N(3)−Fe1−N(1)	82.281(91)
		N(3)−Fe1−N(4)	97.749(90)
		N(3)−Fe1−N(6)	86.451(88)
Fe1−N4	1.9132(19)	N(4)−Fe1−O(1)	85.952(85)
		N(4)−Fe1−O(3)	94.125(85)
		N(4)−Fe1−N(1)	179.036(86)
		N(4)−Fe1−N(6)	81.846(90)
Fe1−N6	1.9653(22)	–	–
Fe1−O1	1.8533(20)	O(1)−Fe1−N(6)	88.264(89)
Fe1−O3	1.856(2)	O(3)−Fe1−O(1)	96.984(86)
		O(3)−Fe1−N(1)	84.913(86)
		O(3)−Fe1−N(6)	173.169(89)

Packing diagram of complex **1** has been shown in Fig. 2.11. Short range forces and non−covalent interactions and H−bonding interactions are important in supramolecular chemistry, crystal engineering and biochemistry.[418]
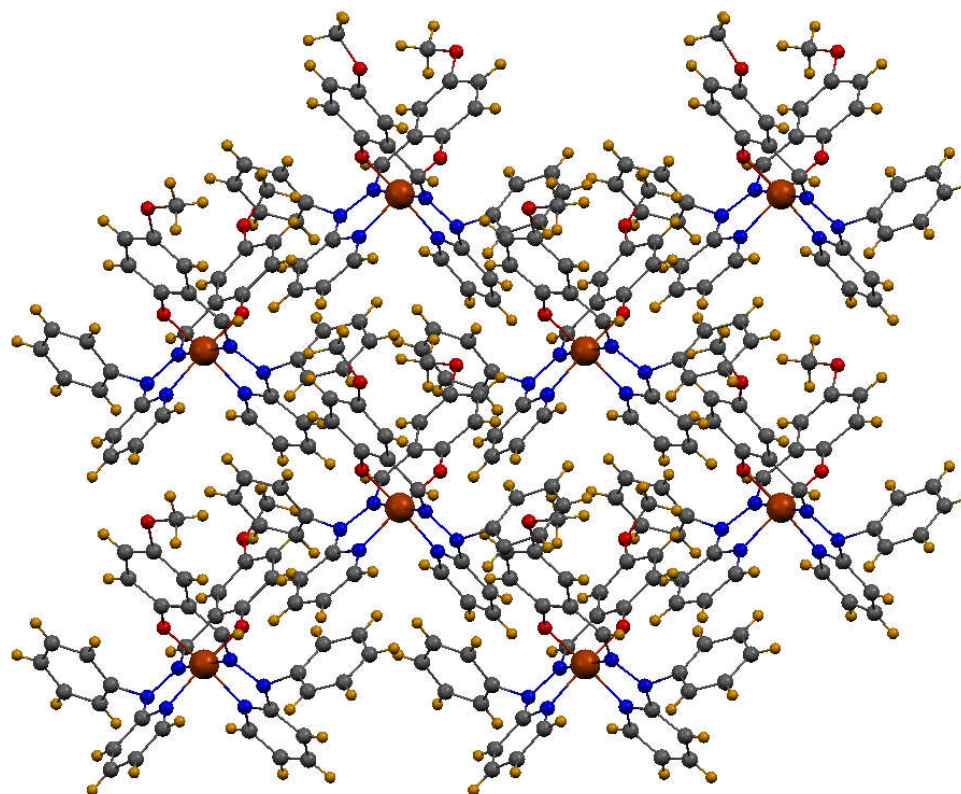
Fig. 2.11 Packing diagram of complex **1**

In the present complex H−bonding interactions were not observed although non−covalent types of interactions were found as shown in Fig. 2.12. Non−covalent interactions were found between the C2−H31 and O2−H6 at distance 2.828 and 2.596 Å (Table 2.8).
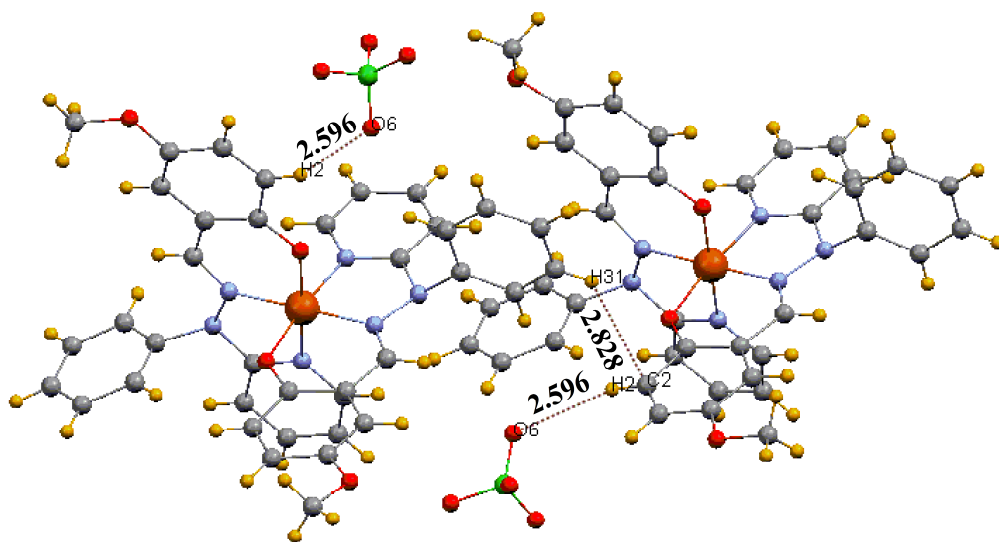
Fig. 2.12 Non−covalent interactions in **1**

Table 2.8 Non−covalent interactions in complex **1**

Atom	Distance (Å)
C2−H2·····O6	2.596
H2−C2·····H31	2.828

2.3.4. Density functional theory (DFT) calculations

We have performed the geometrical optimization for the complex **1** by DFT calculations. The highest occupied molecular orbital (HOMO) and the lowest unoccupied molecular orbital (LUMO) of complex have been depicted in Fig. 2.13−2.14. From the molecular orbital diagram it has been concluded that HOMO orbitals have contribution of ligand only (Fig. 2.13).

(a)   (b)
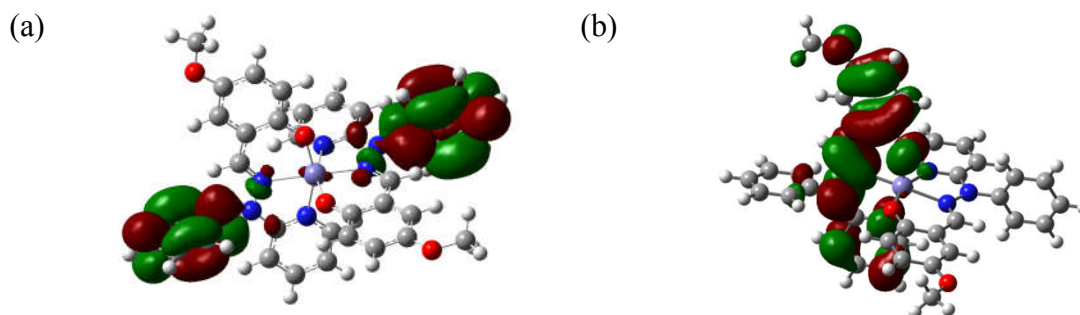
Fig. 2.13 Molecular orbital diagram of HOMO (a) alpha and (b) beta of complex **1**

On the other hand, LUMO orbitals have partial contribution from metal as well as ligand as shown in Fig. 2.14.

(a)   (b)
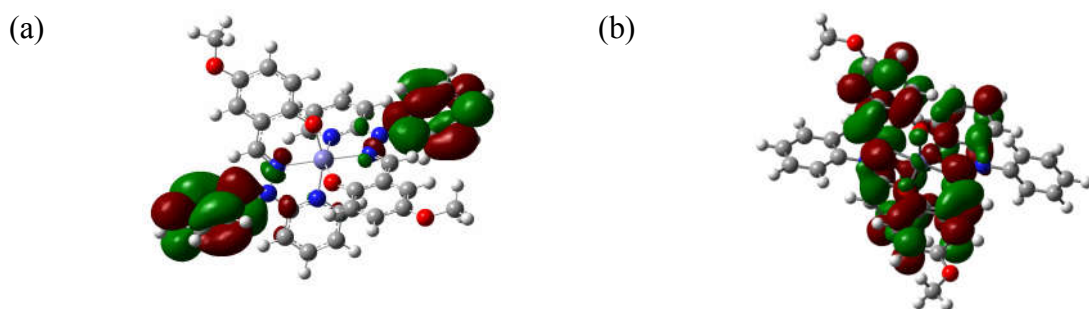
Fig. 2.14 Molecular orbital diagram of LUMO (a) alpha and (b) beta of complex **1**

The characteristic structural parameters (bond distances, bond angles) were calculated. The experimental and calculation data showed good agreement as depicted in the Table 2.9.

Table 2.9 Comparison of theoretical and experimental bond lengths and bond angles of

complex **1** using S=6

Bond lengths (Å)			Bond angles (°)		
	X–ray	DFT		X–ray	DFT
Fe1–N1	1.9143(20)	2.187	N(1)–Fe1–O(1)	94.118(86)	98.88
			N(1)–Fe1–N(6)	99.117(92)	74.35
Fe1–N3	1.9699(22)	2.158	N(3)–Fe1–O(1)	173.049(89)	157.44
			N(3)–Fe1–O(3)	88.644(89)	89.46
			N(3)–Fe1–N(1)	82.281(91)	102.37
			N(3)–Fe1–N(4)	97.749(90)	74.05
			N(3)–Fe1–N(6)	86.451(88)	88.28
Fe1–N4	1.9132(19)	2.201	N(4)–Fe1–O(1)	85.952(85)	84.27
			N(4)–Fe1–O(3)	94.125(85)	99.00
			N(4)–Fe1–N(1)	179.036(86)	175.11
			N(4)–Fe1–N(6)	81.846(90)	101.99
Fe1–N6	1.9653(22)	2.155	–	–	–
Fe1–O1	1.8533(20)	1.900	O(1)–Fe1–N(6)	88.264(89)	90.19
Fe1–O3	1.856(2)	1.908	O(3)–Fe1–O(1)	96.984(86)	100.24
			O(3)–Fe1–N(1)	84.913(86)	84.18
			O(3)–Fe1–N(6)	173.169(89)	157.39

To optimize excited state transition TD–DFT were also performed on the optimized
geometry and data have been summarized in Table 2.10.

Table 2.10 Calculated TD–DFT excitation energies (in eV), oscillator strengths (f), and nature

of transitions in the complex **1**

Transitions (% Contribution)	E (eV) calcd/exp	Oscillator strength (*f*)	λ_{theo} (nm)	λ_{Exp} (nm)
HOMO–10→HOMO–4(25%) HOMO–9→ HOMO–3(48%) HOMO–8→HOMO–4(27%)	2.41/2.42	0.0329	513	504
HOMO–7 →HOMO–3(50%) HOMO–5→ HOMO–2 (24%)	3.11/3.13	0.0021	397	396
HOMO–9 →LUMO–4(31%) HOMO–9→ HOMO–3(26%)	3.39/3.39	0.0096	365	365
HOMO–9→HOMO–3(41%) HOMO–10→HOMO–4(37%)	3.98/4.00	0.0096	311	310

2.3.5. Electrochemical studies

2.3.5.1. Ligands

In dichloromethane solutions, ligands were subjected to electrochemical investigation. As shown in Fig. 2.15 ill–defined anodic waves were found for all the ligands.[199] Ligands do not show any redox property in the range −1.0 to 0.6 V *vs.* Ag/AgCl. Irreversible oxidations in the potential range 0.8 to 1.8 V were observed for all the ligands. This is probably due to the presence of phenolic moiety in the ligand system.
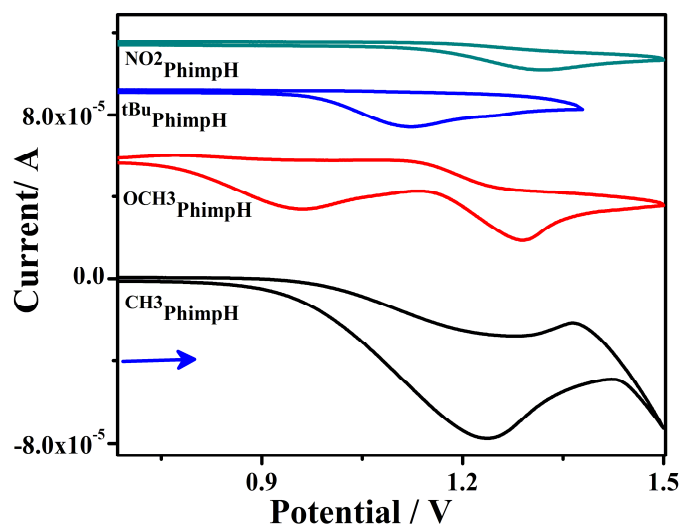
Fig. 2.15 Cyclic voltammograms of a 10^{-3} M solutions of ligands in dichloromethane at a scan rate of 0.1 V/s

2.3.5.2. Iron complexes

Ligands did not show any redox activity in the range of -1.0 to 0.6 V, hence the peak associated in this range is probably having metal character as Fe(III)/Fe(II) couple (Fig. 2.16). In all the complexes cyclic voltammetric studies show an oxidation in potential range 0.8 to 1.8 V as found in ligand system. The oxidation potential observed in case of iron complexes shifted slightly in the anodic direction with respect to the free ligands. The $E_{1/2}$ values found for Fe(III)/(II) couple and along with the ligand centered oxidations were found to be lower than the reported values.[419]

Table 2.11 Electrochemical data for ligands and iron(III) complexes at 298 K[a] *vs* Ag/AgCl

Compound	Fe(III)/Fe(II)			Ligand−centred		
	E^1_{pa}/V	E^1_{pc}/V	$E^1_{1/2}$[b], V (ΔE_p[c], mV)	E^1_{pa}	E^2_{pa}	$E^2_{1/2}$[b], V (ΔE_p[c], mV)
^{CH3}PhimpH	–	–	–	1.2329	–	
^{OCH3}PhimpH	–	–	–	0.9540 1.2817	–	
^{NO2}PhimpH	–	–	–	1.3042	–	
^{tBu}PhimpH	–	–	–	1.1149	–	
1	–0.132	–0.224	–0.178 (92)	1.106 1.353	1.050	
2	–0.133	–0.219	–0.176 (86)	1.123 1.272	–	
3	–0.257	–0.388	–0.322(131)	1.272	1.142	1.207 (130)
4	0.323	0.203	0.263 (120)	1.331		

[a]Measured in dichloromethane using 0.1 M tetrabutylammonium perchlorate (TBAP).[b] $E_{1/2}$ values were calculated as average of anodic (E_{pa}) and cathodic (E_{pc}) peak potentials and [c]ΔE_p = E_{pa} – E_{pc} at scan rate of 0.1 V/s
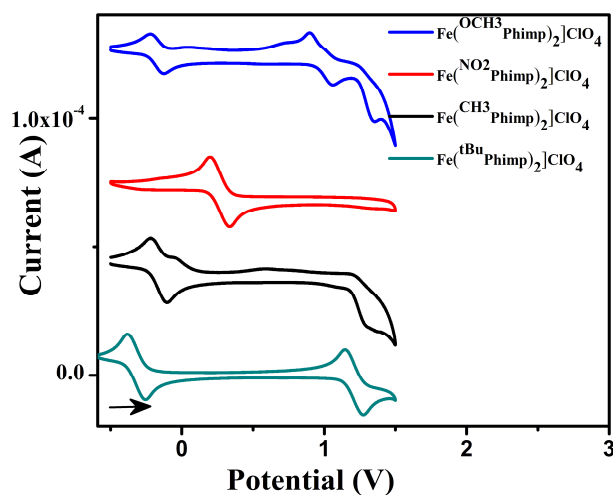
Fig. 2.16 Cyclic voltammograms of 10^{-3} M solutions of complexes **1**, **2**, **3** and **4** at a scan rate of 0.1 V/s

2.3.5.3. Effect of substituent on redox property: Hammett plot

The value of the Hammett parameter (σ_p) designates the relative electron withdrawing or electron–donating effect of a particular substituent at para position. Fig. 2.17 indicates that the substituents at para position have significant effect on the value of potential. A linear relationship was observed between the $E_{1/2}$ and the Hammett σ_p parameter. The electron withdrawing nature of NO_2 decreases the electron density on metal center and hence metal is more prone to reduced as compare to electron donating group. Hence electron withdrawing groups shifted the Fe(III)/Fe(II) couple to more positive potentials.[420]
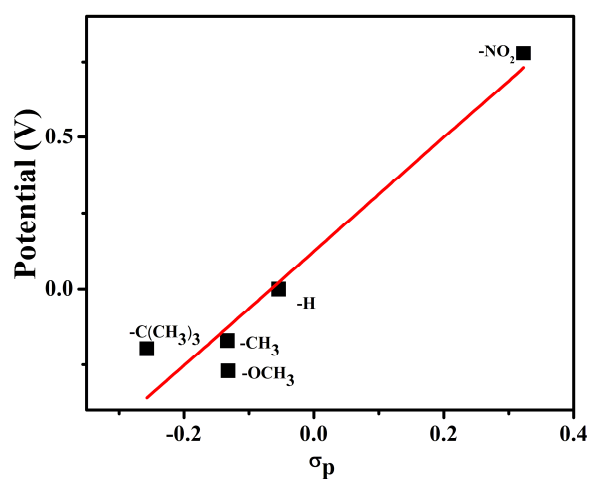
Fig. 2.17 Dependence of $E_{1/2}$ of Fe(III)/Fe(II) couple *vs* σ_p of the ligand para–substituents, with the para–substituent R group specified

2.3.6. Nuclease activity

DNA cleavage activity of complex **3** was studied by gel electrophoresis in tris buffer using supercoiled *pBR322* DNA. Complex **3** has ability to generate stable phenoxyl radical as compare to other complex. To access the DNA cleavage activity of **3**, *pBR322* DNA was incubated with the variable concentration of complex at 37°C for 3 h (Fig. 2.18).

Fig. 2.18 Gel electrophoresis separations showing the cleavage of SC *pBR322* DNA (100 ng) using complex **3** in a 0.1 M buffer containing 10% DMF and incubated at 37 °C for 3 h. Lane 1: DNA control, lane 2: DNA + Fe(ClO$_4$)$_3$.xH$_2$O (100 μM), lane 3: DNA + ^{tBu}PhimpH (100 μM), lanes 4−7: DNA + **3** = 10, 25, 50 and 100 μM, respectively, lane 8: DNA +10% DMF

DNA cleavage experiment showed complete disappearance of nicked circular (NC) and supercoiled (SC) bands at higher concentration (25−100 μM) without any external agent. These observations indicated extensive DNA degradation and DNA cleavage at multiple positions.[421] Hence complex was found to be efficient in DNA cleavage activity in absence of any oxidizing or reducing agent. These data clearly indicate self–activated DNA cleavage by the complex[268]

2.3.7. Protease activity

Similarly protease activity of complex **3** has been investigated. Bovine serum albumin (BSA) was incubated with variable concentration of complex **3** to observe the effect of concentration of metal complex in protease activity. Lanes 6−7 clearly showed protein cleavage activity at concentration 50 μM and 100 μM in Fig. 2.19(a). However, we have performed this experiment for 3 hours only. We have increased the incubation time with similar concentrations of complex **3** and found out efficient cleavage after 20 hours (Fig.2.19(b)). Complex **3** at 50 μM and 100 μM concentrations cleaves the BSA effeciently. These results support the non–specific cleavage of BSA into very small fragments.[360]

(a)   (b)
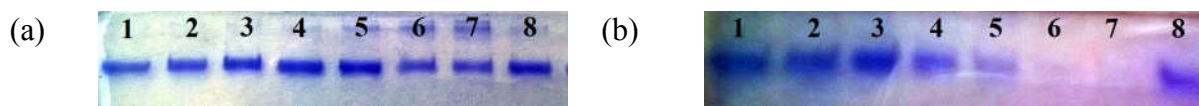
Fig. 2.19 SDS−PAGE of BSA (4 μM) incubated with complex **3** in a 0.1 M buffer containing 10% DMF incubated at variable temperature and concentrations of complex at 50 °C (a) 3 h (b) 20 h. Lane 1: BSA, lane 2: BSA + Fe(ClO$_4$)$_3$.xH$_2$O (100 μM), lane 3: BSA + ^{tBu}PhimpH (100 μM), lane 4: BSA + **3** (10 μM), lane 5: BSA + **3** (25 μM), lane 6: BSA + **3** (50 μM), lane 7: BSA + **3** (100 μM), lane 8: BSA + DMF (10%)

It has been found out that cleavage of peptide bond in BSA is time dependent. Similar concentration of complex was found to be more efficient for protease at higher incubation period. Hence it has been found out that compound is effective in nuclease as well as in protease activity.

2.3.8. DPPH assay

DPPH (2,2−diphenyl−1−picrylhydrazine) is an intensely violet−colored stable free radical which is used to determine the antioxidant properties of different amines, phenols, natural products, foods etc *via* disappearence of color.[422–425] Violet color of DPPH disappears during estimations of antioxidant property. Experiment was performed in 0.1 M phosphate buffer containing 10% DMF. DMF solution of complex **3** (4×10^{-5} M) was taken with DPPH radical (1.2 × 10^{-4} M) and a decrease in absorbance was observed at 540 nm (Fig. 2.20).
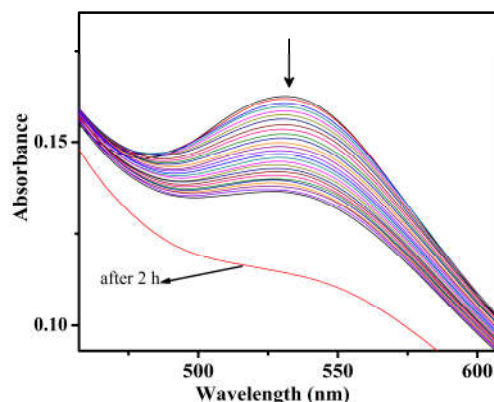
Fig. 2.20 Disappearance of absorption band of DPPH radical at 540 nm using complex **3** in 0.1 M phosphate buffer containing 10% DMF solution

To optimize the possible role of reactive oxygen species (ROS) DPPH assay was performed. During these studies disappearance of band due to the stable free radical was observed which indicated possible involvement of reactive oxygen species.

2.3.9. Oxidation of *o*–aminophenol and phenoxazinone synthase activity

Oxidation of *o*–aminophenol (OAP) in presence of catalytic amount of iron complexes were performed under aerobic condition in methanol at room temperature. The change in absorbance at 430 nm ($\varepsilon=24\times10^3$ $M^{-1}cm^{-1}$) a characteristic of 2–aminophenoxazin–3–one formed, was optimized as a function of time (2 h) to follow the reaction kinetics. Complexes were taken in minor amount as compared to the substrate to maintain the reaction conditions under pseudo–first order reaction. The bands formed for complexes **1** and **2** have been described in Fig. 2.21. We have also utilized iron complexes without any substituent reported elsewhere for the present studies.[426]
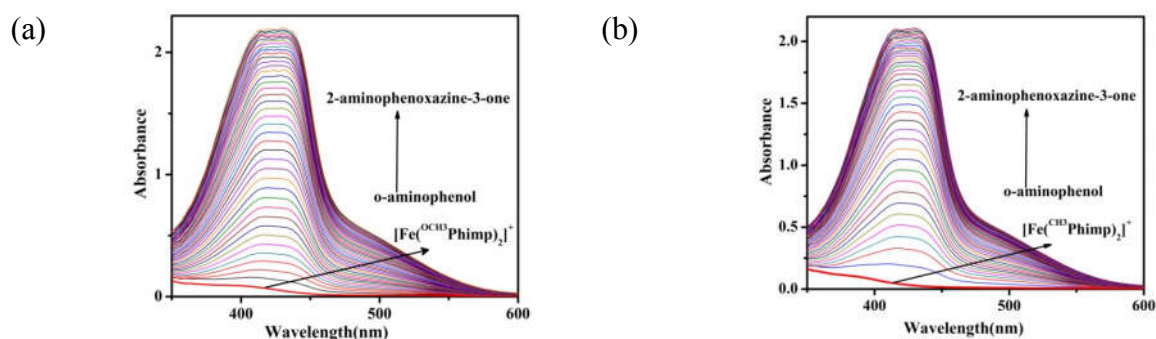
Fig. 2.21 Time resolved electronic absorption spectral changes for the oxidation of *o*–aminophenol (1×10^{-2} mol dm^{-3}) catalyzed by the complexes (1×10^{-5} mol dm^{-3}) (a) **1** (b) **2** at 25 °C in aerobic environment (3 min interval)

Similarly in–situ oxidation was optimized for complexes **3** and **4** in methanol as shown in Fig. 2.22.

93

(a)   (b)
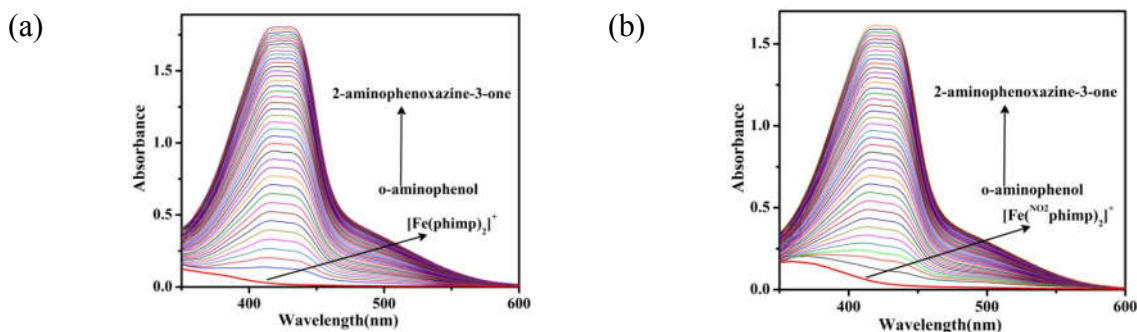
Fig. 2.22 Time resolved electronic absorption spectral changes for the oxidation of
o−aminophenol (1×10^{-2} mol dm^{-3}) catalyzed by the complexes (1×10^{-5} mol dm^{-3}) (a) **3**
(b) **4** at 25 °C in aerobic environment (3 min interval)

Oxidation was performed for the complex **5** using UV−visible spectrophotometer and
formation of band formed was observed similar to the other complexes (Fig. 2.23).
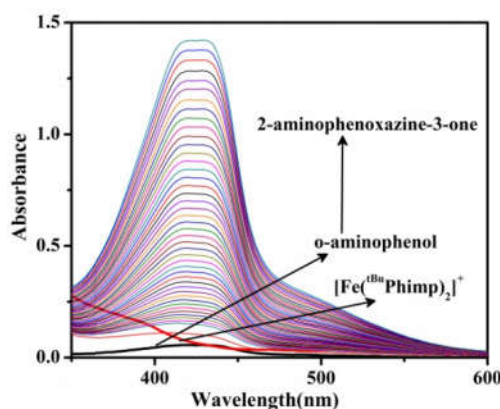
Fig. 2.23 Time resolved electronic absorption spectral changes for the oxidation of
o−aminophenol (1×10^{-2} mol dm^{-3}) catalyzed by the complex **5** (1×10^{-5} mol dm^{-3})
at 25 °C in aerobic environment (3 min interval)

All the complexes were found to be effective in catalyzing the o−aminophenol oxidation
at ambient conditions.

To optimize the effect of substituents on the oxidation of o−aminophenol a plot between
absorbance versus time due to the generation of 2−aminophenoxazine−3−one (APX) at 430 nm
has been drawn as shown in Fig. 2.24.

(a)

(b)
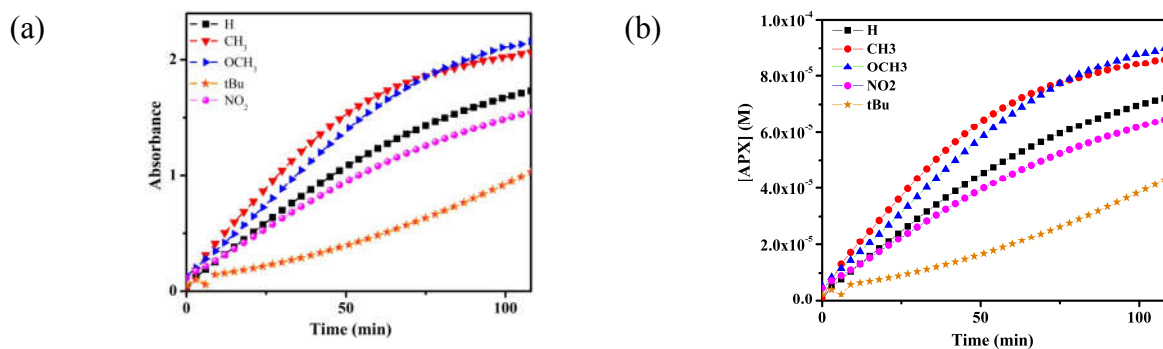
Fig. 2.24 Time dependent absorption spectral studies for oxidation of $o-$aminophenol (a) change in absorbance (b) concentration of 2−aminophenoxazine−3−one (APX) formed for all the complexes observed at 430 nm

Table 2.12 TOF, TON and rate of reaction of $o-$aminophenol oxidation for complexes

Complex	TOF(h^{-1})	TON based on catalyst	$V_{max}(Ms^{-1})$
1	17.03	34.06	4.43×10^{-8}
2	16.92	33.84	1.15×10^{-8}
3	14.55	27.66	6.57×10^{-9}
4	13.83	29.10	1.04×10^{-9}
5	16.89	33.78	1.82×10^{-9}

From the studies, it can be concluded that oxidation of $o-$aminophenol is found to be higher in complexes **1**, **2** having electron donating group ($-OCH_3, -CH_3$). Despite the higher electron donating tendency of $tert-$butyl substituent in the complex **3**, oxidation of $o-$aminophenol was found to be lower than complexes **1** and **2**. This could be probably due to the bulkiness of the $tert-$butyl substituent at $o-$ and $p-$ positions which could possibly create steric hindrance while interacting with the substrate. The electron withdrawing group $-NO_2$ was also found to be less efficient as that of complexes with or without any substituent.

2.3.9.1. Kinetics of oxidation of *o*–aminophenol (OAP)

To gain better insight into the mechanism of oxidation of *o*–aminophenol method of initial rates was evaluated by monitoring the increase in band at 430 nm corresponding to the APX formed.

To optimize the effect of reactants such as substrate, catalyst concentration on rate of reactions, kinetic studies were carried out in the following steps:

(i) Varying substrate concentration at constant complex concentration.

(ii) Varying complex concentration at constant substrate concentration.

Rate of reactions were calculated using initial rate method. Pseudo–first order reaction condition was maintained by using complex as minor component and at least 10 equivalents of substrate during experiments.[163] All the experiments were performed in triplicates to check the reproducibility and authenticity of the data.

2.3.9.1.1. Rate dependence on variation of substrate concentration

During substrate concentration variation, concentrations of complexes were kept fixed while the variations of substrates were monitored. Absorption spectral studies were performed as a function of time at λ_{max} of 430 nm (band originated due to the formation of 2–aminophenoxazine–3–one (APX)). Initial rates of reactions were calculated using linear regression from the slope of the plot between absorbance and time. The initial rates of reactions were calculated as a function of [OAP] concentration varied between 50 µM to 500 µM in case of all complexes. At constant concentration of catalyst (5 µM) (complex **1–5**), rate saturation kinetics were observed for all the iron complexes (Fig. 2.25–2.27).

(a)

(b)
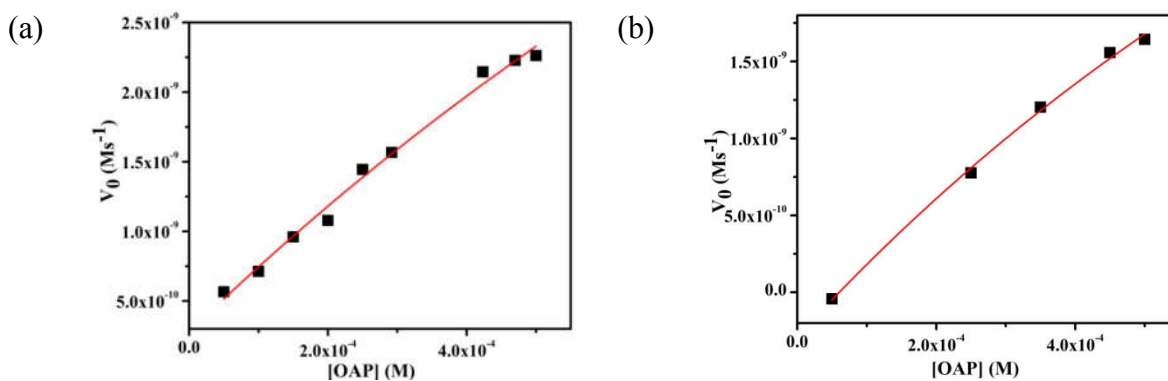
Fig. 2.25 Plot of initial rates *vs.* substrate concentration obtained for the oxidation of *o*−aminophenol catalyzed by complexes (5 μM) (a) **1** (b) **2** at ambient temperature in methanol. Symbols and lines representing the experimental and simulated values respectively

(a)

(b)
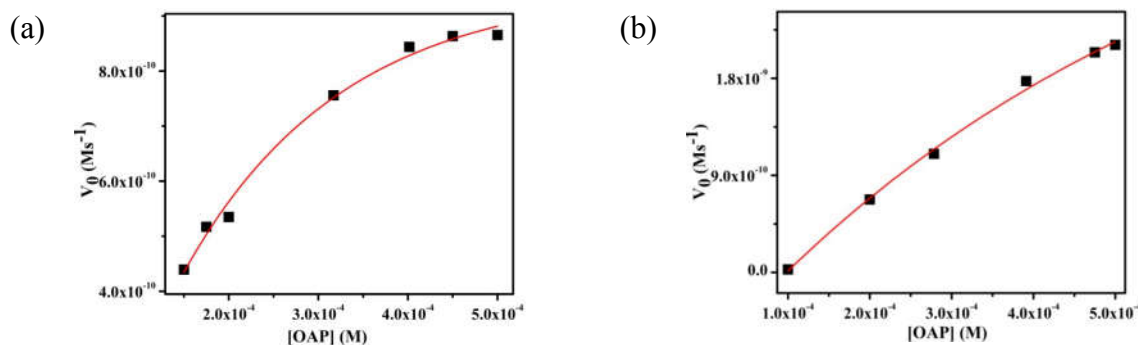
Fig. 2.26 Plot of initial rates *vs.* substrate concentration obtained for the oxidation of *o*−aminophenol catalyzed by complexes (5 μM) (a) **3** (b) **4** at ambient temperature in methanol. Symbols and lines representing the experimental and simulated values respectively
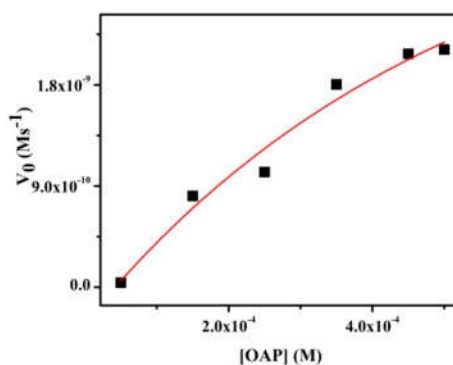
Fig. 2.27 Plot of initial rates versus substrate concentration obtained for the oxidation of *o*−aminophenol catalyzed by complex (5 μM) **5** at ambient temperature in methanol. Symbols and lines representing the experimental and simulated values respectively

97

When varying the concentration of substrate, a saturation type curve was observed. Under the given experimental conditions, saturation kinetics was found for the initial rates (V_0) versus [OAP] concentrations (Fig. 2.26–2.28). This indicates that an intermediate complex–substrate adduct formed during pre–equilibrium process and this irreversible metal–based oxidant formation is probably the rate–determining step of the catalytic cycle.[393]

2.3.9.1.2. Rate dependence on variation of catalyst concentration

During catalyst concentration variation, concentrations of substrate were kept fixed while the variations of complexes were observed. Absorption spectral studies were performed as a function of time at λ_{max} 430 nm. The initial rates of reactions were calculated as a function of complex concentrations varied between 5 μM to 50 μM in case of all complexes. At constant concentration of substrate (500 μM) (complex **1–5**), rate saturation kinetics were observed for all the iron complexes (Fig. 2.28–2.30).
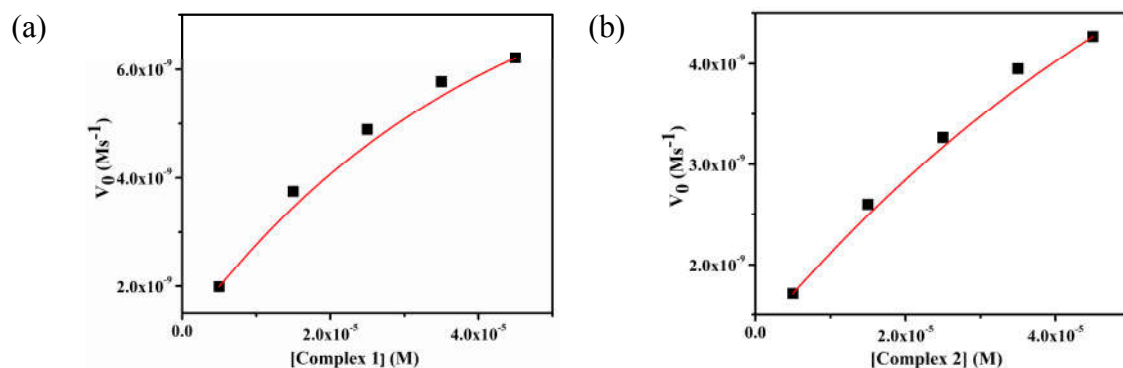
Fig. 2.28 Plot of initial rates *vs.* complex concentration obtained for the oxidation of *o*–aminophenol catalyzed by complexes (a) **1** and (b) **2** at ambient temperature in methanol. Symbols and lines representing the experimental and simulated values respectively

(a)

(b)
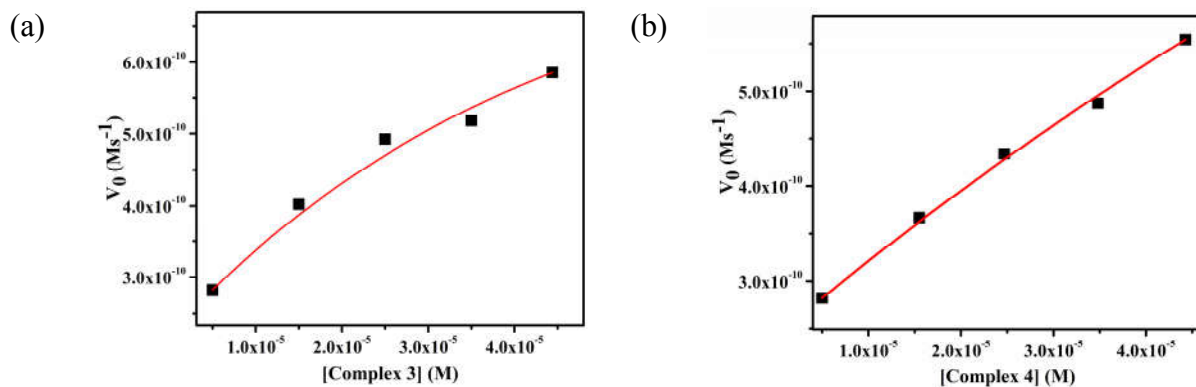
Fig. 2.29 Plot of initial rates *vs.* complex concentration obtained for the oxidation of *o*−aminophenol catalyzed by complexes (a) **3** and (b) **4** at ambient temperature in methanol. Symbols and lines representing the experimental and simulated values respectively
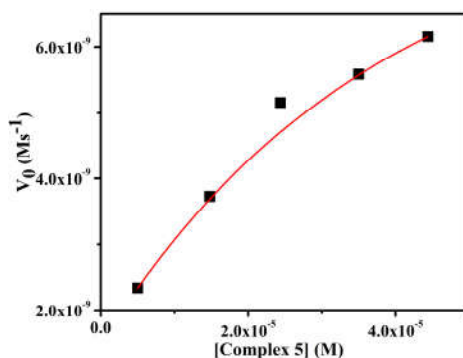
Fig. 2.30 Plot of initial rates *vs.* complex concentration obtained for the oxidation of *o*−aminophenol catalyzed by complex **5** at ambient temperature in methanol. Symbols and lines representing the experimental and simulated values respectively

To gain better insight into the order of reaction logarithmic plots of these values were drawn.

2.3.9.1.3. Order of reaction

A general rate of reaction can be derived using the following equation:

$$-d[OAP]/dt = d[APX]/dt = K_1 [OAP]^m[Complex]^n$$

To evaluate the rate of reaction and order of reaction the logarithm of initial rate of reaction was plotted against ln [OAP] at a fixed concentration of catalyst[163] as shown in Fig. 2.31−2.33.

99

(a)

(b)
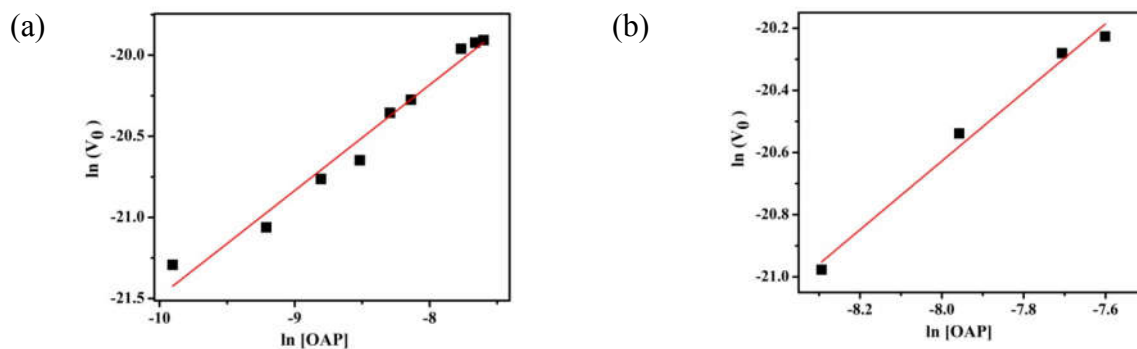
Fig. 2.31 Logarithmic plot of initial rates *vs.* substrate concentration obtained for the oxidation of *o*−aminophenol catalyzed by complexes (a) **1** (b) **2** at ambient temperature in methanol. Symbols and lines representing the experimental and simulated values respectively

(a)

(b)
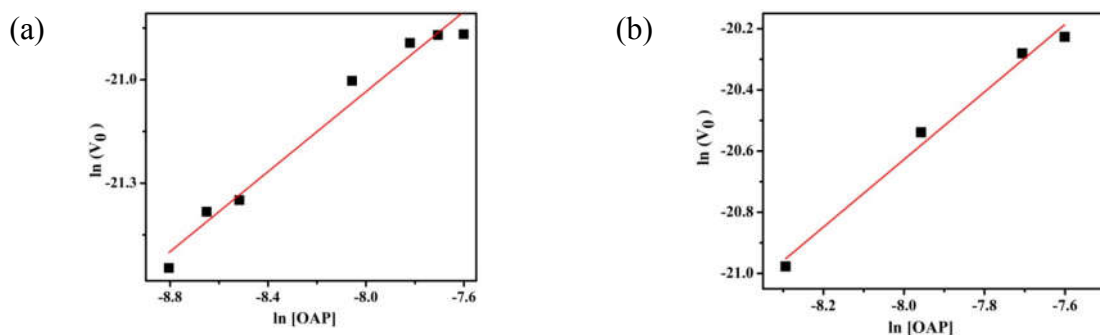
Fig. 2.32 Logarithmic plot of initial rates *vs.* substrate concentration obtained for the oxidation of *o*−aminophenol catalyzed by complexes (a) **3** (b) **4** at ambient temperature in methanol. Symbols and lines representing the experimental and simulated values respectively
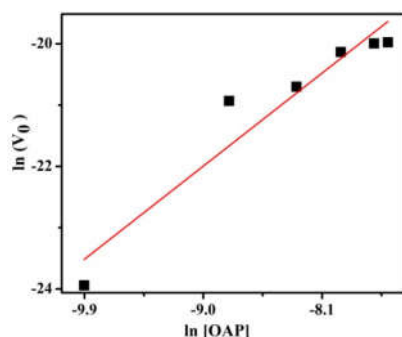
Fig. 2.33 Logarithmic plot of initial rates *vs.* substrate concentration obtained for the oxidation of *o*−aminophenol catalyzed by complexes **5** at ambient temperature in methanol. Symbols and lines representing the experimental and simulated values respectively

From the plot it is clear that logarithm of rate of reaction is linearly dependent on the substrate concentration. Slopes of these plots give the value closer to 1 (m=0.77 (complex **1**), 1.02 (complex **2**), 0.89 (complex **3**), 1.11 (complex **4**) and 0.92 (complex **5**)) in all the complexes respectively.

2.3.9.1.4. Order of reaction for catalyst

Similarly, logarithmic plot of rate of reaction versus complex concentration were drawn. These plots were found to be linear indicating that the rate of reaction depends on the concentration linearly in complexes **1**–**5**.

(a)   (b)
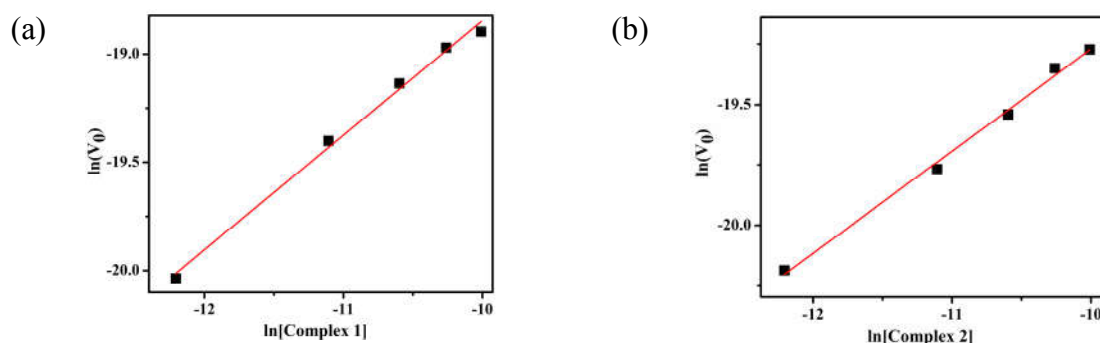
Fig. 2.34 Logarithmic plot of initial rates versus catalyst concentration obtained for the oxidation of o−aminophenol catalyzed by complexes (a) **1** (b) **2** at ambient temperature in methanol. Symbols and lines representing the experimental and simulated values respectively

(a)   (b)
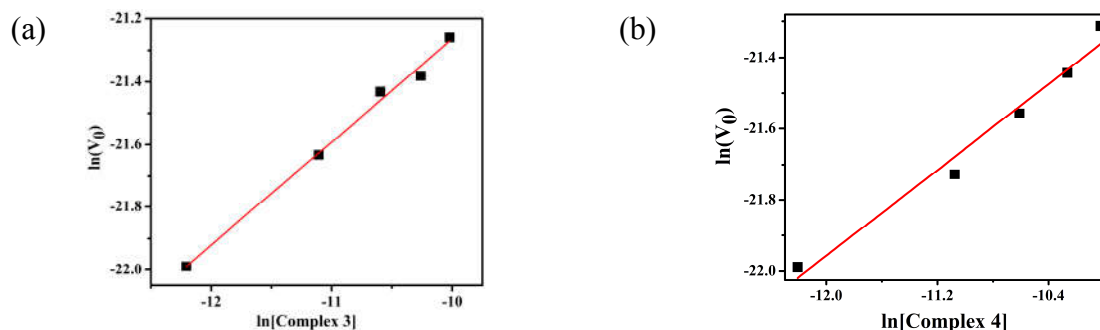
Fig. 2.35 Logarithmic plot of initial rates $vs.$ catalyst concentration obtained for the oxidation of o−aminophenol catalyzed by complexes (a) **3** (b) **4** at ambient temperature in methanol. Symbols and lines representing the experimental and simulated values respectively

101
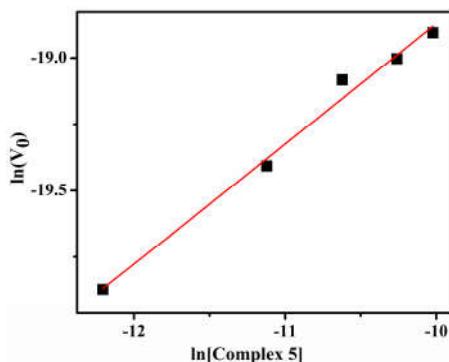
Fig. 2.36 Logarithmic plot of initial rates *vs.* catalyst concentration obtained for the oxidation of *o*−aminophenol catalyzed by complexes **5** at ambient temperature in methanol. Symbols and lines representing the experimental and simulated values respectively

From the above plot, it can be concluded that logarithm of rate of reaction is linearly dependent on the complex concentration. Slopes of these plots give the value close to 0.5 (n=0.52 (m=0.77 (complex **1**), 0.42 (complex **2**), 0.54 (complex **3**), 0.47 (complex **4**) and 0.45 (complex **5**)) in all the complexes.

Overall reaction can be derived as

$$-d[OAP]/dt = d[APX]/dt = K_1 [OAP]^1 [Complex]^{0.5}$$

Hence from the experiments it has been found out that the reaction followed 1.5th order of reaction kinetics in the given experimental conditions.

2.4. Conclusions

In the present study we synthesized tridentate ligands ^{OCH3}PhimpH, ^{CH3}PhimpH, ^{tBu}PhimpH and ^{NO2}PhimpH having N_2O donors. These ligands were analyzed and characterized with various spectroscopic techniques such as IR, UV−visible, GC−MS, NMR spectral studies. The ligands were utilized to synthesize the mononuclear bis iron complexes. Complexes were characterized using IR, UV−visible, ESI−MS spectral studies. Magnetic properties of

complexes were also analyzed. Conductivity measurements show the uni–univalent (1:1) electrolytic behavior of complexes in solutions. All the studies supported the formation of $[Fe(^{OCH3}PhimpH)_2](ClO_4)$ (**1**), $[Fe(^{CH3}PhimpH)_2](ClO_4)$ (**2**), $[Fe(^{tBu}PhimpH)_2](ClO_4)$ (**3**) and $[Fe(^{NO2}PhimpH)_2](ClO_4)$ (**4**) complexes. Molecular structure of complex **1** was determined by single crystal X–ray analysis. Investigation of electrochemical studies suggested metal centred as well as ligand centred oxidation. Complex **3** gave rise to effective nuclease as well as protease activity. From the studies it was found that the complex is capable in exhibiting self–activated nuclease and protease activity. Possible involvement of any radical species was further confirmed using DPPH assay. These iron complexes exhibited phenoxazinone synthase activity *via o*–aminophenol oxidation. Kinetic studies on phenoxazinone synthase clearly indicated higher activity of complexes capable of generating stable phenoxyl radical.

2.5. Experimental section

2.5.1. Materials and instrumental methods

Precursors (substituted aldehydes) for synthesis of ligands have been prepared from corresponding substituted phenols using a reported procedure.[427] However, *p*–cresol, *p*–methoxy phenol, *p*–methyl phenol and anhydrous $MgCl_2$ were purchased from Himedia Laboratories Pvt. Ltd, Mumbai, India. Salicyldehyde was purchased from SRL, Mumbai, India. 3,5–di–*tert*–butyl–2–hydroxybenzaldehyde, $Fe(ClO_4)_3.xH_2O$ were purchased from Sigma–Aldrich. Solvents used for spectroscopic studies were HPLC grade and purified by standard procedures before use.[396] Elemental analysis was carried out on an Elemental model Vario EL–III. Infrared spectra were recorded as KBr pellets on a Nicolet NEXUS Aligent 1100 FT–IR spectrometer, using 50 scans and are reported in cm^{-1}. Electronic spectra were recorded in CH_2Cl_2 and CH_3OH with an Evolution 600, Thermo Scientific UV–Visible spectrophotometer using cuvettes of 1 cm path length. Molar conductivities were determined in dimethylformamide (DMF) at 10^{-3} M at 25 °C with a Systronics 304 conductometer. Magnetic susceptibilities were determined at 300 K with a Cryogenic vibrating sample magnetometer. Cyclic voltammetric studies were performed on a CH–600 electroanalyser in CH_2Cl_2 with 0.1 M tetrabutylammonium perchlorate (TBAP) as a supporting electrolyte. The working electrode, reference electrode and auxiliary electrode were glassy carbon, Ag/AgCl and a Pt wire electrode, respectively. The concentration of the compounds was of the order of 10^{-3} M. The ferrocene/ferrocenium couple occurs at $E_{1/2}$= +0.52 V (72) V versus Ag/AgCl under the similar experimental conditions.

2.5.2. Synthesis of ligands

2.5.2.1. Synthesis of ^{OCH3}PhimpH

To a methanolic solution of 2–hydroxy–5–methoxybenzaldehyde (152 mg, 1.00 mmol), 2–(1–phenylhydrazinyl)pyridine (185.0 mg, 1.00 mmol) was added in 10 mL of methanol. The reaction mixture was stirred at room temperature. Within 30 min a white solid began to separate out and stirring was continued for further 2 h. A white precipitate was filtered, washed with small amount of methanol and then dried in vacuum. ^{CH3}PhimpH was recrystallized from dichloromethane. Yield: 63%. ESI–MS pos (CH$_3$CN, m/z): 320.1321(M+H)$^+$, 342.1134 (M+Na)$^+$, 358.0879 (M+K)$^+$. Selected IR data (KBr, ν_{max}/cm^{-1}): 3426, ν_{OH}, 1586, $\nu_{C=Nimine}$. UV–visible [CH$_2$Cl$_2$, λ_{max}/nm (ε/M^{-1}cm^{-1})]: 356 (38,000), 318 (38,340), 230 (39,680). ^{1}H–NMR (CDCl$_3$, δ/ppm, 400 MHz): 11.29 (1H, s), 8.27(1H, d, J=5.0 Hz), 7.67–7.51 (4H, m), 7.35(1H, s), 7.32–7.28(2H, m), 6.96(2H, t, J=9.8 Hz), 6.84 (2H, m), 6.50 (1H, d, J= 2.3 Hz), 3.71 (3H, d, 1.4Hz). ^{13}C–NMR (CDCl$_3$, δ/ppm, 400 MHz): 156.73, 152.52, 151.58, 148.40, 140.87, 137.93, 137.65, 130.93, 130.00, 129.32, 118.78, 117.51, 116.84, 116.73, 114.05, 108.92, 55.93. Anal. Calcd for C$_{19}$H$_{17}$N$_3$O$_2$: C, 71.46; H, 5.37; N, 13.16, Found: C, 70.92; H, 5.14; N, 12.98.

2.5.2.2. Synthesis of ^{CH3}PhimpH

Ligand was synthesized by similar procedure adopted for ^{OCH3}PhimpH using 2–hydroxy–5–methylbenzaldehyde (136 mg, 1.00 mmol) instead of 2–hydroxy–5–methylbenzaldehyde. Yield: 60%. ESI–MS (CH$_3$CN, m/z): 304.4157(M+H)$^+$, 326.4093 (M+Na)$^+$. Selected IR data (KBr, ν_{max}/cm^{-1}): 3404, ν_{OH}, 1588, $\nu_{C=Nimine}$. UV–visible [CH$_2$Cl$_2$, λ_{max}/nm (ε/M^{-1}cm^{-1})]: 393 (4,410), 363 (7,880), 320 (9,110), 246 (6,590). ^{1}H–NMR (CDCl$_3$, δ/ppm, 400 MHz): 11.47 (1H, s), 8.25 (1H, m), 7.57 (4H, m), 7.31(4H, m), 7.00 (2H, m), 6.91 (1H, d, J= 8.2 Hz), 6.81 (1H), 1.25 (3H, s). ^{13}C–NMR (CDCl$_3$, δ/ppm, 400 MHz): 156.78, 155.17, 148.34, 141.51, 137.99,

137.67, 130.99, 130.94, 130.42, 130.06, 129.32, 128.35, 118.49, 116.62, 116.59, 108.87, 20.42.

Anal. Calcd for $C_{19}H_{17}N_3O$: C, 75.23; H, 5.65; N, 13.85, Found: C, 75.87; H, 5.00; N, 12.53.

2.5.2.3. Synthesis of ^{NO2}PhimpH

Ligand was prepared using the procedure employed for ^{CH3}PhimpH starting from 2–hydroxy–5–nitrobenzaldehyde (167.0 mg, 1.00 mmol). Yield: 52%. ESI–MS (CH₃CN, m/z): 335.1126 (M+H)⁺. Selected IR data (KBr, v_{max}/cm^{-1}): 3448, v_{OH}, 1587, $v_{C=Nimine}$. UV–visible [CH₂Cl₂, λ_{max}/nm ($\varepsilon/M^{-1}cm^{-1}$)]: 345 (14,150), 320 (11,690), 300 (10,900), 246 (3,410). ¹H–NMR (CDCl₃, δ/ppm, 400 MHz): δ 8.40–8.35 (1H, m), 8.10 (1H, dd, J = 9.2, 2.7 Hz), 7.96 (1H, d, J = 2.3 Hz), 7.72–7.65 (2H, m), 7.63–7.51 (2H, m), 7.38 (1H, s), 7.34–7.29 (2H, m), 7.08 (1H, d, J = 9.2 Hz), 6.93 (1H, dd, J = 6.6, 5.3 Hz), 6.69 (1H, d, J = 8.2 Hz), 5.30 (1H, s) ¹³C–NMR (DMSO–d₆, δ/ppm, 500 MHz): 163.03, 138.04, 131.34, 130.07, 129.69, 125.70, 125.50, 119.02, 117.61, 117.47, 109.16 Anal. Calcd for $C_{18}H_{14}N_4O_3$: C, 64.66; H, 4.22; N, 16.76, Found: C, 65.47; H, 4.50; N, 16.52.

2.5.3. Synthesis of metal complexes

Caution! Perchlorate salts of metal complexes with organic ligands are potentially explosive. Only a small quantity of material should be prepared and handled carefully.

2.5.3.1. Synthesis of [Fe(^{OCH3}Phimp)₂](ClO₄) (1)

To a solution of ^{OCH3}PhimpH (638 mg, 2.00 mmol) in dichloromethane (8 mL) was added Et₃N (202 mg, 2.00 mmol) followed by a methanolic solution of Fe(ClO₄)₃.xH₂O (354 mg, 1 mmol). After complete addition of reactants solution mixture was further stirred for 3–4 h at room temperature. A brown color solution was filtered and filtrate was evaporated to dryness. The complex was recrystallized using ether diffusion into a mixture of dichloromethane/methanol. Yield: 82%. Selected IR data (KBr, v_{max}/cm^{-1}): 1610, $v_{C=Nimine,}$ 1307, $v_{C–Ophenol,}$ 1092, 622, $v_{ClO4−}$. UV–visible [CH₃OH, λ_{max}/nm ($\varepsilon/M^{-1}cm^{-1}$)]: 504 (900), 396

(5,870), 365 (8,490), 310 (17,250), 237 (22,880). μ_{eff} (300 K): 3.88 BM. $\Lambda_M/\Omega^{-1}cm^2mol^{-1}$ (in DMF): 65 (1:1). Anal. Calcd for $C_{38}H_{32}N_6O_8FeCl$: C, 57.63; H, 4.07; N, 10.61, Found: C, 56.48; H, 3.89; N, 9.59.

2.5.3.2. Synthesis of [Fe(^CH3^Phimp)$_2$](ClO$_4$) (2)

Complex [Fe(^CH3^Phimp)$_2$](ClO$_4$) was synthesized using above mentioned procedure using ^CH3^PhimpH as a ligand. Yield: 68%. Selected IR data (KBr, ν_{max}/cm^{-1}): 1611, $\nu_{C=Nimine,}$ 1307, $\nu_{C-Ophenol,}$ 1092, 622, ν_{ClO4-}. UV–visible [CH$_3$OH, λ_{max}/nm ($\varepsilon/M^{-1}cm^{-1}$)]: 557 (900), 493 (940), 374 (9,430), 314 (23,540), 242 (25,340). μ_{eff} (300 K): 2.91 BM. $\Lambda_M/\Omega^{-1}cm^2mol^{-1}$ (in DMF): 60 (1:1). Anal. Calcd for $C_{38}H_{32}N_6O_6FeCl$: C, 60.05; H, 4.24; N, 11.06, Found: C, 58.47; H, 4.10; N, 10.58.

2.5.3.3. Synthesis of [Fe(^tBu^Phimp)$_2$](ClO$_4$) (3)

Similar procedure was followed for complex [Fe(^tBu^Phimp)$_2$](ClO$_4$) using ^tBu^PhimpH (804 mg, 2.00 mmol) as a ligand. A brown color solution was filtered and filtrate was evaporated to dryness. Yield: 76%. Selected IR data (KBr, ν_{max}/cm^{-1}): 1612, $\nu_{C=Nimine,}$ 1309, $\nu_{C-Ophenol,}$ 1094, 622, ν_{ClO4-}. UV–visible [CH$_3$OH, λ_{max}/nm ($\varepsilon/M^{-1}cm^{-1}$)]: 560 (1,540), 483 (1,480), 375 (9,420), 314 (23,540), 244 (22,880). μ_{eff} (300 K): 5.14 BM. $\Lambda_M/\Omega^{-1}cm^2mol^{-1}$ (in DMF): 63 (1:1). Anal. Calcd for $C_{52}H_{60}N_6O_6FeCl$: C, 65.31; H, 6.32; N, 8.79, Found: C, 61.40; H, 5.75; N, 6.93.

2.5.3.4. Synthesis of [Fe(^NO2^Phimp)$_2$](ClO$_4$) (4)

Complex was synthesized using procedure employed for [Fe(^tBu^Phimp)$_2$](ClO$_4$) and ^NO2^PhimpH as a ligand. Yield: 55%. Selected IR data (KBr, ν_{max}/cm^{-1}): 1606, $\nu_{C=Nimine,}$ 1301, $\nu_{C-Ophenol}$ 1098, 623, ν_{ClO4-}. UV–visible [CH$_3$OH, λ_{max}/nm ($\varepsilon/M^{-1}cm^{-1}$)]: 545 (440), 350 (15,300), 300 (16,750), 237 (13,270). μ_{eff} (300 K): 3.34 BM. $\Lambda_M/\Omega^{-1}cm^2mol^{-1}$ (in DMF): 58 (1:1). Anal. Calcd for $C_{36}H_{26}N_8O_{10}FeCl$: C, 52.61; H, 3.19; N, 13.63, Found: C, 51.14; H, 2.80; N, 11.59.

2.5.4. Nuclease activity

Cleavage of plasmid DNA was performed using agarose gel electrophoresis. Supercoiled *pBR322* DNA (100 ng) in TBE (pH 8.2) was treated with iron complexes **3** (10–100 μM) dissolved in DMF (10%). The samples were incubated for 2 h at 37 °C and loaded buffer (25% bromophenol blue and 30% glycerol) was added after incubation. The agarose gel (0.8%) containing 0.4 μg/mL of EB was prepared and the electrophoresis of the DNA cleavage products was performed on it. The gel was run at 70 V for 90 min in TBE buffer and the bands were identified by placing the stained gel under an illuminated UV lamp. The fragments were photographed by using gel documentation system (BIO RAD).

2.5.5. Protease activity

The stock solutions of BSA were prepared by dissolving BSA (1×10^{-4} mol L^{-1}) in 0.1 M phosphate buffer at pH 7.2 and kept at 0─4 °C for three days under dark conditions and then diluting with 0.1 M phosphate buffer (pH 7.2) to the preferred concentration. The concentration of protein solution was determined from the absorption spectral data using the molar absorptivity value of $\varepsilon_{280} = 44720$ for BSA.(ref) During protein cleavage studies representative complex **3** (10–100 μM) was incubated with BSA (4 μM) in TBE buffer pH 7.4 at 50 °C for 3 h and 20 h respectively. During protein cleavage studies DMF content was kept below 10%. On completion of incubation period samples were subjected to loading buffer 100 mM Tris HCl (pH 6.8), 4% (w/v) sodium dodecyl sulphate, 0.2% (w/v) bromophenol blue, 20% (v/v) glycerol. Protein was denatured by keeping it in hot water at 90°C for 3 minutes. Finally, samples were analyzed using discontinuous SDS–PAGE in a Genei vertical gel electrophoresis apparatus. Experiments were carried out at 80 V (stacking) and 100 V (resolving). Coomassie blue solution was utilized for staining (1 h) and destaining was performed in a mixture of water/ methanol/acetic acid mixture for 3 h.

2.5.6. DPPH assay

DPPH assay was performed in 0.1 M phosphate buffer solution using 10% DMF. Stocks of DPPH and complex **3** were prepared in DMF due to insolubility in buffer.

2.5.7. Measurement of oxidation of o−aminophenol and determination of the concentration of the phenoxazinone

Solutions of complexes **1**−**5** and o−aminophenol were prepared in methanol under aerobic conditions. Concentration of the phenoxazinone formed was calculated using molar extinction coefficient 24×10^3 $M^{-1}cm^{-1}$ at 435 nm.

2.5.8. Density functional theory (DFT) calculations

DFT calculations for complex **1** was carried out using *Gaussian 03* program.[428−430] The Becke's three parameters hybrid exchange functional with the Lee-Yang-Parr (LYP) non−local correlation functional was used for the computational study.[430] During calculations, the basis set used for iron center was the LANL2DZ effective core potential and 6−31G(d) for the ligand atoms (C, H, N, O and Cl). The X−ray coordinates of complex **1** were utilized as input data for geometry optimization. The Gauss View−4 was used to generate the pictorial representation of frontier molecular orbitals.

2.5.9. X−ray structure determination

The X−ray data collection complex **1** was performed at 293 K. Crystal data, data collection parameters and refinement details of the structure determinations have been summarized in Table 2.13.

Table 2.13 Crystallographic parameters of complex **1**

Empirical formula	$C_{38}H_{32}N_6O_8ClFe$
Formula weight (gmol^{-1})	792.00
Temperature /K	293 K
λ (Å) (Mo–Kα)	0.71073
Crystal system	Monoclinic
Space group	P 21
a (Å)	12.728(3)
b (Å)	10.377(2)
c (Å)	12.929(3)
α (°)	90.00
γ (°)	90.00
β (°)	96.682(11)
V (Å^3)	1696.0(7)
Z	2
ρ_{calc} (gcm^{-3})	1.551
Crystal size (mm)	0.19 × 0.17 × 0.16
F(000)	818.0
Theta range for data collection	1.59–30.60
Index ranges	−18<h<18,−14<k<14,−17<l<17
Refinement method	Full matrix least–squares on F^2
Data/restraints/parameters	9300/13/489
GOF^a on F^2	0.989
R$_1$^{b} [I > 2σ(I)]	0.0452
R$_1$[all data]	0.0623
wR$_2$^{c} [I > 2σ(I)]	0.1071
wR$_2$ [all data]	0.1179

^{a}GOF = $[\Sigma[w(F_o^2–F_c^2)^2] /M–N)]^{1/2}$ (M = number of reflections, N = number of parameters refined). ^{b} R$_1$ = $\Sigma\|F_o|–|F_c\|/\Sigma|F_o|$, ^{c} wR$_2$ = $[\Sigma[w(F_o^2–F_c^2)^2]/\Sigma [w(F_o^2)^2]]^{1/2}$

Chapter-3

Generation of Phenoxyl Radical Species, Nuclease and Protease Activity Studies on Manganese Complexes derived from Tridentate Ligand having N_2O Donor

3.1. Abstract

Tridentate ligands ^{OCH3}PhimpH, ^{CH3}PhimpH and ^{tBu}PhimpH having N_2O donors coordinates to manganese(III) after deprotonation affording a series of mononuclear manganese complexes. All the complexes were characterized by elemental analysis, IR and UV–visible spectral studies. Magnetic moments and conductivity measurements suggested the formulation of manganese complexes [Mn(^{OCH3}Phimp)$_2$]ClO$_4$ (**5**), [Mn(^{CH3}Phimp)$_2$]ClO$_4$ (**6**) and [Mn(^{tBu}Phimp)$_2$]ClO$_4$ (**7**) respectively. Molecular structure of **7** was determined by X–ray crystallography and structural features were also explored. Cyclic voltammetric studies were also monitored for all the complexes in the series. DFT and TD–DFT calculations were monitored for representative metal complex to optimize geometrical, structural and electronic parameters. Phenoxyl radical complexes were generated at low temperature using [(NH$_4$)$_2$[Ce^{IV}(NO$_3$)$_6$] in CH$_3$CN solution and were characterized by absorption spectral studies. Representative complex **7** exhibited nuclease as well as protease activity without any external agent.

3.2. Introduction

Manganese and iron have similar chemical and physical properties[1] and both metals show various oxidation states in different ligand environment. Manganese can behave as divalent cation such as calcium, magnesium showing Lewis acidity. On the other hand, it can also behave as a redox active metal responding between II, III and IV. However in photosystem II role of manganese is unique.[431] Manganese is redox active and biologically relevant, hence complexes of manganese are used for various magnetic and catalytic reactions.[432–436] This metal ion is found in the active site of several metalloenzymes such as catalase[436–439], superoxide dismutase,[59,440] manganese dioxygenase,[23] and ribonucleotide reductase[441] etc. Hence manganese complexes have been utilized to explore the structural and functional modelling of various metalloenzymes.[442] There has been considerable interest in metallopharmaceutical research where researchers are more focused towards manganese complexes having biological and oxidative activities.[443,444] Ligand environment around metal centre also plays crucial role to execute such activities. Complexes having nitrogen and phenol donor(s) have been extensively used to study manganese chemistry. In continuation of this, such manganese complexes used for structural and functional mimicking of galactose oxidase (Scheme 1.7–1.8 chapter 1).[192,445] Similar manganese complexes have also been utilized to study nuclease and protease activities[275,446–450] It is important to note that manganese salen type of complexes have been used for Jacobsen catalyst which is used in the asymmetric epoxidation of unfunctionalized olefins.[451–453]

^{CH3}**PhimpH**   R$_1$- H, R$_2$-CH$_3$
^{OCH3}**PhimpH**   R$_1$- H, R$_2$-OCH$_3$
^{tBu}**PhimpH**   R$_1$=R$_2$-3,5 di-tert-butyl
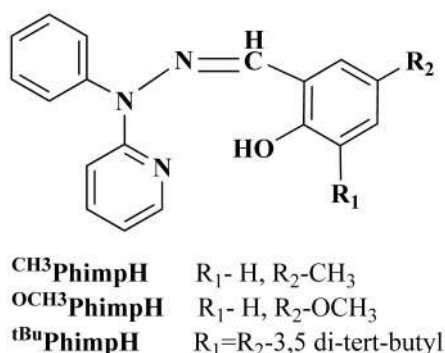
Fig. 3.1 Tridentate ligands with abbreviations used in the present work

In the present chapter, we have synthesized manganese(III) complexes derived from tridentate ligands having N$_2$O donor. Complexes [Mn(^{OCH3}Phimp)$_2$]ClO$_4$ (**5**), [Mn(^{CH3}Phimp)$_2$]ClO$_4$ (**6**) and [Mn(^{tBu}Phimp)$_2$]ClO$_4$ (**7**) were characterized using IR, UV–visible, ESI–MS spectral studies. Magnetic and electrochemical properties were also examined using these complexes. Molecular structure of **7** was determined by X–ray crystallography. Due to the presence of phenolato moiety in ligand framework, phenoxyl radical generation and stability of manganese–coordinated phenoxyl radical species were studied using absorption spectral studies. Theoretical (DFT, TD-DFT) calculations were performed to optimize geometry and characteristic structural parameters were evaluated. Electronic spectral properties were also scrutinized using TD–DFT calculation and data obtained were compared with the experimental values. Complex **7** was used for nuclease and protease activity studies.

3.3. Results and discussion

3.3.1. Synthesis and characterization of ligands

Synthesis and characterization of tridentate ligand having N$_2$O donor have been already described in chapter 1.

3.3.2. Synthesis and characterization of metal complexes

Synthesis of mononuclear manganese(III) complexes were carried out at ambient temperature in air. To a stirred solution of deprotonated ligand was added Mn(ClO$_4$)$_2$.6H$_2$O

dropwise in a ratio of 2:1 respectively. Similar complexes were also synthesized following a different procedure using $Mn(OAc)_3.2H_2O$ as a starting metal salt using $MeOH:H_2O$ (9:1) as solvent system. Procedures followed for the synthesis of all the complexes were same. Schematic representation of the synthesis of complexes **5–7** have been assigned in the Scheme 3.1.

^{OCH3}PhimpH	R_1- H, R_2-OCH$_3$		**5**	[Mn(^{OCH3}Phimp)$_2$]ClO$_4$
^{CH3}PhimpH	R_1- H, R_2-CH$_3$		**6**	[Mn(^{CH3}Phimp)$_2$]ClO$_4$
^{tBu}PhimpH	R_1=R_2-3,5 di-tert-butyl		**7**	[Mn(^{tBu}Phimp)$_2$]ClO$_4$
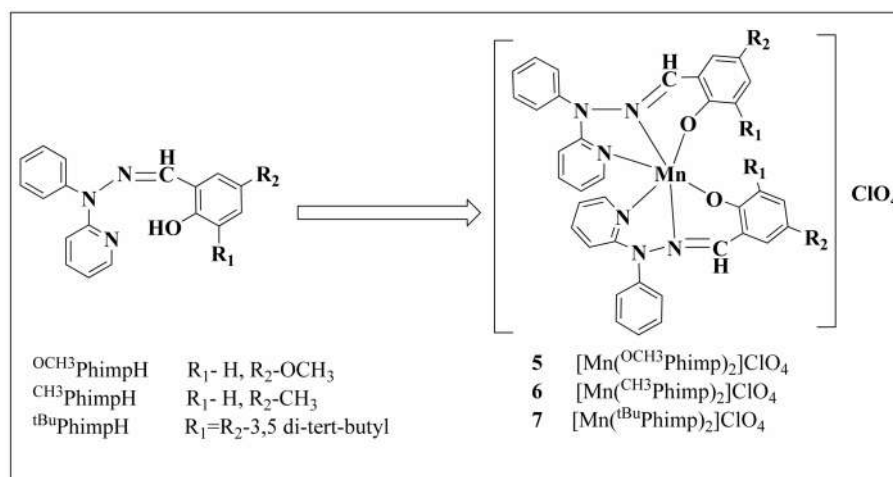
Scheme 3.1 Schematic representation of synthesis of manganese complexes

3.3.2.1. IR spectral studies

A significant shift (~20 cm^{-1}) in stretching frequencies for $\nu_{-HC=N}$ suggested the coordination of azomethine nitrogen (–HC=N–) to metal centre.[396] A strong and sharp band due to azomethine moiety ($\nu_{-HC=N}$) was observed in the range 1600–1610 cm^{-1} in all the three manganese complexes. Bands in the region near ~1090 cm^{-1} together with a band at ~623 cm^{-1} were observed in all manganese(III) complexes. These bands clearly assigned to non−coordinated perchlorate ions.[401] Experimental values of IR data for all the complexes have been listed in Table 3.1.

Table 3.1 Data for IR and conductivity studies of complexes

Complex	IR data $(cm^{-1})^a$			Conductivity data $(\Omega^{-1}cm^2mol^{-1})^b$
	ν_{O-H}	$\nu_{-HC=N}$	ν_{ClO4^-}	
5	3433	1603	1089, 624	58.0 (1:1)
6	3432	1607	1094, 623	61.0 (1:1)
7	3431	1608	1092, 621	56.0 (1:1)

[a]Using KBr pellets, [b]Solvent: dimethylformamide

3.3.2.2. Electronic absorption spectral studies

UV−visible spectra of complexes **5**–**7** have been shown in Fig. 3.2 and data have been summarized in Table 3.2. Band originated above 400 nm in all the complexes was assigned to phenolato oxygen to manganese(III) ligand to metal charge transfer transitions.[454] Bands at lower energy around 300 nm were assigned n–π* in nature and high energy band around 230 nm as π –π* transitions.[174,403,405]

Table 3.2 Electronic absorption spectral data of manganese complexes

Complex	UV−visible data $(\lambda_{max}/nm, \varepsilon/M^{-1}cm^{-1})^a$
5	498 (520), 400 (51,780), 308 (15,380), 236 (20,400), 201 (31,010)
6	402 (8,390), 332 (17,100), 305 (17,810), 237 (26,280), 202 (44,820)
7	422 (11,900), 340 (41,100), 306 (47,700), 242(69,700), 205 (97,000)

[a]UV−visible data in methanol
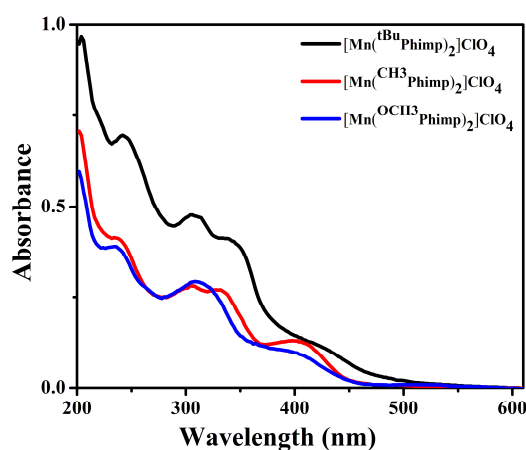
Fig. 3.2 UV−visible absorption spectra of manganese(III) complexes in methanol

3.3.2.3. Conductivity studies

Molar conductivity measurements were performed using complexes **5–7** in DMF at ca. 10^{-3} M. Values obtained for complexes **5**, **6** and **7** have been found 58, 61 and 56 respectively at 25 °C indicating the uni–univalent (1:1) electrolytic behavior in DMF solution[406] (Table 3.1).

3.3.2.4. Magnetic moment studies

Magnetic moments were calculated for complexes **5**, **6** and **7** at 300 K. The values of magnetic moments were found to be 4.84, 4.91 and 4.97 BM respectively. These values indicated the presence of high–spin magnetically diluted d^4 manganese(III) metal centre.[455,456]

3.3.2.5. ESI–MS spectral studies

Complexes **5** and **7** were subjected to the ESI–MS spectral studies to confirm the proper synthesis of metal complexes. All the complexes showed characteristic peak corresponding to $[M-ClO_4]^+$ in acetonitrile solution under positive ion mode. ESI–MS spectrum of complex **5** displayed peak at 659.1977 corresponding to $[M-ClO_4]^+$ as shown in Fig. 3.3.
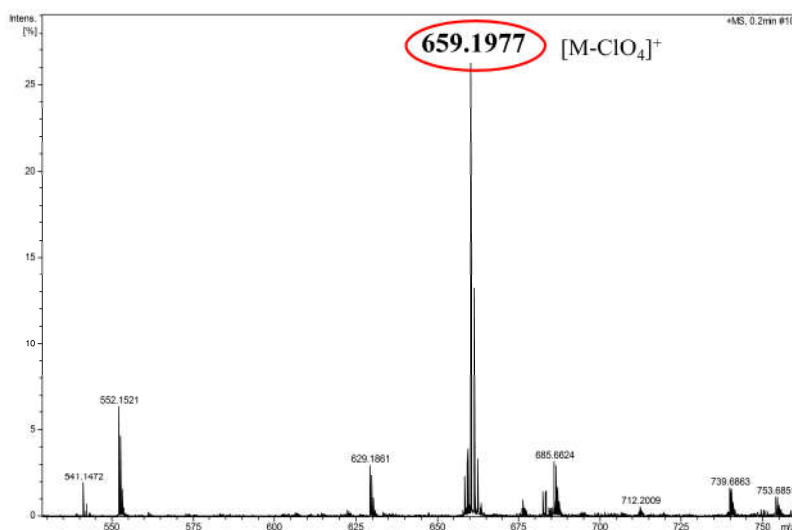
Fig. 3.3 ESI–MS spectrum of complex **5** in acetonitrile solution under positive ion mode

Complex **7** displayed peak corresponding to $[M–ClO_4]^+$ at 855.4180 in acetonitrile solution under positive ion mode (Fig. 3.4).
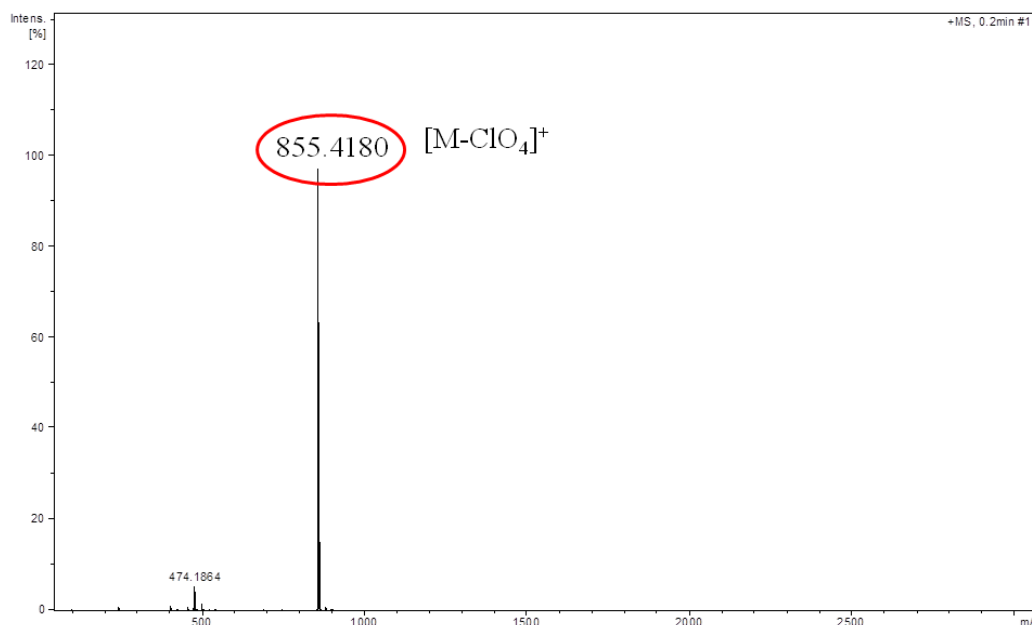
Fig. 3.4 ESI–MS spectrum of complex **7** in acetonitrile solution under positive ion mode

3.3.3. Molecular structure of complex 7

Molecular structure of complex **7** has been shown in Fig. 3.5. Single crystals of X–ray diffraction quality were grown in the dichloromethane:methanol (1:1) solvent system on slow evaporation. Crystallographic data and details of refinement and data collection have been described in Table 3.9.
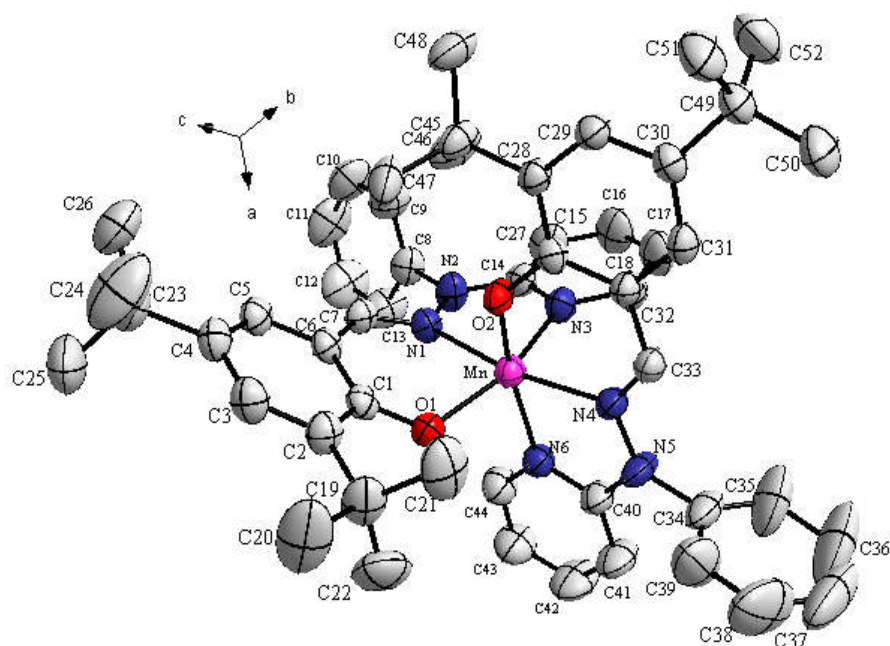
Fig. 3.5 Thermal ellipsoid diagram of the crystal structure of **7** showing the atom numbering scheme and thermal ellipsoids (50% probability level). Hydrogen atoms are omitted for clarity

Complex crystallized in triclinic P−1 space group in a distorted octahedral geometry. Manganese(III) metal centre is surrounded by two ligands in meridional fashion having N_4O_2 donor atoms. The trans atoms exhibited an N(4)−Mn−N(1), O(2)−Mn−N(6) and N(3)−Mn−O(1) angle of 167.02°, 164.13° and 154.04° respectively. Trans angles considerably deviates from the linearity as described in Table 3.3. Bond distances between Mn−N$_{py}$ are found to be very similar and vary in the narrow range from 2.039 Å (Mn−N6) to 2.157 Å (Mn−N3). Bond distances for Mn−N$_{im}$ 2.184 Å (Mn−N1) and 2.099 Å (Mn−N4) are also comparable to the reported manganese(III) high−spin metal centred complexes.[456–460] [482-486] Manganese to phenolato bond distances were found to be 1.924 Å (Mn−O1) and 1.836 Å (Mn−O2) and consistent to the reported in literature.[456–460] A considerable distortion from ideal octahedral geometry was observed due to ligand rigidity imposed by the adjacent five−and six−membered chelate rings.[461] Characteristic bond lengths and bond angles have been described in the Table 3.3.

117

Table 3.3 Selected bond lengths (Å) and angles (°) of complex **7**

Bond length (Å)		Bond angles (°)	
Mn–N1	2.184(22)	N(1)–Mn–O(1)	81.79(89)
		N(1)–Mn–N(6)	104.50(92)
Mn–N3	2.157(24)	N(3)–Mn–O(1)	154.04(89)
		N(3)–Mn–O(2)	95.32(94)
		N(3)–Mn–N(1)	73.77(88)
		N(3)–Mn–N(4)	93.28(93)
		N(3)–Mn–N(6)	91.82(93)
Mn–N4	2.099(24)	N(4)–Mn–O(1)	111.13(93)
		N(4)–Mn–O(2)	89.29(93)
		N(4)–Mn–N(1)	167.02(94)
		N(4)–Mn–N(6)	76.14(94)
Mn–N6	2.039(26)	–	–
Mn–O1	1.924(21)	O(1)–Mn–N(6)	85.82(91)
Mn–O2	1.836(21)	O(2)–Mn–O(1)	93.77(89)
		O(2)–Mn–N(1)	91.12(91)
		O(2)–Mn–N(6)	164.13(97)

Importance of non–covalent interaction in crystal engineering and supramolecular chemistry is widely known.[418] Packing diagram of the complex **7** has been shown in the Fig. 3.6.
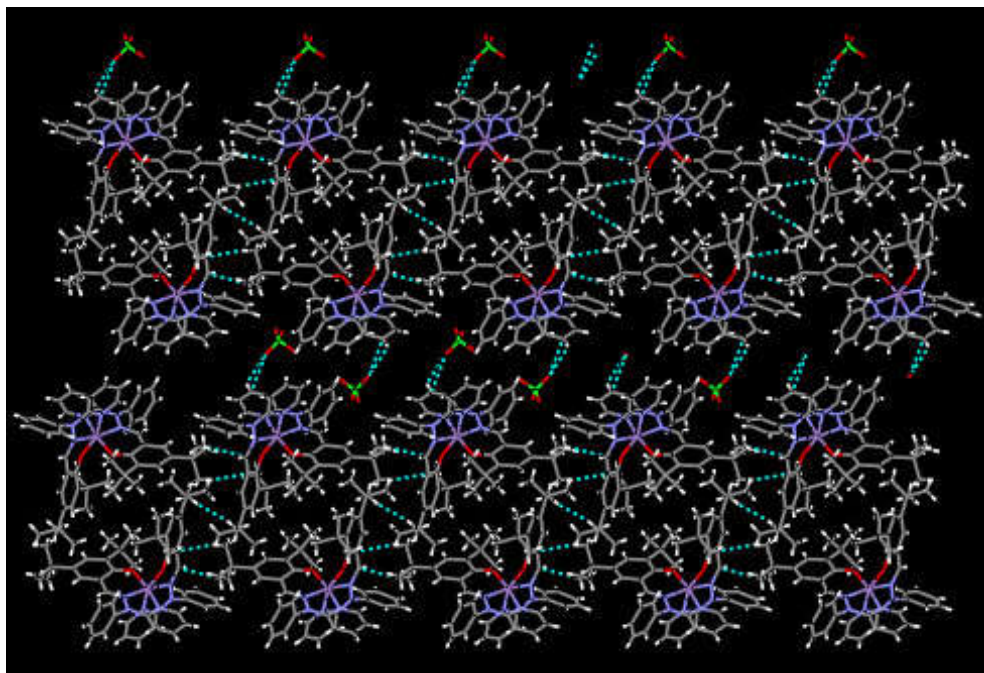
Fig. 3.6 Packing diagram of complex **7**

Complex **7** exhibited non−covalent interactions which have been depicted in the Fig. 3.7 and listed in Table 3.4. Non−covalent interactions were observed between O atoms of perchlorate ion and aromatic hydrogens of pyridine rings. Protons of *tert*−butyl group exhibit non−covalent interactions with the aromatic ring having phenolato moiety in the ligand frame.
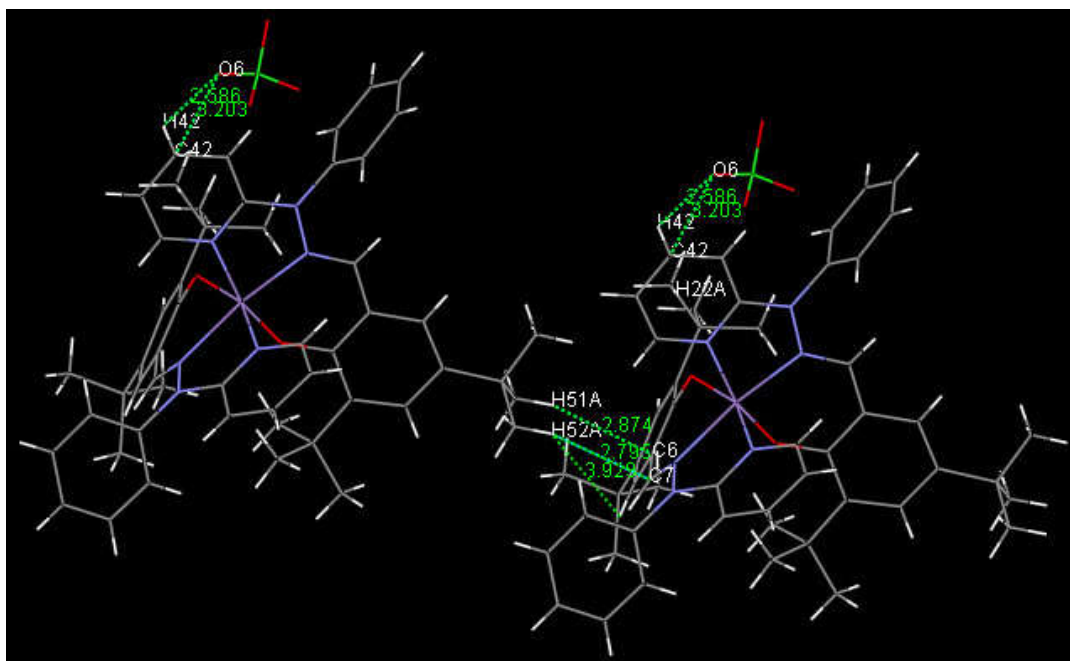
Fig. 3.7 Non–covalent interactions in **7**

Table 3.4 Non–covalent interactions in complex **7**

Atom	Distance (Å)
C42–H42·····O6	2.686
H6–C6·····H51	2.874
H7–C7·····H52	2.796

3.3.4. Density functional theory (DFT) calculations

DFT calculations were performed to optimize the geometry of complex **7** and structural parameters were also monitored. The highest occupied molecular orbital (HOMO) and the lowest unoccupied molecular orbital (LUMO) of complexes have been depicted in Fig. 3.8–3.9.

(a) (b)
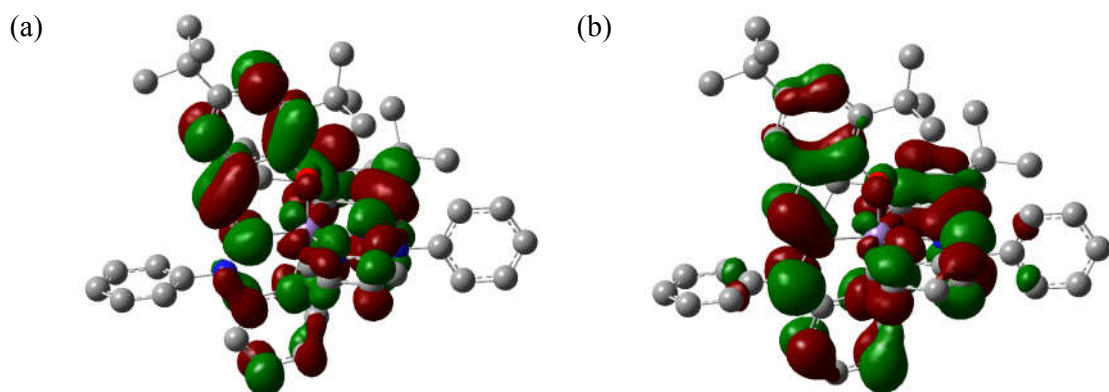
Fig 3.8 Molecular orbital diagram of HOMO (a) alpha and (b) beta of complex **7**

(a) (b)
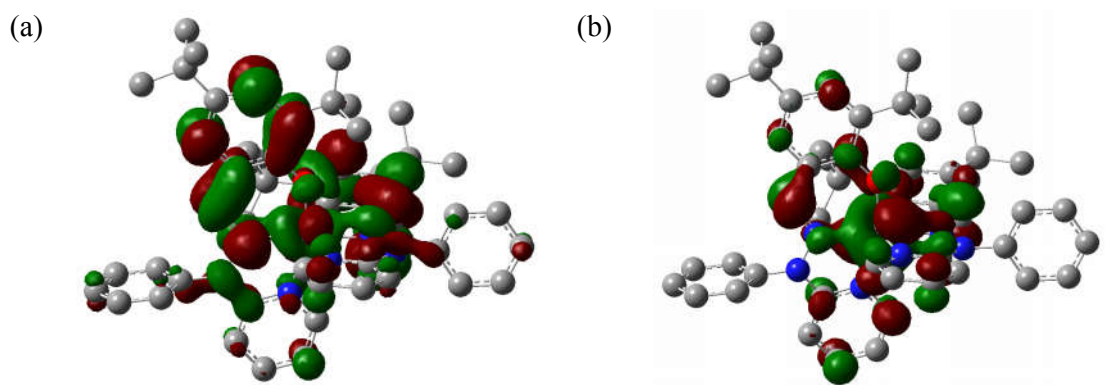
Fig 3.9 Molecular orbital diagram of LUMO (a) alpha and (b) beta of complex **7**

HOMO and LUMO orbital were having mixed contribution from the metal as well as ligands. Structual parameters were consistent with that obtained from single crystal X–ray spectroscopy (Table 3.5).

121

Table 3.5 Comparison of theoretical and experimental bond lengths and bond angles of

complex **7** using S=6

	Bond lengths (Å)			Bond angles (°)		
	X–ray	DFT			X–ray	DFT
Mn–N1	2.184(22)	2.194	N(1)–Mn–O(1)		81.79(89)	97.88
			N(1)–Mn–N(6)		104.50(92)	75.57
Mn–N3	2.157(24)	2.090	N(3)–Mn–O(1)		154.04(89)	161.51
			N(3)–Mn–O(2)		95.32(94)	89.69
			N(3)–Mn–N(1)		73.77(88)	99.48
			N(3)–Mn–N(4)		93.28(93)	75.58
			N(3)–Mn–N(6)		91.82(93)	88.52
Mn–N4	2.099(24)	2.193	N(4)–Mn–O(1)		111.13(93)	86.58
			N(4)–Mn–O(2)		89.29(93)	97.92
			N(4)–Mn–N(1)		167.02(94)	173.24
			N(4)–Mn–N(6)		76.14(94)	99.47
Mn–N6	2.039(26)	2.090	–		–	–
Mn–O1	1.924(21)	1.868	O(1)–Mn–N(6)		85.82(91)	89.68
Mn–O2	1.836(21)	1.868	O(2)–Mn–O(1)		93.77(89)	97.68
			O(2)–Mn–N(1)		91.12(91)	86.57
			O(2)–Mn–N(6)		164.13(97)	161.48

Electronic spectral properties were also monitored for the complex **7** and compared with the experimental values. Table 3.6 shows contribution of orbitals associated to the particular transitions. Experimental and theoretical data was found to be fairly consistent.

Table 3.6 Calculated TD–DFT excitation energies (in eV), oscillator strengths (f), and

nature of transitions in the complex **7**

Transitions (% Contribution)		E (eV)	Oscillator	λ_{theo}	λ_{exp}
Alpha orbitals (%)	Beta orbitals (%)	theo/exp	strength (f)	(nm)	(nm)
HOMO–1➢LUMO+2 (45)	HOMO–1➢LUMO+2(4)	2.92/2.42	0.0002	424	422
HOMO ➢ LUMO+1 (45)	HOMO➢LUMO+5 (3)				
HOMO ➢ LUMO+4 (2)					
HOMO–3➢LUMO+4(13)	HOMO➢LUMO+6 (39)	3.64/3.64	0.0390	340	340
HOMO–1➢LUMO+4(11)	HOMO–4➢LUMO (23)				
HOMO–2➢ LUMO+3(8)	HOMO–1➢LUMO+3(17)				
HOMO ➢ LUMO+3(8)	HOMO ➢LUMO+8(15)				
HOMO–4➢ LUMO+3(6)	HOMO–3➢LUMO+3(3)				
HOMO–5➢ LUMO+1(5)	HOMO–2➢LUMO+4(3)				
HOMO–6➢ LUMO(4)	HOMO–3➢LUMO+1(44)				

3.3.5. Electrochemical studies

Redox properties of metal complexes have been investigated using electrochemical studies in dichloromethane solution. Redox potentials associated with all the complexes have been shown in the Table 3.7. Ligands do not show any redox activity in the range of −1.0 to 0.6 V *vs.* Ag/AgCl as described in the chapter 2. Hence peak found in the range is mainly attributed to the molecular orbital that is having metal character as Mn(III)/Mn(II) couple. All the complexes exhibited quasi–reversible redox process and follow the order **5** > **7** > **6** (Table 3.7). In all the complexes peak found in the potential range 0.8 to 1.8 V are probably associated with some ligand associated oxidation.[445]

Table 3.7 Electrochemical data for manganese(III) complexes at 298 K[a] *vs* Ag/AgCl

Complex	Mn(III)/Mn(II)			Ligand centre		
	E^1_{pa}/V	E^1_{pc}/V	$E^1_{1/2}$[b], V (ΔE_p[c], mV)	E^2_{pa}	E^2_{pa}	$E^2_{1/2}$[b], V (ΔE_p[c], mV)
5	0.325	0.101	0.213 (224)	1.160	0.972	0.188(188)
6	−0.132	−0.230	−0.181 (98)	1.052	1.210	0.979 (144)
				1.351	0.906	1.275 (141)
7	0.238	0.994	0.127 (222)	0.994	0.871	0.932 (123)

[a]Measured in dichloromethane using 0.1 M tetrabutylammonium perchlorate (TBAP). [b]$E_{1/2}$ values were calculated as average of anodic (E_{pa}) and cathodic (E_{pc}) peak potentials and [c]$\Delta E_p = E_{pa} - E_{pc}$ at scan rate of 0.1 V/s.

Cyclic voltammogram of complexes **5**–**7** have been depicted in Fig. 3.10
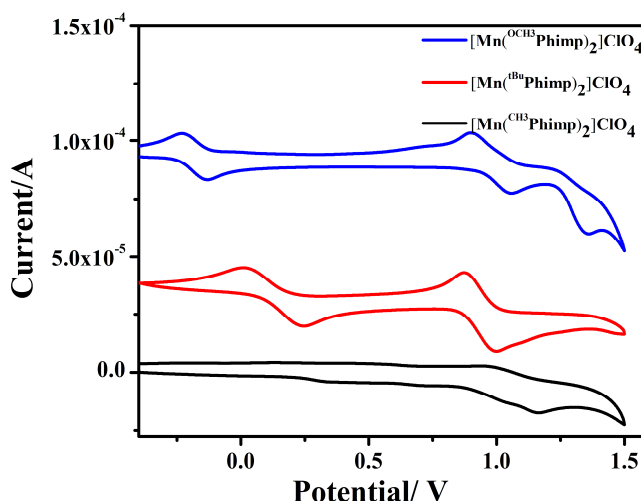
Fig. 3.10 Cyclic voltammograms of 10^{-3} M solution of complexes **5**, **6** and **7** at a scan rate of 0.1 V/s

3.3.6. Generation of phenoxyl radical

Generation of phenoxyl radical complexes were monitored by oxidation of complexes **5**–**7** using $(NH_4)_2[Ce^{IV}(NO_3)_6]$ (CAN) in acetonitrile solutions. These chemistry are very important for the active site modeling of galactose and glyoxal oxidase metalloenzymes.[462,463] UV–visible spectral properties were utilized to observe the generation of phenoxyl radical complex during addition of CAN to the solutions of metal complexes at low temperature (0°C). Upon addition of CAN, charge transfer band of the

124

complex **5** at 420 nm was decreased and shifted to the higher wavelength (432 nm). Appearance of the new low intense broad band at 600 nm was also observed is probably due to the generation of phenoxyl radical complex. Titration of variable amount of CAN was also performed to optimize proper concentration of CAN for band generation (Fig. 3.11).
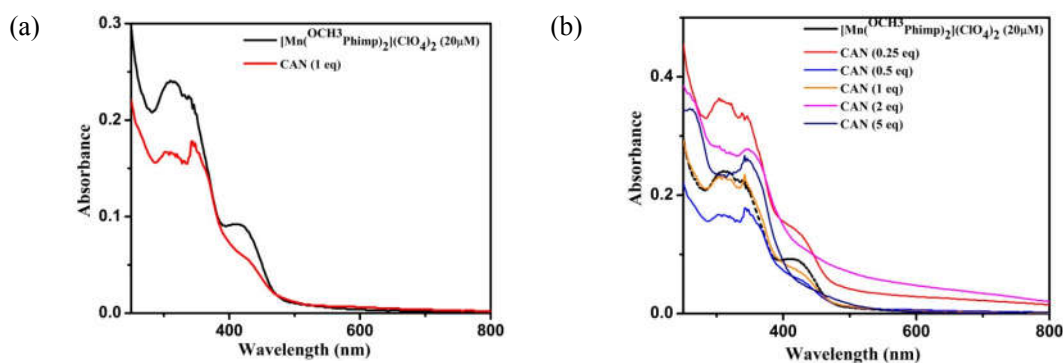
Fig. 3.11 (a) In situ generation of phenoxyl radical using 1 eq of CAN in acetonitrile, (b) titration of complex **5** with variable concentration of CAN in acetonitrile at 0°C

Similarly during the addition of CAN to the solution of complex **6** in acetonitrile, changes were observed in electronic spectral properties. The band monitored at 400 nm in the complex **6** was found to be shifted to 413 nm on addition of CAN to the acetonitrile solution of the same. A broad band was also observed at 620 nm as shown in the Fig. 3.12. A similar titration to optimize proper concentration of CAN for the generation of phenoxyl radical was also performed (Fig. 3.12b).
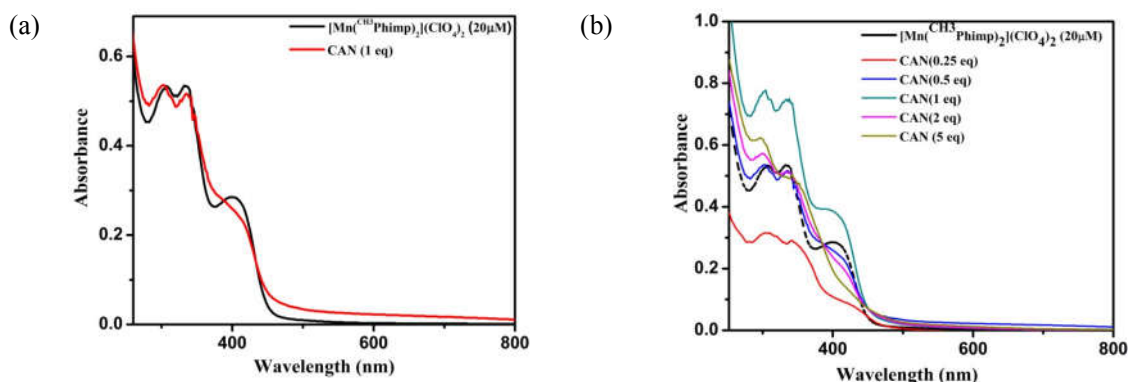
Fig. 3.12 (a) In situ generation of phenoxyl radical using 1 eq of CAN in acetonitrile, (b) titration of complex **6** with variable concentration of CAN in acetonitrile at 0°C

Similar behavior to the above complexes was observed in case of complex **7**. Charge transfer band found at 400 nm was shifted to higher wavelength (420 nm) along with a broad band at 620 nm with the addition of CAN. Fig. 3.13 depicts the change observed during the addition of CAN and titration performed for the optimization of proper concentration of CAN for the generation of phenoxyl radical complex. Table 3.8 shows band generated during the addition of CAN in the acetonitrile solution of complexes **5–7**.
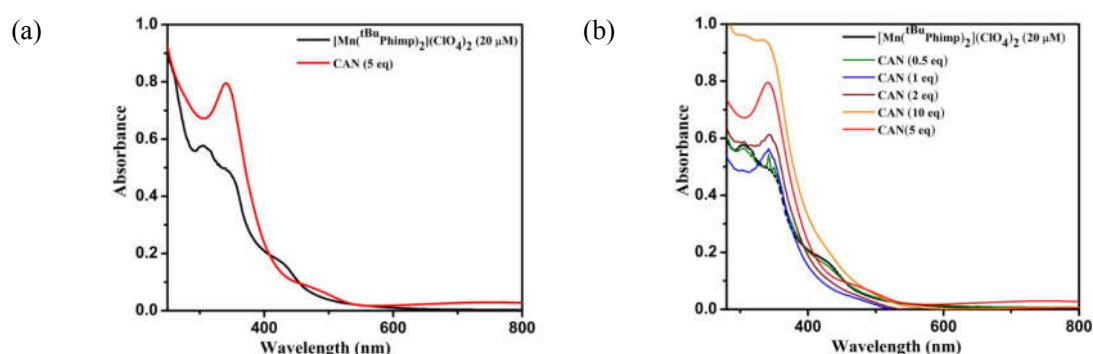
Fig. 3.13 (a) In situ generation of phenoxyl radical using 1 eq of CAN in acetonitrile, (b) titration of complex **7** with variable concentration of CAN in acetonitrile at 0°C

Table 3.8 UV–visible data of phenoxyl radical of complexes **5–7**

Complex	λ_{max} (nm)[a]
5	432, 600
6	413, 620
7	420, 620

[a] new bands originated during the addition of CAN in acetonitrile at 0°C

The new band generated at 600 nm is probably similar to the band due to phenoxyl radical and manganese(III) ion as described earlier.[193] These band generated *via* addition of CAN are fairly similar to that generated electrochemically.[464] The broad band generated at higher wavelength (>600 nm) is probably due to the (phenolate to manganese(III) charge

126

transfer transition (LMCT) from the π_p orbital on the phenolate oxygen to the half–filled manganese(III) $d\pi^*$ orbital[445,465] while the band originated at ~400 nm is due to the LMCT process originated from the p_π orbital to the d_σ^* orbital transitions of the coordinated phenoxyl radical.[268,466] Hence it can be concluded from the UV–visible spectral studies that phenoxyl radical were generated in solution in all the three complexes. The intensities of the characteristic bands at about 420 nm and 600 nm depend on the addition of amount of CAN.

Stabilities of phenoxyl radical in complexes **5–7** were also optimized using absorption spectral studies. The stability of phenoxyl radical was monitored at 432 nm and the radical was found to be stable for 80 sec for complex **5**. The decay profile of phenoxyl radical has been shown in the Fig. 3.14. The stability of radical generated for complex **6** was also monitored at 413 nm similar to that of complex **5** and found to be 85 sec. In case of complex **7** the stability of radical was slightly higher (100 sec) as compared to complex **5** and **6** (Fig. 3.14). The order of complexes stability was found to be **7**> **6** > **5** at lower energy transition. Complex **7** was found to be most stable probably due to the presence of electron donating group in ligand framework.[268] From the studies it can be concluded that radical species generated was unstable and decomposes within few seconds.
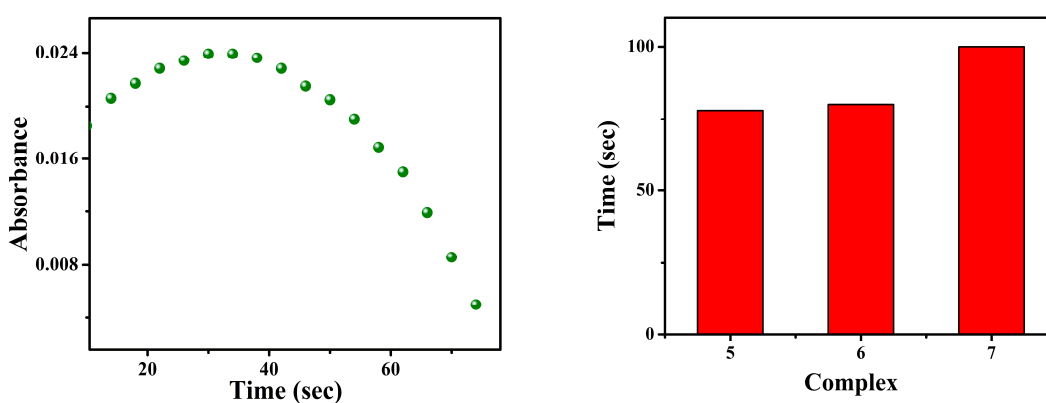
Fig. 3.14 Stability of phenoxyl radical formed on addition of CAN (2eq) in complex **5** (100 μM) with time

3.3.7. Nuclease activity

Oxidative DNA cleavage activity of complex **7** was investigated. Complex **7** was incubated with *pBR322 DNA* for 2 h. Complex **7** has been utilized because this complex is capable of generating stable phenoxyl radical as compare to other complex. Variable concentration of complex **7** was utilized to incubate with DNA. Fig. 3.15 indicates that with the variation of complex concentrations in lane 3–6 (10 μM, 25 μM, 50 μM and 100 μM respectively) nuclease activity increases. It is observed here that the complex showed self−activated nuclease activity i.e. the complex is efficient in DNA cleavage activity without any oxidizing and reducing agents.
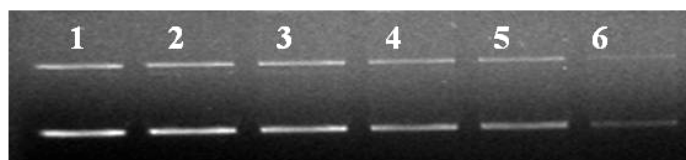
Fig. 3.15 Gel electrophoresis separations showing the cleavage of supercoiled *pBR322* DNA (100 ng) using complexes **7** in a 0.1 M phosphate buffer containing 10% DMF and incubated at 37 °C for 2 h. Lane 1: DNA control, lane 2: DNA control + DMF (10%), lane 3−6, DNA + **7** (10 μM, 25 μM, 50 μM and 100 μM respectively)

3.3.8. Protease activity

Complex **7** was used as a representative complex to monitor protein cleavage activity. BSA was subjected to SDS–PAGE at 50 °C with 3 h incubation with the variation of concentrations of complex **7** as depicted in Fig. 3.16. BSA was incubated with variable concentrations of complex to optimize the effect of concentration of complex. It was concluded that at 50 μM and 100 μM concentrations, band of BSA becomes faded as compared to the BSA alone. These results support the non−specific cleavage of BSA into very small fragments.[360] Hence complex **7** exhibited self−activated nuclease activity without any reducing or oxidizing agent.
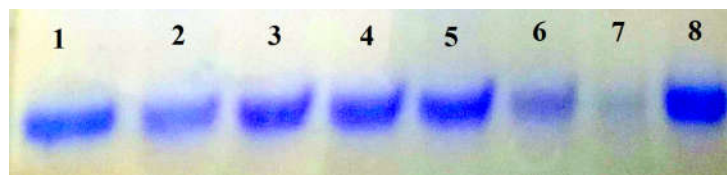
Fig. 3.16 SDS−PAGE of BSA (4 μM) incubated with complex **7** in a 0.1 M buffer containing 10% DMF incubated at variable temperature and concentration of complex at 50 °C for 20 h. Lane 1: BSA, Lane 2: BSA + Fe(ClO$_4$)$_3$.xH$_2$O (100 μM), Lane 3: BSA + ^{tBu}PhimpH (100 μM), Lane 4: BSA + **7** (10 μM), Lane 5: BSA + **7** (25 μM), Lane 6: BSA + **7** (50 μM), Lane 7: BSA + **7** (100 μM), Lane 8: BSA + DMF (10%)

3.3.9. DPPH assay

DPPH (2,2–diphenyl–1–picrylhydrazine) was utilized to study any rective oxygen species involved as described in chapter 2. Violet color of DPPH disappears during antioxidant property quantification estimations. Experiment was performed in 0.1 M phosphate buffer containing 10% DMF. DMF solution of complex **7** ($4×10^{-5}$ M) was taken with DPPH radical ($1.2 × 10^{-4}$ M) and a decrease in absorbance was observed at 540 nm (Fig. 3.17).
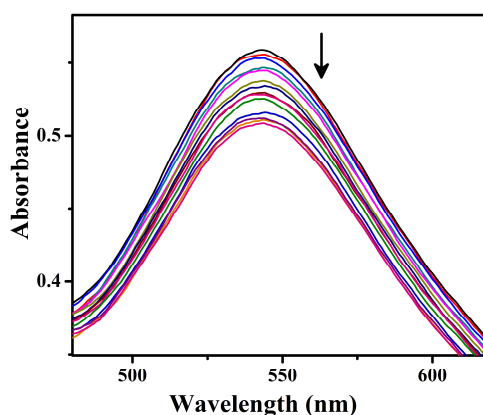
Fig. 3.17 Disappearance of absorption band of DPPH radical at 540 nm using complex **7** in 0.1 M phosphate buffer containing 10% DMF solution

3.4. Conclusions

A series of novel mononuclear manganese complexes have been synthesized using tridentate ligands ^{OCH3}PhimpH, ^{CH3}PhimpH and ^{tBu}PhimpH having N$_2$O donors.

Hexa–coordinated manganese complexes [Mn(^{OCH3}Phimp)$_2$]ClO$_4$ (**5**), [Mn(^{CH3}Phimp)$_2$]ClO$_4$ (**6**) and [Mn(^{tBu}Phimp)$_2$]ClO$_4$ (**7**) have been synthesized and characterized using various spectroscopic studies. Molecular structure of complex **7** has been determined using single crystal X–ray diffraction study. Theoretical calculations (DFT, TD–DFT) were also performed and electronic as well as structural parameters were evaluated. Redox properties were also examined for all the three complexes by cyclic voltammetric studies. Phenoxyl radical generation was studied for complexes using absorption spectral studies. Stability order for phenoxyl radical species generated in solution was found to be **7** > **6** > **5**. Complex **7** was further used for nuclease and protease activity. Complex **7** found to be potent self–activated artificial chemical nuclease as well as protease. To the best of our knowledge generation of reactive oxygen species and/or radical were responsible for nuclease and protease activity.

3.5. Experimental section

3.5.1. Materials and instrumental methods

Analytical reagents were utilized for synthesis purpose. Metal salts $Mn(ClO_4)_2.6H_2O$ and $Mn(CH_3COO)_3.2H_2O$ (Sigma Aldrich, Steinheim, Germany) were used as obtained. Sodium perchlorate was purchased from Himedia Laboratotries PVT. LTD., Mumbai, India. The supercoiled *pBR322* DNA and CT−DNA were purchased from Bangalore Genei (India) and stored at 4 °C. Agarose (molecular biology grade) and ethidium bromide were obtained from Sigma Aldrich. Tris (hydroxymethyl) amino methane−HCl (Tris−HCl) buffer and phosphate buffer were prepared in deionised water.

3.5.2. Synthesis of metal complexes

Caution! Perchlorate salts of metal complexes with organic ligands are potentially explosive. Only a small quantity of material should be prepared and handled carefully.

3.5.2.1. Synthesis of $[Mn(^{OCH3}Phimp)_2](ClO_4)$ (5)

Method A

A batch of triethylamine (Et_3N) (133.3 mg, 1.32 mmol) was added to stirred solution of ligand ($^{OCH3}PhimpH$) (421.0 mg, 1.32 mmol) in 10 mL methanol. After stirring for half an hour, a batch of $Mn(ClO_4)_2 \cdot 6H_2O$ (238.0 mg, 0.66 mmol) in 5 mL of methanol was added dropwise. The colour of solution changed to brown. Reaction was further stirred for 3 h, solvent was evaporated to give brown solid which was washed with small amount of methanol, diethylether and dried in vacuum. Yield: 65%. Selected IR data (KBr, v_{max}/cm^{-1}): 1603, $v_{C=Nimine,}$ 1089, 624, $v_{ClO4}-$. UV−visible [CH_3OH, λ_{max}/nm ($\varepsilon/M^{-1}cm^{-1}$)]: 498 (520), 400 (51,780), 308 (15,380), 236 (20,400), 201 (31,010). μ_{eff} (303 K): 4.84 BM. $\Lambda_M/\Omega^{-1}cm^2mol^{-1}$ (in DMF): 58 (1:1). Anal. Calcd for $C_{38}H_{32}N_6O_8Mn$: C, 57.69; H, 4.08; N, 10.62, Found: C, 56.88; H, 4.15; N, 8.44.

Method B

To a solution ^{OCH3}PhimpH (638 mg, 2.00 mmol) in dichloromethane (8 mL) was added a methanol:water (4.5:0.5 mL) solution of Mn(CH$_3$COO)$_3$.2H$_2$O (268 mg, 1.00 mmol) dropwise. After complete addition reaction mixture was further stirred for 3–4 h at room temperature. Sodium perchlorate (140 mg, 1.00 mmol) was added to the reaction mixture. A brown color solution was stirred for half an hour and filtered. Filtrate was evaporated to dryness. The complex was recrystalized using ether diffusion into a mixture of acetonitrile/methanol.

3.5.2.2. Synthesis of [Mn(^{CH3}Phimp)$_2$](ClO$_4$) (6)

Method A

Complex **6** was synthesized following the similar procedure as mentioned above using ^{CH3}PhimpH (606 mg, 2.00 mmol) as a ligand. Yield: 68%. Selected IR data (KBr, ν_{max}/cm^{-1}): 1607, $\nu_{C=Nimine}$, 1094, 623, ν_{ClO4}–. UV–visible [CH$_3$OH, λ_{max}/nm (ε/M^{-1}cm^{-1})]: 402 (8,390), 332 (17,100), 305 (17,810), 237 (26,280), 202 (44,820). μ_{eff} (303 K): 4.91 BM. Λ_M/Ω^{-1}cm^{2}mol^{-1} (in DMF): 61 (1:1). Anal. Calcd for C$_{38}$H$_{32}$N$_6$O$_6$Mn: C, 60.13; H, 4.25; N, 11.07, Found: C, 59.87; H, 4.01; N, 9.78.

Method B

Similar as followed for complex **5** instead of ligand ^{OCH3}PhimpH, ^{CH3}PhimpH was used.

3.5.2.3. Synthesis of [Mn(^{tBu}Phimp)$_2$](ClO$_4$) (7)

Method A

Complex **7** was synthesized following the similar procedure as mentioned above using ^{tBu}PhimpH (804 mg, 2.00 mmol) as a ligand. A brown color solution was stirred for half an hour and filtered. Filtrate was evaporated to dryness. The complex was recrystalized using ether diffusion into a mixture of dichloromethane:methanol. Yield: 59%. Selected IR data (KBr, ν_{max}/cm^{-1}): 1608, $\nu_{C=Nimine}$, 1092, 621, ν_{ClO4}–. UV–visible [CH$_3$OH, λ_{max}/nm (ε/M^{-1}cm^{-}

^{1})]: 422 (11,900), 340 (41,100), 306 (47,700), 242 (69,700), 205 (97,000). μ_{eff} (303 K): 4.97 BM. $\Lambda_M/\Omega^{-1}cm^2mol^{-1}$ (in DMF): 56 (1:1). Anal. Calcd for $C_{52}H_{60}N_6O_6Mn$: C, 65.37; H, 6.33; N, 8.80, Found: C, 63.43; H, 6.51; N, 7.59.

Method B

Similar as followed for complex **5** instead of ligand ^{OCH3}PhimpH, ^{tBu}PhimpH was used.

3.5.3. Generation of the phenoxyl radical complexes

Phenoxyl radical species of the manganese complexes **5**–**7** were generated *in situ* by adding $(NH_4)_2[Ce^{IV}(NO_3)_6]$ (CAN) into a CH_3CN solution of phenolate complexes (1.0×10^{-4} M) in UV cell at 0 °C.

3.5.4. Nuclease activity

As mentioned in chapter 2.

3.5.5. Protease activity

As mentioned in chapter 2.

3.5.6. DPPH assay

As mentioned in chapter 2.

3.5.7. Density functional theory (DFT) calculations

As described in chapter 2.

3.5.8. X–ray structure determination

The X–ray data collection for complexes **7** was performed at 293 K. Crystal data, data collection parameters and refinement details of the structure determinations of complexes **7** summarized in Table 3.9.

Table 3.9 Crystallographic parameter of complex **7**

Empirical formula	$C_{52}H_{60}N_6O_6ClMn$
Formula weight (gmol^{-1})	955.48
Temperature /K	293 K
λ (Å) (Mo–Kα)	0.71073
Crystal system	Triclinic
Space group	P –1
a (Å)	10.656(3)
b (Å)	12.775(4)
c (Å)	20.582(6)
α (°)	94.402(15)
γ (°)	101.938(14)
β (°)	95.490(17)
V (Å^3)	2715.1(13)
Z	2
ρ_{calc} (gcm^{-3})	1.169
Crystal size (mm)	0.16 × 0.14 × 0.13
F(000)	1008.0
Theta range for data collection	1.00–28.52
Index ranges	–14<h<14,–17<k<16,–26<l< 27
Refinement method	Full matrix least–squares on F^2
Data/restraints/parameters	13344/0/608
GOF^a on F^2	0.990
R$_1$^{b} [I > 2σ(I)]	0.0668
R$_1$[all data]	0.1319
wR$_2$^{c} [I > 2σ(I)]	0.1769
wR$_2$ [all data]	0.2030

^{a} GOF = $[\Sigma[w(F_o^2-F_c^2)^2]/M-N)]^{1/2}$ (M = number of reflections, N = number of parameters refined). ^{b} R$_1$ = $\Sigma\|F_o\|-\|F_c\|/\Sigma\|F_o\|$, ^{c} wR$_2$ = $[\Sigma[w(F_o^2-F_c^2)^2]/\Sigma[w(F_o^2)^2]]^{1/2}$

Chapter-4

Synthesis and Characterization of Mononuclear Manganese Complexes Derived from Ligand having Tridentate 3N Donor: SOD, DNA Binding, Nuclease and Protease Activity

4.1. Abstract

Ligands H–N₃L (1-phenyl-1-(pyridine-2-ylmethyl)-2-(pyridine-2-ylmethylene)hydrazine) and Me–N₃L (1-phenyl-2-(1-(pyridin-2-yl)ethylidene)-1-(pyridin-2-ylmethyl)hydrazine) have been designed and synthesized. These ligands were characterized using various spectroscopic techniques such as IR, UV-visible, GC-MS and NMR spectral studies. Synthesized ligands have been utilized to prepare mononuclear complexes of manganese. A series of manganese complexes Mn(H–N₃L)Cl₂ (**8**), [Mn(H–N₃L)₂](ClO₄)₂ (**9**), Mn(Me–N₃L)Cl₂ (**10**) and [Mn(Me–N₃L)₂](ClO₄)₂ (**11**) were synthesized and characterized by spectroscopic techniques. Molecular structure of complex **10** was determined by single crystal X-ray diffraction technique. Redox properties were investigated for all the complexes. Theoretical calculations (DFT, TD–DFT) were performed using complex **10** and the geometrical, structural and electronic parameters were also investigated. Complexes **8**, **9**, **10** and **11** were employed to catalyze the dismutation of superoxide using xanthine-xanthine oxidase-nitroblue tetrazolium (NBT) assay. DNA interaction studies were monitored using all complexes. Representative complex **8** exhibited nuclease as well as protease activities in presence of oxidising agent (H₂O₂).

4.2. Introduction

Being biologically relevant metal ion, manganese chemistry has become an interesting area to explore.[467–469] Manganese is present in the active site of several enzymes such as oxygen evolving complex (OEC),[470,471] manganese lipoxygenase,[472–475] manganese dioxygenase,[23] manganese catalase,[431] superoxide dismutase,[476–479] arginase,[33] ribonucleotide reductases[480] etc. Among them considerable attention has been paid to the structural and functional modelling of mononuclear manganese enzymes such as peroxidase,[481,482] dioxygenase,[124] superoxide dismutase.[87,483–490] Superoxide dismutase are enzymes which catalyze the conversion of superoxide radical (O_2^-) to oxygen (O_2) and hydrogen peroxide (H_2O_2).[67] These impart significant role in protecting biological systems against the damage mediated by reactive oxygen species (ROS). These are defense enzymes in cells which are exhibiting important role in several pathological and disease states arising due to oxidative damage.[82] Due to lower toxicity, manganese complexes (II,III) have been utilized as potent SOD mimic.[76,491,492] It has been reported that native SOD enzymes interact with DNA and could exhibit nuclease activity.[493,494] In this regard, designing and synthesis of manganese complexes derived from nitrogen donor is gaining interest in SOD [75,79,84,88,495] as well as in DNA interaction studies.[242,496–498] Complexes derived from these ligands could be utilized to better understand their mode and mechanism of interaction with DNA. These complexes could be used for medicinal purpose. During administration of these drugs, these can interact with other biomolecules such as protein inside body.[360] Designing of artificial protease is important to control tumor malignancy as an anti−metastasis agents.[499–503]
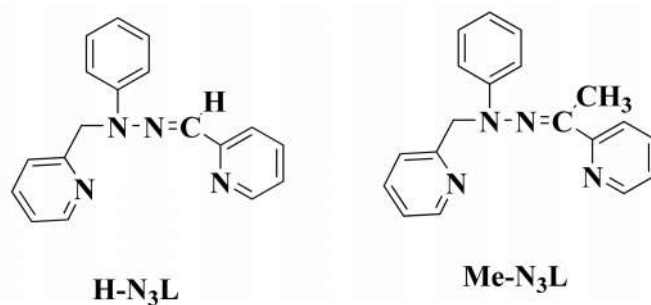
Fig. 4.1 Tridentate ligands with abbreviations used in the present work

Herein, we have synthesized tridentate meridional ligands (Fig. 4.1) having one imine donor and two pyridine donors. Synthesis of ligands and their manganese complexes Mn(H−N$_3$L)Cl$_2$, (**8**), [Mn(H−N$_3$L)$_2$](ClO$_4$)$_2$, (**9**), Mn(Me−N$_3$L)Cl$_2$, (**10**) and [Mn(Me−N$_3$L)$_2$](ClO$_4$)$_2$, (**11**) have been described in the present chapter. Molecular structure of representative complex **10**·CH$_3$COCH$_3$ has been established by X−ray crystallography. Electrochemical studies of the complexes were also performed. Synthesized complexes were utilized to investigate the superoxide dismutase activity using nitro blue tetrazolium (NBT) assay and DNA interaction studies were also explored. Nuclease and protease activities of synthesized manganese complexes were also performed.

4.3. Results and discussion

4.3.1. Synthesis and characterization of ligands

Tridentate ligands H−N$_3$L and Me−N$_3$L have been synthesized in two steps (i) Synthesis of amine (ii) Synthesis of Schiff's base derived from amine with corresponding aldehyde. The overall schematic representation of synthesis of ligands has been depicted in Scheme 4.1.
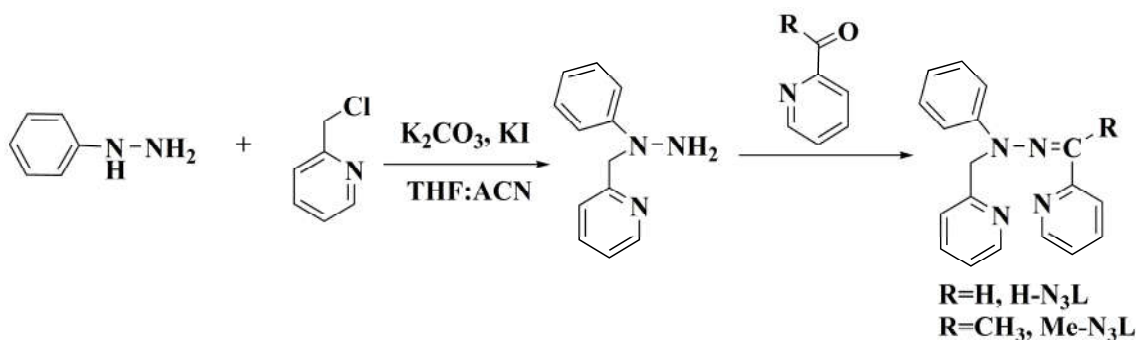
Scheme 4.1 Schematic representation of synthesis of ligands

4.3.1.1. Synthesis of 1−phenyl−1−(pyridine−2−ylmethyl)hydrazine

Amine 1−phenyl−1−(pyridine−2−ylmethyl)hydrazine has been prepared by refluxing phenyl hydrazine and 2−(chloromethyl)pyridine hydrochloride in tetrahydrofuran:acetonitrile (1:1) using a modified procedure to increase the yield.[504]

4.3.1.2. Synthesis of Schiff's base

Ligand H−N$_3$L was synthesized using 1−phenyl−1−(pyridine−2−ylmethyl)hydrazine and 2−pyridinecarboxaldehyde at refluxing temperature in methanol. Similar procedure was followed for Me−N$_3$L using 2−acetylpyridine instead of 2−pyridinecarboxaldehyde.

Table 4.1 Physical analysis data of ligands

Ligand	Empirical formula	Formula weight (g/mol)	Yield (%)	Color	Analysis found (Calc%)		
					% C	% H	% N
H−N$_3$L	C$_{18}$H$_{16}$N$_4$	288	72	yellow	71.53 (74.98)	5.09 (5.59)	17.66 (19.43)
Me−N$_3$L	C$_{19}$H$_{18}$N$_4$	302	68	yellow	74.85 (75.47)	5.80 (6.00)	19.42 (18.53)

4.3.1.3. IR spectral studies

Ligands H−N$_3$L and Me−N$_3$L exhibited characteristic peak of azomethine (−CH=N−) moiety at 1594 and 1593 cm^{-1} respectively.

4.3.1.4. Electronic absorption spectral studies

137

UV–visible spectra of both the ligands H–N_3L and Me–N_3L were recorded in methanol. The ligand H–N_3L exhibited bands 238, 295 and 342 nm respectively on the other hand ligand, Me–N_3L showed band 251, 280 and 341 nm. These bands were found to be intramolecular π–π* or n–π* transitions in nature.[505,506] Table 4.2 depicts characteristic spectroscopic data for the ligands.

Table 4.2 Characteristic IR and UV–visible data of ligands

Ligands	Characterstic IR data $(cm^{-1})^a$ $\nu_{-CH=N}$	UV–visible data $(\lambda_{max}/nm, \varepsilon/M^{-1}cm^{-1})^b$
H–N_3L	1594	342 (20,220), 295 (5,830), 238 (14,470)
Me–N_3L	1593	341 (6,210), 280 (6100), 251 (14,980)

^{a}Using KBr pellets, ^{b}Solvent: Methanol
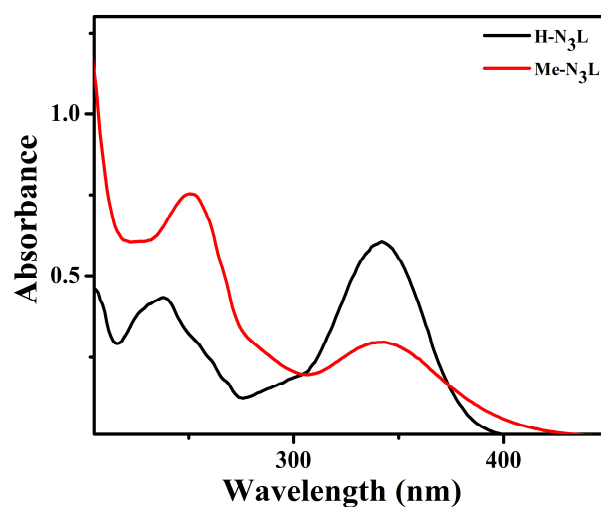
Fig. 4.2 Electronic absorption spectra of ligands in methanolic solutions

4.3.1.5. GC–MS spectral studies

Mass spectral analysis of H–N_3L exhibited peak corresponding to the molecular ion at m/z value of 288 (Fig. 4.3).
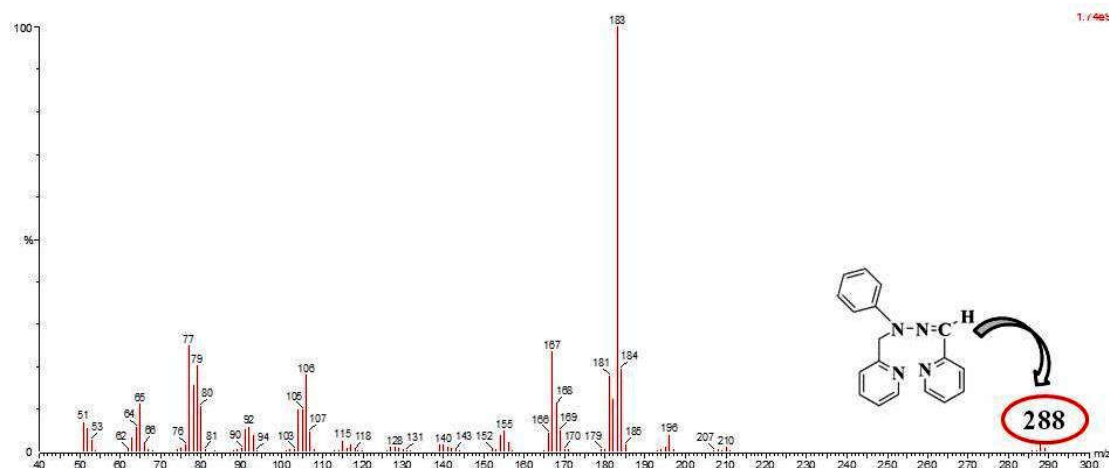
Fig. 4.3 GC−MS spectrum of H−N₃L in methanolic solution

4.3.1.6 NMR spectral studies

NMR analysis of ligands were performed in the CDCl$_3$ and ^{1}H and ^{13}C−NMR spectra of ligands have been depicted in Fig. 4.4–4.7. ^{1}H−NMR spectrum of H−N$_3$L exhibited characteristic peak at 5.30 and 8.6 ppm for two methylene proton (−CH$_2$) and azomethine proton (−CH=N−) respectively.
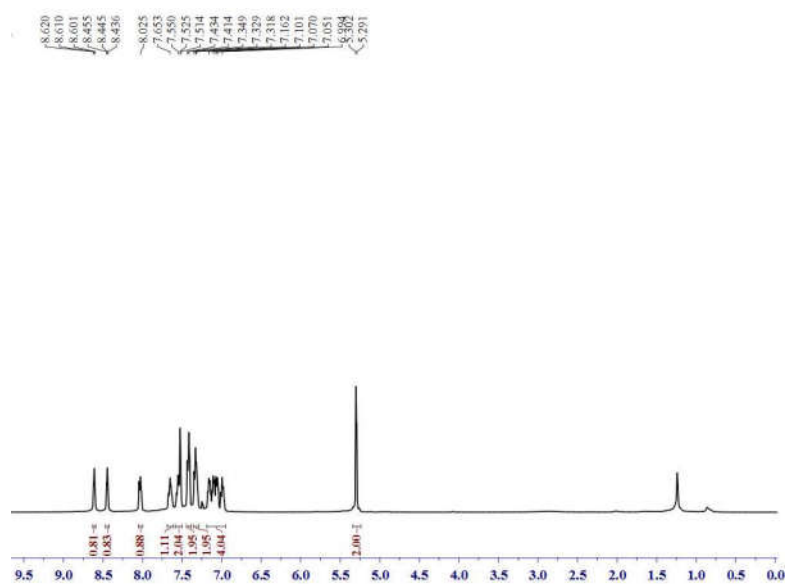
Fig. 4.4 ^{1}H−NMR spectrum of H−N$_3$L in CDCl$_3$

Ligand Me–N$_3$L showed characteristic peak at 2.36, 5.0 and 8.6 ppm for three methyl protons (–CH$_3$), two methylene proton (–CH$_2$) and azomethine proton (–CH=N–) respectively.
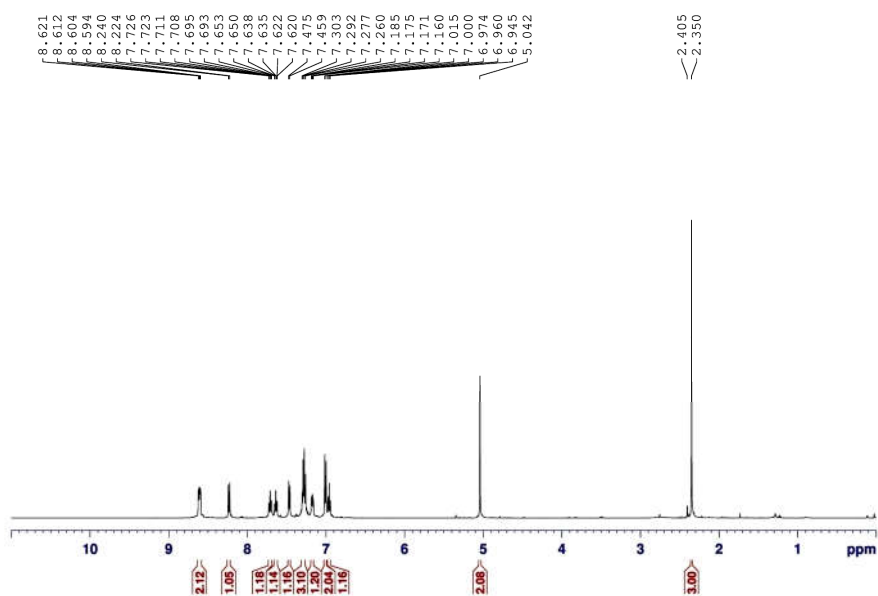
Fig. 4.5 ^{1}H–NMR spectrum of Me–N$_3$L in CDCl$_3$

^{13}C–NMR spectral studies were also carried out for ligand H–N$_3$L and Me–N$_3$L in CDCl$_3$ and have been shown in Fig. 4.6 and 4.7 respectively.
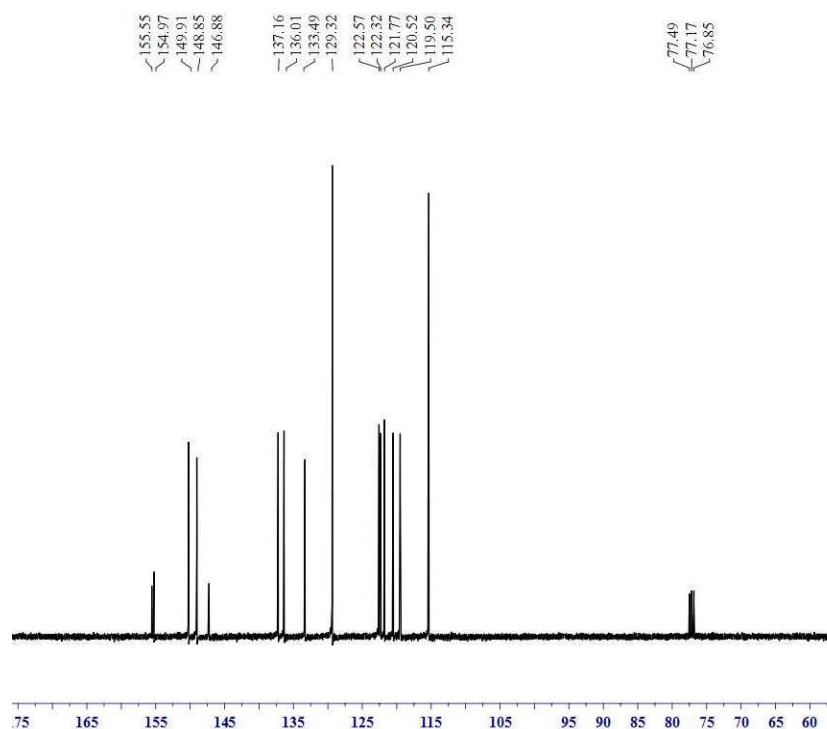
Fig. 4.6 ^{13}C–NMR spectrum of H–N$_3$L in CDCl$_3$
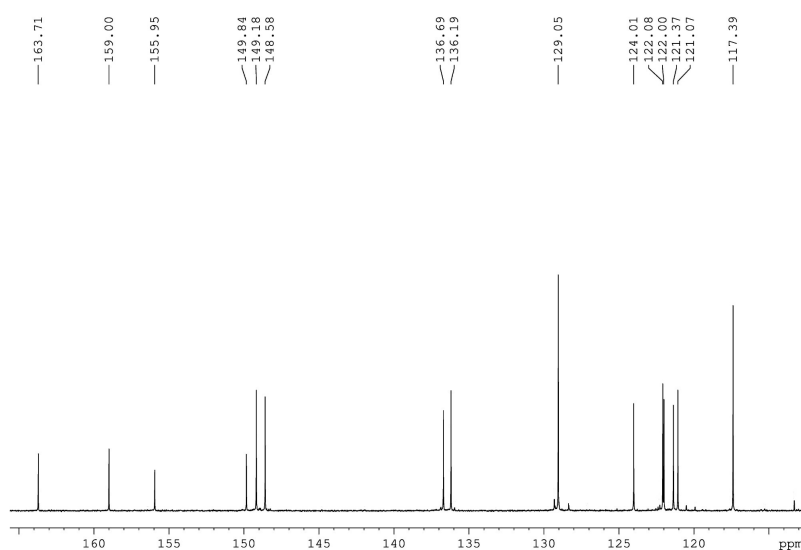
Fig. 4.7 ^{13}C–NMR spectrum of Me–N$_3$L in CDCl$_3$

4.3.2. Synthesis and characterization of metal complexes

Mononuclear manganese complex Mn(H–N$_3$L)Cl$_2$, (**8**) was synthesized using MnCl$_2$·4H$_2$O and ligand H–N$_3$L in equimolar ratio. Two equivalent of ligand H–N$_3$L and

141

Mn(ClO$_4$)$_2$·6H$_2$O were utilized to prepare bis complex of [Mn(H−N$_3$L)$_2$](ClO$_4$)$_2$, (**9**) in ethanol:methanol (1:1) solvent mixture. Similar procedure were followed to prepare Mn(Me−N$_3$L)Cl$_2$, (**10**) and [Mn(Me−N$_3$L)$_2$](ClO$_4$)$_2$, (**11**), using equimolar ratio of ligand Me−N$_3$L with MnCl$_2$·4H$_2$O in case of **10** and two equivalent of ligand with Mn(ClO$_4$)$_2$·6H$_2$O in case of complex **11**. The schematic representation of synthetic procedures of complexes **8**, **9**, **10** and **11** have been summarized in Scheme 4.2.
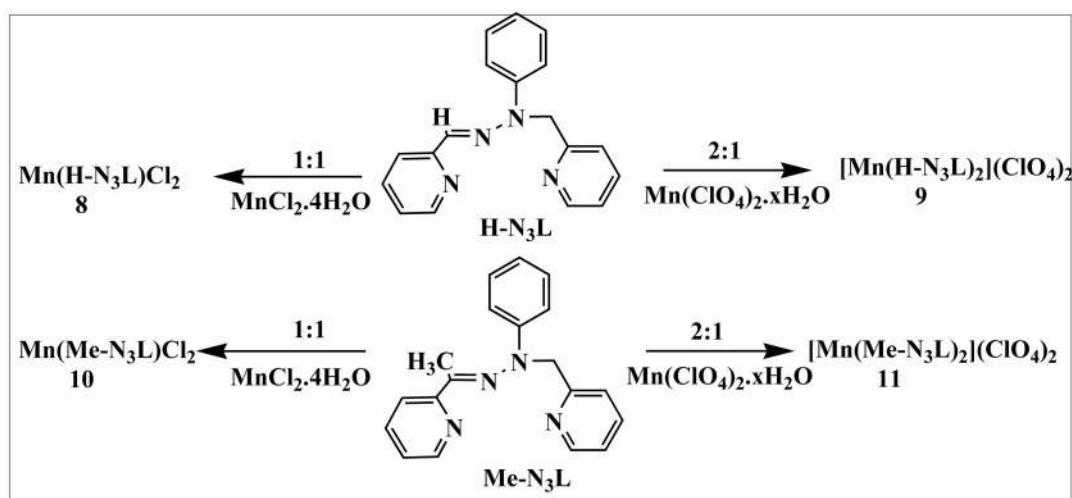
Scheme 4.2 Schematic representation of manganese complex synthesis

4.3.2.1. IR spectral studies

Coordination of ligand with the metal was analyzed primarily on the basis of IR spectral studies. During IR spectral studies azomethine $\nu_{-HC=N}$ band for free ligands were observed at ~1595 cm^{-1}. Coordination of the nitrogen to the metal centre resulted into shift in the stretching frequency of the $\nu_{-HC=N}$ indicates the possible ligation to metal centre in all the manganese complexes.[507] Bands near 1090 cm^{-1} together with a band at 623 cm^{-1} were found in complexes **9** and **11**. These bands suggested the presence of non−coordinated perchlorate ion to the metal centre.[401] The experimental IR data for all complexes have been tabulated and as given in Table 4.3.

Table 4.3 Data for IR and conductivity studies of complexes

Complex	IR data (cm^{-1})^a		Conductivity
	$\nu_{-HC=N}$	ν_{ClO4^-}	$(\Omega^{-1}cm^2mol^{-1})^b$
8	1602	–	28 (neutral)
9	1604	1092, 623	130 (1:2)
10	1595	–	22 (neutral)
11	1600	1096, 623	142 (1:2)

^{a}Using KBr pellets, ^{b}Solvent: dimethylformamide

4.3.2.2. Electronic absorption spectral studies

Absorption spectral studies for all the complexes were performed in methanol. UV–visible data and spectra of all the complexes have been shown in Table 4.4 and Fig. 4.8. Complexes **8**–**11** showed band below 400 nm which could be due to intraligand π–π* transitions or charge transfer transition in manganese(II). Manganese(II) having d^5 (high spin) electronic transitions are laporte as well as spin forbidden. Possibility of d–d transition is also ruled out due to the presence of d^5 (high spin) in octahedral geometry which is spin forbidden.[18] Hence bands associated with complexes **8**–**11** are intraligand n–π* and π–π*transitions.[508]

Table 4.4 Electronic spectral data of manganese complexes

Complex	UV–visible data (λ_{max}/nm, ε/M^{-1}cm^{-1})^a
8	341 (15,330), 294 (3,960), 236 (9,580), 203 (14,710)
9	344 (7,000) 252 (19,440), 225 (16,560), 204 (25,780)
10	344 (5,980), 251(17,670), 225 (13,720), 202 (26,210)
11	343 (14,970), 251 (44,290), 220 (50,460), 206 (57,260)

^{a}UV–visible data in methanol
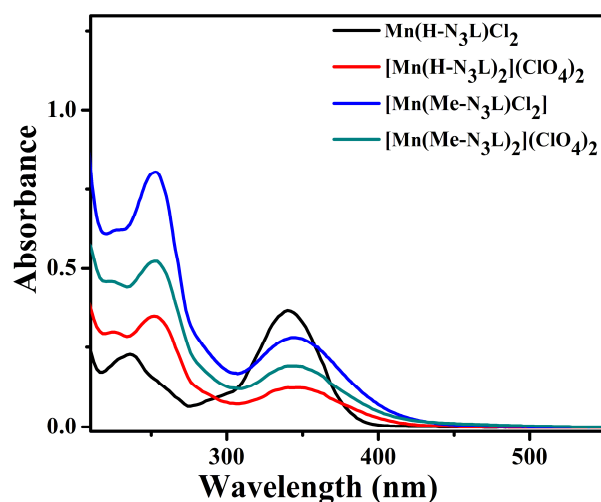
Fig. 4.8 UV−visible absorption spectra of manganese(II) complexes in methanol

4.3.2.3. Conductivity studies

Experimental values obtained for molar conductivity have been presented in Table 4.3. The molar conductivity measurements were determined in DMF at ca. 10^{-3} M. The values obtained for complex **8** (28) and **10** (22) exhibited the neutral non–electrolytic nature of the complexes in solution. On the other hand, complex **9** and **11** have values of molar conductivity 130 and 142 respectively indicating uni–bivalent (1:2) electrolytic behavior in solutions.[406]

4.3.2.4. Magnetic moment studies

To elucidate the magnetic nature of the complexes magnetic moments were calculated for all the complexes. Magnetic moment of complexes **8**, **9**, **10** and **11** were found to be 5.36, 5.21, 5.11 and 5.09 BM respectively suggesting high–spin manganese(II) centre (Table 4.3).[509]

4.3.2.5. ESI–MS spectral studies

Complexes were subjected to mass analyses for further confirmation of proposed structure. ESI–MS of complexes were performed in acetonitrile solution under positive ion mode. Complex **8** exhibited peak at m/z value of 378.0398 corresponding to $[M–Cl]^+$ as depicted in Fig. 4.9.
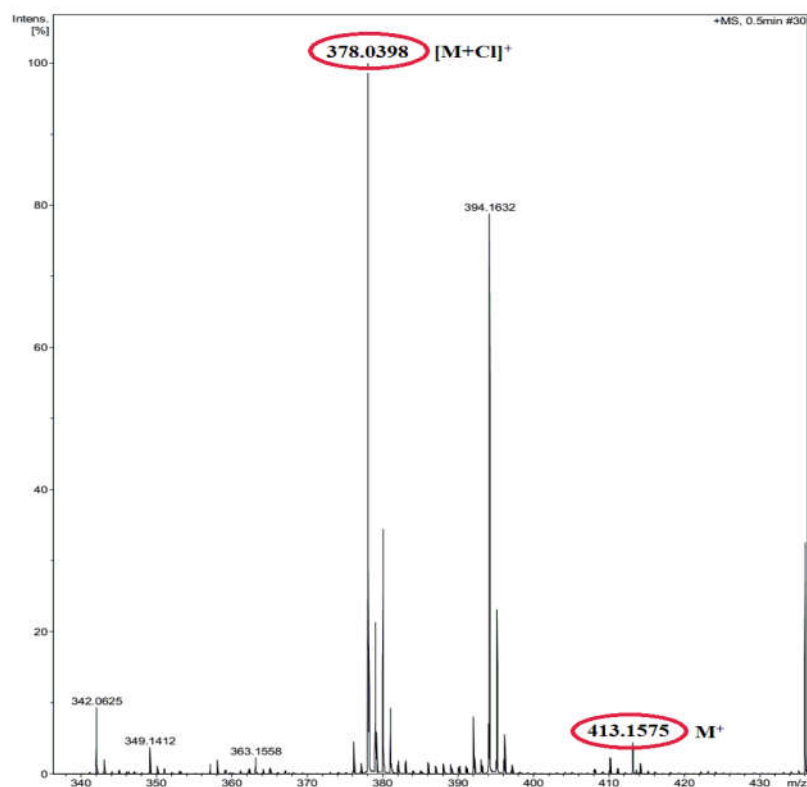
Fig. 4.9 ESI–MS spectrum of **8** in acetonitrile solution under positive ion mode

Complex **10** exhibited characteristic peak at m/z at 450.01, 393.06, 325.14 and 301.14 corresponding to $[M+Na]^+$, $[M-Cl]^+$, $[L+Na]^+$ and $[L+H]^+$ respectively as depicted in Fig. 4.10.

145
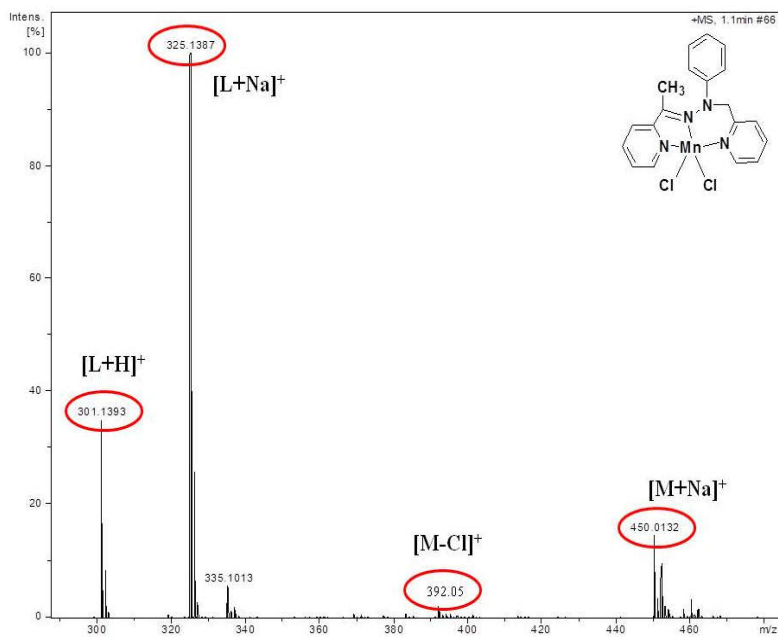
Fig. 4.10 ESI−MS spectrum of **10** in acetonitrile solution under positive ion

During the mass spectral analysis of complex **11** peak at m/z 758.1896 was found due to the formation of $[M-ClO_4]^+$ adduct (Fig. 4.11).

146
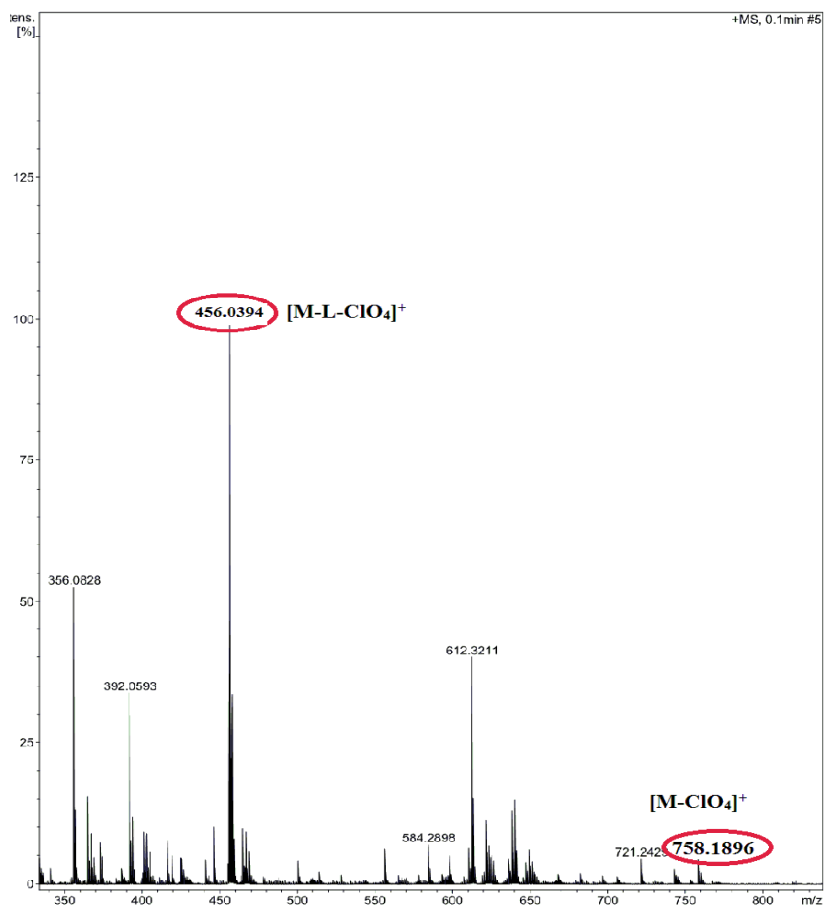
Fig. 4.11 ESI–MS spectrum of complex **11** in acetonitrile solution under positive ion mode

4.3.3. Molecular structures of complex 10·CH₃COCH₃

Single crystal X–ray analysis was performed on representative complex **10**·CH$_3$COCH$_3$. Selected bond lengths, bond angles and crystallographic data have been summarized in Table 4.5 and Table 4.12.

The ORTEP diagram of the complex Mn(Me–N$_3$L)Cl$_2$ (**10**·CH$_3$COCH$_3$) has been shown in Fig. 4.12. Crystals of complex **10**·CH$_3$COCH$_3$ were obtained by diffusion of diethylether to a solution of **10**·CH$_3$COCH$_3$ at room temperature in acetone within a week. Complex **10** was crystallized in monoclinic space group *P 21/n* consisting of mononuclear manganese(II) complex with three nitrogens one from imine and two from pyridine donor of Me–N$_3$L ligand coordinated in meridional fashion and remaining sites were occupied by two chlorine atoms. All the three nitrogen atoms and one chlorine Cl(2) is in the equatorial plane. Cl(1) is found perpendicular to the plane of rest coordinated atoms. The structural index parameter (τ) is found to be 0.22 which supports the square pyramidal geometry of the complex **1**. Mn1 is situated 0.616 A° above the plane. Mn1–N$_{py}$ bond lengths are in the range of 2.41 A° and in good agreement to the reported values.[510,511] but longer then Singh and co–worker.[512] Mn1–N$_{imine}$ bond distance is comparable to the reported.[513,514] and Mn1–Cl bond lengths are in the range of 2.379 Å and are in good agreement[511,513] but smaller to previously reported values.[515]

(a)   (b)
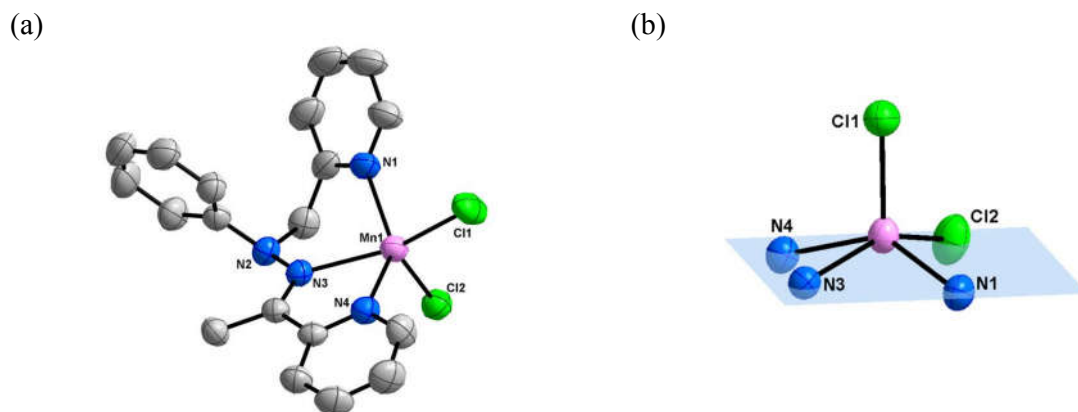
Fig. 4.12 (a) Thermal ellipsoid diagram of the crystal structure of **10**.CH_3COCH_3 showing the atom numbering scheme and thermal ellipsoids (50% probability level). Hydrogen atoms are omitted for clarity and (b) square pyramidal geometry of manganese(II) centre

Table 4.5 Selected bond lengths (Å) and angles (°) of complex **10**

Bond lengths (Å)		Bond angles (°)	
Mn1–N1	2.241(2)	N(1)–Mn1–N(3)	81.73(8)
Mn1–N3	2.311(19)	N(1)–Mn1–Cl(1)	106.77(7)
		N(1)–Mn1–N(4)	138.78(9)
		N(3)–Mn1–N(4)	70.26(8)
Mn1–N4	2.239(2)	N(1)–Mn1–Cl(2)	97.313(7)
Mn1–Cl1	2.365(8)	N(3)–Mn1–Cl(1)	99.261(6)
		N(3)–Mn1–Cl(2)	152.00(7)
Mn1–Cl2	2.393(8)	N(4)–Mn1–Cl(1)	107.05(6)

<div align="center">

N(4)–Mn1–Cl(2)   94.120(6)

Cl(1)– Mn1–Cl(2)   107.708(4)

</div>

In terms of supramolecular chemistry π–stacking interaction with aryl hydrogen and hydrogen bonding network are very significant.[418] Two types of non–covalent interactions observed in the packing diagram of complex **10**. Firstly, the aryl hydrogen–pyridine ring (C–H–π) weak interaction (distance 3.364 Å) shown in Fig. 4.13.
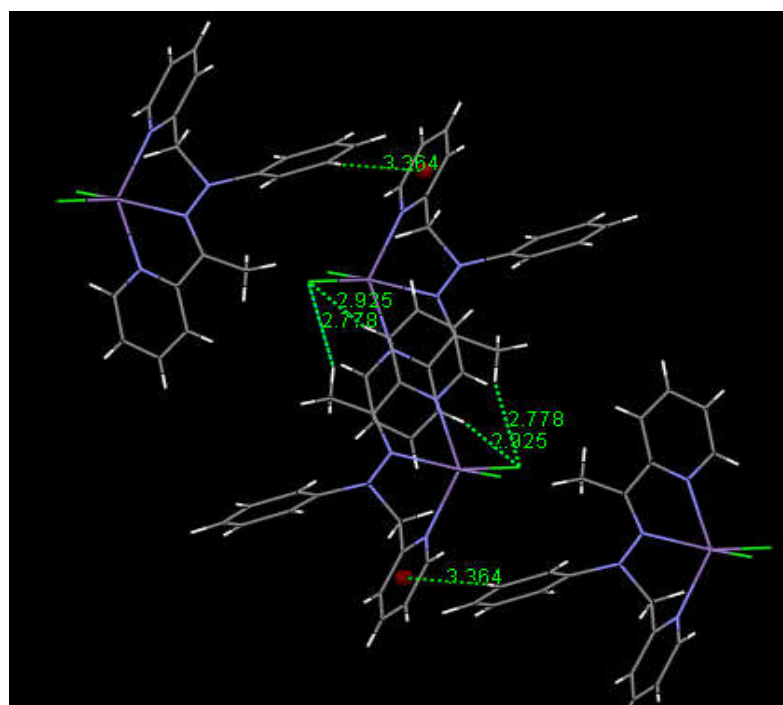
Fig. 4.13 C–H–π interactions in packing diagram of complex **10**

Secondly, hydrogen bonding was found in between aryl hydrogen and oxygen (acetone) atom (2.853 Å). Along with this, similar interactions were observed between aryl hydrogen and chlorine (2.925Å) atom and methylene hydrogen and chlorine atom (2.778 Å) as shown in Fig. 4.14.

<div align="center">149</div>
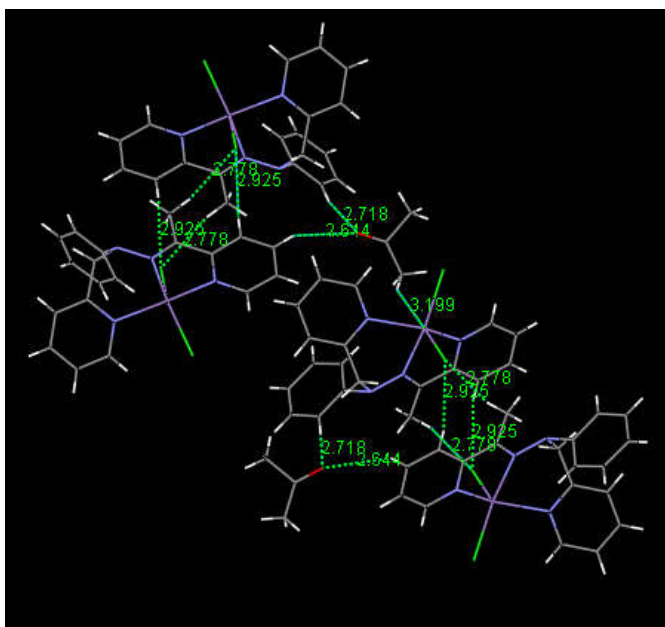
Fig. 4.14 H–bonding interactions in packing diagram of complex **10**

Solvent acetone was also present in the crystal lattice and is 3.199 Å away from the

Mn1. Packing diagram of complex **10** have been shown in Fig. 4.15 and hydrogen bond

geometries have been depicted in the Table 4.6.
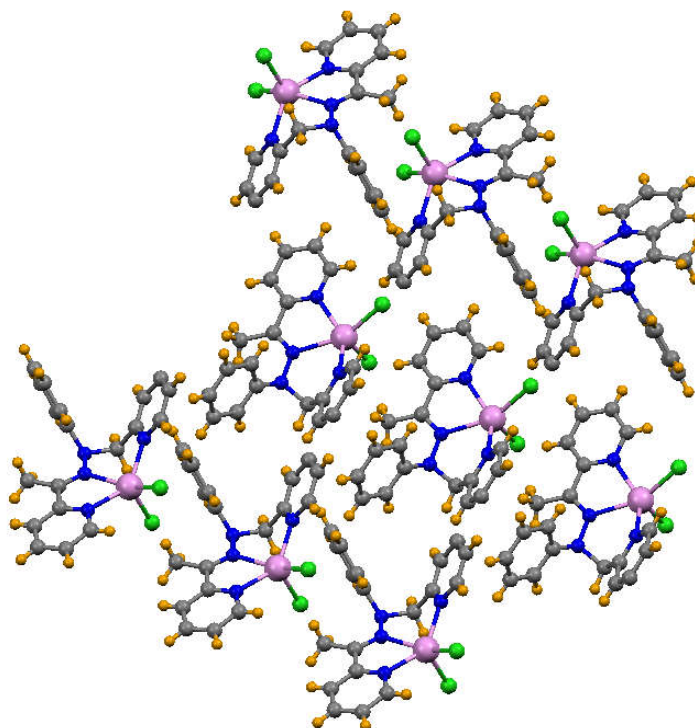
Fig. 4.15 Packing diagram of complex **10**

Table 4.6 Hydrogen bonding geometries of complex **10**

D─H.....A	D─H (Å)	D.......A (Å)	H.......A (Å)	D─H.......A (°)
C6─H6B.........Cl1	0.970(3)	3.715(3)[a]	2.852(1)[a]	148.76(17)[a]
C14─H14C.....N2	0.960(3)	2.784(4)[a]	2.602(2)[a]	98.27(19)[a]
C12─H12........N3	0.930(3)	2.882(4)[a]	2.602(2)[a]	98.00(19)[a]
C1─H1............Cl2	0.930(4)	3.445(4)[a]	2.788(1)[a]	128.49(23)[a]
C19─H19........Cl2	0.930(4)	3.460(4)[a]	2.858(1)[a]	123.53(22)[a]
C16─H16........Cl1	0.930(3)	3.822(3)[b]	2.925(1)[b]	162.64(19)[b]
C14─H14B.....Cl1	0.960(3)	3.696(3)[b]	2.778(1)[b]	160.35(18)[b]
C6─H6A….....O1	0.970(3)	3.664(9)[c]	2.815(8)[c]	146.69(22)[c]
C8─H8…........O1	0.930(4)	3.601(8)[c]	2.717(8)[c]	159.09(27)[c]
C17─H17…....O1	0.930(3)	3.338(6)[d]	2.645(5)[d]	131.91(23)[d]
C3─H3............Cl1	0.930(4)	3.868(4)[e]	2.949(1)[e]	169.79(24)[e]

C22─H22A.....Cl1	0.960(9)	3.759(.8)^f	2.983(1)^f	138.89(50)^f

Symmetry Equivalents: (a) x,y,z; (b) −x+2,−y,−z; (c) x+1/2,−y+1/2,+z−1/2; (d) −x+1/2+1,+y−1/2,−z+1/2 (e) −x+1/2+2,+y+1/2,−z+1/2 (f) x−1,+y,+z

4.3.4. Density functional theory (DFT) calculations

Density functional theory (DFT) has become an effective tool to elucidate structural, electronic and spectral properties of molecules.[516,517] To optimize the geometry of the complex **10** density functional theory (DFT) was performed. Fig. 4.16 and 4.17 represent the HOMO and LUMO of alpha and beta molecular orbitals respectively.

(a)   (b)
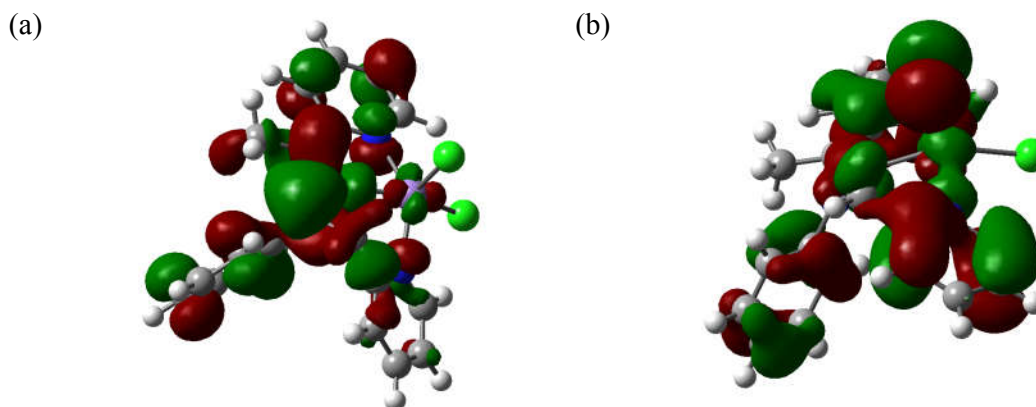
Fig. 4.16 Molecular orbital diagram of HOMO (a) alpha and (b) beta of complex **10**

All the theoretical calculations were performed in the gas phase.

(a)   (b)
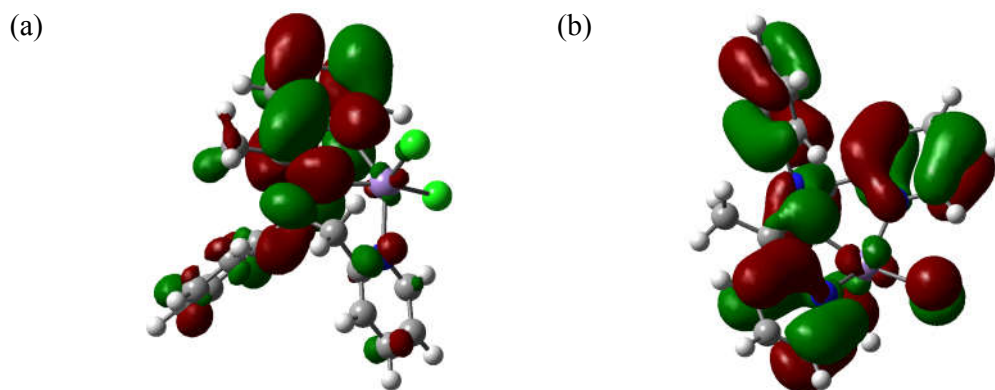
Fig. 4.17 Molecular orbital diagram of LUMO (a) alpha and (b) beta of complex **10**

152

Selected bond angles and bond distances obtained from optimized geometries were compared with the available X–ray crystallographic data which showed minimum deviations in solid as well as in gas phase (Table 4.7).

Table 4.7 Comparison of theoretical and experimental bond lengths and bond angles of complex **10** using S=6

Bond lengths (Å)			Bond angles (°)		
	X–ray	DFT		X–ray	DFT
Mn(1)–N(1)	2.241	2.236	N(1)–Mn1–N(3)	81.588	82.96
Mn(1)–N(3)	2.311	2.331	N(1)–Mn1–Cl(1)	106.809	90.72
			N(1)–Mn1–N(4)	138.788	71.24
			N(3)–Mn1–N(4)	70.408	71.28
Mn(1)–N(4)	2.239	2.236	N(1)–Mn1–Cl(2)	97.313	95.54
Mn(1)–Cl(1)	2.365	2.404	N(3)–Mn1–Cl(1)	99.261	104.05
			N(3)–Mn1–Cl(2)	152.007	145.18
Mn(1)–Cl(2)	2.393	2.476	N(4)–Mn1–Cl(1)	107.05	106.02
			N(4)–Mn1–Cl(2)	94.120	90.70
			Cl(1)– Mn1–Cl(2)	107.708	117.24

TD–DFT calculations were also performed for complex **10** to estimate the electronic properties of complex and characteristic transitions along with their contribution as depicted in Table 4.8.

Table 4.8 Calculated TD−DFT excitation energies (in eV), oscillator strengths (f), and

nature of transitions in the complex **10**

Composition(% Contribution)	E (eV)	Oscillator strength (f)	λ_{theo} (nm)	λ_{exp} (nm)
HOMO−1 ➔ LUMO+5 (35%)	4.6022	0.0162	269	253
HOMO−2 ➔ LUMO+4 (29%)				
HOMO−2 ➔ LUMO+3 (11%)				
HOMO−7 ➔ LUMO+2 (22%)	4.4667	0.0052	277	277
HOMO−2 ➔ LUMO+3 (21%)				
HOMO−10 ➔ LUMO (9%)				
HOMO−1 ➔ LUMO+1 (100 %)	3.5859	0.0032	345	345

4.3.5. Electrochemical studies

Redox properties of manganese complexes have been studied by cyclic voltammetry (CV) studies in dimethylformamide solutions. All the manganese complexes exhibited irreversible redox processes. The onset potentials, i.e. potentials where the complexes start oxidizing have been shown in Table 4.9. These are probable corresponding to Mn(II)/(III) redox processes. In addition to this, an anodic peak was also observed in ligands as well as in all the manganese complexes. This anodic peak is probably due to some ligand centred activity. Data have been given in Fig. 4.18 and listed in Table 4.9.

Table 4.9 Electrochemical data for manganese(II) complexes at 298 K[a] *vs* Ag/AgCl

Compound	Mn(II)/Mn(III) E (V)
8	1.213
9	1.040
10	1.272
11	1.048

[a]Measured in dimethyformamide using 0.1 M tetrabutylammonium perchlorate (TBAP)
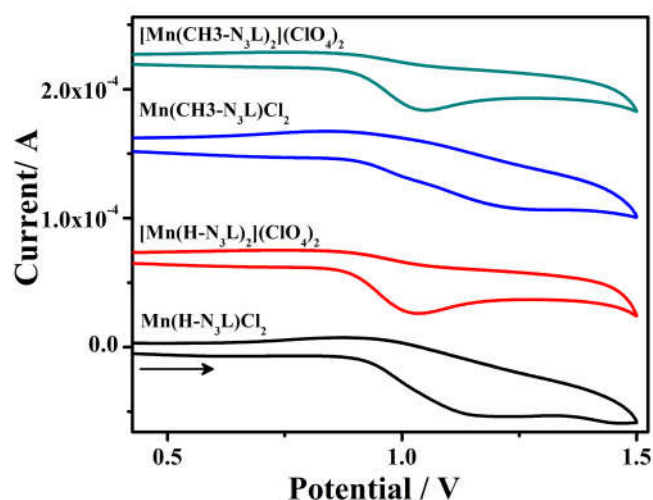
Fig. 4.18 Cyclic voltammograms of 10^{-3} M solutions of complexes **8**, **9**, **10** and **11** at a scan rate of 0.1 V/s

4.3.6. Superoxide dismutase (SOD) activity

Superoxide dismutase (SOD) activities of the complexes were determined at 298 K following indirect method xanthine/xanthine oxidase/nitroblue tetrazolium assay.[497] Superoxide radicals ($O^{2\bullet-}$) were generated in situ using xanthine/ xanthine oxidase system and detected spectrophotometrically by monitoring the absorbance at 560 nm due to the formation of formazan from NBT (nitroblue tetrazolium). The SOD activities of all the four complexes have been depicted in the Table 4.10. Complexes **8**, **10** exhibited better activity as compared to reported manganese complex.[81,82,86,87] Complexes **9**, **11** was also proved to be a better SOD mimic as compared to the published one.[87] These complexes were having values in the range of micromolar (μM) and found to be potent applicants as SOD mimic (Fig. 4.19-4.20).

Table 4.10 IC$_{50}$ values for **8**, **9**, **10** and **11** complexes

Complex	IC$_{50}$ (μM)^a
8	3.36
9	11.39

10	2.56
11	9.04

[a]IC_{50} values are the average of two replicate experiments

(a) (b)
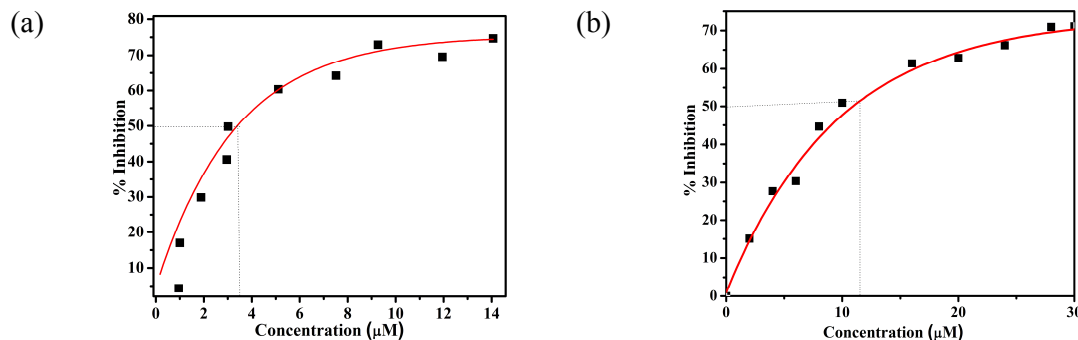
Fig. 4.19 SOD activities of complexes (a) **8** and (b) **9** (DMF) using xanthine oxidase-nitro blue tetrazolium (NBT) assay

(a) (b)
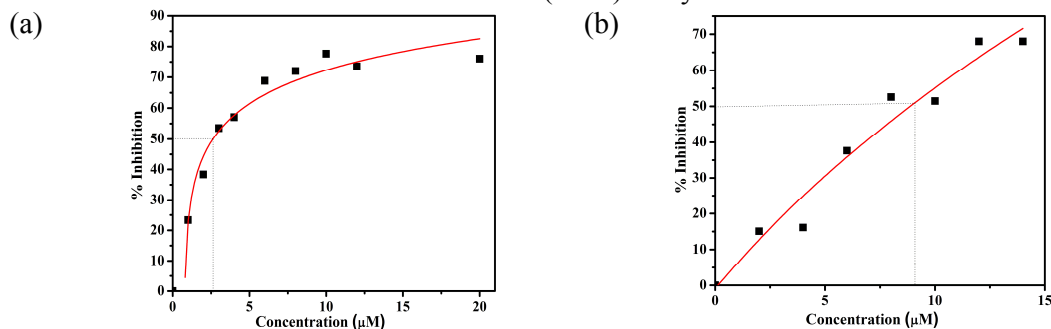
Fig. 4.20 SOD activities of complexes (a) **10** and (b) **11** (DMF) using xanthine oxidase-nitro blue tetrazolium (NBT) assay

4.3.7. DNA binding activity

All the biological activities were performed in 0.1 M phosphate buffer pH 7.2. Hence stabilities of complexes in buffer during the experiments were observed. Small change in absorbance without any shift in wavelengths (λ_{max}) predicted the stability of these manganese complexes in the above buffer solution (Fig. 4.21–4.22).
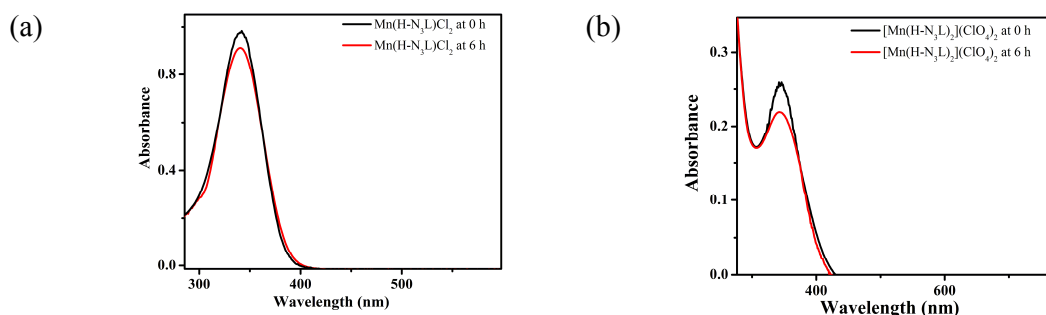
Fig. 4.21 Stability of complexes **8** and **9** in 0.1 M phosphate buffer (pH 7.2) solution for 6 h
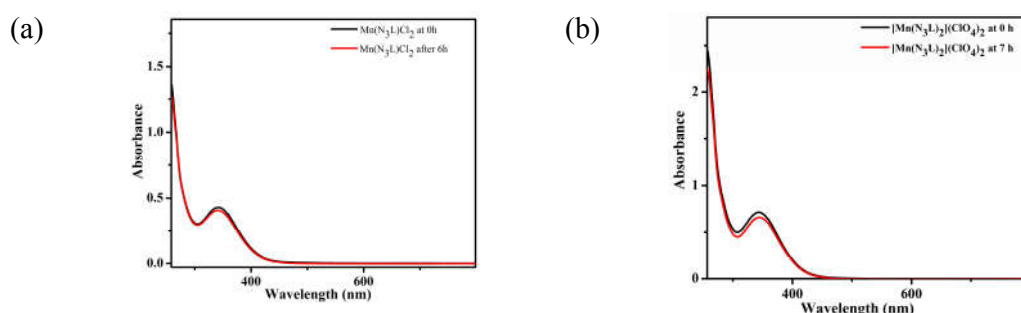
Fig. 4.22 Stability of complexes **10** and **11** in 0.1 M phosphate buffer (pH 7.2) solution for 6 h

Binding of DNA with complexes was investigated using absorption spectral studies. To achieve this, the absorption spectra of complexes in the absence and presence of calf thymus DNA (CT–DNA) at different concentrations were measured. Upon successive addition of CT–DNA, UV–visible absorption band of metal complexes showed hypochromism in all manganese complexes without any appreciable shift in wavelength. Hypochromism indicates probable mode of binding can be intercalative or electrostatic due to π–π* stacking interaction.[518] The intrinsic binding constants K_b for complexes have been determined using Wolfe–Shimer equation[519] and shown in Table 4.11.[520] The value of K_b in complex **8** suggests strong binding of the complex with DNA as the value is closer to the classical intercalator ethidium bromide.[509,521] The K_b value is lesser as compared to the value reported.[241,498] but is more as compared to H. Wu *et.al.*[241] In most cases, the existence of hypochromism for all complexes could be considered as first evidence that the binding of

157

the complexes involving intercalation between the base pairs of CT−DNA.[522] Although the exact mode of binding cannot be merely proposed by UV−visible spectroscopic titration studies. Absorption spectra of complexes **8** and **9** in 0.1 M phosphate buffer (pH 7.2) in the presence of increasing DNA concentration have been shown in Fig. 4.23−4.26.

Table 4.11 Values of binding constants (K_b) for complexes **8**−**11**

Complex	$K_b\,(M^{-1})$
8	2.62×10^4
9	1.6×10^4
10	5.16×10^3
11	1.0×10^4
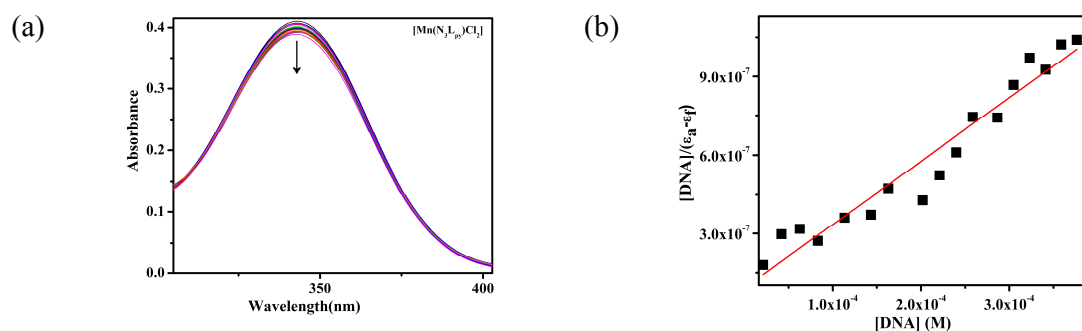
Fig. 4.23 (a) Absorption spectra of **8** (100 μM) (b) Plot of [DNA]/ε_A−ε_F *vs* [DNA] in 0.1 M phosphate buffer (pH 7.2) in presence of increasing DNA concentration (0−200 μM). Arrows show the absorbance changes upon increasing DNA concentration

(a)

(b)
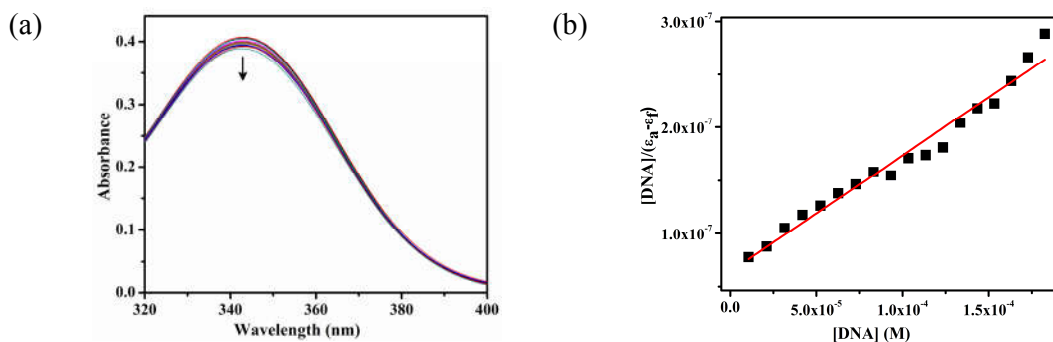
Fig. 4.24 (a) Absorption spectra of **9** (100 µM) (b) Plot of [DNA]/ε_A−ε_F *vs* [DNA] in 0.1 M phosphate buffer (pH 7.2) in presence of increasing DNA concentration (0−340 µM). Arrows show the absorbance changes upon increasing DNA concentration

(a)

(b)
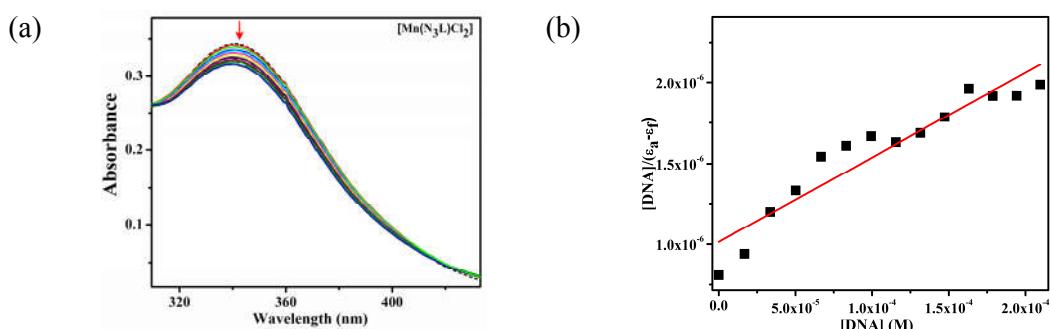
Fig. 4.25 (a) Absorption spectra of **10** (100 µM) (b) Plot of [DNA]/ε_A−ε_F *vs* [DNA] in 0.1 M phosphate buffer (pH 7.2) in presence of increasing DNA concentration (0−209 µM). Arrows show the absorbance changes upon increasing DNA concentration

(a)

(b)
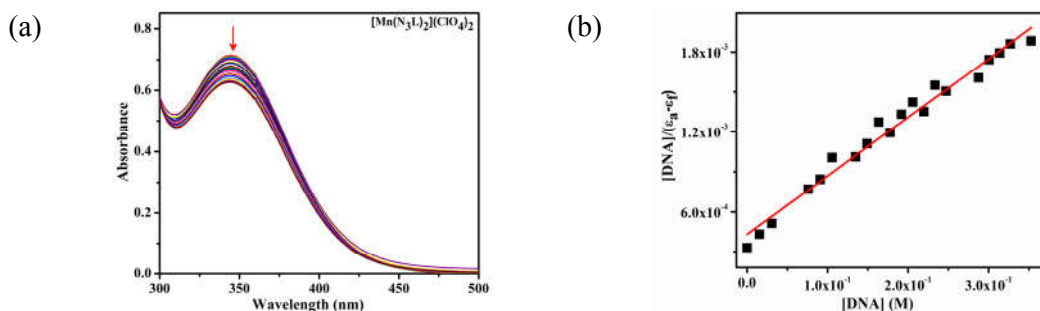
Fig. 4.26 (a) Absorption spectra of complexes **11** (100 µM) (b) Plot of [DNA]/ε_A−ε_F *vs* [DNA] in 0.1 M phosphate buffer (pH 7.2) in presence of increasing DNA concentration (0−366 µM). Arrows show the absorbance changes upon increasing DNA concentration

Competitive binding of ethidium bromide *vs.* complexes with DNA using fluorescence spectral studies were performed to get better insight into the mechanism. Ethidium bromide (EB) emits intense fluorescence in the presence of DNA due to its strong intercalation

159

between DNA base pairs. The competitive binding of metal complex with DNA may lead to the decrease in the enhanced fluorescence due to the EB. The fluorescence quenching curve of ethidium bromide bound to DNA by the complexes have been shown in Fig. 4.27–4.30. Stern−Volmer quenching constant Ksv for all the complexes were obtained by Stern−Volmer plot which are described in Table 4.12. The values are comparable to that of reported by M. Zampakou *et. al.* which suggests that these complexes can probably interact with intercalative mode to CT DNA.[498] The Ksv values for the complexes **8** and **9** is more as compared to the value reported by H. Wu *et al*[498] but comparable to that reported by M. Zampakou *et al*.[498] It can be concluded that the binding of complex with DNA is probably intercalative.
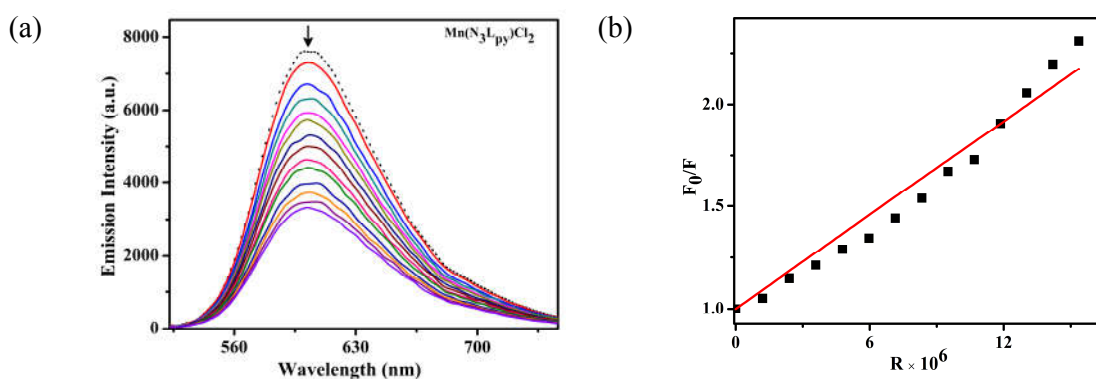
Fig. 4.27 EtBr–DNA fluorescence quenching titration of complex **8** (0–40μM). Stern−Volmer plots of F_0/F versus [R] for complex shown. Tests was performed in the conditions of 0.1 M phosphate buffer (pH 7.2) at 298 K [C_{DNA}] = 25μM, [C_{EtBr}] = 0.5 μM; λ_{ex} = 250 nm, λ_{em} = 585nm
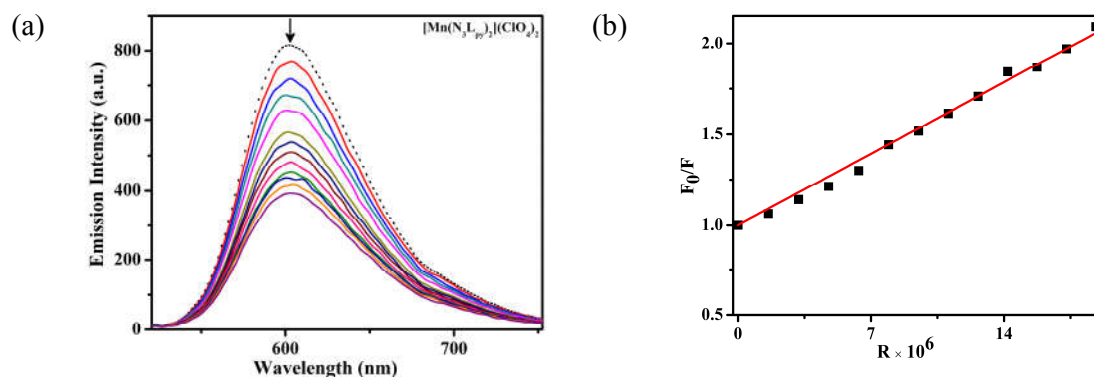
Fig. 4.28 EtBr–DNA fluorescence quenching titration of complex **9** (0–40μM).

160

Stern−Volmer plots of F_0/F versus [R] for complex shown. Tests was performed in the conditions of 0.1 M phosphate buffer (pH 7.2) at 298 K [C_{DNA}] = 25μM, [C_{EtBr}] = 0.5 μM; λ_{ex} = 250 nm, λ_{em} = 585nm

(a)　　　　　(b)
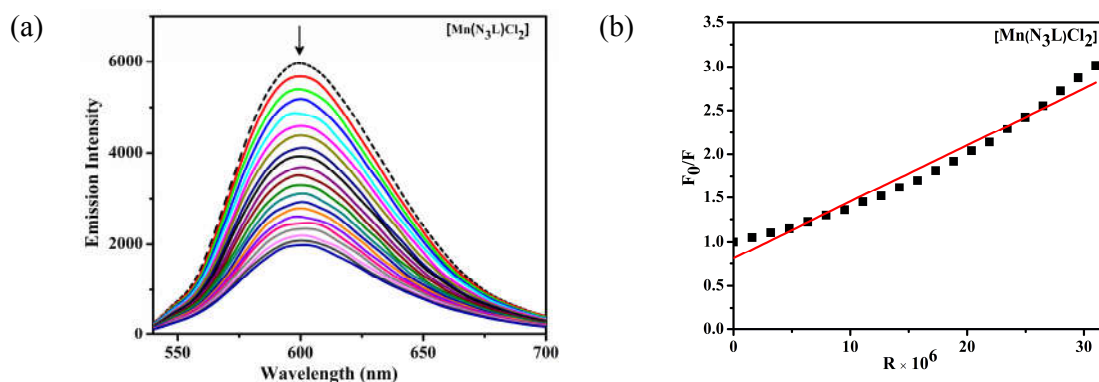
Fig. 4.29 EtBr–DNA fluorescence quenching titration of complex **10** (0–40μM). Stern−Volmer plots of F_0/F versus [R] for complex shown. Tests was performed in the conditions of 0.1 M phosphate buffer (pH 7.2) at 298 K [C_{DNA}] = 25μM, [C_{EtBr}] = 0.5 μM; λ_{ex} = 250 nm, λ_{em} = 585nm

(a)　　　　　(b)
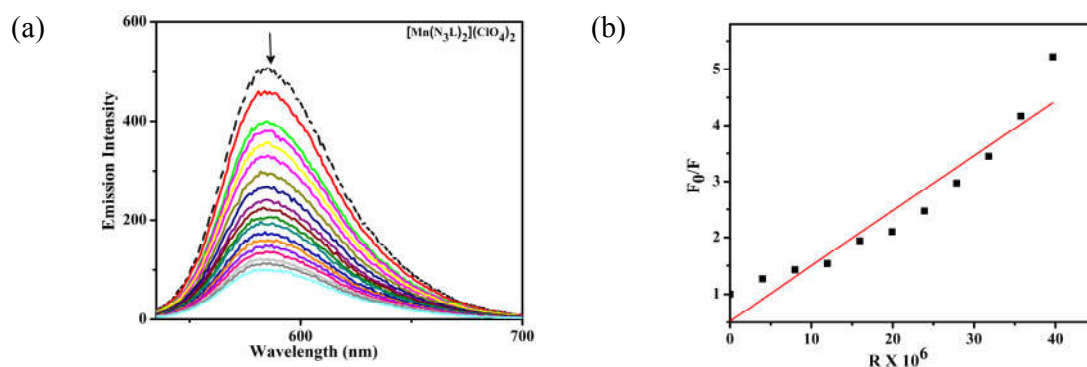
Fig. 4.30 EtBr–DNA fluorescence quenching titration of complex **11** (0–40μM). Stern−Volmer plots of F_0/F versus [R] for complex shown. Tests was performed in the conditions of 0.1 M phosphate buffer (pH 7.2) at 298 K [C_{DNA}] = 25μM, [C_{EtBr}] = 0.5 μM; λ_{ex} = 250 nm, λ_{em} = 585nm

Table 4.12 Values of Stern–Volmer quenching constants of complexes

Complex	K_{SV} (M^{-1})
8	7.64×10^4
9	5.6×10^4
10	6.47×10^4
11	1.0×10^5

For further confirmation of interaction of complexes with DNA, circular dichroism (CD) spectroscopic studies were performed. CD spectrum of CT–DNA was recorded in the range 225–300 nm in 0.1 M phosphate buffer (pH 7.2) and it has been observed that there was one positive band at 278 nm due to base stacking and one negative band at 246 nm due to helicity for a right handed B–form of DNA.[446,523] Data indicates appreciable decrease in mono complexes **8** and **10** mainly in the positive band (Fig. 4.31) while in complexes **9** and **11** a significant change is observed for both the positive and negative bands of DNA (Fig. 4.31). This indicates that the interaction of complexes with the DNA interfere with helicity as well as base stacking of DNA. However there was no shift in λ_{max} could be observed. This probably designate that the probable mode of coordination could be intercalative in nature.
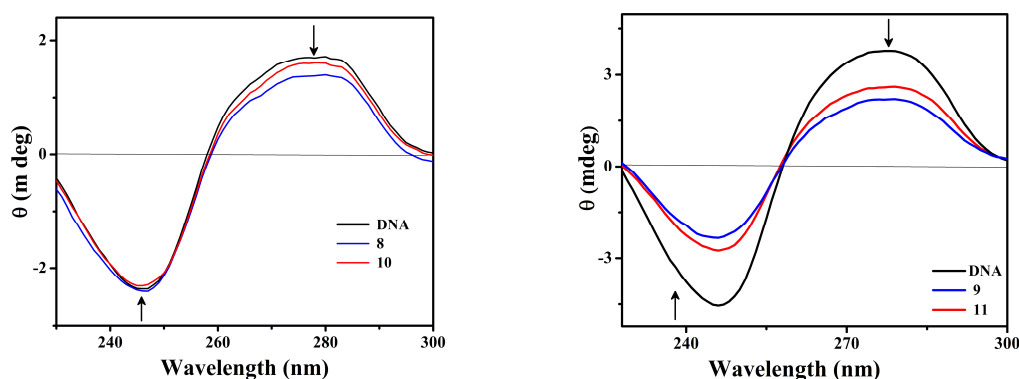
Fig. 4.31 Circular dichroism spectra in 0.1 M phosphate buffer (pH 7.2) after 10 min incubation at 25 °C. (a) **8** and **10** (b) **9** and **11** with CT–DNA and its interaction with complexes spectra recorded in 5% dimethylformamide

4.3.8. Nuclease activity

Nuclease studies were investigated by the conversion of supercoiled *pBR322* plasmid DNA to nicked circular DNA forms. Supercoiled *pBR322* DNA in trisboric acid–EDTA buffer (TBE) (pH 8.2) was treated with complexes **8** in dimethylformamide (10%) in the presence or absence of additives. The oxidative DNA cleavage by the complexes were studies in the presence of H_2O_2 (oxidizing agent). The samples were incubated at 37 °C

temperature. Complex **8** was having variable concentration was subjected for nuclease studies (Fig. 4.32).
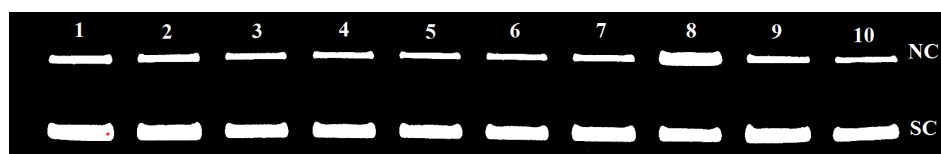
Fig. 4.32 Gel electrophoresis separations showing the cleavage of supercoiled *pBR322* DNA (100 ng) by variable concentration of complexes **8** in 10% DMF incubated at 37 °C for 2 h. Lane 1: DNA, lane 2: DNA + FeCl$_3$ (100 μM), lane 3: DNA + H−N$_3$L, lane 4: DNA + **8** (10 μM), lane 5: DNA + **8** (25 μM), lane 6: DNA + **8** (50 μM), lane 7: DNA + **8** (100 μM), lane 8: DNA+ **8** (100 μM) + H$_2$O$_2$ (100 μM), lane 9: DNA + H$_2$O$_2$ (100 μM), lane 10: DNA + DMF (2 μL)

Quantitative determination of band was also observed using band area as shown in Fig. 4.33. NC form was found to be higher in presence of H$_2$O$_2$. Hence complex **8** showed excellent nuclease activity in presence of oxidizing agent H$_2$O$_2$.
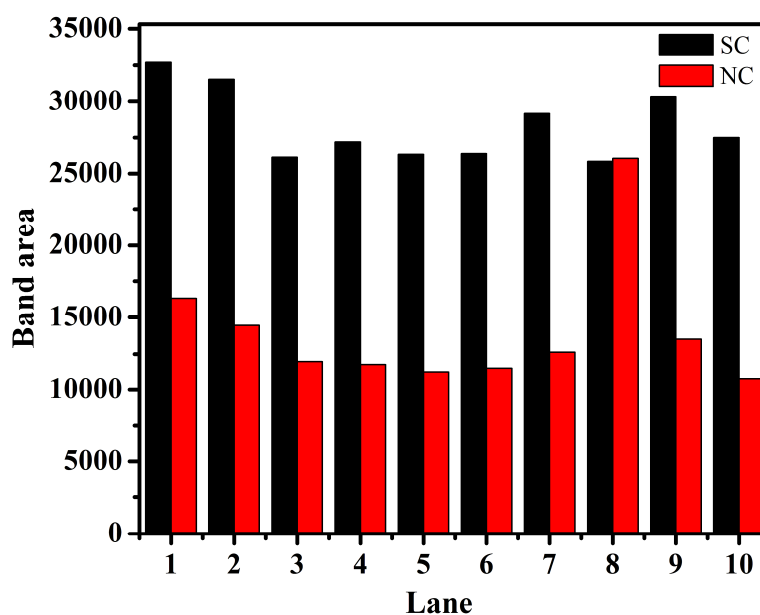
Fig. 4.33 Bar diagram representation of SC and NC form during nuclease activity of complex

4.3.9. Protease activity

The efficiency of complex **8**·to cleave peptide bonds of BSA as substrate was monitored using SDS−PAGE. The protein (4 μM) was incubated at 50 °C with the variable concentration of complex **8**·in dimethyformamide and for 20 h as shown in the Fig. 4.34

Complex **8**·was found to be efficient for protein cleavage activity at higher concentration although in presence of oxidizing agent H_2O_2 complex **8** cleaved the BSA in small fragments leading to the disappearance of band.[360] Control experiment (lane 10) showed no cleavage in presence of H_2O_2 without any complex.
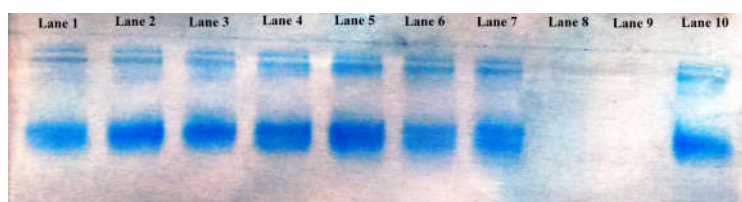
Fig. 4.34 SDS−PAGE of BSA (4 μM) incubated with complexes **8** in a 0.1 M buffer containing 10% DMF incubated at variable tempreture and concentration of complex at 50 °C (a) 3 h (b) 20 h. Lane 1: BSA, lane 2: BSA + Fe(ClO$_4$)$_3$.xH$_2$O (100 μM), lane 3: BSA + ^{tBu}PhimpH (100 μM), lane 4: BSA + DMF (100 μM), lane 5: BSA + **8** (10 μM), lane 6: BSA + **8** (25 μM), lane 7: BSA + **8** (50 μM), lane 8: BSA + **8** (100 μM), lane 9: BSA + **8** (100 μM) +H$_2$O$_2$(100 μM), lane 10: BSA + H$_2$O$_2$(100 μM)

4.4. Conclusions

Herein we designed novel tridentate meridional ligands having 3N donor. These ligands were characterized using IR, UV−visible, GC−MS and NMR spectral studies. Ligands were utilized to synthesize manganese(II) complexes. Complexes Mn(H−N$_3$L)Cl$_2$ (**8**), [Mn(H−N$_3$L)$_2$](ClO$_4$)$_2$ (**9**), Mn(Me−N$_3$L)Cl$_2$ (**10**), [Mn(Me−N$_3$L)$_2$](ClO$_4$)$_2$ (**11**) were isolated in good yield and characterized using various spectroscopic techniques such as IR, UV−visible spectral studies, magnetic moment data and conductivity measurements to confirm the formation of desired complexes. X−ray crystal structures of complex **10**·CH$_3$COCH$_3$ revealed square pyramidal geometry around manganese(II) metal centre. Bond distances and bond angles were in good agreement to the reported manganese(II) metal centre. Electrochemical studies were also optimized for complexes **8–11**. All the complexes were found to be potent SOD mimic and exhibited IC$_{50}$ values in micromolar (μM) range. DNA binding studies of complex **8–11** indicated intercalative mode of

interaction. Complex **8** was also subjected to nuclease and protease activity. Complex **8** found to be an efficient artificial nuclease as well as protease in presence of oxidising agent H_2O_2.

4.5. Experimental section

4.5.1. Materials and instrumental methods

Analytical grade reagents phenylhydrazine, hydrogen peroxide (S. D. Fine, Mumbai, India) and 2–chloromethylpyridine hydrochloride (Sigma Aldrich, Steinheim, Germany), methyl–2–pyridyl ketone (Himedia Laboratories Pvt. Ltd., Mumbai, India), ethylenediaminetetraacetic acid, $MnCl_2.4H_2O$ (Merck Limited, Mumbai, India), and $Mn(ClO_4)_2.6H_2O$ (Sigma Aldrich, Steinheim, Germany) were used as obtained.

The supercoiled *pBR322* DNA and CT–DNA were purchased from Bangalore Genei (India) and stored at 4 ˚C. Agarose (molecular biology grade) and ethidium bromide were obtained from Sigma Aldrich. Xanthine, nitro blue tetrazolium (NBT) and catalase were obtained from Himedia and xanthine oxidase (XO) from bovine milk was purchased from Sigma. Tris(hydroxymethyl)aminomethane–HCl (Tris–HCl) buffer and phosphate buffer were prepared in deionised water. All the chemical are of reagent grade and used as purchased. Solvents used for spectroscopic studies were HPLC grade and purified by standard procedures before use. Electronic spectra were recorded in methanol and phosphate buffer solution with UV–2450, Shimadzu, UV–visible spectrophotometer using cuvettes of 1 cm path length. Fluorescence spectra were recorded by RF5301PC Shimadzu spectrofluorophotometer. Circular dichroism (CD) spectra were recorded on Chirascan circular dichroism spectrometer, Applied photophysics, UK.

4.5.2. Synthesis of ligands

4.5.2.1. Synthesis of 1–phenyl–1–(pyridine–2–ylmethyl)–2–(pyridine–2–ylmethylene)hydrazine (H–N₃L)

Synthesis of ligand 1–phenyl–1–(pyridine–2–ylmethyl)–2–(pyridine–2–ylmethylene)hydrazine (H–N₃L) was performed in two steps: (i) Synthesis of amine and (ii) Synthesis of Schiff's base of amine with corresponding aldehyde.

4.5.2.1.1. Synthesis of amine 1–phenyl–1– (pyridine–2–ylmethyl)hydrazine

Amine has been prepared using a modified procedure to improve the yield and avoid side products as reported previously.[504]

To a 100 mL solution of phenylhydrazine (108 mg, 1.00 mmol), 2–(chloromethyl)pyridine hydrochloride (164 mg, 1.00 mmol) in THF:ACN (1:1) added potassium carbonate (414 mg, 3.00 mmol,) and potassium iodide portion–wise (166 mg, 1.00 mmol). Reaction mixture kept on refluxing for 4 h. Solvent was evaporated red–brown color oil separated out. Oily compound was taken in CH_2Cl_2 and washed with $NaHCO_3$ (aq) and brine, dried over sodium sulphate. Solvent was evaporated and red color oil was used as obtained. Purity of compound was checked using TLC. Yield: 78 %.

4.5.2.1.2. Synthesis of 1–phenyl–1–(pyridine–2–ylmethyl)–2–(pyridine–2–ylmethylene)hydrazine (H–N₃L)

1–phenyl–1–(pyridine–2–ylmethyl)hydrazine (199 mg, 1.00 mmol) was taken in 5 mL methanol and stirred. A solution of pyridine 2–carboxaldehyde (108 mg, 1.00 mmol) was taken in methanol and added to the stirred solution of amine. Reaction was continued to stirr for further 4–5 h at ambient temperature. Evaporation of solvent gave rise to yellow–red oil which was used without further purification. Purity of compound was checked using TLC. Yield: 72%. GC–MS (MeOH, m/z): 288 (M⁺). Selected IR data (KBr, v_{max}/cm^{-1}): 1594 $v_{C=Nimine}$. UV–visible [MeOH, λ_{max}/nm ($\varepsilon/M^{-1}cm^{-1}$)]: 342 (20,220), 295 (5,830), 238 (14,470). ¹H–NMR (CDCl₃, δ/ppm, 400 MHz): 8.62 (1H, d, J = 4.1 Hz), 8.46 (1H, t, J = 3.9 Hz), 8.04 (1H, dd, J = 7.6, 4.8 Hz), 7.70–7.61 (1H, m), 7.59–7.51 (2H, m), 7.43 (2H, d, J = 8.2 Hz), 7.37–7.29 (2H, m), 7.19–7.04 (3H, m), 7.00 (1H, q, J = 6.3 Hz), 5.31 (2H, d, J = 4.6

Hz). ^{13}C–NMR (CDCl$_3$, δ/ppm, 400 MHz): 155.55, 154.97, 149.91, 148.85, 146.88, 137.16, 136.01, 133.49, 129.32, 122.57, 122.32, 121.77, 120.52, 119.50, 115.34. Anal. Calcd for C$_{18}$H$_{16}$N$_4$: C, 74.98; H, 5.59; N, 19.43, Found: C, 71.53; H, 5.09; N, 17.66.

4.5.2.2. Synthesis of 1−phenyl−2−(1−(pyridin−2−yl)ethylidene)−1−(pyridin−2−ylmethyl)hydrazine (Me−N$_3$L)

1−phenyl−2−(1−(pyridin−2−yl)ethylidene)−1−(pyridin−2−ylmethyl)hydrazine (Me−N$_3$L) was prepared according to modified method reported previously.[504] Yield: 68%. GC–MS (MeOH, m/z): 302 (M$^+$). Selected IR data (KBr, ν_{max}/cm^{-1}): 1593 $\nu_{C=Nimine}$. UV−visible [MeOH, λ_{max}/nm (ε/M^{-1}cm^{-1})]: 341 (6,210), 280 (6100), 251 (14,980). ^{1}H–NMR (CDCl$_3$, δ/ppm, 400 MHz): 8.608 (dd, J=4.5 Hz, 8.75 Hz, 2H), 8.232 (d, J=8 Hz, 1H), 7.710 (t, J=7.75 Hz, 1H), 7.637 (t, J=7.75 Hz, 1H), 7.467 (d, J=8Hz, 1H), 7.290 (m, 3H), 7.173 (dd, J= 5 Hz, 7.25 Hz, 1H), 7.007 (d, J=7.5, 2H), 6.960 (t, J=7.5 Hz, 1H), 5.042 (s, 2H), 2.35 (s, 3H). ^{13}C–NMR (CDCl$_3$, δ/ppm, 400 MHz): 163.71, 159.00, 155.95, 149.84, 148.58, 136.69, 136.19, 129.05, 124.01, 122.08, 122.01, 121.37, 121.07, 117.39. Anal. Calcd for C$_{19}$H$_{18}$N$_4$: C, 75.47; H, 6.00; N, 18.53, Found: C, 74.85; H, 5.80; N, 19.42.

4.5.3. Synthesis of metal complexes

Caution! Perchlorate salts of metal complexes with organic ligands are potentially explosive. Only a small quantity of material should be prepared and handled carefully.

4.5.3.1. Synthesis of Mn(H−N$_3$L)Cl$_2$ (8)

A batch of (99 mg, 0.5 mmol) MnCl$_2$.4H$_2$O in 3 mL of ethanol was added dropwise to stirred methanolic solution (10 mL) of (140 mg, 0.5 mmol) ligand H−N$_3$L. The color of solution changed to orange. The orange solution stirred for 3 h. On slow evaporation of solvent an orange color crystalline compound was obtained which was filtered and washed with small amount of ethanol and diethylether. Yield: 62%. Selected IR data (KBr, ν_{max}/cm^{-1}): 1602, $\nu_{C=Nimine}$. UV−visible [CH$_3$OH, λ_{max}/nm (ε/M^{-1}cm^{-1})]: 203 (14,710), 236 (9,580), 294 (3,960), 341 (15,330). μ_{eff} (300 K): 5.36 BM. Λ_M/Ω^{-1}cm^{2}mol^{-1} (in DMF): 28. ESI–

MS(Positive ion mode, CH_3CN): m/z =378 $[M–Cl]^+$. Anal. Calc. For $C_{18}H_{16}N_4Cl_2Mn$: C, 52.20; H, 3.89; N, 17.12. Found C, 50.87; H, 3.95; N, 16.48.

4.5.3.2. Synthesis of $[Mn(H–N_3L)_2](ClO_4)_2$ (9)

To a stirred methanolic (5–8 mL) solution of ligand $H–N_3L$ (1.00 mmol, 288 mg), a batch of $Mn(ClO_4)_2.xH_2O$ (127 mg, 0.5 mmol) in 3 mL of methanol was added dropwise. A significant color change was observed to yellowish orange and reaction mixture was further stirred for 3–4 h. Solvent was removed by slow evaporation leading to a crystalline compound. Yield: 58%. Selected IR data (KBr, v_{max}/cm^{-1}): 1604, $v_{C=Nimine}$1092, 623 v_{ClO4}. UV–visible [CH_3OH, λ_{max}/nm ($\varepsilon/M^{-1}cm^{-1}$)]: 204 (25,780), 225 (16,560), 252 (19,440), 344 (7,000). μ_{eff} (300 K): 5.21 BM. $\Lambda_M/\Omega^{-1}cm^2mol^{-1}$ (in DMF): 130. Anal. Calc. For $C_{36}H_{32}N_8O_8Cl_2Mn$: C, 52.06; H, 3.88; N, 13.49. Found C, 51.45; H, 3.12; N, 14.03.

4.5.3.3. Synthesis of $Mn(Me–N_3L)Cl_2 \cdot CH_3COCH_3$ ($10 \cdot CH_3COCH_3$)

A batch of (99 mg, 0.5 mmol) $MnCl_2.4H_2O$ in 3 mL of ethanol was added dropwise to stirred solution of (151 mg, 0.5 mmol) ligand ($Me–N_3L$) in 15 mL of methanol. The color of solution changed to orange and stirred for 3 h. Orange color precipitate was obtained which was filtered and washed with small amount of ethanol and diethylether. Crystals were grown in acetone diffusion of ether. Yield: 66%. Selected IR data (KBr, v_{max}/cm^{-1}): 1595, $v_{C=Nimine}$. UV–visible [CH_2Cl_2, λ_{max}/nm ($\varepsilon/M^{-1}cm^{-1}$)]: 202 (26,210), 225 (13,720), 251(17,670), 344 (5,980). μ_{eff} (300 K): 5.11 BM. $\Lambda_M/\Omega^{-1}cm^2mol^{-1}$ (in DMF): 22. ESI–MS–(Positive ion mode, CH_3CN): m/z = 450.01 $[M+Na]^+$, 393.06 $[M–Cl]^+$, 325.14 $[L+Na]^+$ and 301.14 $[L+H]^+$. Anal. Calc. For $C_{19}H_{18}N_4Cl_2Mn$: C, 53.29; H, 4.24; N, 13.08. Found C, 52.27; H, 3.67; N, 13.03.

4.5.3.4. Synthesis of $[Mn(Me–N_3L)_2](ClO_4)_2$ (11)

A batch of (127 mg, 0.5 mmol) $Mn(ClO_4)_2.xH_2O$ in 3 mL of methanol was added dropwise, to the stirred solution of (302 mg, 1.00 mmol) ligand ($Me–N_3L$) in 10 mL of

methanol. The color of solution changed to yellow orange. Yellow orange solution was stirred for 3−4 h. Yellow orange solid was separated out which was filtered and washed with methanol and small amount of diethylether. Yield: 53%. Selected IR data (KBr, ν_{max}/cm^{-1}): 1600, $\nu_{C=Nimine}$, 1096, 623 $\nu_{ClO4−}$. UV–visible [CH_3OH, λ_{max}/nm ($\varepsilon/M^{-1}cm^{-1}$)]: 206 (57,260), 220 (50,460), 251 (44,290), 343 (14,970). μ_{eff} (300 K): 5.09 BM, $\Lambda_M/\Omega^{-1}cm^2mol^{-1}$ (in DMF): 142. ESI–MS (Positive ion mode, CH_3CN): m/z = 758.18 $[M–ClO4]^+$. Anal. Calc. For $C_{38}H_{36}N_8O_8Cl_2Mn$: C, 53.16; H, 4.23; N, 13.05. Found C, 52.60; H, 3.77; N, 13.43.

4.5.4. Measurement of superoxide dismutase (SOD) activity

Superoxide dismutase activities of complexes **8**, **9**, **10** and **11** were monitored using indirect method using NBT (nitro blue tetrazolium) assay. Superoxide anion was generated in situ enzymetically using xanthine/xantine oxidase system and detected spectrophotometrically by reduction of NBT to blue colour formazan dye. Formation of formazan dye gives rise to band at 560 nm.[396] Addition of complexes to this will reduce the absorbance of this band due to the tendency of complexes to demolish the superoxide ion. The assay was carried out in phosphate buffer (50 mM) at pH 7.8 using 0.2 mM xanthine, 0.12 mM NBT, 0.07 U/mL xanthine oxidase and catalase 1000 U/mL (final volume = 750 μL). The tested compounds were dissolved in DMF and the final concentration of DMF in reaction mixture was 0.1% in phosphate buffer at pH 7.8. The reaction was initiated by adding 0.07 U/mL xanthine oxidase and measurement was started after incubation of 15 min for each measurement. IC_{50} value for SOD activity was defined as the concentration of the compound for the 50 % inhibition of the NBT absorbance due to the superoxide radicals generated during the reaction.

4.5.5. DNA–binding activity

Absorbance titration experiment were carried out with at constant complex concentration varying the CT–DNA concentration in 0.1 M phosphate buffer (pH 7.2) containing 10% DMF. Fluorescence quenching experiments were carried out by the

successive addition of complexes to the DNA (25 µM) solutions containing 5 µM ethidium bromide (EB) in 0.1 M phosphate buffer (pH 7.2). For better solubility of complexes, 10% DMF was also used. These samples were excited at 250 nm and emissions were observed between 500–700 nm. Stern–Volmer quenching constants were calculated using the given equation

$$I_0 / I = 1 + K_{sv} Q,$$

Where I_0 and I are the fluorescence intensities in the absence and presence of complex and Q is the concentration of quencher (complexes). K_{sv} is a linear Stern–Volmer constant and given by the ratio of slope to intercept in the plot of I_0 / I versus Q.[396] Circular dichroism (CD) spectra of CT–DNA in absence and presence of the manganese complexes were recorded with a 0.1 cm path length cuvette after 10 min incubation at 25 °C. The concentration of the complexes and CT–DNA were 50 and 200 µM respectively.

4.5.6. Nuclease activity

As described in the chapter 2.

4.5.7. Protease activity

As described in the chapter 2.

4.5.8. Density functional theory (DFT) calculations

As described in the chapter 2.

4.5.9. X–ray structure determination

The X–ray data collection for complex **10** was performed at 296 K using Mo–Kα (0.71073). Crystal data, data collection parameters and refinement details of the structure determinations has been summarized in Table 4.13.

Table 4.13 Crystallographic parameters of complex **10**

Empirical formula	$C_{22}H_{23}N_4OCl_2Mn$
Formula weight (gmol^{-1})	485.28
Temperature /K	296(2)
λ (Å) (Mo–Kα)	0.71073
Crystal system	Monoclinic
Space group	P 21/n
a (Å)	7.8634(2)
b (Å)	17.4229(3)
c (Å)	17.1614(3)
α (°)	90.00
γ (°)	90.00
β (°)	90.4300(10)
V (Å^3)	2351.10(8)
Z	4
ρ_{calc} (gcm^{-3})	1.371
Crystal size (mm)	0.20 × 0.19 × 0.14
F(000)	1000.0
Theta range for data collection	1.67–28.010
Index ranges	–10<h<10,–23<k<22,–22<l<22
Refinement method	Full matrix least–squares on F^2
Data/restraints/parameters	5658/0/282
GOF^a on F^2	0.777
R$_1$^{b} [I > 2σ(I)]	0.0434
R$_1$[all data]	0.0758
wR$_2$^{c} [I > 2σ(I)]	0.1579
wR$_2$ [all data]	0.2073

^{a} GOF = $[\Sigma[w(F_o^2 - F_c^2)^2] / M - N)]^{1/2}$ (M = number of reflections, N = number of parameters refined). ^{b} $R_1 = \Sigma \| F_o | - | F_c \| / \Sigma | F_o |$, ^{c} $wR_2 = [\Sigma[w(F_o^2 - F_c^2)^2]/\Sigma [w(F_o^2)^2]]^{1/2}$

Chapter-5

Synthesis and Characterization of Mononuclear Iron Complexes Derived from Ligand having Tridentate 3N Donor: DNA Binding and Nuclease Activity

5.1. Abstract

Tridentate ligands H–N_3L and Me–N_3L have been utilized to synthesized mononuclear iron complexes. Complexes Fe(H–N_3L)Cl_3 **(12)** [Fe(H–N_3L)$_2$]$(ClO_4)_2$ **(13)** Fe(Me–N_3L)Cl_3 **(14)** and [Fe(Me-N_3L)$_2$]$(ClO_4)_2$ **(15)** have been synthesized and characterized using elemental analysis, IR, UV–visible and ESI–MS spectral studies. Magnetic moments and conductivity measurements also supported the formulated structures of the complexes. NMR spectral studies were also performed for complexes **13** and **15** due to the presence of low–spin Fe(II) metal centre. Structural and geometrical aspects were monitored using DFT calculations. TD–DFT calculations were also performed to optimize the electronic properties. Electrochemical studies were also investigated for representative complex. Due to the stability in buffer complexes were subjected to the DNA interaction studies. DNA binding studies were monitored using UV–visible, fluorescence and CD spectral studies. Nuclease activity was monitored for the representative complexes and exhibited oxidative nuclease in presence of oxidizing agent (H_2O_2).

5.2. Introduction

Mononuclear iron complexes having tridentate 3N donors are of extreme current interest in several areas of chemical research such as structural and functional modelling of mononuclear iron enzymes such as catechol dioxygenase (CDO),[524,525] superoxide dismutase (SOD).[526] Several groups are interested in designing oxidation catalyst with such kind of mononuclear iron complexes. Chemistry of iron with the nitrogen donor ligands has been an interesting area to explore.[527–529] In this regard, Que and co–workers have utilized a tetradentate ligand TPA for the synthesis of iron complexes. These complexes were utilized for the functional modelling of non–heme iron enzymes capable of alkane functionalization.[530] Hitomi and co–workers have reported iron complexes derived from ligands having nitrogen donors. These complexes were found to be potent applicant in the hydroxylation of alkane C–H bonds with high selectivity.[531] Roelfes *et. al.* have synthesized iron complexes using N4Py a pentadentate ligand. This complex was proved to be an efficient catalyst for diverse substrate oxidation reactions.[532] Iron complexes derived from nitrogen donor ligands have been shown remarkable magnetic properties as in spin state crossover[533–535] and also used as polymerization catalyst.[536] We have been working with ligand Pyimpy, Me−Pyimpy and recently reported spontaneous reduction and nuclease activities of corresponding iron complexes.[507] Such types of ligands are similar to bis iminopyridine ligands reported by Chirik and co–workers which have shown several type of interesting activities.[537–541]

As a part of our ongoing research[396,497,542,543,398,544–551] we have designed ligand H−N$_3$L, Me−N$_3$L and synthesized mononuclear iron complexes Fe(H−N$_3$L)Cl$_3$ (**12**), [Fe(H−N$_3$L)$_2$](ClO$_4$)$_2$ (**13**), Fe(Me−N$_3$L)Cl$_3$ (**14**) and [Fe(Me−N$_3$L)$_2$](ClO$_4$)$_2$ (**15**). These complexes were characterized spectroscopically using IR, UV–visible, NMR and ESI–MS spectral studies. Theoretical calculations were also elucidated geometrical and structural

parameters. TD–DFT calculations were monitored for the representative complex **12** to study the electronic properties. Electrochemical studies were also performed for complexes **12** and **13**. These complexes were found to be stable in aqueous buffer system and hence subjected to DNA binding and nuclease studies. Complex **12** exhibited effective oxidative cleavage in presence of H_2O_2.
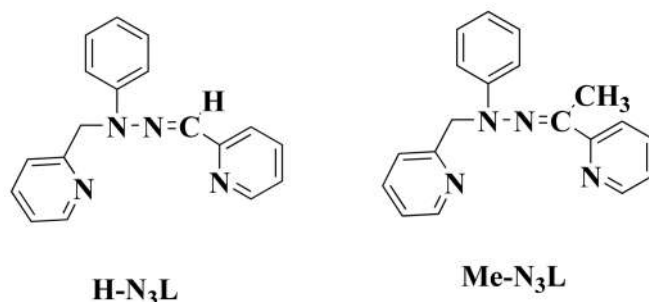
Fig. 5.1 Tridentate ligands with abbreviation used in the present work

5.3. Results and discussion

5.3.1. Synthesis and characterization of ligands

Tridentate ligands H−N$_3$L and Me−N$_3$L have been synthesized in two steps (i) Synthesis of amine (ii) Synthesis of Schiff's base using amine with corresponding aldehyde as described in chapter 4.

5.3.2. Synthesis and characterization of metal complexes

Mononuclear iron complex Fe(H−N$_3$L)Cl$_3$, **12** was synthesized using Et$_4$N[FeCl$_4$] and ligand H−N$_3$L in equimolar ratio. Two equivalent of ligand H−N$_3$L and Fe(ClO$_4$)$_2$.xH$_2$O were utilized to prepare bis complex of [Fe(H−N$_3$L)$_2$](ClO$_4$)$_2$, **13** in ethanol:methanol (1:1) solutions. Similar procedures were followed to prepare Fe(Me−N$_3$L)Cl$_3$, **14** and [Fe(Me−N$_3$L)$_2$](ClO$_4$)$_2$, **15** using equimolar ratio of ligand Me−N$_3$L with Et$_4$N[FeCl$_4$] in case of complex **14** and two equivalent of ligand with one equivalent of Fe(ClO$_4$)$_2$.xH$_2$O in

case of complex **15**. The schematic representation of synthetic procedures of complexes **12**, **13**, **14** and **15** has been summarized in Scheme 5.1.
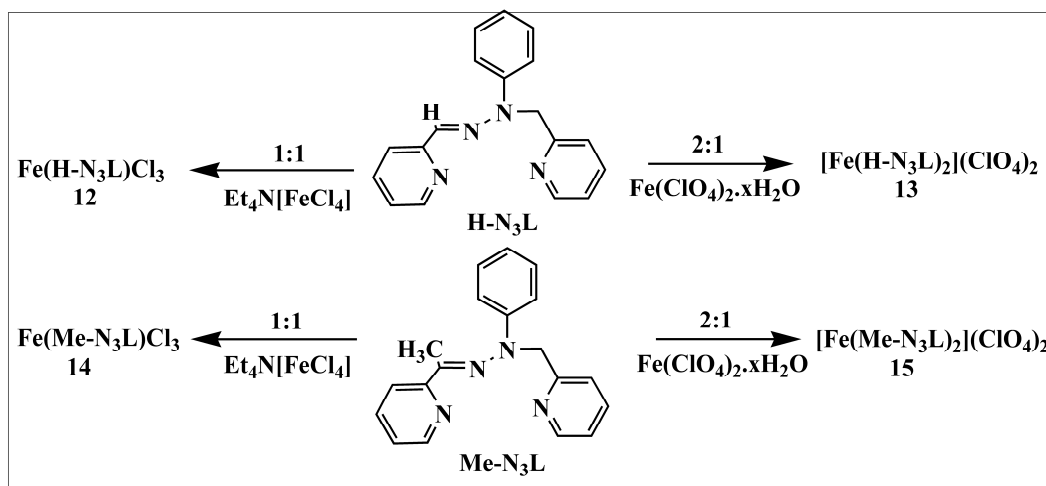
Scheme 5.1 Schematic representation of synthesis of iron complexes

5.3.2.1. IR spectral studies

During IR spectral studies characteristic azomethine ($v_{-HC=N}$) band for free ligands were observed at ~1595 cm^{-1}. On metal complexation all the iron complexes exhibited shift in stretching frequency. These shifts exhibited the probable coordination of azomethine with the metal during complex formation.[552,553] Complex **13** and **15** also showed characteristic band near 1090 cm^{-1} together with a band at 623 cm^{-1} for non−coordinated perchlorate ion.[401] The experimental IR data for all complexes have been deposited in Table 5.1.

Table 5.1 Data for IR and conductivity studies for complexes

Complex	IR data (cm^{-1})^a		Conductivity data ($\Omega^{-1}cm^2mol^{-1}$)^b
	$v_{-HC=N}$	$v_{ClO4}-$	
12	1606	–	52 (neutral)
13	1606	1091, 623	156(2:1)
14	1595	–	41 (neutral)
15	1597	1095, 618	148(2:1)

^{a}Using KBr pellets, ^{b}Solvent: Dimethylformamide

5.3.2.2. Electronic absorption spectral studies

Absorption spectral studies were also performed for all the complexes in methanol and depicted in Fig. 5.2 and Table 5.2. High energy band observed below 250 nm is probably due to the intraligand $\pi-\pi^*$ and $n-\pi^*$ transitions. The band originated at higher wavelength in the range 400–550 nm could be due to $d-\pi^*$, chloro to iron and other LMCT transitions.[554,555]

Table 5.2 Electronic absorption spectral data of iron complexes

Complex	UV−visible data (λ_{max}/nm, ε/M^{-1}cm^{-1})[a]
12	452 (500), 343 (7,520), 300 (4,930), 259 (7,960), 221 (10,740)
13	550(210), 340 (31,290), 294 (11,010), 258 (14,840), 238 (24,160)
14	435 (790), 329 (3,980), 260 (6,500), 225 (8,220)
15	552(350), 345(8,720), 285(9,790), 250(27,740)

[a]UV−visible data of complexes in methanol
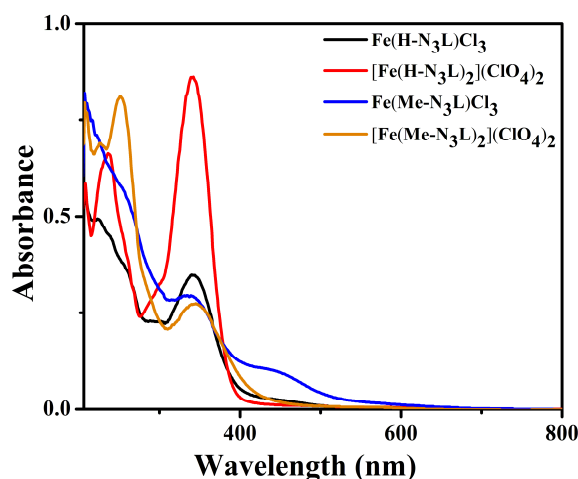
Fig. 5.2 UV−visible absorption spectra of iron complexes in methanol

5.3.2.3. Conductivity studies

The molar conductivity was measured at 25 °C in dimethylformamide at ca. 10^{-3} M. Data have been deposited in Table 5.1. Values for mononuclear complexes **12** and **14** were

found to be 52 and 41 $\Omega^{-1}cm^2mol^{-1}$ respectively. These values suggested neutral electrolytic behavior of the complexes in solution. Complexes **13** and **15** were having the values 156 and 148.0 $\Omega^{-1}cm^2mol^{-1}$ respectively. These values confirmed uni–bivalent (1:2) electrolytic behavior of complexes in solution.[556]

5.3.2.4. Magnetic moment studies

Effective magnetic moments for all the complexes were also calculated. Magnetic moments for complex **12** and **14** were found to be 5.63 and 5.94 BM at 303 K. The values indicated the presence of high spin iron(III) metal centre in the complexes.[411] Complexes **13** and **15** have the value of magnetic moment 2.31 and 2.04 BM at 303 K. These values are employed for the low–spin iron(II) electronic configuration.[557,558] NMR spectra of metal complexes **2** and **4** also supports the presence of low–spin iron(II) center.

5.3.2.5. ESI–MS spectral studies

ESI–MS spectra of the complexes were also recorded in acetonitrile solution at positive ion mode. Complex **12** exhibited peak at m/z 414.1428 corresponding to the $[M–Cl]^+$ as shown in Fig. 5.3.
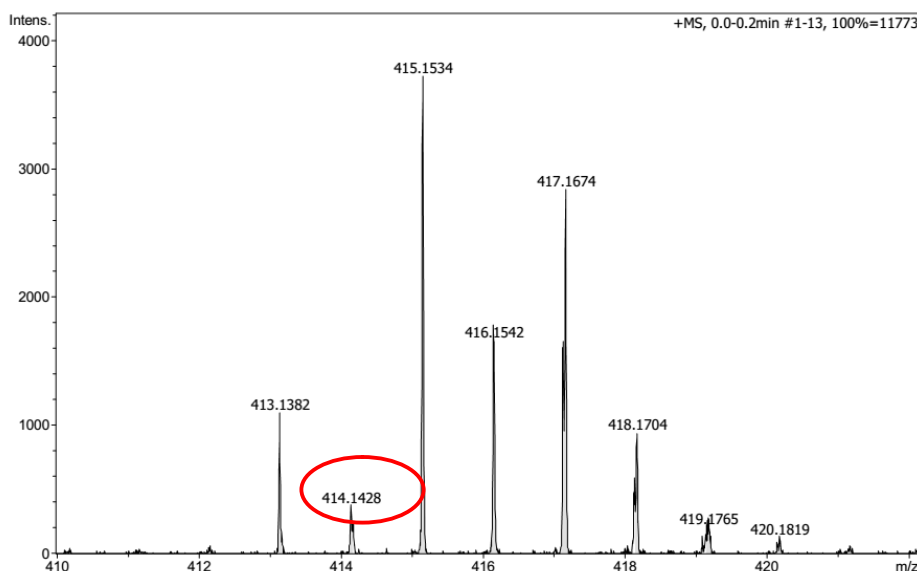
Fig. 5.3 ESI–MS spectrum of complex **12** in acetonitrile under positive ion mode

Similarly, studies performed for complex **13** exhibited peak corresponding to the m/z 731.1615 for $[M-ClO_4]^+$ in acetonitrile solution (Fig. 5.4).
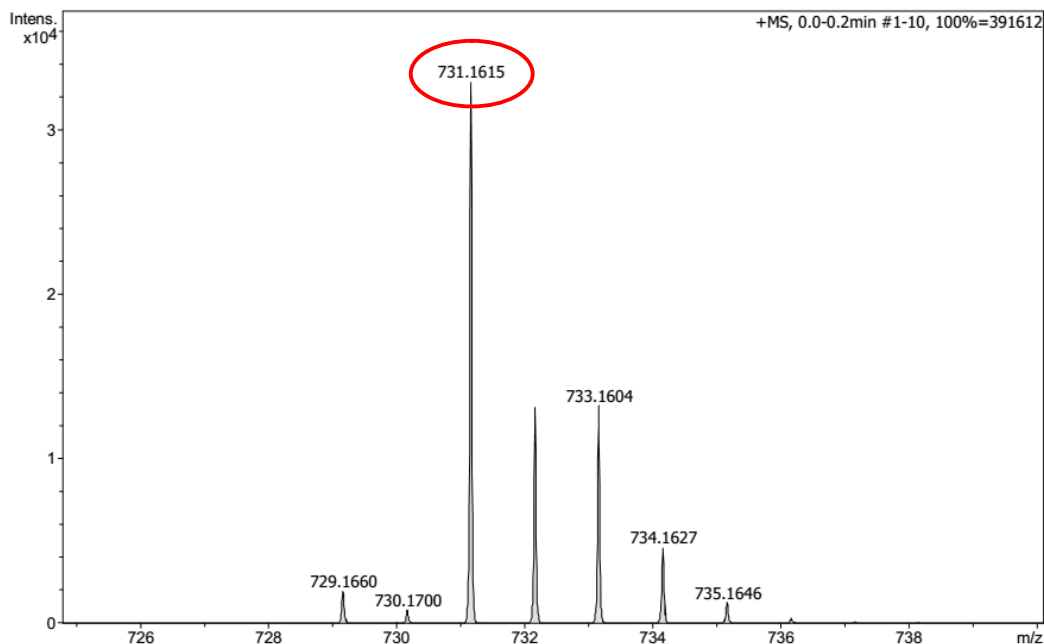
Fig. 5.4 ESI−MS spectrum of complex **13** in acetonitrile under positive ion mode

ESI−MS spectrum of **14** in acetonitrile solutions under positive mode exhibiting the peaks corresponding to $[M-Cl]^+$, $[L+Na]^+$ and $[L+H]^+$ at m/z: 428.02 (1.92%) $[M-Cl]^+$, 325.14 (25.24%) $[L+Na]^+$, 301.14 (65.10%) $[L+H]^+$ respectively (Fig. 5.5).
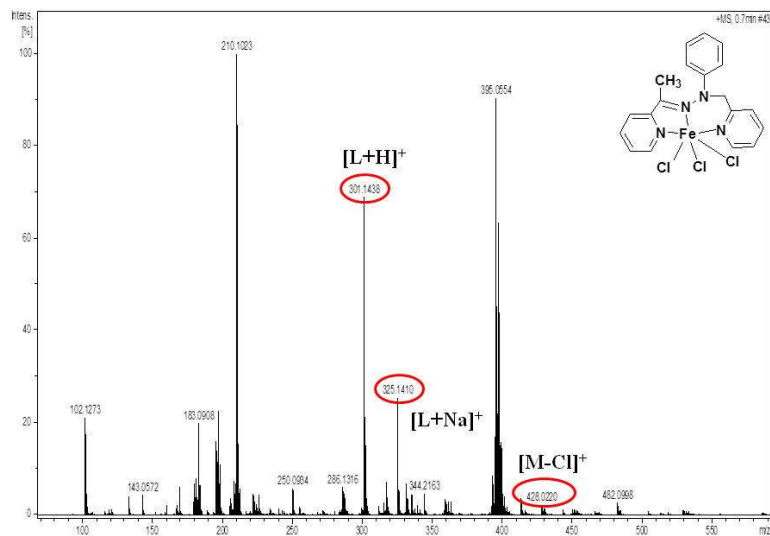
Fig. 5.5 ESI−MS spectrum of complex **14** in acetonitrile under positive ion mode

ESI−MS studies performed for complex **15** showed peak at m/z 759.1790 corresponding to the $[M-ClO_4]^+$ in acetonitrile solution (Fig. 5.6).

179
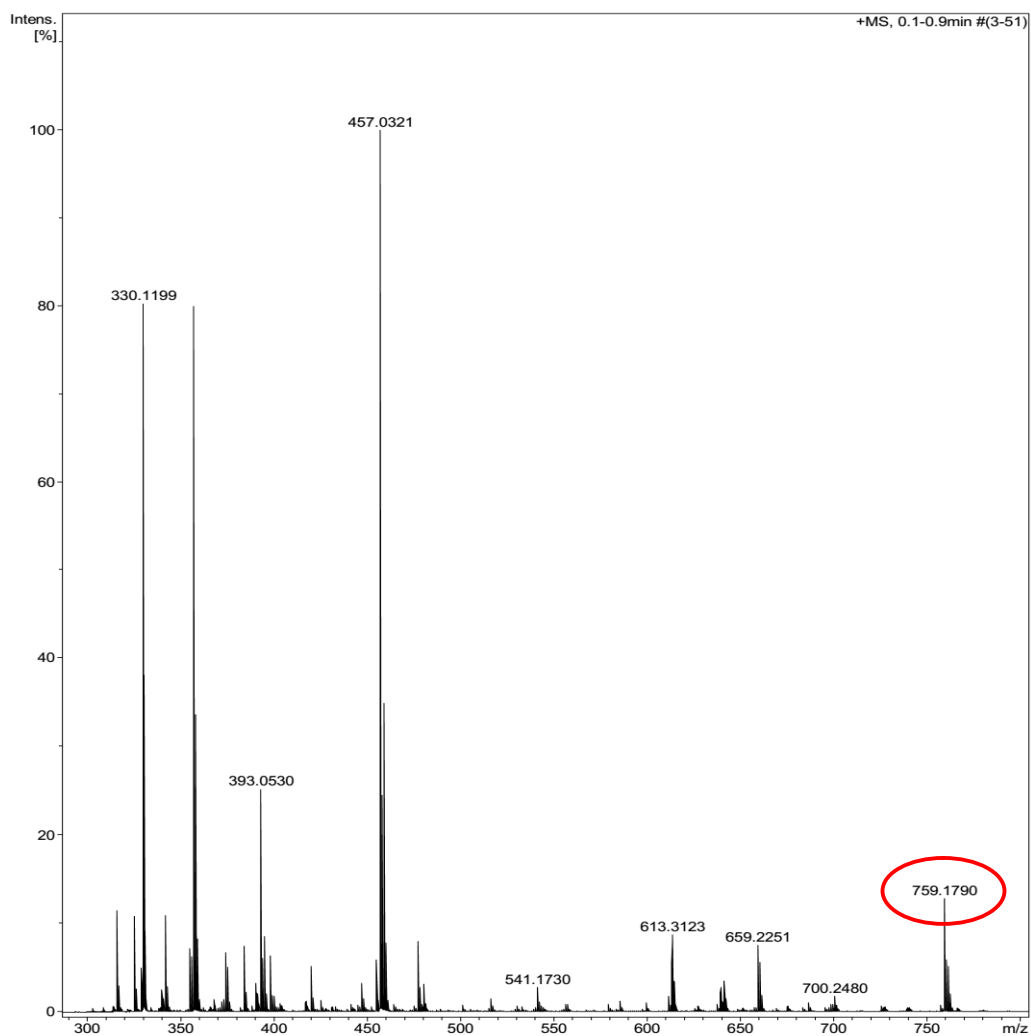
Fig. 5.6 ESI–MS spectrum of complex **15** in acetonitrile under positive ion mode

5.3.2.6. NMR spectral studies

Presence of iron(II) low–spin metal centre the complexes **13** and **15** afforded NMR spectra. However coordination of the ligand with iron metal ion afforded a change in chemical shift as compared to the free ligand. ^{1}H and ^{13}C–NMR spectral data for both the complexes have been shown in Fig. 5.7–5.10.
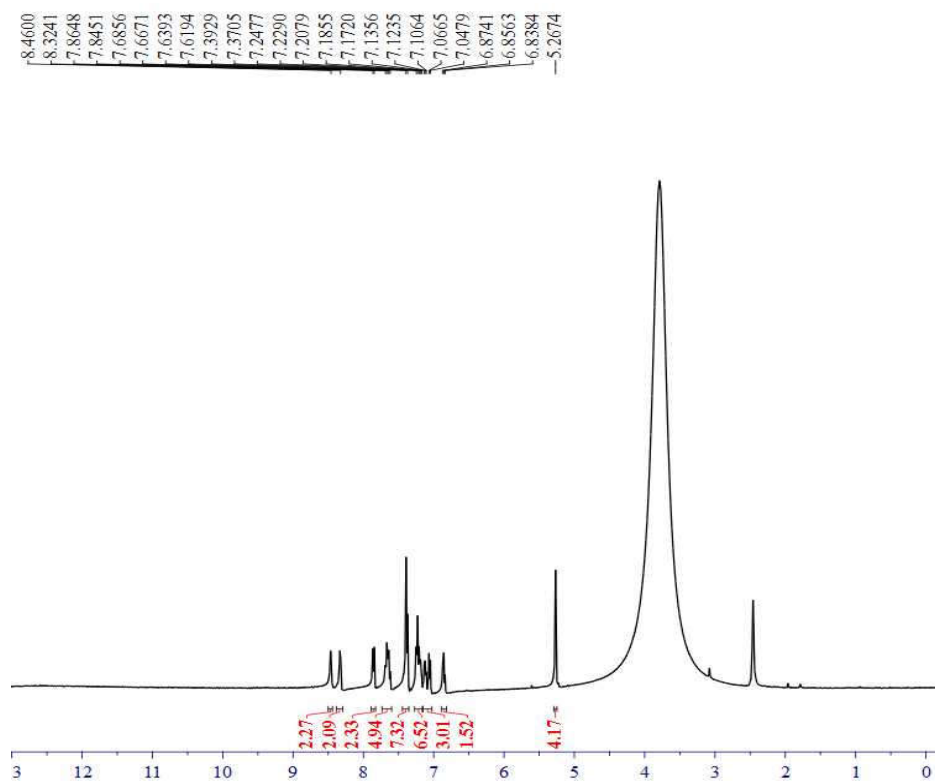
Fig. 5.7 ^{1}H–NMR spectrum of **13** in deuteriated DMSO
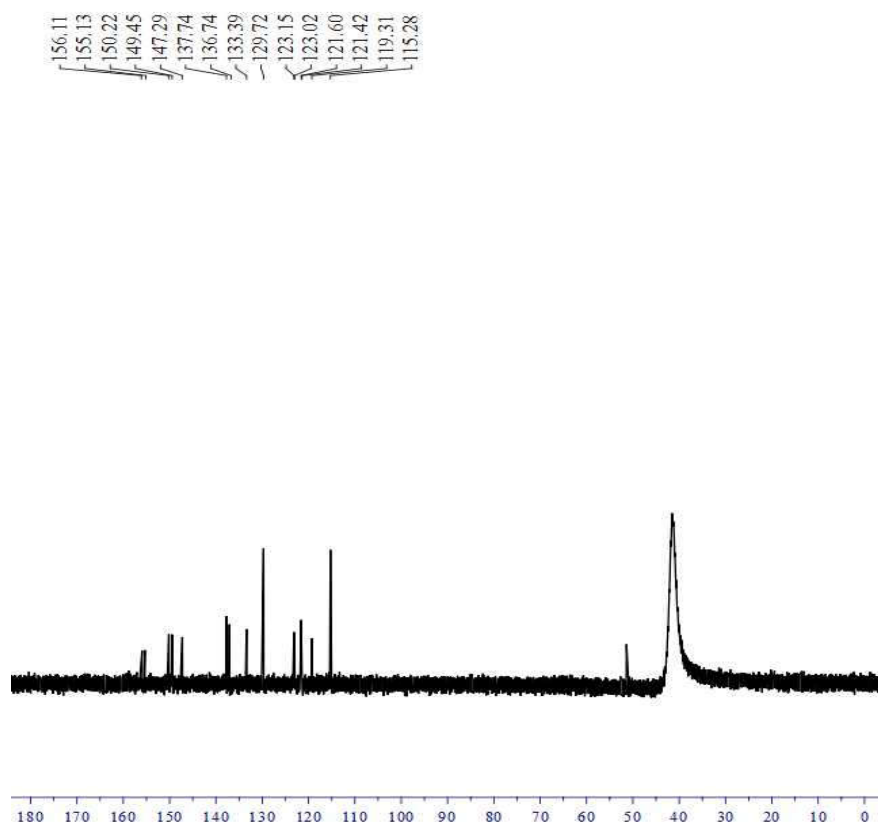
Fig. 5.8 ^{13}C–NMR spectrum of **13** in deuteriated DMSO
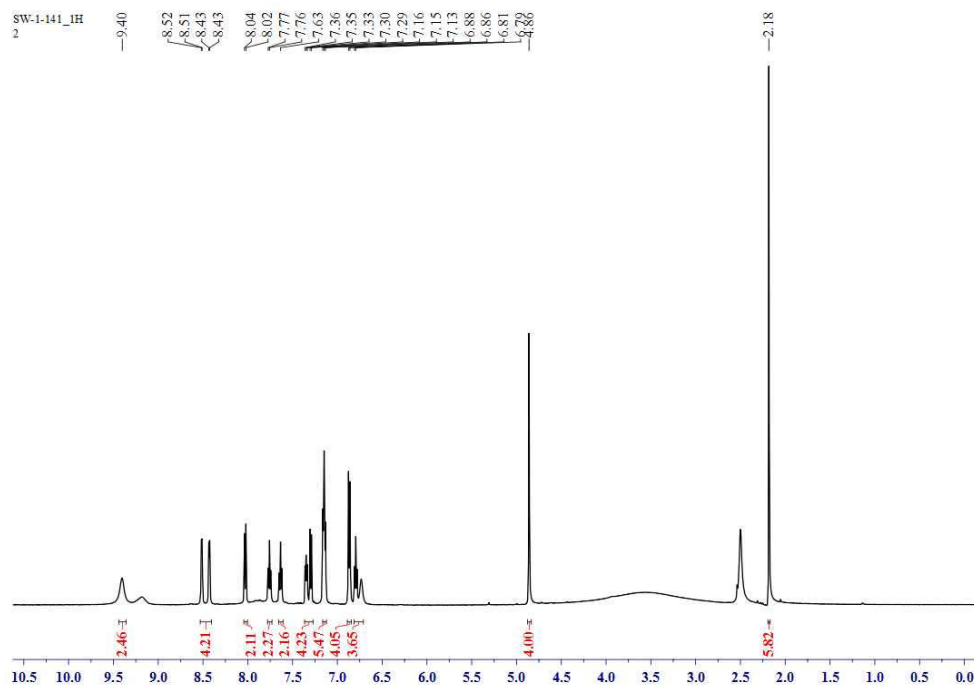
Fig. 5.9 ^{1}H–NMR spectrum of **15** in deuteriated DMSO

182
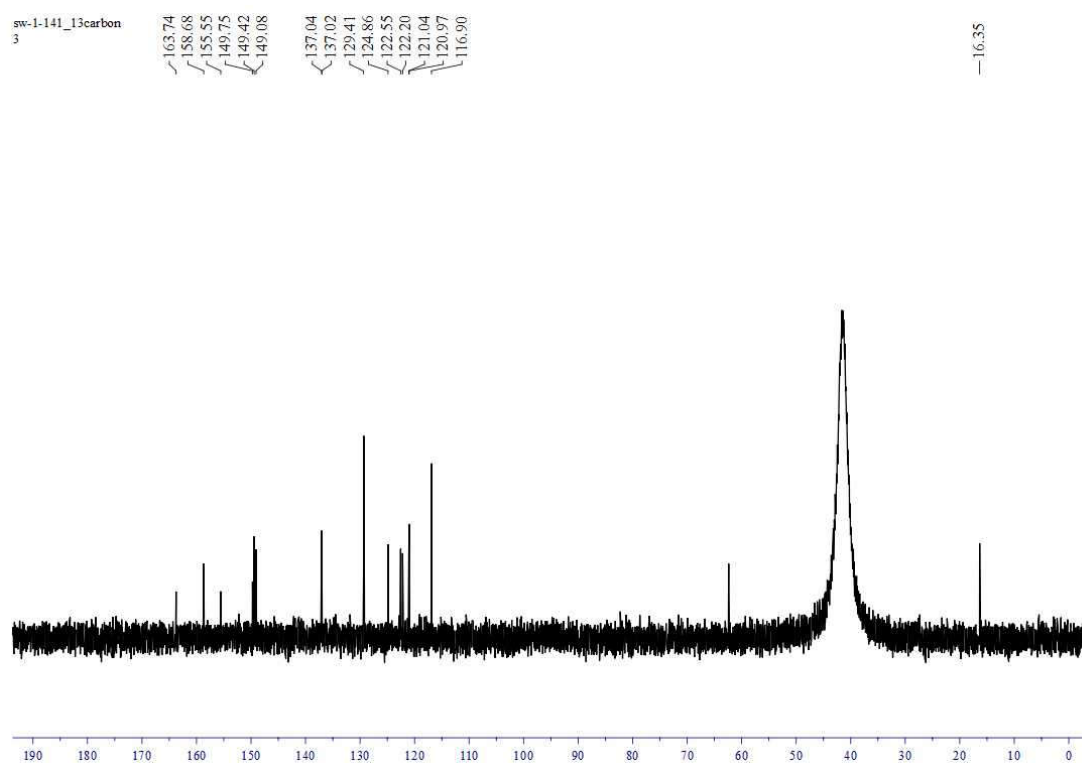
Fig. 5.10 ^{13}C–NMR spectrum of **15** in deuteriated DMSO

5.3.3. Density functional theory (DFT) calculations

Density functional theory (DFT) calculations have been found useful to determine the geometrical and structural properties of metal complexes.[516,559–561] Herein we have performed DFT calculations to elucidate the structural property of complex **12**. Optimized structure of complex **12** has been depicted in Fig. 5.11 and characteristic structural parameters have been summarized in Table 5.3.
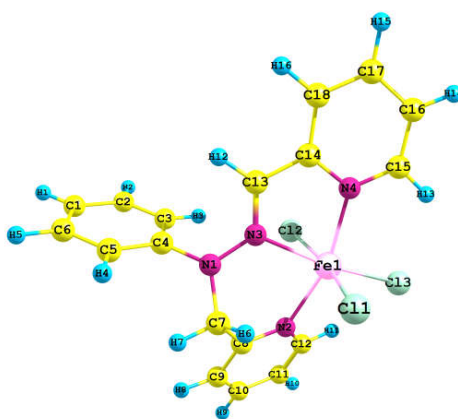
Fig. 5.11 Optimized geometry of the complex **12** using DFT

Table 5.3 Selected bond lengths (Å) and angles (°) of complexes **12** obtained using

DFT

Bond lengths (Å)		Bond angles (°)	
	DFT		**DFT**
Fe(1)−N(2)	2.186	Cl(3)−Fe1−N(2)	99.55
		N(2)−Fe1−Cl(1)	92.95
		N(2)−Fe1−Cl(2)	83.56
		N(2)−Fe1−N(3)	88.25
		N(2)−Fe1−N(4)	161.72
Fe(1)−N(3)	2.252	Cl(3)−Fe1−N(3)	171.83
		N(3)−Fe1−N(4)	74.87
Fe(1)−N(4)	2.145	Cl(3)−Fe1−N(4)	97.08
Fe(1)−Cl(1)	2.399	Cl(1)−Fe1−Cl(2)	166.37
		Cl(1)−Fe1−N(3)	85.06
		N(4)−Fe1−Cl(1)	92.53
		N(2)−Fe1−Cl(1)	92.95
Fe(1)−Cl(2)	2.454	N(4)−Fe1−Cl(2)	87.03
		Cl(2)−Fe1−N(3)	81.67
Fe(1)−Cl(3)	2.328	Cl(3)−Fe1−Cl(2)	96.71
		Cl(3)−Fe1−Cl(1)	96.87

Time dependent DFT (TD–DFT) calculations were also performed on the optimized structure of the complex to verify the electronic transitions in the UV–visible spectrum with the theoretical one. All the theoretical calculations were performed in the gas phase. The HOMO and LUMO have been depicted in the Fig. 5.12.

HOMO (α)   **LUMO (α)**

HOMO (β)   **LUMO (β)**
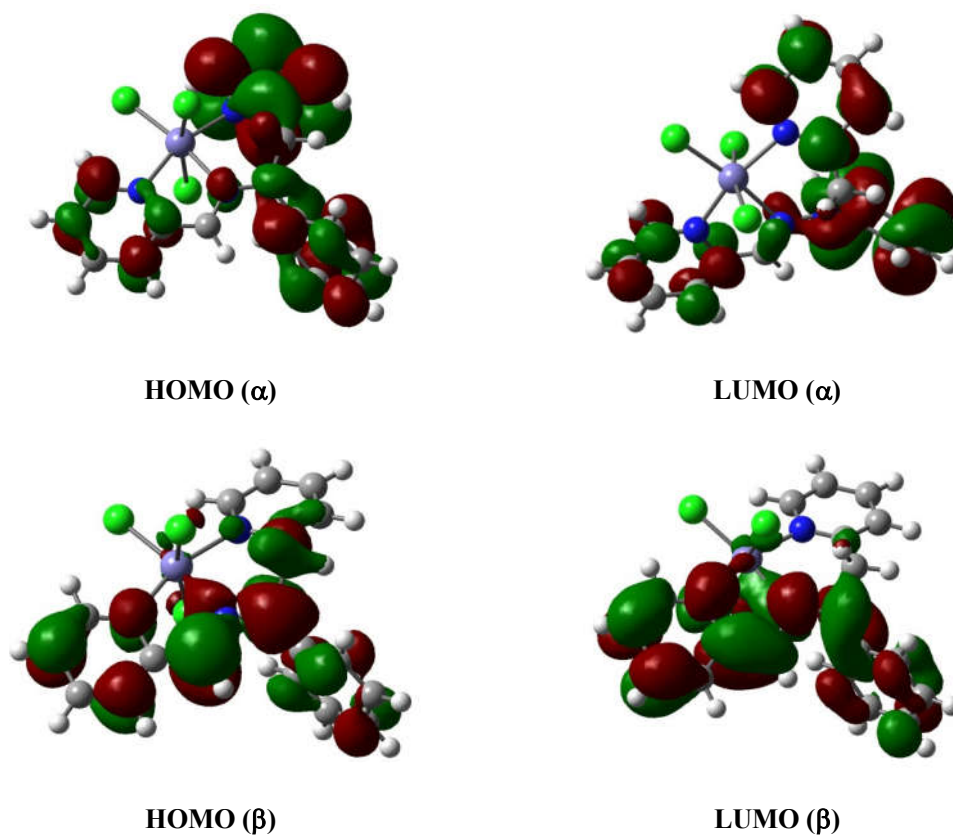
Fig. 5.12 HOMO and LUMO of complex **12**

TD–DFT calculations show contribution of molecular orbitals associated with the electronic transition and characteristic transitions have been depicted in Table 5.4.

Table 5.4 Calculated TD–DFT excitation energies (in eV), oscillator strengths (f), and

nature of transitions in the complex **12**

Composition(% Contribution)	E (eV)	Oscillator strength (f)	λ_{theo} (nm)	λ_{exp} (nm)
HOMO–3→ LUMO+6 (29%) HOMO–7→ LUMO+4 (13%)	4.1401	0.0511	299.47	300
HOMO–5 → LUMO (74%) HOMO–4 → LUMO+5 (11%)	3.6216	0.0077	342.9	342.35
HOMO–7→ LUMO (23 %) HOMO–1→ LUMO+1 (15 %)	2.7422	0.0002	452.13	452

The theoretical and experimental values were found to be in good agreement. Fig. 5.13

exhibit distribution of HOMO–LUMO orbitals calculated using DFT calculations.

Alpha HOMO	Alpha LUMO	Beta HOMO	Beta LUMO
HOMO	LUMO	HOMO	LUMO
HOMO–1	LUMO+1	HOMO–1	LUMO+1
HOMO–2	LUMO+2	HOMO–2	LUMO+2

| HOMO–3 | LUMO+3 | HOMO–3 | LUMO+3 |
| HOMO–4 | LUMO+4 | HOMO–4 | LUMO+4 |
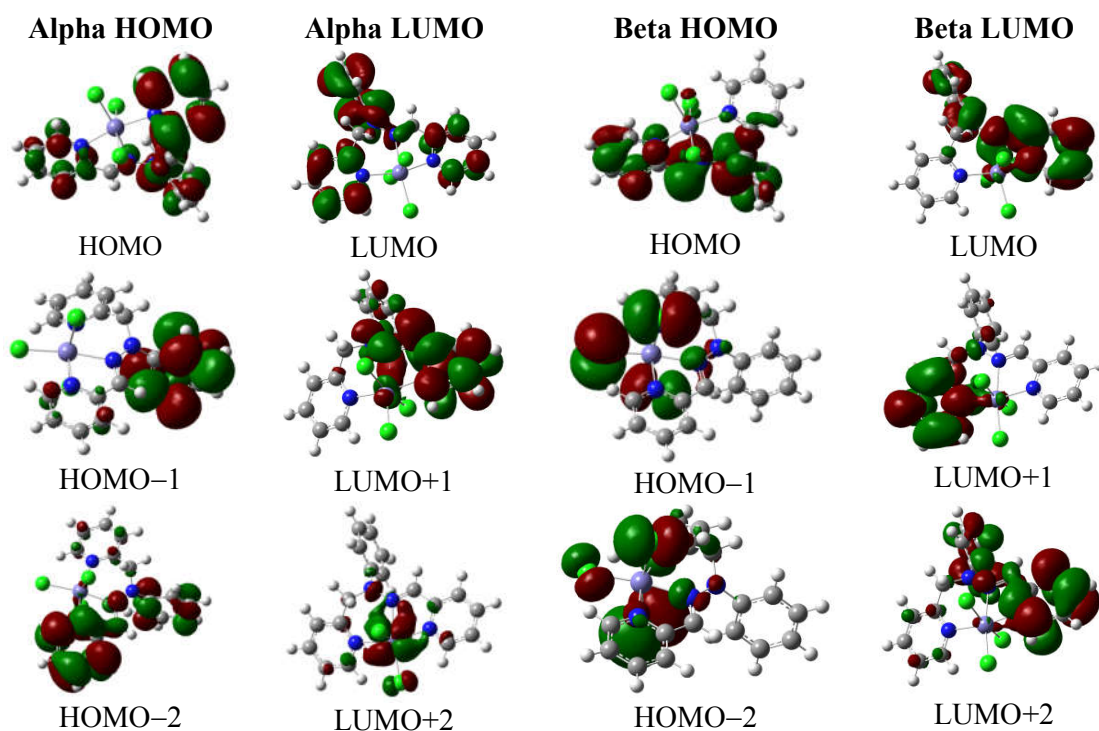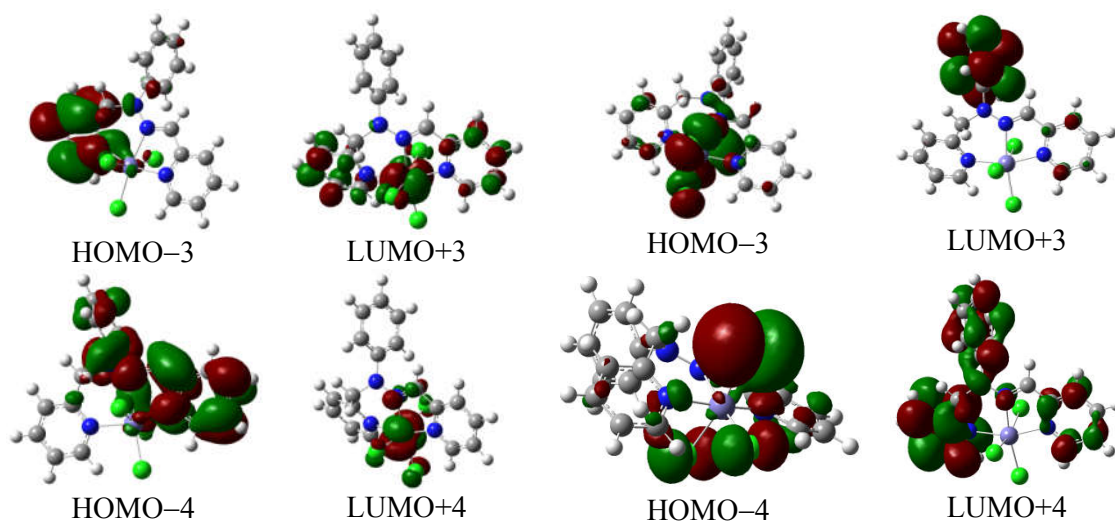
Fig. 5.13 A pictorial representation of HOMO–LUMO distribution calculated using TD–DFT calculations

5.3.4. Electrochemical studies

Redox properties of the metal complexes were investigated using electrochemical studies at a glassy carbon electrode using Ag/AgCl reference electrode. Fig. 5.14 shows cyclic voltammograms associated with the metal complexes **12** and **13** in acetonitrile solution. Both the complexes **12** and **13** showed a reversible peak at −0.85 and −0.97 V probably associated with Fe(III)/Fe(II) redox behavior. Both the complexes showed irreversible peak at −0.35 and −0.78 V for complexes **12** and **13** respectively.
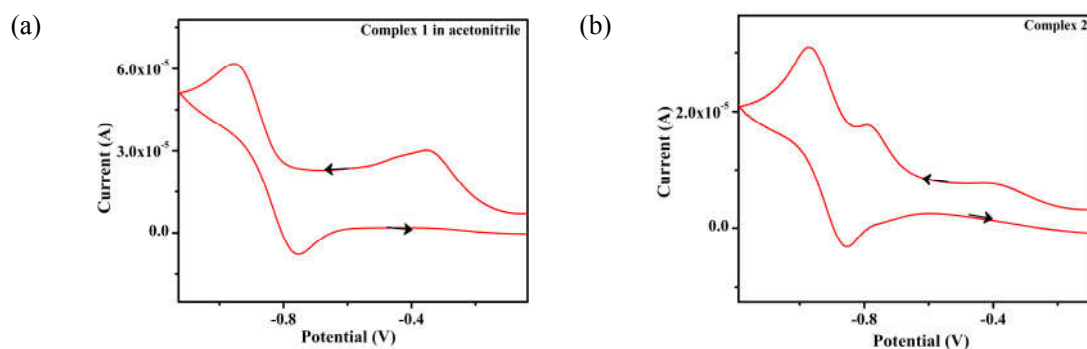
Fig. 5.14 Cyclic voltammograms of 10^{-3} M solution of complexes (a) **12** and (b) **13** in acetonitrile solutions

5.3.5. DNA binding studies

Synthesized iron complexes were subjected to the DNA interaction studies using absorption, fluorescence and circular dichroism spectral studies. To investigate the DNA interaction studies of the complexes, stability of complexes were determined in the buffer solution. All the complexes were found to be stable in the buffer for more than 6 h. Fig. 5.15−5.16 shows the stability of complexes in buffer. No shift was observed in the band only a decrease in absorbance was observed. Small decrease in absorbance could be probably due to the slow precipitation of the compounds. This indicated that the complexes retained their composition for the particular period of time. Hence complexes could be utilized for further DNA interaction studies.
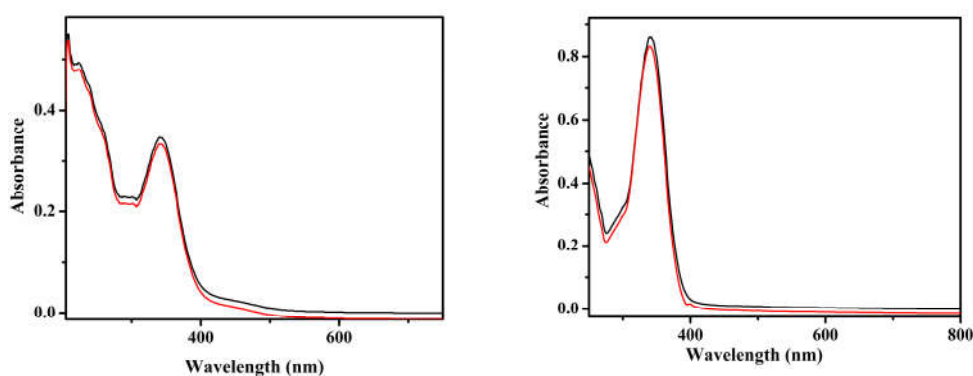
Fig. 5.15 Stability of complexes **12** and **13** in 0.1 M phosphate buffer (pH 7.2) solution for 6 h
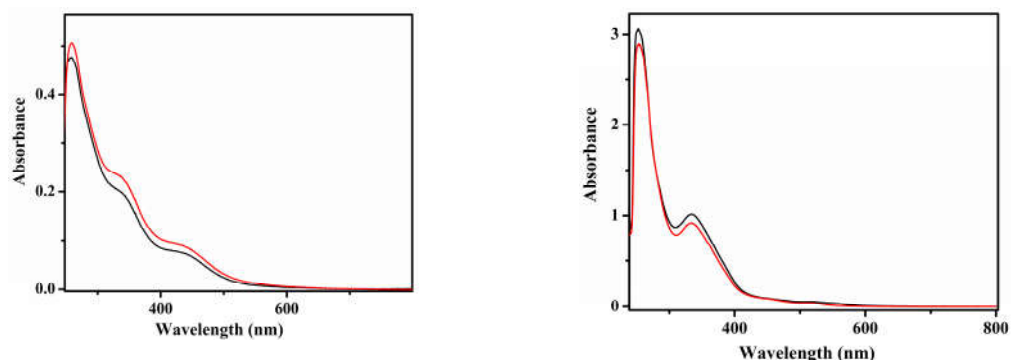
Fig. 5.16 Stability of complexes **14** and **15** in 0.1 M phosphate buffer (pH 7.2) solution for 6 h

Absorption spectral studies have been utilized for preliminary investigation of interactions of CT–DNA with the complexes. During experiments, small amount of DNA was added to a fixed complex concentration. Experiments were performed at physiological pH and changes in electronic properties were monitored. The UV–visible data for all the complexes have been depicted in the Fig. 5.17–5.20.
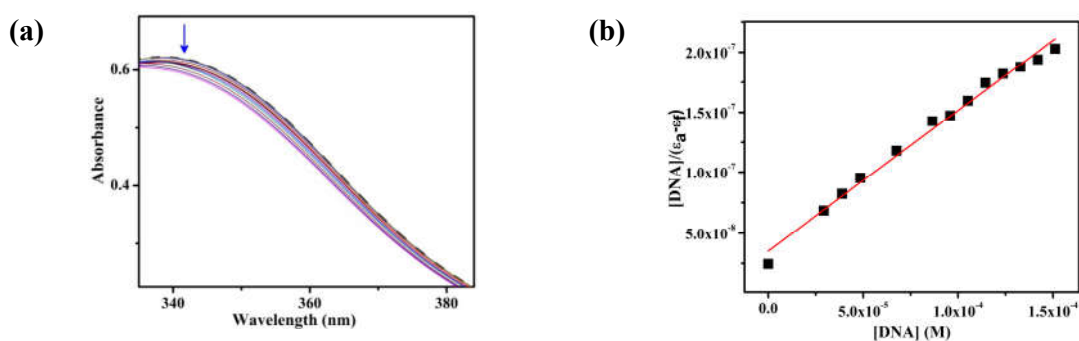
Fig. 5.17 Absorption spectra of complex **12** in 0.1 M phosphate buffer (pH 7.2) in the presence of increasing DNA concentration. (a) [**12**] = 70 µM, [DNA] = 0–150 µM, (b) Plot of [DNA]/ε_a–ε_f *vs* [DNA] for the calculation of K_b of complex **12**. Arrow indicates change in the absorbance with the increasing DNA concentration

(a)

(b)
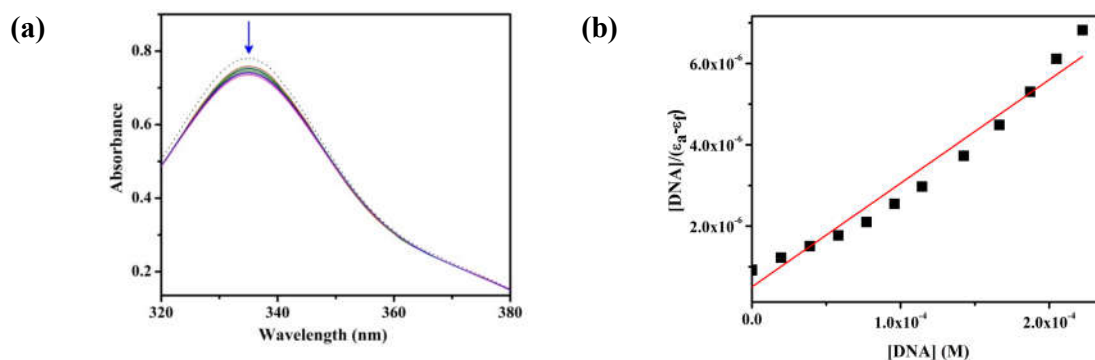
Fig. 5.18 Absorption spectra of complex **13** in 0.1 M phosphate buffer (pH 7.2) in the presence of increasing DNA concentration. (a) [**13**] = 100 μM, [DNA] = 0–250 μM, (b) Plot of [DNA]/ε_a–ε_f *vs* [DNA] for the calculation of K_b of complex **13**. Arrow indicates change in the absorbance with the increasing DNA concentration

(a)

(b)
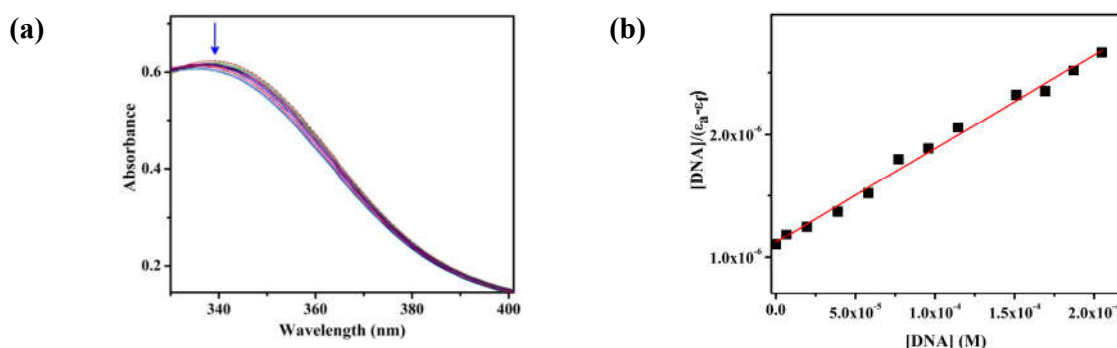
Fig. 5.19 Absorption spectra of complex **14** in 0.1 M phosphate buffer (pH 7.2) in the presence of increasing DNA concentration. (a) [**14**] = 70 μM, [DNA] = 0–200 μM, (b) Plot of [DNA]/ε_a–ε_f *vs* [DNA] for the calculation of K_b of complex **14**. Arrow indicates change in the absorbance with the increasing DNA concentration

(a)

(b)
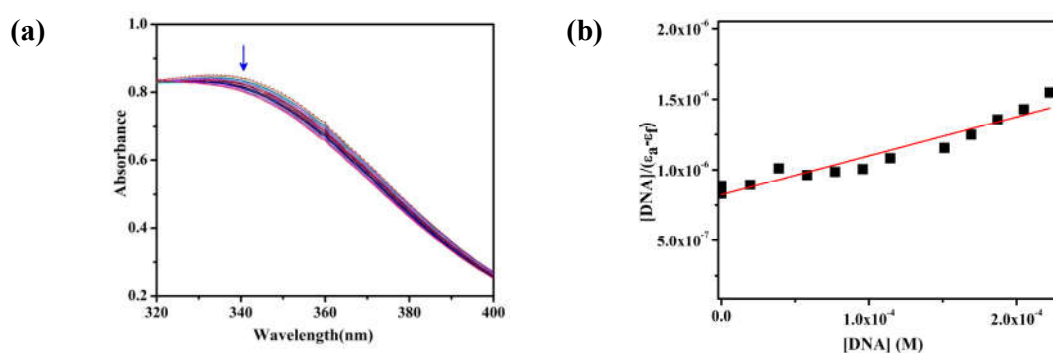
Fig. 5.20 Absorption spectra of complex **15** in 0.1 M phosphate buffer (pH 7.2) in the presence of increasing DNA concentration. (a) [**15**] = 100 μM, [DNA] = 0–220 μM, (b) Plot of [DNA]/ε_a–ε_f *vs* [DNA] for the calculation of K_b of complex **15**. Arrow indicates change in the absorbance with the increasing DNA concentration

During the interaction of CT–DNA with the complexes a change is observed in the intra ligand transition at 340 nm. Hypochromism was observed in all the four complexes **12–15** without any shift in wavelength. Binding constant (K_b) has been evaluated using Wolfe–Shimer equation[519] and have been tabulated in Table 5.5. The strength of binding is determined in terms of binding constant (K_b). The values of intrinsic binding constants (K_b) for complexes are in the range of 10^3–10^4 M^{-1}. These values are lower than the standard intercalator EB.[562] These hypochromism along with the value of binding constant proposed binding of DNA probably through intercalation attributed to π–π* stacking interaction between the aromatic chromophore of ligands and DNA base pairs.[563–565] The values for K_b are comparable to the reported values for the iron complexes.[566] Interaction of DNA with the complexes cannot be concluded only using UV–visible absorption studies. Hence fluorescence and CD spectral studies must be performed to explain the accurate mode of interaction.

Table 5.5 Binding constants (K_b) for complexes

Complex	K_b (M^{-1})
12	3.29×10^4 (Hypochromism)
13	5.01×10^4 (Hypochromism)
14	6.82×10^3 (Hypochromism)
15	3.35×10^3 (Hypochromism)

From the UV−visible interaction studies it can be calculated that all the complexes were found to be interactive with the CT−DNA in given experimental condition.

Ethidium bromide (EB) displacement assay was performed using fluorescence spectral studies. EB is not itself fluorescent but in presence of DNA it becomes fluorescent. During studies displacement of EB with the complex is monitored. In order to optimize these properties a fixed amount of DNA is used with EB and titrated with a fixed amount of

complexes at regular interval. Quenching in fluorescence emission intensity was observed due to the displacement of EB from the CT–DNA. The extent of quenching was calculated in terms of Stern–Volmer constant (K_{SV}) using linear Stern–Volmer equation (Fig. 5.21–5.24).

(a)

(b)
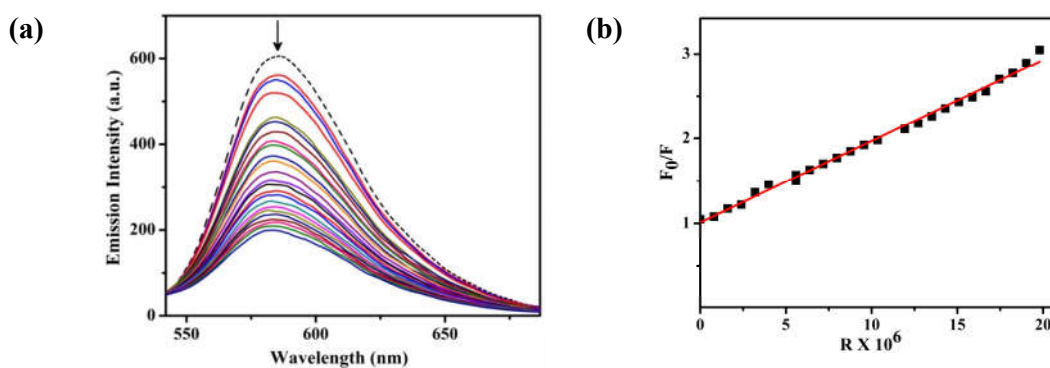
Fig. 5.21(a) EB–DNA fluorescence quenching titration complex **12** (0–20 µM).(b) Stern−Volmer plots of F_o/F versus [R] for complex shown. Tests were performed in the conditions of 50 mM phosphate buffer (pH 7.2) at 298 K [C_{DNA}] = 25 µM, [C_{EtBr}] = 0.5 µM; λ_{ex} = 250 nm, λ_{em} = 585 nm

(a)

(b)
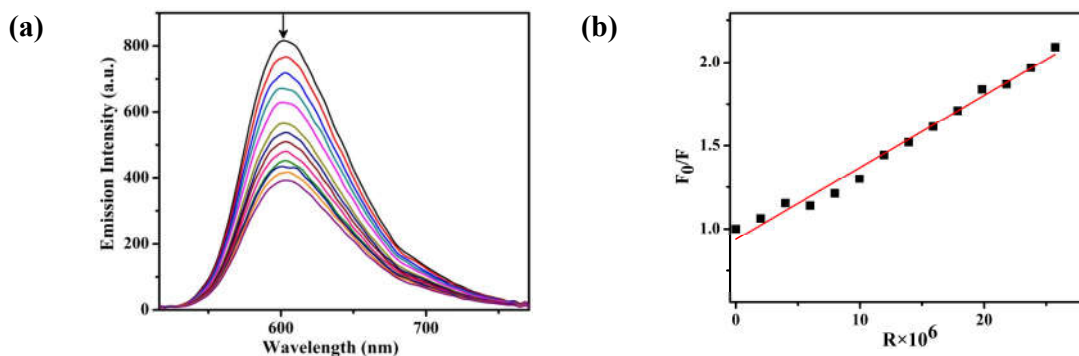
Fig. 5.22 (a) EB–DNA fluorescence quenching titration complex **13** (0–28 µM).(b) Stern−Volmer plots of F_o/F versus [R] for complex shown. Tests were performed in the conditions of 50 mM phosphate buffer (pH 7.2) at 298 K [C_{DNA}] = 25 µM, [C_{EtBr}] = 0.5 µM; λ_{ex} = 250 nm, λ_{em} = 585 nm

(a)

(b)
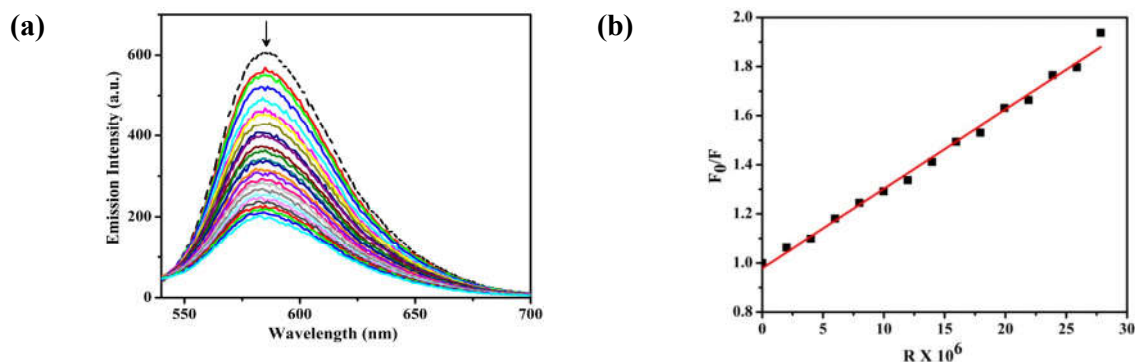
Fig. 5.23 (a) EB–DNA fluorescence quenching titration complex **14** (0–28 µM).(b) Stern−Volmer plots of Fo/F versus [R] for complex shown. Tests were performed in the conditions of 50 mM phosphate buffer (pH 7.2) at 298 K [CDNA] = 25 µM, [CEtBr] = 0.5 µM; λex = 250 nm, λem = 585 nm

(a)

(b)
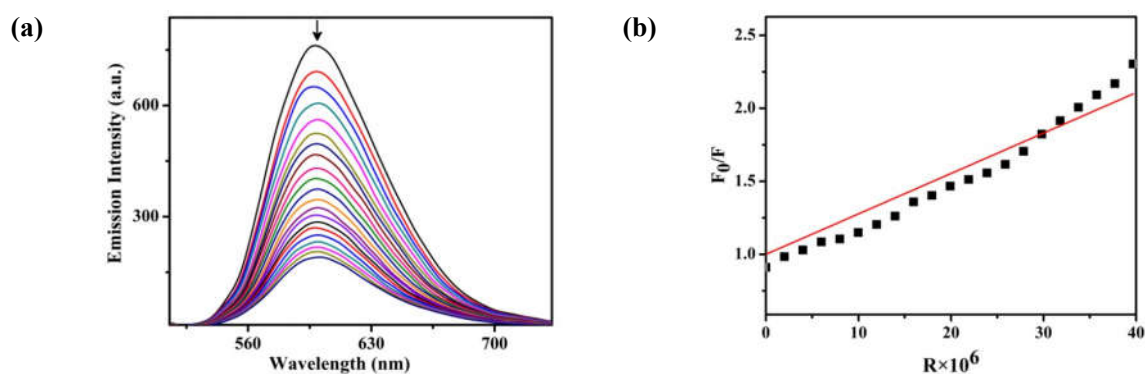
Fig. 5.24 (a) EB–DNA fluorescence quenching titration complex **15** (0–40 µM). (b) Stern−Volmer plots of F_o/F versus [R] for complex shown. Tests were performed in the conditions of 50 mM phosphate buffer (pH 7.2) at 298 K C_{DNA} = 25 µM, C_{EtBr} = 0.5 µM; $λ_{ex}$ = 250 nm, $λ_{em}$ = 598 nm

Stern–Volmer plots clearly indicated that the fluorescence quenching of EB bound CT–DNA in the presence of complexes **12**–**15** and also in good linear agreement with the Stern–Volmer equation. These data suggested that the complexes bound with CT–DNA and values of Stern–Volmer constant (K_{SV}) have been summarized in the Table 5.6.

Table 5.6 Stern–Volmer quenching constant (Ksv) for complexes

Complex	$K_{SV}(M^{-1})$
12	9.2×10^4
13	4.0×10^4
14	3.2×10^4
15	2.7×10^4

The values of K_{SV} are found to be lesser then classical intercalator.[562] Hence the partial displacement was observed in all the four complexes. The studies performed indicated probable mode of interaction with the CT–DNA is partial intercalation.[567,568]

During circular dichroism studies conformational changes in CT–DNA observed on interaction of metal complexes. DNA shows two bands in CD spectra, a positive band at 275 nm due to base stacking and a negative band at 245 nm due to helicity. The iron complexes were not optically active and did not exhibit any CD spectra in the range 200–800 nm. On interaction with metal complexes CD spectra showed a decrease in the negative as well as in positive bands (Fig. 5.25) which represents significant interaction of CT–DNA with metal complexes. No shift in wavelength observed which indicates that these complexes do not affect the conformational changes of DNA.[352] These studies also suggested intercalative mode of interaction with the DNA.[569–571]
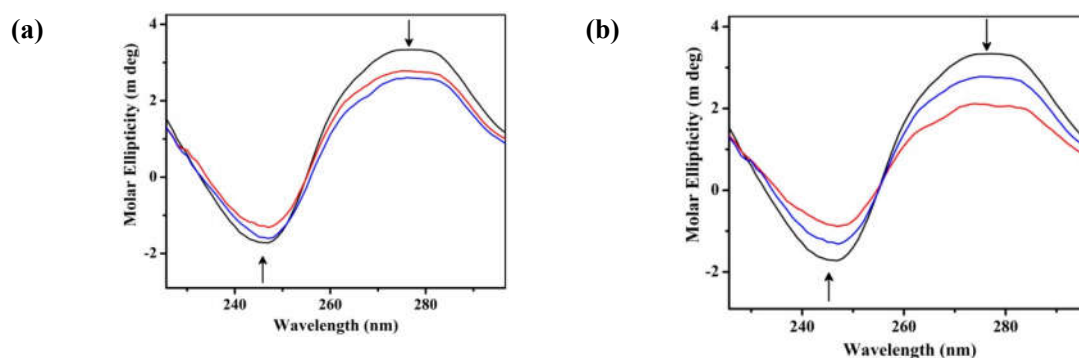
Fig. 5.25 Circular dichroism spectra in 0.1 M phosphate buffer (pH 7.2) after 10 min incubation at 25 °C. (a) **12** (red) and **14** (blue) (b) **13** (red) and **15** (blue) with CT–DNA (black) and its interaction with complexes spectra recorded in 5% dimethylformamide

5.3.6. Nuclease activity

Nuclease activity of the representative complex **12** in presence of H_2O_2 was evaluated (Fig. 5.26). Cleavage of supercoiled *pBR322* DNA was observed with the complex **12** using gel electrophoresis. During the studies DMF content was kept below 10 %. Variable concentration of complex **12** was employed to optimize the cleavage activity. Fig. 5.26 depicts that intensity of the circular SC form decreases, while that of NC form increase (lane 4–7) without any activating agents. When an oxidising agent H_2O_2 was added to the DNA the NC form further increased (lane 8).
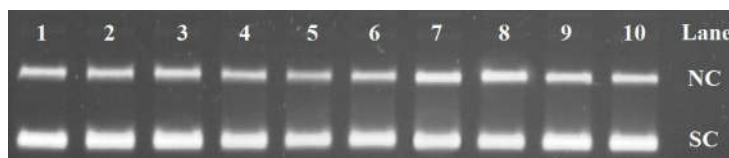
Fig. 5.26 Gel electrophoresis separations showing the cleavage of supercoiled *pBR322* DNA (100 ng) by variable concentration of complexes **12** in 10% DMF incubated at 37 °C for 2 h. Lane 1: DNA, lane 2: DNA + FeCl$_3$ (100 μM), lane 3: DNA + H−N$_3$L, lane 4: DNA + **12** (10 μM), lane 5: DNA + **12** (25 μM), lane 6: DNA + **12** (50 μM), lane 7: DNA + **1** (100 μM), lane 8: DNA+ **12** (100 μM) + H$_2$O$_2$ (100 μM), lane 9: DNA + H$_2$O$_2$ (100 μM), lane 10: DNA + DMF (10%)

Quantitative representation of cleavage has been depicted in the Fig. 5.27. From the activity it is clear that with the increased amount of complex concentration the DNA is cleaved and a mixture of nicked DNA and supercoiled DNA obtained in presence of H_2O_2.
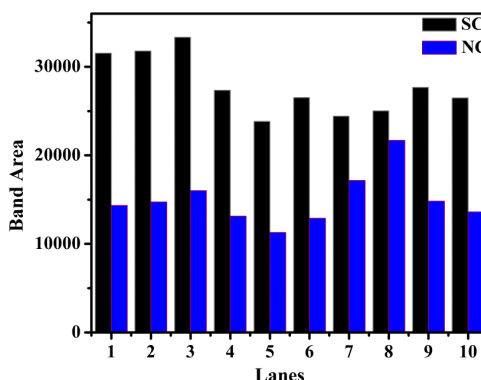
Fig. 5.27 Bar diagram representation of SC and NC form during nuclease activity of complex

5.4. Conclusions

A new family of mononuclear iron complexes have been synthesized and characterized using various spectroscopic techniques. ESI–MS and NMR spectral studies clearly indicated the formation of complexes. DFT and TD–DFT calculations were performed on complex **12** to optimize geometrical and structural parameters. Redox properties of complexes of were examined by electrochemical studies and the results indicated Fe(III)/Fe(II) redox behavior. For advancement of medicinal inorganic chemistry a better understanding of mechanism of metal complexes interaction with the DNA is needed. Hence DNA interaction studies were performed utilizing these complexes. DNA binding studies were optimized using absorption, fluorescence and circular dichroism spectral studies. These studies indicated interaction is probably due to the intercalation mode of binding. Complex **12** was subjected to the nuclease activity. Complex **12** was effective artificial chemical nuclease in presence of H_2O_2 under physiological pH. Oxidative reactivity studies of these complexes are under progress.

5.5. Experimental section

5.5.1. Materials and instrumental methods

Anhydrous $FeCl_3$ was purchased from Rankem, New Delhi, India, $Fe(ClO_4)_2.xH_2O$, 2–chloromethylpyridine hydrochloride from Sigma Aldrich, Steinheim, Germany.

5.5.2. Synthesis of metal complexes

Caution! Perchlorate salts of metal complexes with organic ligands are potentially explosive. Only a small amount of material should be prepared and handled with caution.

5.5.2.1. Synthesis of Fe(H−N₃L)Cl₃ (12)

To a solution of H–N₃L (144 mg, 0.5 mmol) in methanol:ethanol (1:1) was added similar equivalent of $NEt_4[FeCl_4]$ (163 mg, 0.5 mmol) in 2 mL methanol:ethanol (1:1) dropwise. Reaction mixture was continued to stirr for 3 h and filtered. Evaporation of solvent afforded a red–brown colored precipitate. Yield: 70%. Selected IR data (KBr, v_{max}/cm^{-1}): 1606, $v_{C=Nimine}$. UV–visible [CH_3OH, λ_{max}/nm ($\varepsilon/M^{-1}cm^{-1}$)]: 452 (500), 343 (7,520), 300 (4,930), 259 (7,960), 221 (10,740). μ_{eff} (303 K): 5.91 BM. $\Lambda_M/\Omega^{-1}cm^2mol^{-1}$ (in DMF): 52. ESI–MS (m/z): 414.1428 $[M–Cl]^+$. Anal. Calc. For $C_{18}H_{16}N_4Cl_3Fe$: C, 52.08; H, 3.89; N, 13.50. Found C, 49.97; H, 4.05; N, 13.32.

5.5.2.2. Synthesis of [Fe(H−N₃L)₂](ClO₄)₂ (13)

Ligand H–N₃L (144 mg, 0.5 mmol) was taken in 10 mL of methanol and stirred. To this stirred solution $Fe(ClO_4)_2.xH_2O$ (63 mg, 0.25 mmol) in 2–3 mL of methanol was added drop wise. Color changes to red and reaction was stirred further for 3–4 h. Reaction was filtered and left for solvent evaporation. Evaporation of solvent ended up with crystalline complex. Yield: 68%. Selected IR data (KBr, v_{max}/cm^{-1}): 1606, $v_{-C=N}$, 1091, 623, v_{ClO4-}. UV–visible [CH_3OH, λ_{max}/nm ($\varepsilon/M^{-1}cm^{-1}$)]: 340 (31,290), 294 (11,010), 258 (14,840), 238 (24,160). μ_{eff} (303 K): 2.10 BM. $\Lambda_M/\Omega^{-1}cm^2mol^{-1}$ (in DMF): 156. ESI–MS (m/z): 731.1615

$[M–ClO_4]^+$. Anal. Calc. For $C_{36}H_{32}N_8Cl_2O_8Fe$: C, 52.00; H, 3.88; N, 13.48. Found C, 51.77; H, 3.22; N, 13.02.

5.5.2. 3. Synthesis of Fe(Me–N₃L)Cl₃ (14)

To a solution of Me–N₃L (151 mg, 0.5 mmol) in methanol:ethanol (1:1) was added similar equivalent of NEt₄[FeCl₄] (163 mg, 0.5 mmol) in 2 mL methanol:ethanol (1:1) dropwise. Reaction mixture was continued to stirr for 3 h and filtered. Evaporation of solvent afforded red–brown colored precipitate. Yield: 64%. Selected IR data (KBr, ν_{max}/cm^{-1}): 1595, $\nu_{C=Nimine}$. UV–visible [CH₃OH, λ_{max}/nm ($\varepsilon/M^{-1}cm^{-1}$)]: 435 (790), 329 (3,980), 260 (6,500), 225 (8,220). μ_{eff} (303 K): 5.40 BM. $\Lambda_M/\Omega^{-1}cm^2mol^{-1}$ (in DMF): 41 ESI–MS (m/z): 428.0220 $[M–Cl]^+$, 325.1410 $[L+Na]^+$, 301.1438 $[L+H]^+$. Anal. Calc. For $C_{19}H_{18}N_4Cl_3Fe$: C, 53.18; H, 4.23; N, 13.06. Found C, 51.85; H, 4.42; N, 12.83.

5.5.2.4. Synthesis of [Fe(Me–N₃L)₂](ClO₄)₂ (15)

To the stirred solution of ligand Me–N₃L (151 mg, 0.5 mmol) in 10 mL of methanol was added a methanolic solution Fe(ClO₄)₂.xH₂O (63 mg, 0.25 mmol) was added drop wise. A dark red color precipitate appeared. The reaction mixture was stirred further for 4 h. Reaction was filtered and solvent was removed. The solid obtained after evaporation was washed with small amount of methanol and diethylether. Complex was recrystallized for further analysis. Yield: 63%. Selected IR data (KBr, ν_{max}/cm^{-1}): 1597, $\nu_{–C=N}$,1091, 623, $\nu_{ClO4}-$. UV–visible [CH₃OH, λ_{max}/nm ($\varepsilon/M^{-1}cm^{-1}$)]: 552 (350), 345 (8,720), 285 (9,790), 250 (27,740). μ_{eff} (303 K): 2.04 BM. $\Lambda_M/\Omega^{-1}cm^2mol^{-1}$ (in DMF): 148. ESI–MS (m/z): 759.1790 [M–ClO₄]. Anal. Calc. For $C_{38}H_{36}N_8Cl_2O_8Fe$: C, 53.10; H, 4.22; N, 13.04. Found C, 52.88; H, 4.19; N, 12.92.

5.5.3. Density functional theory (DFT) calculations
As described in previous chapters.

5.5.4. DNA-binding and cleavage activity
As described in chapter 4.

Chapter-6

Sensing of Metal Ions(Iron and Mercury) Using Naphthyl Based Probes in Aqueous Medium:Applications in Living cells and Logic Gates

6.1. Abstract

Naphthylamine–based probe (N-(2-aminoethyl)naphthalen-1-amine) NED1 was utilized for the detection of Hg(II), Fe(II), Fe(III) in mixed aqueous media *via* fluorescence quenching. These sensitive metal ions bind with the probe by forming a 1:1 complex. Time resolved fluorescence and quantum yield of probe NED1 in absence as well as in presence of metal ions were investigated. Extent of binding probe with sensitive metal ions was calculated. Sensitivity of the probe in presence of other metal ions was examined using competitive binding studies. Probe NED1 displayed sensitivity towards Hg(II) during *in vitro* as well as *in vivo* studies. This multianalyte probe demands biological applications in cell imaging and in logic gates.

6.2. Introduction

Designing and synthesis of fluorescent probes which are selective and sensitive for monitoring heavy and transition metal ions is an important and demanding area of research due to the prominent role of metal ions in environment and biology.[327–329] Over the last several decades, an outstanding development of small fluorescent molecule with selectivity towards metal ions has been dragged attention of the researchers. These study generally helps us to understand transport and localization along with the physiological and pathological effect of metal ions in the cell.[331] Due to high sensitivity, rapid response and simplicity, fluorescence has gained much awareness for the detection of several chemical analytes.[332] Detection of Hg(II) in aqueous media is important as it is one of the toxic metal ion which severely affects environment and living beings.[572–576] On the other hand, iron is also an important biological relevant transition metal playing crucial roles in several catalytic and enzymatic reactions and could become dangerous due to its improper concentration.[3,333] Till date various fluorescent probes based on single metal ion detection have been explored.[577] However, a multi analyte recognition *via* a single probe has received a great interest.[345,578–581] Most of these probes have been synthesized using multistep synthesis and tedious methods. Among them, several probes have solubility in organic solvents only, it restricts their utilization in *in vivo* applications. Hence a probe which could work in aqueous media is needed to monitor accumulation of these metals in living cells. Hence a probe which could work in aqueous media or in mixed aqueous media along with working in physiological pH is highly demanding for living cell applications.[345–347] A multi analyte responsive probe is also very important for designing in molecular logic gates and molecular keypad lock devices.[582–586] Recently, we have designed and synthesized fluorescent probe based on naphthylamine showing sensing for single metal ion Fe(III).[587,588] This prompted us to synthesize other naphthylamine based fluorescent probes which may provide us multianalyte responsive probe as well as logic gates and molecular

keypad   lock   devices.   Herein   we   have   reported   probe
N−(2−aminoethyl)naphthalen−1−amine (NED1) and its photophysical properties in mixed aqueous media. To avoid tedious method used for synthesis of a sensor we have chosen a probe which is neither time consuming and also cost effective and has application in living cell as well as in logic gates. To the best of our knowledge there is no report of a multianalyte responsive probe for Hg(II), Fe(II) and Fe(III) based on naphthylamine.[589,590]

In the present work, we have chosen N−(2−aminoethyl)naphthalen−1−amine (NED1) because of this molecule could easily be derivatized in several ways to synthesize a series of naphthyl based fluorescent probes. Such variety of fluorescent probe contains metal binding motif which could provide us probable chelation enhanced quenching (CHEQ) as well as enhancement of fluorescence activity during metal coordination. To the best of our knowledge this moiety is found to be chelated to platinum.[591]
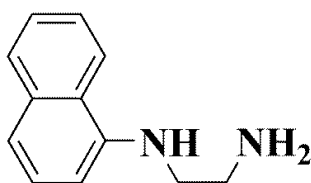
Fig. 6.1 Probe N−(2−aminoethyl)naphthalen−1−amine (NED1) used in present work

6.3. Results and discussion

6.3.1. Synthesis and characterization of probe NED1

Probe NED1 was obtained commercially in form of hydrochloride salt and used directly neutralizing the hydrochloride salt of N−(2−aminoethyl)naphthalen−1−amine with potassium hydroxide.

To optimize the proper neutralization of the hydrochloride salt GC−MS data was also recorded (Fig. 6.2) which showed the molecular ion peak supporting the proper

neutralization of the probe NED1. Purity of NED1 was also confirmed using thin layer chromatography.
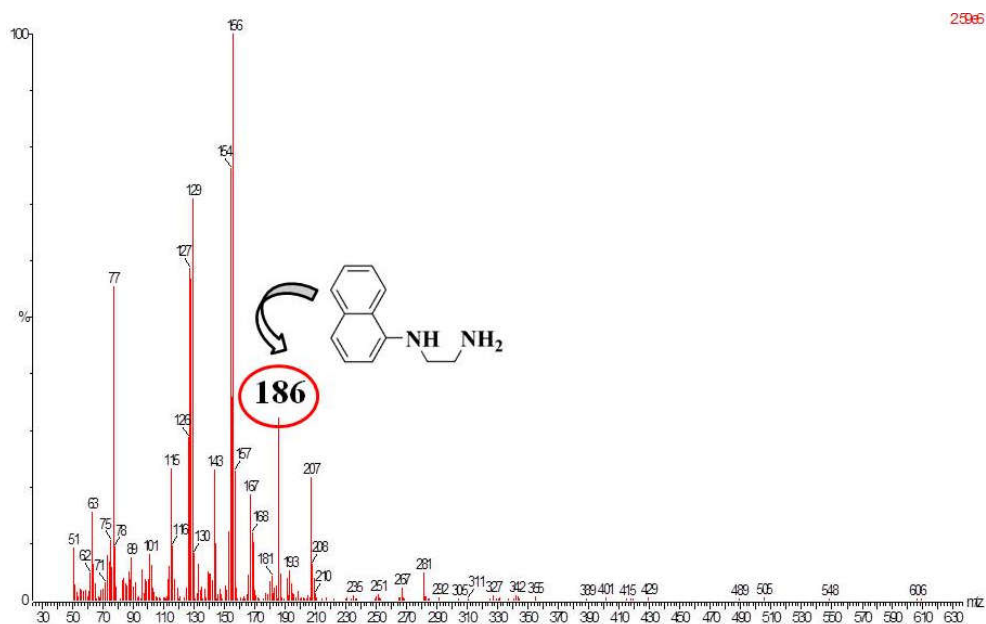
Fig. 6.2 GC−MS spectrum of N−(2−aminoethyl)naphthalen−1−amine NED1

ESI−MS spectral study was also performed to justify the neutralization which showed peaks at (m/z) 185.04 corresponding to $[M-H]^+$ under positive ion mode in acetonitrile solution solution.

201
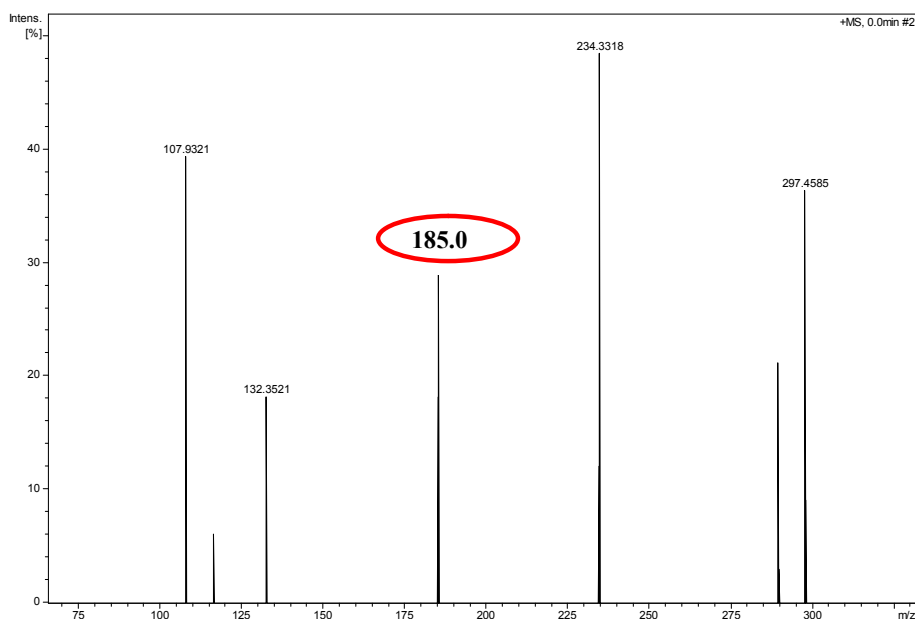
Fig. 6.3 ESI−MS spectrum of NED1 in acetonitrile under positive mode

6.3.2. Absorption spectral studies

Absorption spectral studies of probe NED1 was monitored in mixed aqueous media. Titration of probe NED1 was performed with the sensitive metal ions. During experiments only freshly prepared stock solution of metal ions have been used in water as described by Xu and co−workers, Chereddy *et al*. and Anslyn and co−workers[341,592,593] and no precipitation were observed during experiment (2 hrs) in the stock as well as in the cuvette. Absorption spectra of probe NED1 at different concentrations of Hg(II) has been depicted in Fig. 6.4. Probe NED1 showed a band around 320 nm which was due to charge transfer transition between donor amine and acceptor naphthyl moiety.[583] During titration two isosbestic points at 290 nm and 345 nm appeared. Appearance of a shoulder near 390 nm is probably due to metal to ligand charge transfer (MLCT) transition.[594] These experiment clearly indicated significant change in donor−acceptor property of naphthylamine chromophore and chelation of Hg(II) to the probe (Fig. 6.4).[595]
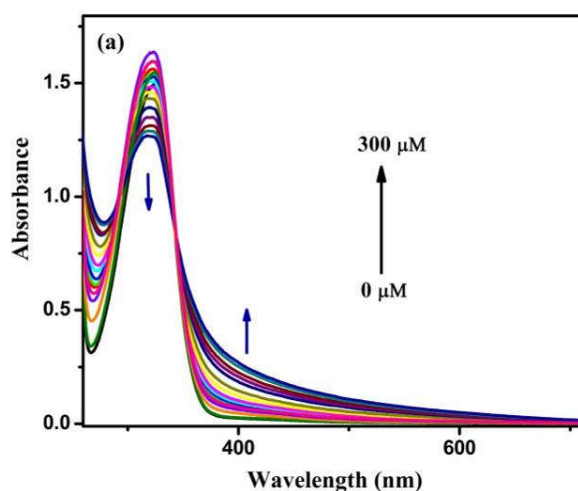
Fig. 6.4 UV−visible spectra of probe NED1 (50 μM) upon addition of $HgCl_2$ (0−300 μM) in mixed solvent media (0.1% DMSO in 100 mM phosphate buffer, pH 7.4)

Similarly, electronic absorption spectral studies were also monitored using probe NED1 and other sensitive metal ions Fe(II) and Fe(III) (Fig. 6.5). Titration experiments were also carried out for probe NED1 with Fe(II) and Fe(III) to optimize metal ion binding properties. During titration experiments a cation induced hyperchromic shift was observed in case of both the metals (Fig. 6.5).
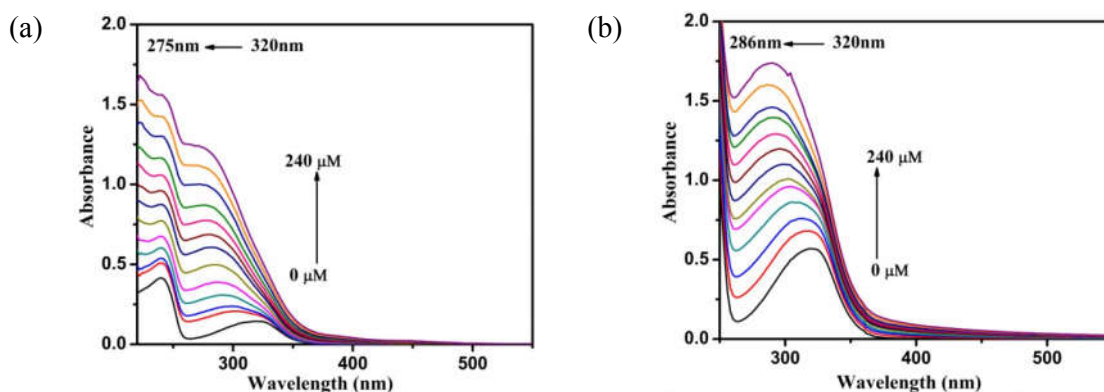
Fig. 6.5 Changes observed in UV−visible spectra of probe NED1 (20 μM) upon addition of (a) $FeCl_2$(0−240 μM) (b) $FeCl_3$(0−240 μM) in mixed solvent media (0.1% DMSO in 100 mM phosphate buffer, pH 7.4)

The greater extent of hyperchromism observed for the absorption band near 320 nm in case of Fe(II), Fe(III) as well as for Cu(II) indicating strong binding of these metal ions with the probe NED1 in ground state (Fig. 6.6).
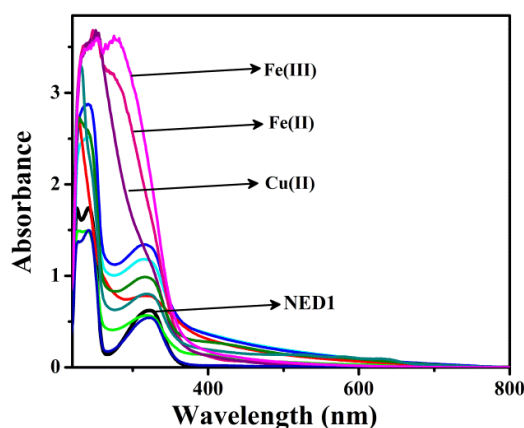
Fig. 6.6 UV−visible spectra of probe NED1 (50 µM) upon addition of 20 equivalents of representative metal ions in mixed solvent media (0.1% DMSO in 100 mM phosphate buffer, pH 7.4)

Control experiments were also performed to nullify the effect of any metal ion or precipitation. During these experiments equal amount of metal salt was added to both the cuvettes. Changes observed in UV−visible spectra indicate that some complexation is occurring which is responsible for the change in spectra and decline the effect due to the metal ion or any precipitation. No precipitation was found till the completion of experiment. Both the stock solutions were having similar concentrations and no major change in color was observed. To exclude the possibilities of Fe(II) and Fe(III) and their chemistry water/buffer mixture, this titration experiments (UV−visible) were repeated in methanol as a control experiment (Fig. 6.7). Similar results to that of the experiments performed in water were obtained.
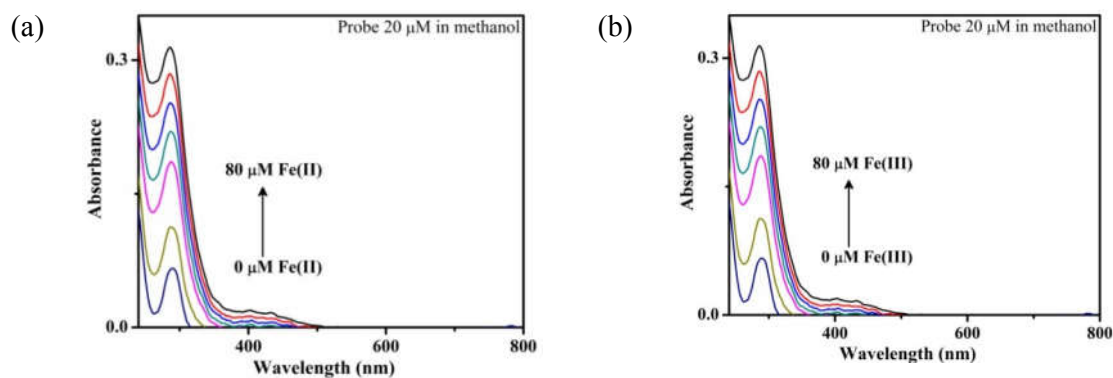
Fig.6.7 UV−visible spectral changes observed during titration with probe NED1 (20 μM) (a) Fe(II) (b) Fe(III) in methanol

To check whether changes in UV−visible spectra were due to chelation with iron, some control experiments using *o*−phenylenediamine as a mimic of chelating motiff were performed. The results obtained in Fig. 6.8 shows similar behavior was observed for probe NED1 and supported probable chelation of motif to iron metal ion.
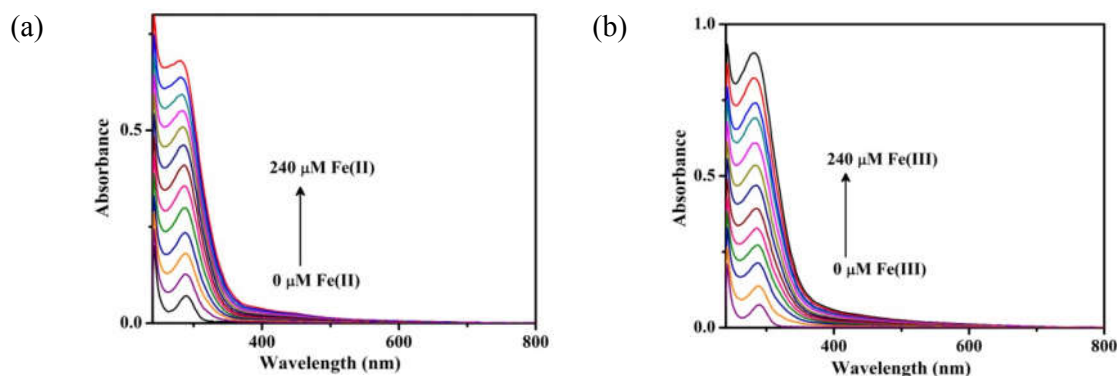
Fig. 6.8 UV−visible spectral changes observed during titration with *o*−phenylenediamine (20μM) in DMSO (a) Fe(II) (b) Fe(III) in 0.1M phosphate buffer solution pH 7.4

Control experiments were also performed in case of iron under anaerobic condition and have been depicted in Fig. 6.9.

(a)

(b)
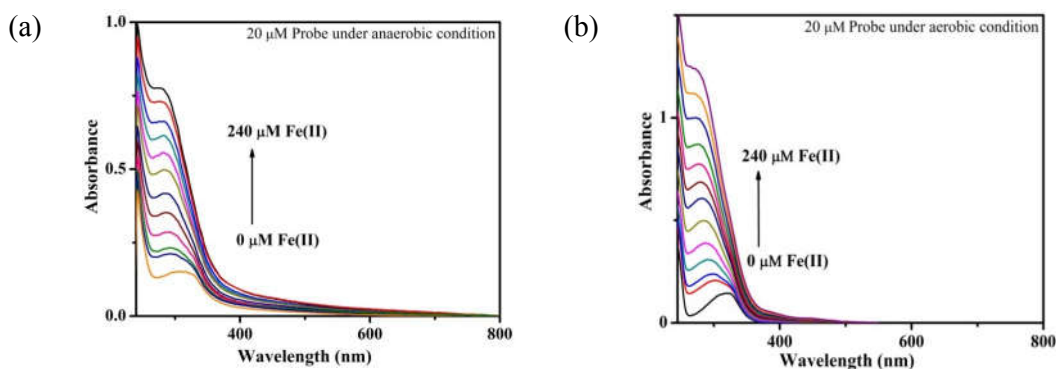
Fig. 6.9 UV−visible spectral changes observed during titration with probe NED1 (20µM) in DMSO (a) Fe(II) under anaerobic conditions (b) Fe(II) under aerobic conditions in 100 mM phosphate buffer solution pH 7.4

6.3.3. Emission spectral studies

Stability of probe NED1 in mixed aqueous media (0.1% DMSO in 100 mM phosphate buffer, pH 7.4) was observed for 30 min (Fig. 6.10). Emission spectral of probe NED1 was also explored.
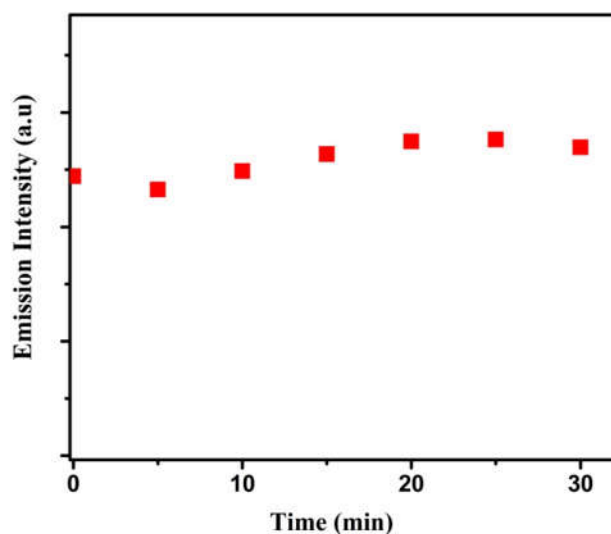
Fig. 6.10 Stability of probe NED1 (10 µM) in mixed solvent media (0.1% DMSO in 100 mM phosphate buffer, pH 7.4) for 30 min at (λ_{ex}= 320 nm)

For better insight into the photophysical properties change in emission intensity of probe NED1 (50 µM) were explored for various representative metal ions such as Ca(II), Mg(II), Mn(II), Fe(II), Co(II), Cr(III), Fe(III), Ni(II), Cu(II), Zn(II) and Hg(II) (in form of

206

their chloride salts) respectively in mixed solvent media (0.1% DMSO in 100 mM phosphate buffer, pH 7.4) (Fig. 6.11).
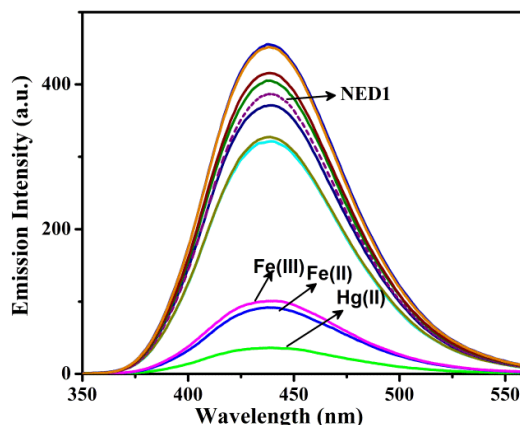
Fig. 6.11 Changes in fluorescence spectra of probe NED1 (50 μM) in presence of 20 equivalents of served metal ions λ_{ex} 320 nm in mixed solvent media (0.1% DMSO in 100 mM phosphate buffer, pH 7.4)

Probe NED1 shows fluorescence emission at wavelength (λ_{em}) 438 nm in mixed aqueous media when excited at 320 nm. After incubation of 2−3 min fluorescence emission intensity becomes constant and with the addition of Hg(II) fluorescence got quenched. Emission intensity of probe NED1 keep on decreasing with the further addition of Hg(II) (Fig. 6.12). The quenching observed was probably due to a heavy atom effect of Hg(II) metal ion and chelation enhanced quenching (CHEQ).[596]
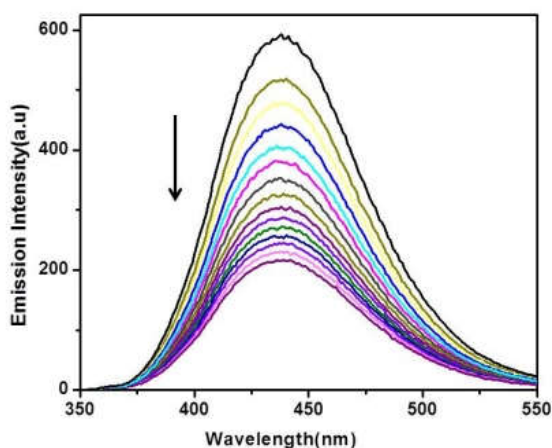
Fig. 6.12 Change in emission spectra on addition of Hg(II) (0−200 μM) in mixed aqueous media (0.1% DMSO in 100 mM phosphate buffer, pH 7.4)

Titration was also performed for the other two sensitive metal ions Fe(II) as well as Fe(III) ions (Fig. 6.13). During fluorescence studies, decrease in emission intensity was observed with the increase in concentration of Fe(II) as well as Fe(III) metal ion. The probable mode of quenching was due to the chelation enhanced quenching in presence of paramagnetic metal ion.[597]

(a)

(b)
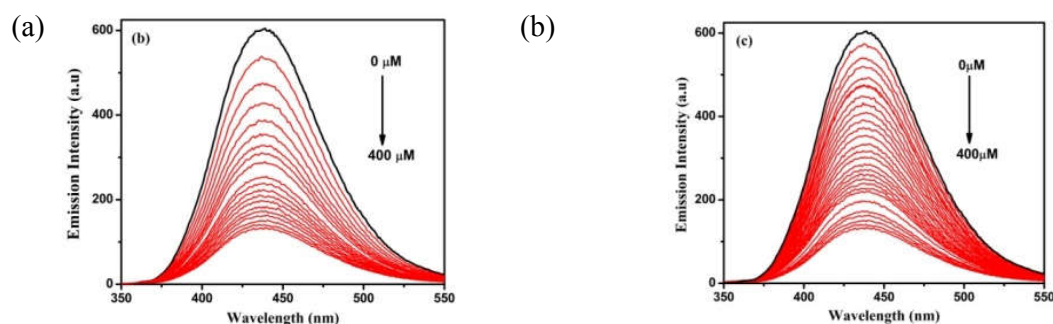
Fig. 6.13 Change in emission spectra on addition of (a) Fe(II) (b) Fe(III) (0−400 μM) in mixed solvent media (0.1% DMSO in 100 mM phosphate buffer, pH 7.4)

6.3.4. Quantum yield and time−resolved measurements

Quantum yield studies of probe NED1 (λ_{ex}: 310 nm) was monitored in mixed solvent media (0.1% DMSO in 100 mM phosphate buffer, pH 7.4), 2−aminopyridine (Φ_F= 0.6) as a reference.[598]

Fluorescence quantum yield of probe NED1 was found to be 0.74 and decrease in quantum yield was found 0.68, 0.52 and 0.65 with the addition of Hg(II), Fe(II) and Fe(III) respectively.

To gain better insight, time resolved fluorescence measurements were also performed in absence and in presence of sensitive metal ions. Fluorescence decay curves followed three exponential decay kinetics for probe NED1 as well as in probe NED1 in presence of Hg(II), Fe(II), Fe(III) (Table 6.1) metal ions respectively.

Table 6.1 Effect of addition of Hg(II), Fe(II) and Fe(III) on fluorescence lifetime (ns) of

probe NED1 (λ_{ex}: 320 nm, λ_{em}: 438 nm)

| Sample | Lifetime (ns) | | | | | | ‹τ› | χ^2 |
| | Component 1 | | Component 2 | | Component 3 | | | |
	τ_1	Emission (%)	τ_2	Emission (%)	τ_3	Emission(%)		
NED1	2.89	38.84	0.82	26.14	14.23	35.02	6.31	1.16
NED1+Hg(II)	1.59	64.96	0.31	15.22	12.24	19.82	3.50	1.11
NED1+Fe(II)	1.92	18.62	13.46	20.37	0.04	61.00	3.12	1.12
NED1+Fe(III)	2.05	20.72	13.54	25.16	0.04	54.13	3.85	1.16

Life time of NED1 was found to be 6.31 ns (χ^2=1.16) and on addition of Hg(II) (20 equivalent) the value decreased to 3.50 ns (χ^2= 1.11) (Fig. 6.14). Faster decay of the excited state was observed in presence of Hg(II) probably due to narrower HOMO–LUMO gap.[583] The similar decrease in life time was observed for all the three metal ions. Decay was faster in presence of Fe(II) and the slowest for Fe(III). These data is consistent to the stronger binding of Fe(II) with the probe NED1 as compared to Hg(II) and Fe(III).[599]
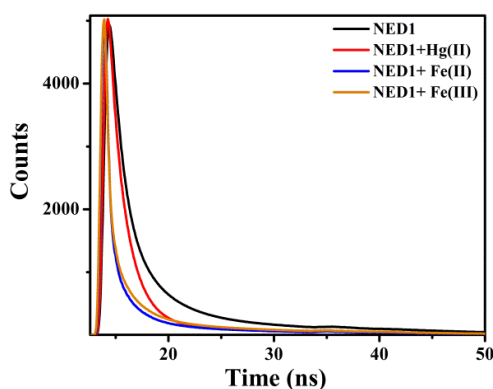
Fig. 6.14 Fluorescence decay profile of NED1 in absence and presence of Hg(II), Fe(II) and Fe(III) in mixed solvent media (0.1% DMSO in 100 mM phosphate buffer, pH 7.4)

6.3.5. Binding stoichiometry and NMR studies

To calculate the binding stoichiometry, Benesi–Hildebrand plot was obtained which suggests 1:1 stoichiometry for all three sensitive metal ions and apparent association constants were also calculated (Table 6.2, Fig. 6.15).[600]

Table 6.2 Apparent association constants (K_{ass}) and Stern–Volmer constants (K_{SV})

Probe NED1 and Metal	$K_{ass}(M^{-1})$	$K_{SV}(M^{-1})$
Hg(II)	6.17×10^3	5.55×10^3
Fe(II)	9.87×10^3	8.39×10^3
Fe(III)	5.18×10^3	8.74×10^3
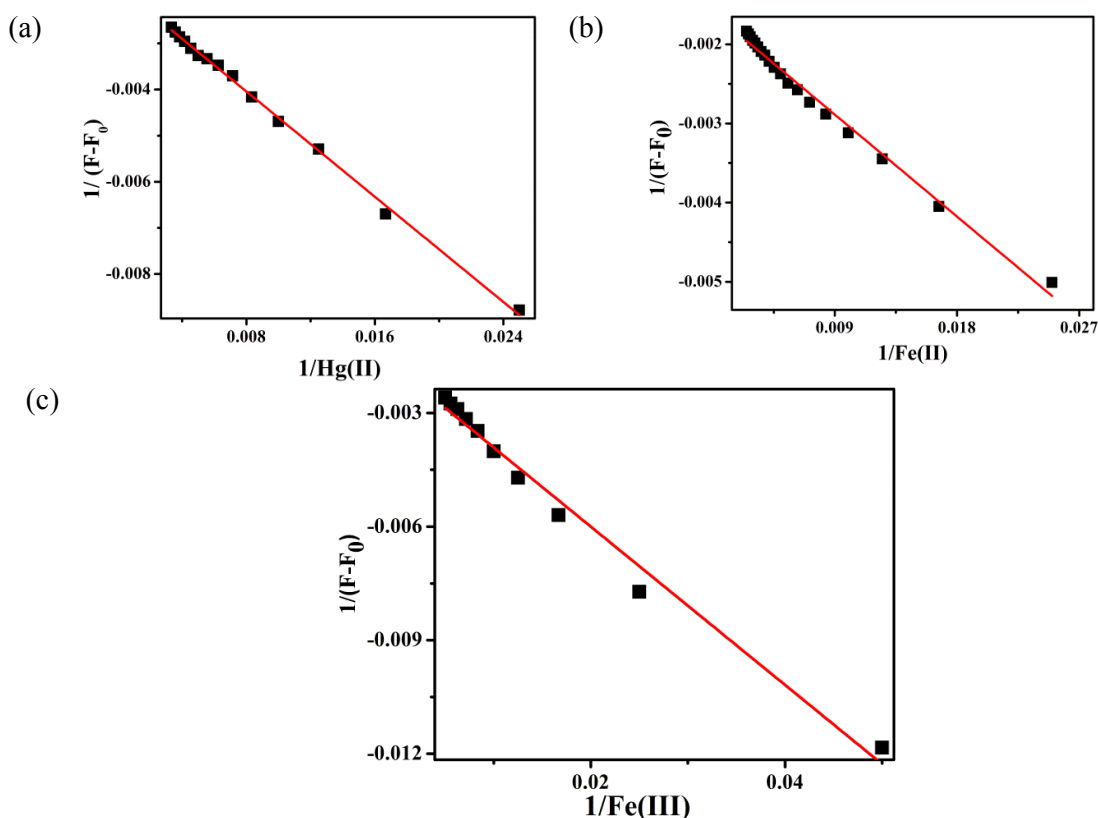
Fig. 6.15 Benesi–Hildebrand plot of probe NED1 at 438 nm depending on the (a) Hg(II). (b) Fe(II) and Fe(III)

These results were also supported by NMR spectral studies (Fig. 6.16). Evaluation of interaction studies of probe NED1 with sensitive metal ion was performed using NMR experiments in [D_6] DMSO. Changes in chemical shifts for aromatic protons (proton present in the napthyl group) as well as aliphatic protons (proton present in $-CH_2$ groups) was observed with the addition of Hg(II) ion. Similar experiments for the iron could not be performed due to the paramagnetic nature of metal ion.
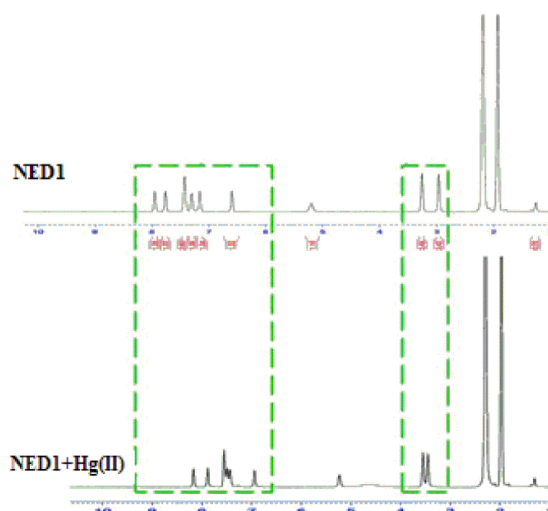
Fig. 6.16 Changes observed during ^{1}H−NMR studies on addition Hg(II) in probe NED1 in [D_6] DMSO

Mass spectral studies were also monitored to find out possible changes in the probe NED1 with the addition of mercury using ESI−MS spectroscopy (Fig. 6.17).
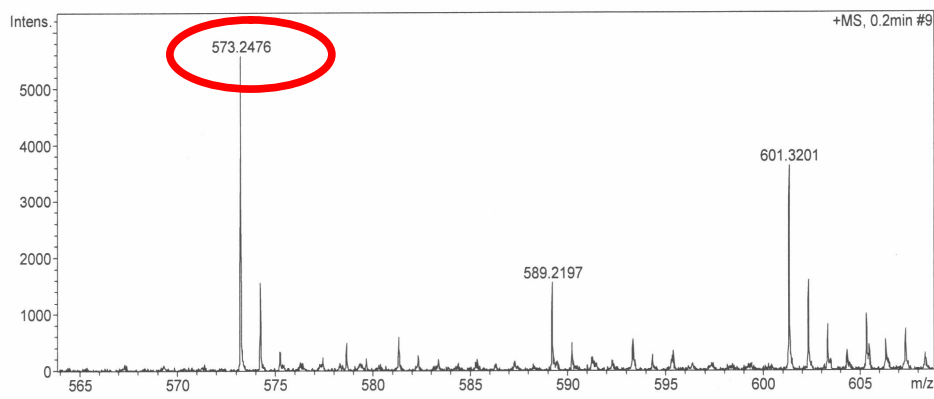
Fig. 6.17 ESI–MS spectrum of [probe NED1+HgCl$_2$.DMSO+K]$^+$ in mixed solvent media (0.1% DMSO in 100 mM phosphate buffer, pH 7.4)

6.3.6. Stern−Volmer quenching constant studies and detection limit

Fluorescence quenching titration was further evaluated using Stern–Volmer equation.[601] Relation between the fluorescence quenching (I_0/I) and the concentration of the quencher (Hg(II), Fe(II) and Fe(III)) has been depicted in Fig. 6.18 is consistent with the Stern–Volmer equation. The extent and efficiency of quenching was calculated in terms of Stern–Volmer constant (Table 6.2).

(c)
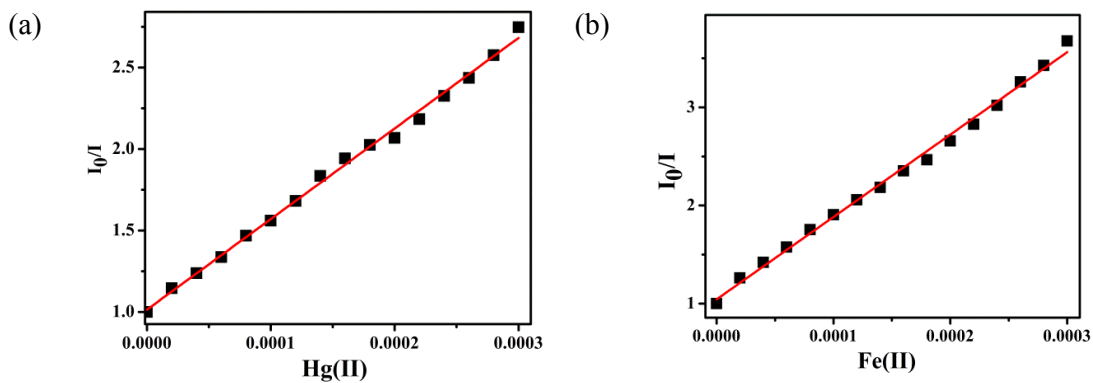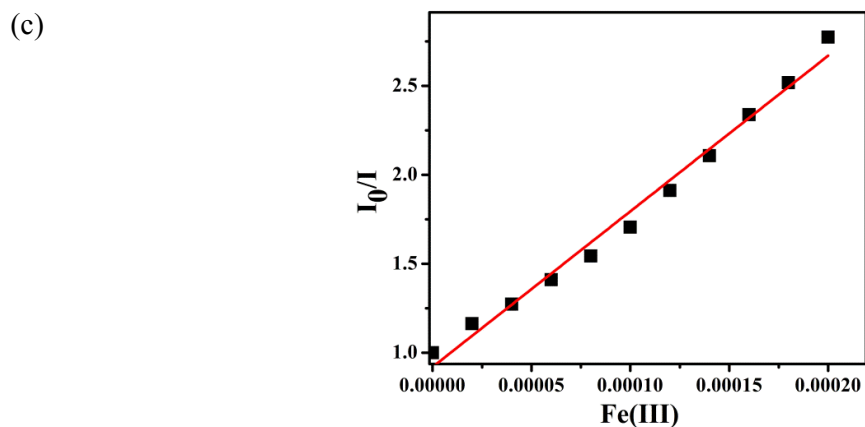
Fig.6.18 Stern−Volmer plot of (a) Hg(II) (b) Fe(II) and (c) Fe(III)

Limit of detection for all the three sensitive metal ions have been calculated. Detection limits were calculated by varying the concentration of Hg(II), Fe(II) as well as for Fe(III) and values were found to be 27.5, 20.93, 27.05 µM respectively.

(a)

(b)

(c)
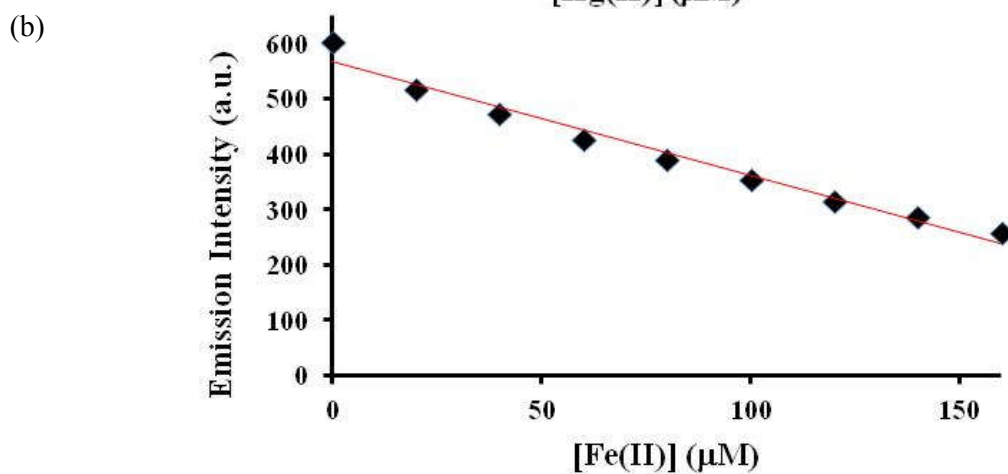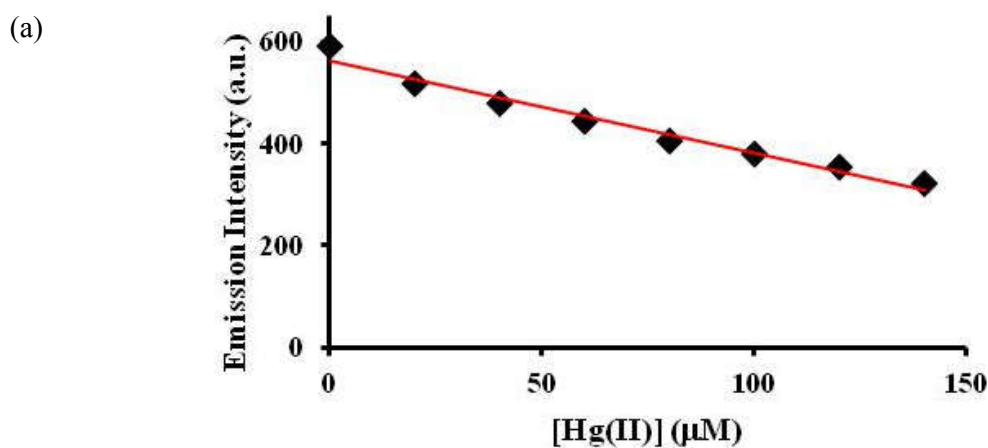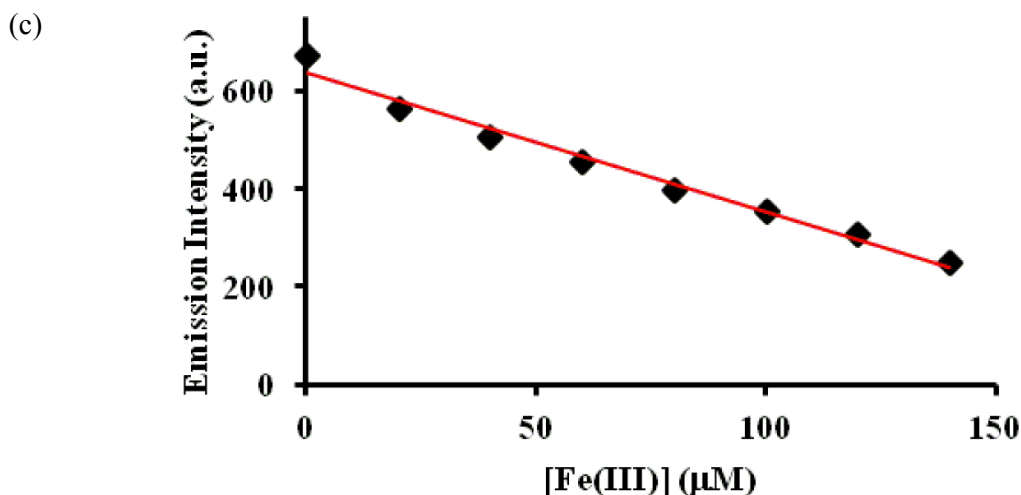
Fig. 6.19 Calculation process of the detection limit of probe NED1 towards (a) Hg(II) (Concentration was linear from 20 μM to 140 μM) (b) Fe(II) (Concentration was linear from 20 μM to 140 μM) and (c) Fe(III) (Concentration was linear from 20 μM to 160 μM) at 438nm

6.3.7. Competitive binding studies

Competitive binding studies of the sensitive metal ions in presence of other served metal ions Ca(II), Mg(II), Mn(II), Fe(II), Co(II), Cr(III) Fe(III), Ni(II), Cu(II), Zn(II) and Hg(II) (as their chloride salts) were also carried out. Fig. 6.20 shows competitive binding studies exhibit no interference of other metal ions in presence of sensitive metal ions. Hence metal ions which are found to be sensitive can be detected even in presence of other metal ions.

(a)

(b)

(c)
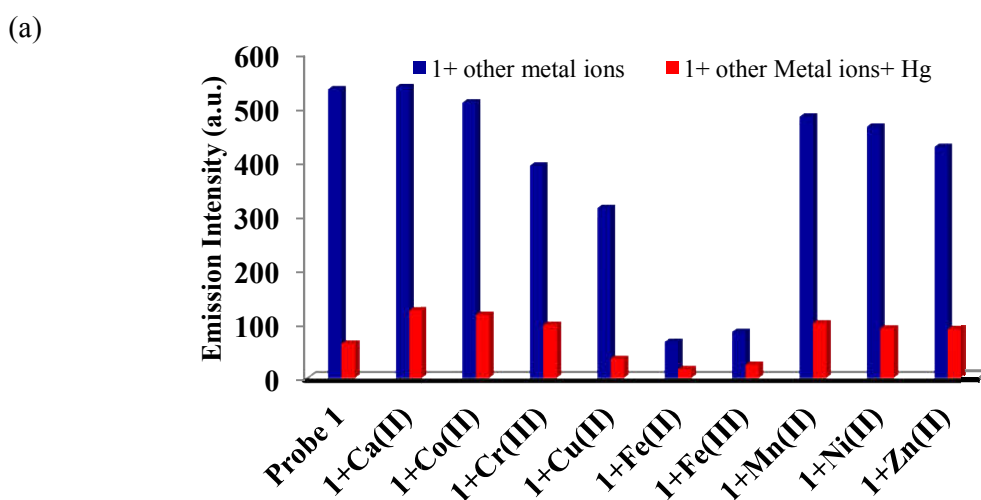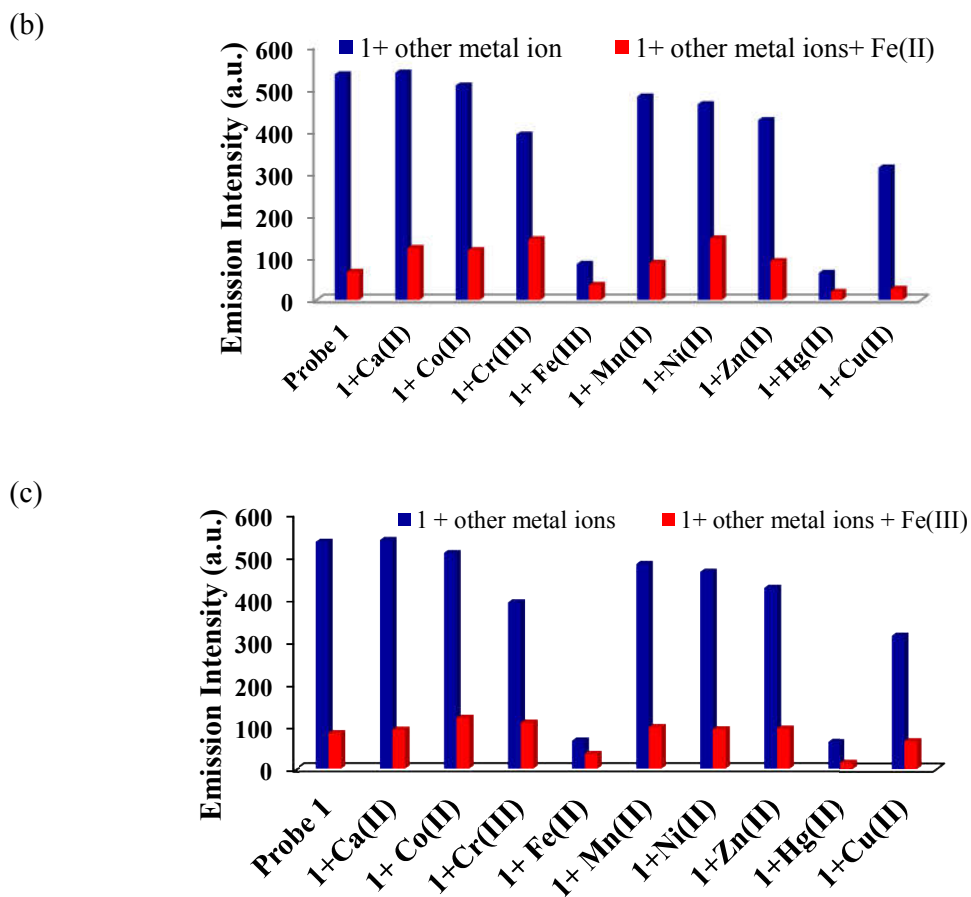
Fig. 6.20 Competitive binding studies: Change in emission intensity of probe NED1 (50 µM) at 438 nm upon addition of 20 equivalents of (a) Hg(II) (b) Fe(II) and (c) Fe(III) along with 20 equivalents of various metal ions (λex=320 nm)

6.3.8. Living cells imaging

In vitro studies prompted to evaluate the performance of probe in living cells. Hence to optimize utility of probe NED1 as an imaging agent for the detection of Hg(II) living cell studies were also performed. Fluorescence microscopic images for the probe and probe and Hg(II) have been depicted in Fig. 6.21. Results obtained clearly indicated that probe NED1 is providing intense fluorescence inside the cell (Fig. 6.21a). Fig. 6.21b explains that the cells are alive in the experimental concentration range of $HgCl_2$. Quenching of fluorescence was observed with the addition of Hg(II) as shown in Fig. 6.21c.

215
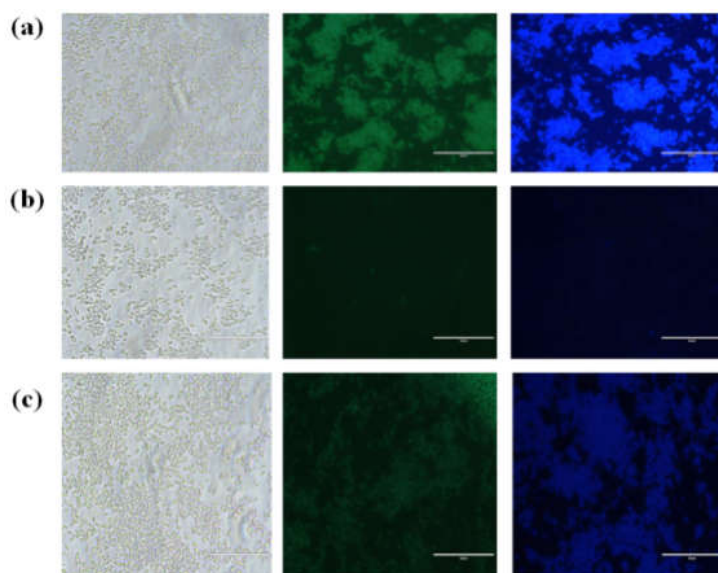
Fig. 6.21 Fluorescence microscopic images of *Candida albicans* cells. (a) Fluorescence image of cells treated with probe NED1 (50 μM) in the absence of HgCl₂ (control); (b) cells supplemented with 10 equivalent HgCl₂ only (c) cells supplemented with probe NED1 and 10 equivalents of HgCl₂ in growth medium for 20 min

6.3.9. Logic gate application

Molecular logic gates are also an interesting area to explore in current research. OR gate is a basic gate which is normally switched on if either one or both inputs are turned on. OR gate can be interpreted if Hg(II)(IN1), Fe(II)(IN2), Fe(III)(IN3) taken as an input while emission intensity at 438 nm as output. Emission intensity 200 a.u. has been taken as a threshold value, above 200 emission intensity gives OUT=0 and emission intensity below 200 gives OUT=1. The truth table and logic function have been shown in Fig. 6.22.

A(IN1)	B(IN2)	C(IN3)	Output(Emission Intensity λem = 438 nm)
0	0	0	0
0	0	1	1
0	1	0	1
0	1	1	1
1	0	0	1
1	0	1	1
1	1	0	1
1	1	1	1
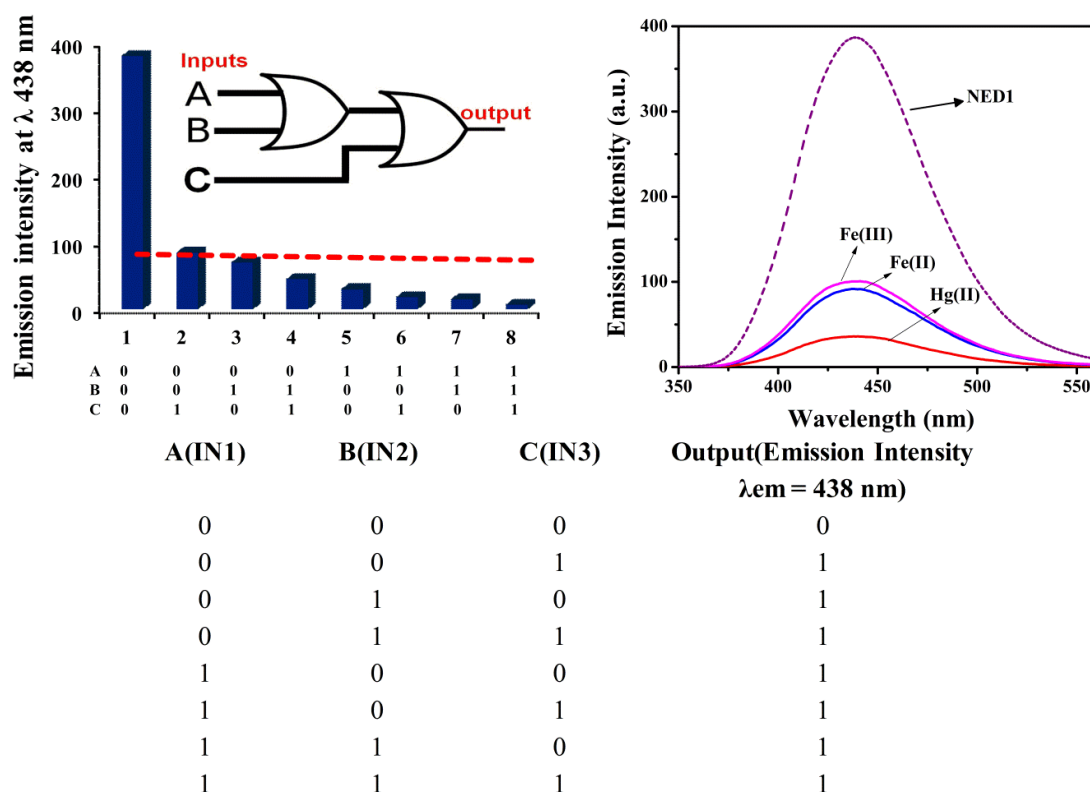
Fig. 6.22 Change in emission spectra and output intensities (bar diagram) of NED1 upon chemical inputs of Hg(II) A, Fe(II) B, Fe(III) C. Truth table indicates OR logic functions

6.4. Conclusions

In conclusion, a naphthylamine based fluorescent probe NED1 was utilized for the metal ion detection using fluorescence spectral studies in mixed aqueous medium. Probe NED1 exhibited selective quenching probably *via* CHEQ in presence of Hg(II), Fe(II), Fe(III). UV−visible and NMR data clearly indicated chelation of above ions to probe NED1. Binding stoichiometry, association constant and Stern−Volmer constants for all the three sensitive metal ions were also calculated. Due to the sensing in mixed aqueous media probe was also subjected for the *in vivo* studies. *In vivo* studies on fluorescence quenching showed sensing of Hg(II) in *Candida albicans* cells. Competitive binding studies clearly articulated that probe NED1 is selective to above three ions. This simple and easytouse probe demands its application in molecular logic gate devices.

6.5. Experimental section

6.5.1. Materials and instrumental methods

N−(2−aminoethyl)naphthalen−1−amine hydrochloride salt was purchased from Sigma Aldrich, Steinheim, Germany and used without further purification. All metal salts used in the synthesis were purchased from commercial source and used directly (without any purification). GC−MS was performed using *PerkinElmer CLARUS 500 GC−Mass spectrometer*; mass spectroscopic measurements were recorded with micROTOF−Q II 10328. The UV−visible spectra were obtained by using Evolution 600, Thermo Scientific UV−visible spectrophotometer. Emission spectra were obtained from RF−5301PC with a 3 cm standard quartz cell. Living cells imaging were recorded by a digital camera connected to the microscope (Evos fl, AMG groups, Carlsbad, CA, USA). DMSO used for studies was HPLC grade.

6.5.2. Synthesis of N−(2−aminoethyl)naphthalen−1−amine, NED1

Probe NED1 was used directly neutralizing the hydrochloride salt of N−(2−aminoethyl)naphthalen−1−amine with saturated solution potassium hydroxide. This neutralized amine was further used and stocks were prepared in DMSO.

6.5.3. Preparation of stock

6.5.3.1. Preparation of stock solution of probe NED1

Stock of probe NED1 was prepared in dimethylsulfoxide. All the experiments were performed with freshly prepared stock solutions and no precipitation was observed within 2 hrs time in the stock as well as in the cuvette. To avoid any precipitation we made very concentrated stock solutions and added a little amount of the stock solution to the solution in cuvette.

6.5.3.2. UV−visible and fluorescence stock preparations

Stock solution of NED1 (1 mM) in DMSO and chloride salt (10 mM) of metals Ca(II), Mg(II), Mn(II), Fe(II), Co(II), Cr(III) Fe(III), Ni(II), Cu(II), Zn(II) and Hg(II) were prepared in water for metal ion sensing.

6.5.4 Determination of fluorescence quantum yield

The fluorescence quantum yield were calculated for probe NED1 as well as probe NED1 and sensitive metal ion using 2−aminopyridine as standard (Φ_F= 0.6) in 0.1 N H$_2$SO$_4$.[597] The probe NED1 as well as probe NED1 and sensitive metal ion were taken in mixed solvent media (0.1% DMSO in 100 mM phosphate buffer, pH 7.4).

$$\emptyset = \emptyset_{std} \left(\frac{I/A}{I_{std}/A_{std}} \right) \left(\frac{\eta}{\eta_{std}} \right)^2 \qquad ($$

6.5.5 Life time measurements

Time resolved fluorescence studies for probe NED1 was carried out in absence as well as presence of sensitive metal ions namely Hg(II), Fe(II) and Fe(III). Laser excitation source of 340 nm was used and decay kinetics was observed at 438 nm. In absence as well as in presence of metal ion probe NED1 followed three exponential decay kinetics. Samples of probe NED1 and NED1 with metal ions were prepared in mixed solvent media (0.1% DMSO in 100mM phosphate buffer, pH 7.4).

6.5.6 Determination of the binding stoichiometry, the apparent association constants K$_{ass}$ and Stern−Volmer constant K$_{SV}$

The apparent association constant (K$_{ass}$) for probe and sensitive metal ion were calculated using Benesi–Hildebrand equation:

$$1/(F - F_0) = 1/\{K_{ass}(F_{max} - F_0)[M]\} + 1/((F_{max} - F_0)$$

Where F is fluorescence intensity for a given concentration of metal ion at λ_{em} 438 nm, F_0 is intensity in absence of metal ion, and F_{max} is maximum fluorescence intensity in presence of metal ion in solution. A graph is obtained by plotting $1/(F-F_0)$ against $1/[M]$. The values of apparent association constant K_{ass} were calculated using slope and line of the plot.[600] Fluorescence quenching titration was further evaluated using Stern–Volmer equation:[601]

$$\frac{I}{I_0} = 1 + K_{SV}[Q]$$

Where I_0 is the emission intensity in absence of quencher, I is emission intensity in presence of quencher (Q) and K_{sv} is SternVolmer constant.

6.5.7. Calculation of detection limit

Limit of detection was calculated using following equation:

Detection limit $= 3\sigma/k$

where σ is the standard deviation of blank measurement, k is the slope between the fluorescence intensity versus metal ion concentration.

6.5.8. *In vitro* cell imaging

Candida albicans was grown in yeast extract peptone dextrose (YEPD) broth medium, and incubated at 30 °C for 48 h with a shaking speed of 120 r/min. Diluted cell suspension (1×10^8 cells/mL) of test microbe was added to separate sterile eppendorf tubes (2 mL) followed by addition of test solutions (probe NED1 (50 µM), $HgCl_2$ (1000 µM) and probe and $HgCl_2$ in respective tube. The eppendorf were then incubated at 30 °C for 4 h to evaluate the fluorescent capturing of prepared solution ($HgCl_2$). After incubation, the tubes were centrifuged and the supernatant was discarded. The pellet was rinsed thrice with PBS (pH 7.4) to remove any extra probe or $HgCl_2$. The stained cells were visualized using fluorescent microscopy.

Chapter-7

Naked Eye Detection of Iron (II) and Iron (III) Metal Ion and Fluorometric Detection of Iron (III) Using Naphthyl Based Probe in Methanol: Logic Gate Application

7.1. Abstract

A novel fluorescent probe (2-((2-(naphthalen-1-ylamino)ethylimino)methyl)phenol) NED2 has been synthesized and characterized by various spectroscopic methods. Photo–physical properties of NED2 have been investigated to study the sensing of metal ions in methanolic solutions. NED2 was found to be highly selective for iron over tested metal ions. Probe NED2 selectively detected iron in both II and III oxidation states giving rise to yellow–brown and purple color respectively. The naked eye detection of iron is useful for the discrimination of II and III oxidation state while fluorescence studies concludes selective and specific sensitivity towards iron(III). Probe was found to be highly sensitive and selective towards iron(III) during fluorimetric detection. DFT calculations were performed. Logic gate application of the probe was also executed.

7.2. Introduction

Design and synthesis of fluorescent probes or chemosensors for the detection of metal ions are significant area of chemical research.[327,329] Among transition metals, iron is one of the most essential element present in the biosystem and exhibit several fundamental roles in different enzymatic and other biological activities.[2,3,333] However, improper concentration of this metal ion could exhibit detrimental effects alone or in a combined state causing diseases like hemochromatosis, cancer etc.[334] Hence detection of the iron and its concentration as well as localizations are extremely important for the cure of such diseases. The most common oxidation states of iron are Fe(II) and Fe(III) which are important for ordinary and related chemistry.[1] Naked eye detection of metal ions is important for qualitative detection as well as quantitative identification. Hence simple and ready to use colorimetric probes are extremely demanding for metal ion sensing.[335] In this regard, fluorescent chemosensors have gained considerable awareness in the recent years because fluorescence measurements are simple, sensitive and easy to handle technique fluorescence.[602] Several colorimetric as well as fluorimetric probes have been described for iron metal ion sensing.[336–339,341–343,603] We have recently reported a simple fluorescent probe for fluorimetric detection of Fe(III).[587] To the best of our knowledge, there is no report of a naphthyl–based probe which could detect iron colorimetrically as well as fluorometrically.[604,605] Multi step synthesis, tedious methods, complicated structures as well as interference from several metals such as Cu(II) and Cr(III) were also observed in reported fluorescence probes for Fe(III).[606–613] In this work, we have designed and synthesized a simple but novel probe 2−((2−(naphthalen−1−ylamino)ethylimino)methyl)phenol (NED2) for the naked eye detection of Fe(II) and Fe(III) (Fig. 7.1). Probe was subjected for the fluorometric detection of Fe(III). The results for the detection of iron will be discussed in the light of theoretical studies *via* DFT calculations. Possible application in the area of logic gates will also be scrutinized.
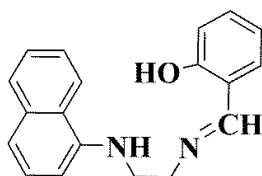
Fig. 7.1 Probe 2−((2−(naphthalen−1−ylamino)ethylimino)methyl)phenol (NED2) used in present work

7.3. Results and discussion

7.3.1. Synthesis of probe NED2

Fluorescent probe 2−((2−(naphthalen−1−ylamino)ethylimino)methyl)phenol NED2 has been synthesized by refluxing N−(1−naphthyl)−ethylenediamine and 2−hydroxybenzaldehyde. Amine N−(1−naphthyl)−ethylenediaminedihydrochloride was neutralized using potassium hydroxide prior to use. Probe NED2 was charcterized using various spectroscopic studies such as IR, UV−visible spectral studies. Structure of probe NED2 was established by spectroscopic techniques ^{1}H−NMR, ^{13}C−NMR and GC−MS spectral studies.

7.3.2. Characterization of NED2

7.3.2.1. IR spectral studies

The characteristic azomethine ($\nu_{-HC=N}$) band for probe was observed at 1581 cm^{-1} in IR spectrum (Fig. 7.2).[396]
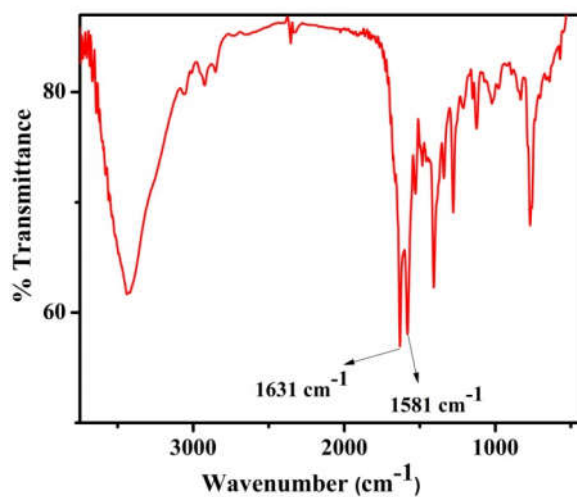
Fig. 7.2 IR spectrum of probe NED2

7.3.2.2. Electronic absorption spectral studies

The electronic absorption study of probe showed bands around 282 and 354 nm (shown in Fig. 7.3). All these bands were assigned as intramolecular $\pi-\pi^*$ and n$-\pi^*$ transitions.[396,402]
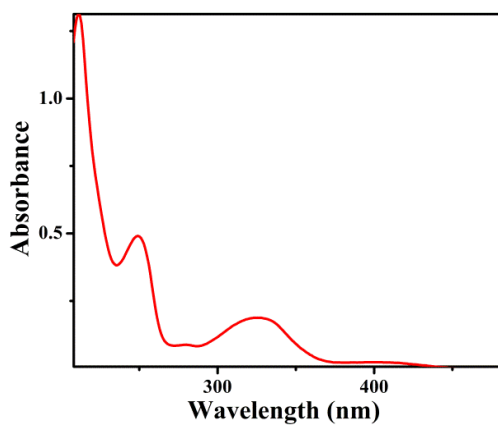
Fig. 7.3 UV−visible absorption spectrum of NED2 (20 μM) in methanol

7.3.2.3. GC-MS spectral studies

GC−Mass spectral studies exhibited peak corresponding to the molecular ion at m/z value of 290 as depicted in the Fig. 7.4.
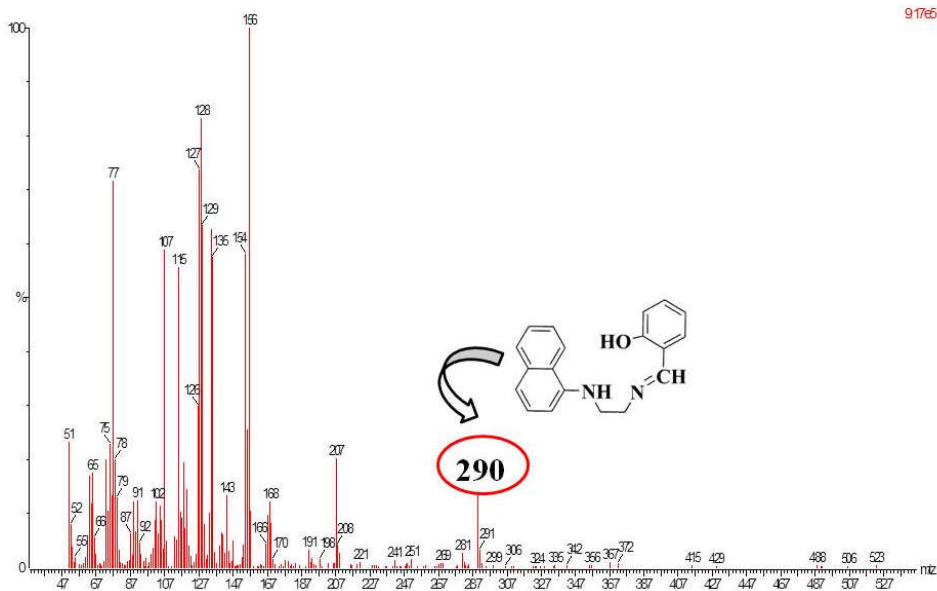
Fig. 7.4 GC−MS spectrum of NED2

7.3.2.4. NMR spectral studies

The ^{1}H−NMR spectrum of the NED2 (Fig. 7.5) exhibited four methylene protons at 3.68 and 3.69 ppm respectively. A singlet for −NH bonded directly to the naphthyl group is at 4.58 ppm. All the aromatic protons were found in the range of 6.69−8.32 ppm. A broad singlet peak at 13.26 ppm was observed due to –OH proton.
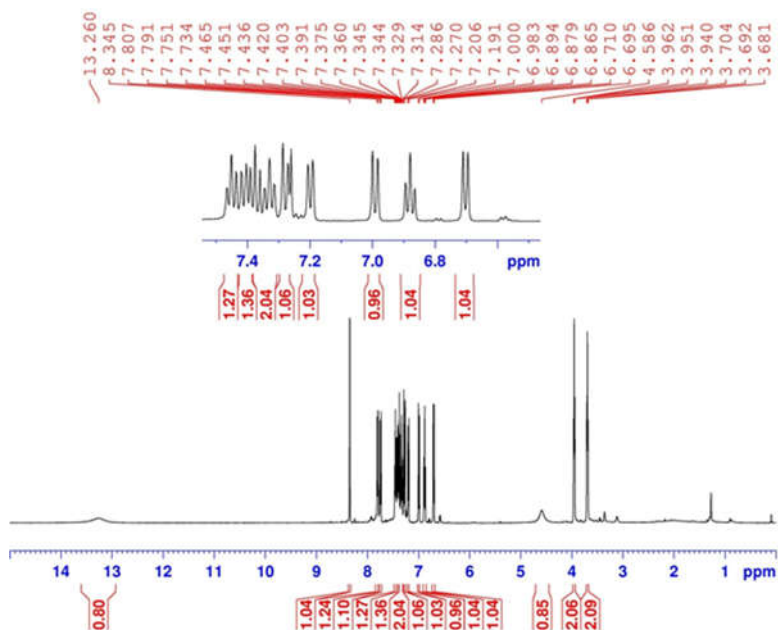
Fig. 7.5 ^{1}H−NMR spectrum of NED2 in CDCl$_3$

To confirm −OH proton a deuterium exchange experiment also performed and confirmed the presence of −OH at 13.26 ppm.
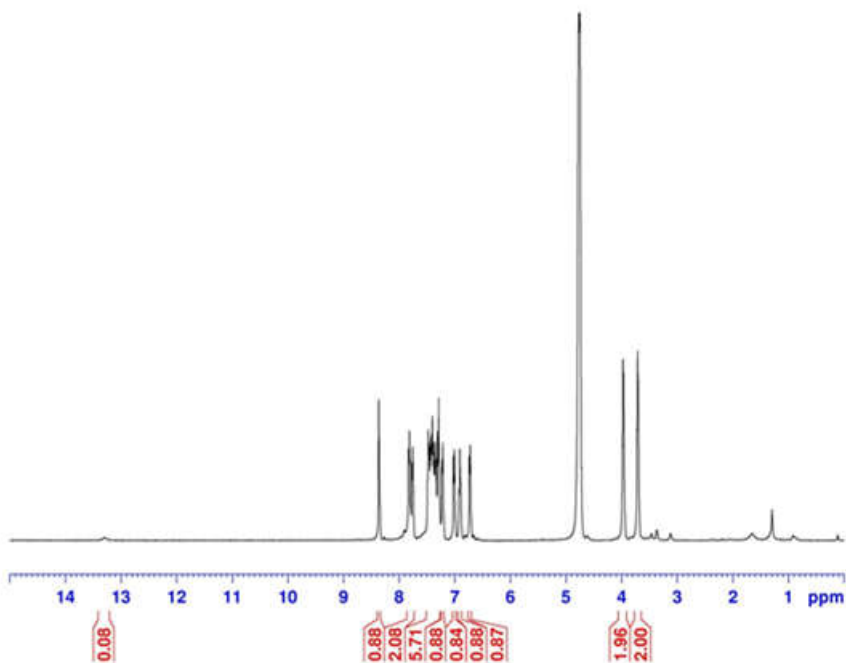
Fig. 7.6 ^{1}H−NMR D$_2$O exchange spectrum of NED2 in CDCl$_3$

^{13}C−NMR spectrum of NED2 has been exhibited in Fig. 7.7. −CH$_2$ carbon showed peak at 44.4 and 58.1 ppm. All the aromatic carbons were found in the range of 104.7−166.7 ppm.
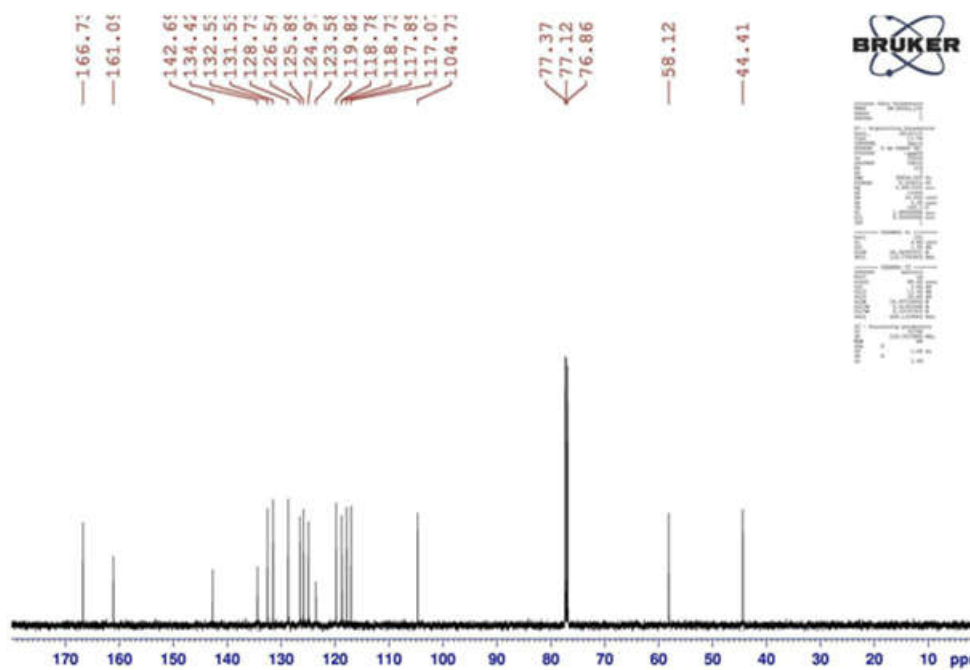
Fig. 7.7 ^{13}C−NMR spectrum of NED2 in CDCl$_3$

To confirm the −CH$_2$ carbon ^{13}C DEPT−135 NMR experiment was also performed which showed peak in negative corresponding to −CH$_2$ carbon and confirms the presence of the same (Fig. 7.8).
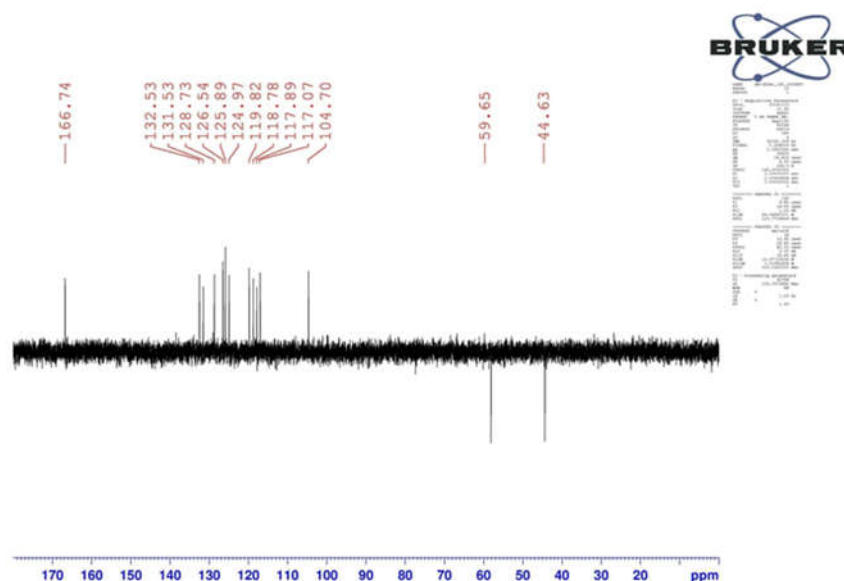
Fig. 7.8 ^{13}C DEPT−135 NMR of NED2 in CDCl$_3$

Table 7.1 Data for UV-visible and NMR spectral studies of probe NED2

UV−visible data (λ_{max}/nm, ε/M^{-1}cm^{-1})[a]	[1]H−NMR[b]	[13]C−NMR[b]
400 (1,190), 325 (9,730), 247 (24,700), 213 (65,560)	13.260 (s, 1H), 8.345 (s, 1H), 8.005 (d, J= 8, 1H), 7.799 (d, J= 8, 1H), 7.742 (d, J= 8.5, 1H), 7.270-7.451 (m, 5H), 7.267 (d, J= 7.5 Hz, 1H), 7.198 (d, J= 7.5, 1H), 6.702 (d, J= 7.5, 1H), 4.586 (s, 1H), 3.318 (dd, 2H), 3.251 (t, 2H)	166.7, 44.41, 58.12, 104.7,117, 117.8, 118.73, 118.78, 119.82, 123.58, 124.97, 125.89, 126.54, 128.73, 131.53, 132.53, 134.42, 142.69, 161.09

[a]Solvent: Methanol, [b]Solvent: CDCl$_3$

7.3.3. Naked eye detection

During the addition of probe NED2 to the metal ions a unique color change was observed. Among the served metal ions only Fe(II) (yellow-brown) and Fe(III) (purple) showed color which can easily be detected *via* "naked eye" (Fig. 7.9). Although several fluorescent probes have been reported for the naked eye detection of iron but there is no

report for discrimination of Fe(II) and Fe(III) using naphthyl–based probe for visible detection.

Fig. 7.9 Naked eye detection of NED2 in the presence of representative metal ions (10 eq)

7.3.4. UV−visible absorption spectral studies

Absorption spectral studies of probe NED2 have been investigated in methanol. UV−visible spectra showed typical naphthalene absorption band at 320 nm corresponding to charge transfer transition between amine and naphthyl group.[583] Probe NED2 exhibited a band around 402 nm in visible region responsible for the slight yellow color of probe. On addition of Fe(II) into the methanolic solution of probe NED2 yellow−brown color appeared and showed an intense absorption band in the visible region around 536 nm. Similarly, the addition of Fe(III) into the methanolic solution gave rise to purple color and showed an intense absorption band in the visible region around 590 nm (Fig. 7.10). The color appeared was due to a charge transfer band originated in the visible region.[614]
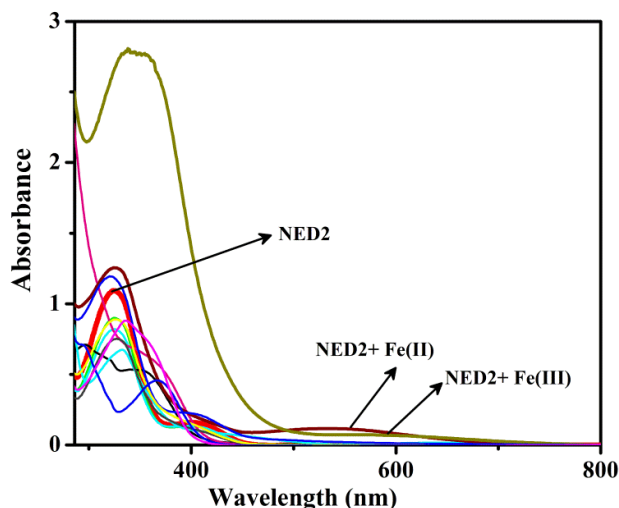
Fig. 7.10 UV−visible spectral change of NED2 (20 µM) in methanol on addition of 10 equivalent of Zn(II), Sn(II), Ni(II), Mn(II), Mg(II), Hg(II), Fe(II), Fe(III), Cu(II), Co(II), Cd(II), Ca(II) and Ba(II)

Further the effect of concentration variation of iron metal ion (Fe(II) and Fe(III)) was monitored using absorption spectral studies. During titration experiments with Fe(II) and Fe(III) ions band increases in the visible region (Fig.7.11−Fig.7.12).
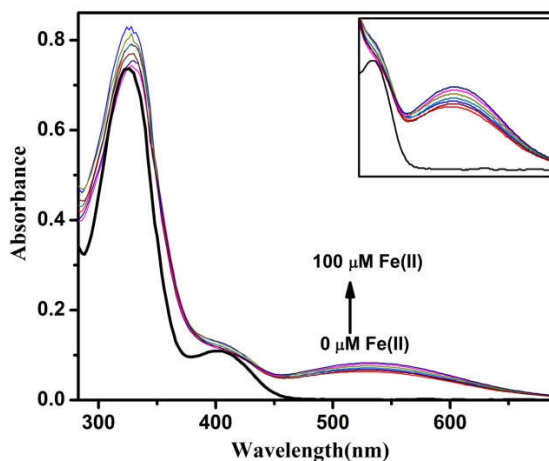
Fig. 7.11 Absorption spectra of NED2 (5 µM) upon addition of different amounts of Fe(II) in methanol
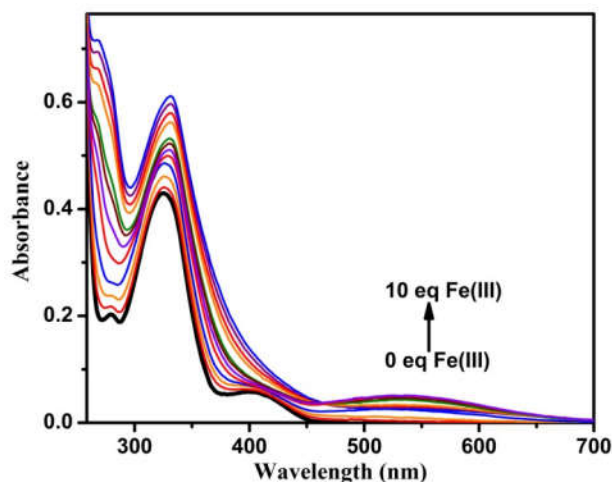
Fig. 7.12 Absorption spectra of NED2 (5 µM) upon addition of different amounts of Fe(III) in methanol

7.3.5. Emission spectral studies

Photophysical properties of probe NED2 were explored in methanol. Probe NED2 was found to be fluorescent at excitation wavelength (λ_{exc}) 320 nm. The wavelength of emission was 420 nm. Maximum emission intensity of probe NED2 was observed after incubation for 5 min and remains constant after that (Fig. 7.13).
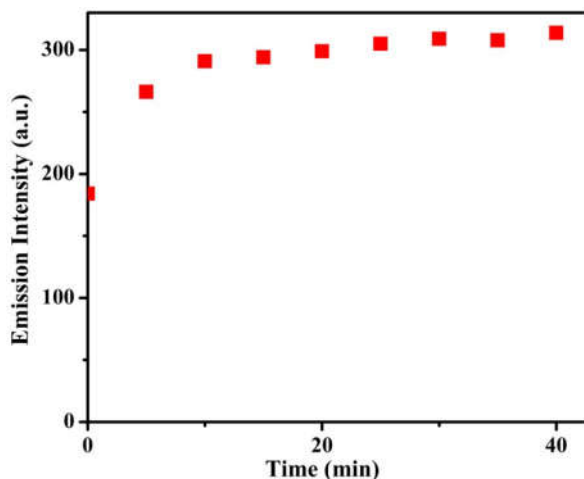
Fig. 7.13 Plot of emission intensity NED2 (5×10^{-5}M) for 40 min at λ_{ex} 320 nm

Upon addition of metal ions Zn(II), Sn(II), Ni(II), Mn(II), Mg(II), Hg(II), Fe(II), Cu(II), Co(II), Cd(II), Ca(II) and Ba(II) to the probe NED2 did not show any appreciable change. While introduction of Fe(III) to the solution of probe NED2 gave rise to quenching in emission intensity with the red shift of 13 nm. On further addition of Fe(III) to the probe a decrease in emission intensity was observed (Fig. 7.14).
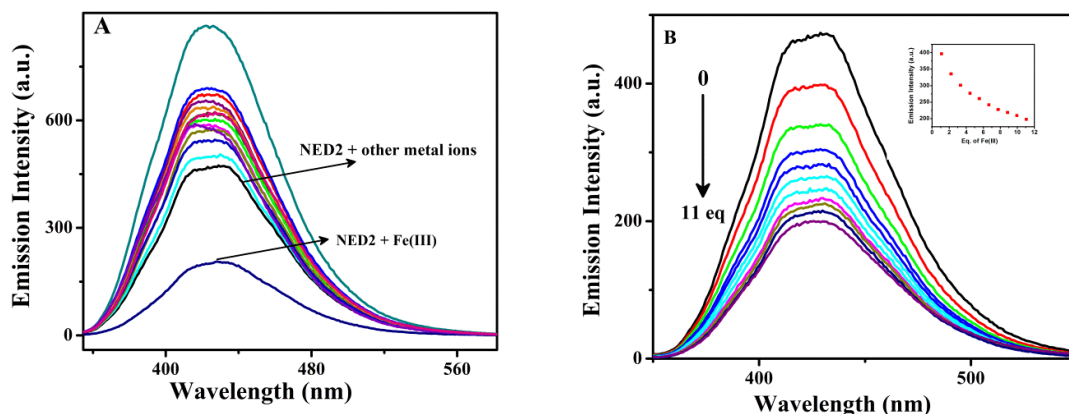
Fig. 7.14 (A) Fluorescence emission spectra of NED2 (20µM) in methanol with 10 equivalent of Zn(II), Sn(II), Ni(II), Mn(II), Mg(II), Hg(II), Fe(II), Fe(III), Cu(II), Co(II), Cd(II), Ca(II) and Ba(II). (B) Fluorescence emission titration spectra of NED2 (20µM) in the presence of varying concentration of Fe(III) in MeOH at λ_{ex} 320 nm. (Inset- change in emission intensity with number of equivalents of Fe(III)

A large stoke shift was observed for maximum excitation and emission wavelength as depicted in Fig. 7.15. Due to large value of stokes shift, fluorescence resonance energy transfer (FRET) is not favorable for the quenching mechanism. Hence the electron transfer could be a probable mechanism for Fe(III) quenching as Fe(III) is a strong Lewis acid and can accept electron easily.[615]
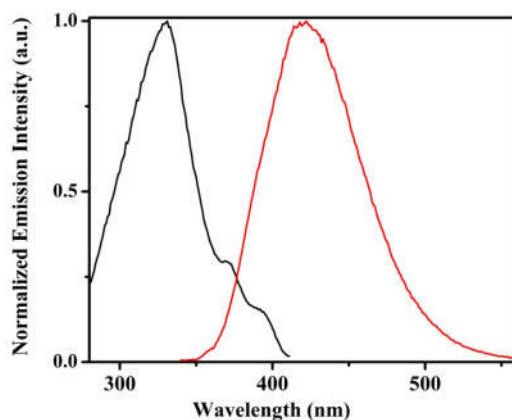
Fig. 7.15 Excitation and emission spectra of probe NED2 (50 μM) in methanol solution. Black line is the excitation spectra, and the blue line is the emission spectra. The maximum excitation and emission are at 330 nm and 420 nm, respectively

7.3.6. Detection of Fe(III) in mixed aqueous media and at variable pH

To optimize possible utilization of probe NED2 for fluorimetric sensing of Fe(III) in the living cell applications, experiments were also performed in water−methanol mixed solvent media. Probe NED2 is insoluble in water hence a mixed aqueous media was utilized for experiments. During absorption spectral studies in mixed aqueous media, the band in visible region which were responsible for color generation completely disappeared (Fig. 7.16).
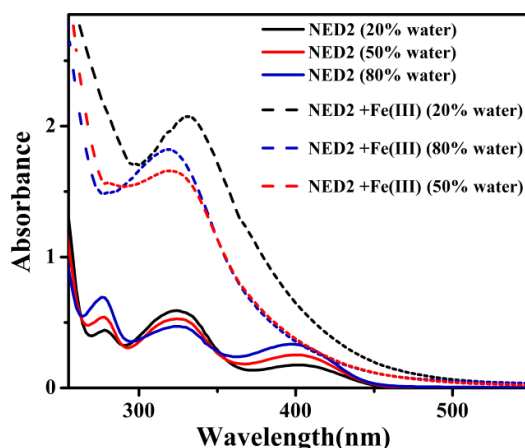
Fig.7.16 Changes observed during absorption spectral studies of NED2 (20 μM) and NED2 and Fe(III) upon addition of different amounts of water in methanol

Experiments were also performed at variable pH in mixed aqueous media (Fig. 7.17) and in this case also band responsible for the naked eye detection was not observed.
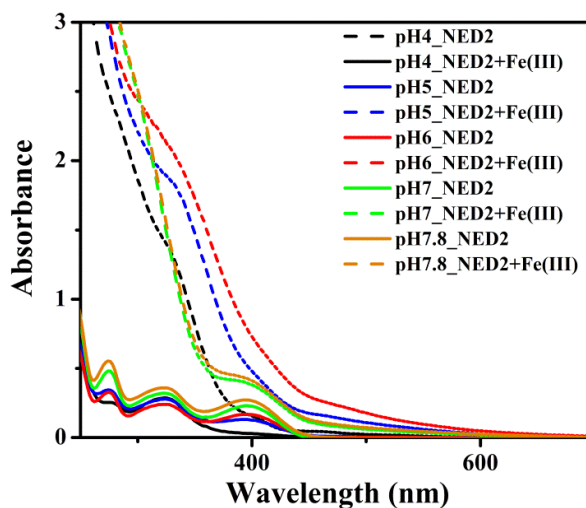
Fig. 7.17 Effect of pH during absorption spectral studies of NED2 (20 µM) and NED2 and Fe(III) in water–methanol (4:1)

Hence naked eye detection was not possible on changing solvent media from methanol to methanol:water as well as for pH variation.

Similar to absorption spectral studies fluorescence properties of probe NED2 were also explored in mixed aqueous media as well as in different pH of the solutions.

In mixed aqueous media sensing of metal ions towards probe changed as compared to sensing in methanol. Although a retention in quenching of Fe(III) observed in both the medium, however selectivity of iron sensing reduced (Fig. 7.18). In methanol, all the metal ions exhibited enhancement of emission intensity as compare to probe NED2 excluding Fe(III). On the other hand, in mixed aqueous media enhancement as well as quenching of emission intensity for different metal ions were observed.
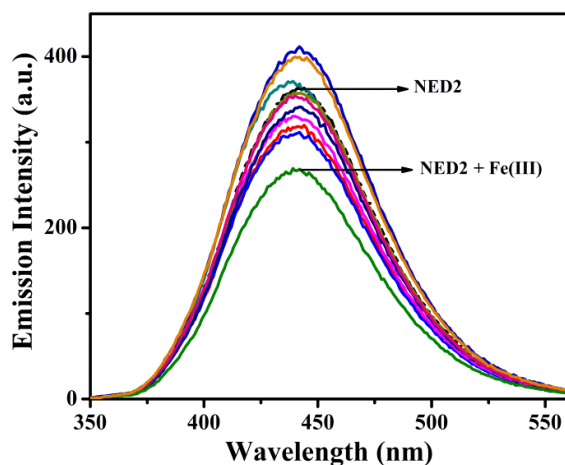
Fig. 7.18 Emission spectral studies of NED2 (20 μM) and other representative metals in water–methanol (4:1)

Effect of water was also observed on Fe(III) metal ion sensing as shown in Fig. 7.19.
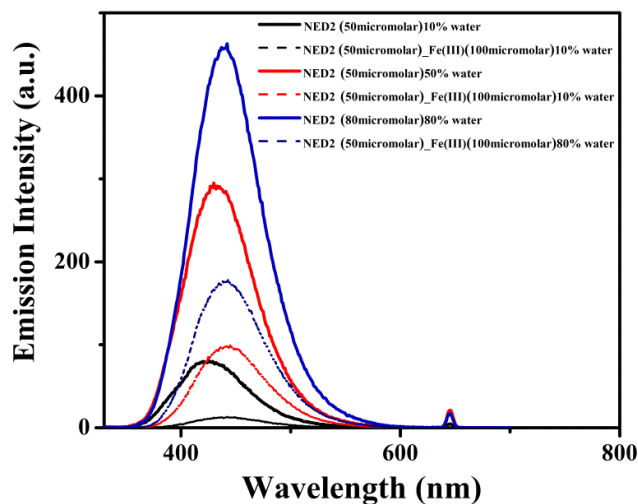
Fig. 7.19 Effect of water during absorption spectral studies of NED2 (20 μM) and NED2 and Fe(III) in water–methanol (4:1)

Fluorescence properties was also observed of probe NED2 and NED2 with the Fe(III) metal ion sensing at variable pH. Data has been deposited in Fig. 7.20.
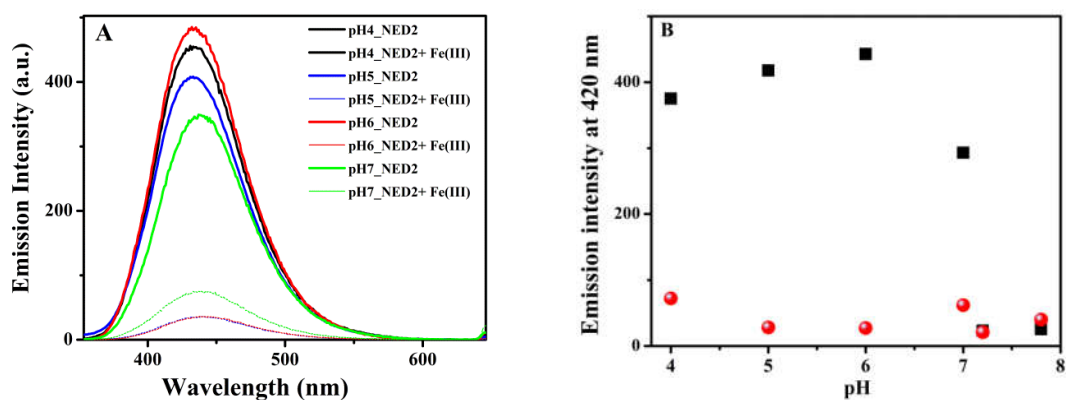
Fig. 7.20 Effect of pH during emission spectral studies of NED2 (20 μM) and NED2 and Fe(III) in water–methanol (4:1)

All these experiments (Fig. 7.16−7.20) suggested that sensitivity and selectivity of Fe(III) fluorescence quenching is medium dependent. These results ruled out the possibility of Fe(III) sensing *via* fluorescence in living cells applications.

7.3.7. Nature of quenching

Stern−Volmer plot, measurement of life time for probe ($\tau = 7.94$ ns) only, probe and Fe(III) (8.09ns) and changes in absorption spectra clearly designate static nature of quenching[616] (Fig. 7.21(A) and (B)).
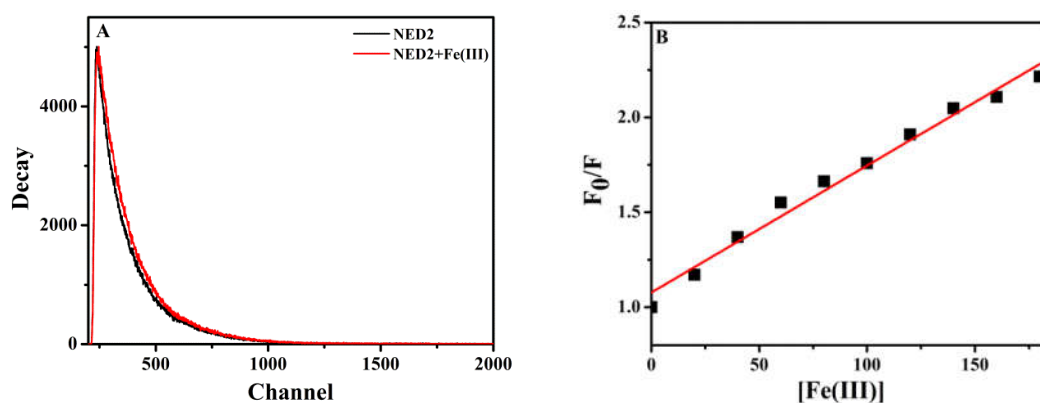
Fig. 7.21 (A) Fluorescence decay profile of NED2 in the presence and absence of Fe(III) in methanol.(B) Stern−Volmer plots for titrations of NED2 with different concentrations of Fe(III) in methanol

Quantum yield values were calculated using 2–aminopyridine as standard. The values for relative quantum yield for probe NED2 as well as for probe NED2 and Fe(III) were found to be 0.03 and 0.005.[613]

7.3.8. Selectivity studies

Competitive binding studies were also performed to study the interference by served metal ions Zn(II), Sn(II), Ni(II), Mn(II), Mg(II), Hg(II), Fe(II), Cu(II), Co(II), Cd(II), Ca(II) and Ba(II) for the detection of Fe(III) using spectrophotometry as well as spectrofluorometry. Interference of metal ion can affect the selectivity of probe NED2 towards Fe(III) and is very crucial for the sensitivity. During competitive binding studies equal concentration of Fe(III) and other metals were taken in methanolic solution. Anti–interference experiment showed that no metal ion interfere with the sensing of Fe(III). Hence probe NED2 is found to be an excellent sensor for Fe(III) even in presence of other metal ions.

During absorption studies wavelength 565 nm was chosen for the mixed metal ion sensing experiment. Bar diagram clearly exhibits the effect of Fe(III) on fluorescence of probe NED2 (Fig. 7.22). Other metal ions did not show any band around 565 nm but on addition of Fe(III) a band arises at 565 nm. Only Cu(II) interfere with the band formation during UV–visible studies.
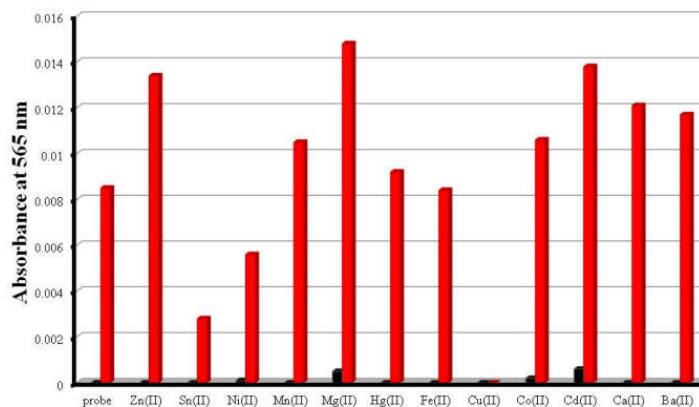
Fig. 7.22 Selectivity of metal ions at wavelength 565 nm in a solution having probe NED2 and metal ions (black bar) and NED2 and metal ions and Fe(III) (red bar) observed using UV−visible absorption spectral studies

Similar to absorption spectral studies, fluorescence studies performed for the competitive binding studies. During experimental condition Fe(III) showed quenching without interference of any other metal ion at wavelength 421 nm (Fig. 7). Hence probe NED2 can be used as highly selective as well as specific fluorimetric sensor for Fe(III) in methanol.
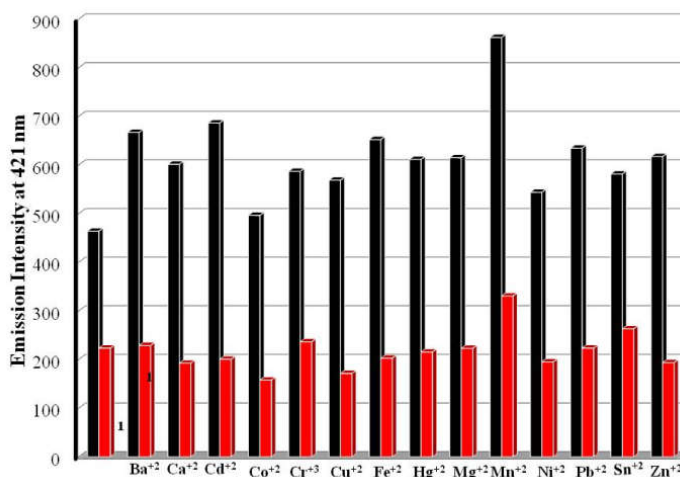
Fig. 7.23 Selectivity of metal ions at wavelength 421 nm in a solution having probe NED2 and metal ions (black bar) and NED2 and metal ions and Fe(III) (red bar) observed using fluorescence spectral studies

7.3.9. Binding stoichiometry of probe NED2 and Fe(III)

Job's plot was used to calculate the binding stoichiometry of probe NED2 and probe NED2 with Fe(III) metal ion.[617] A graph between emission intensity *vs* mole fraction was plotted at wavelength 420 nm. The maxima clearly exhibit 1:1 binding stoichiometry of NED2 with Fe(III) (Fig. 7.24).
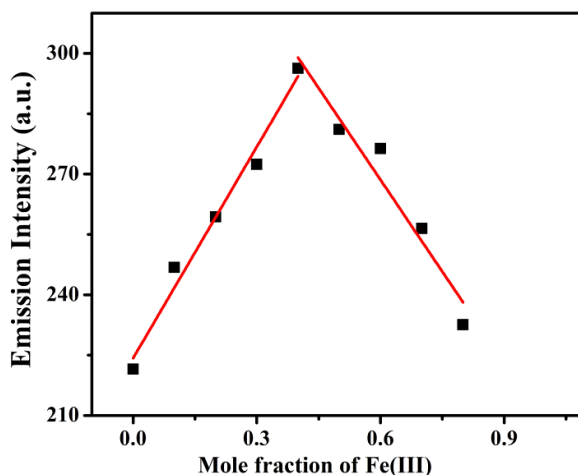
Fig. 7.24 Job's plot of NED2 and Fe(III) in methanol, total concentration of NED2 and Fe(III) were maintained 100 µM and observed at 420 nm

Binding strength of probe NED2 and Fe(III) ion was also measured using Benesi–Hildebrand plot which also supports 1:1 stoichiometry obtained from Job's plot. The value of association constant was found to be $2.884 \times 10^3 \, M^{-1}$ (Fig. 7.25).[618,619]
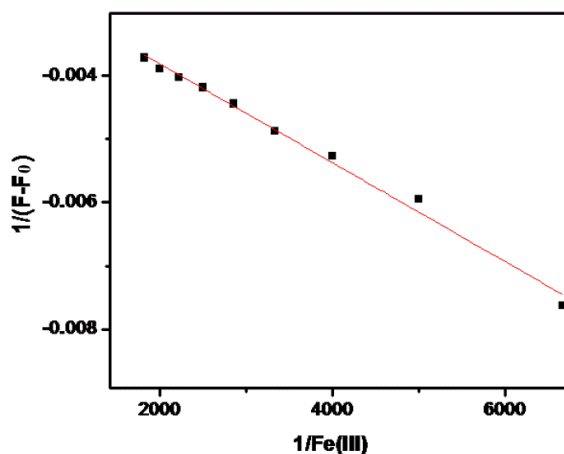
Fig. 7.25 B–H plot for binding of Fe(III) with the probe NED2. Association constant was found to be 2.884×10^3. A good linear fit of the B–H plot supported the 1:1 binding stoichiometry

Electrospray ionization−mass spectral (ESI−MS) studies were also optimized to study the behavior of species formed in solution. Results observed from these experiments supported the 1:1 metal ion and probe NED2 interaction (Fig. 7.26−7.27).
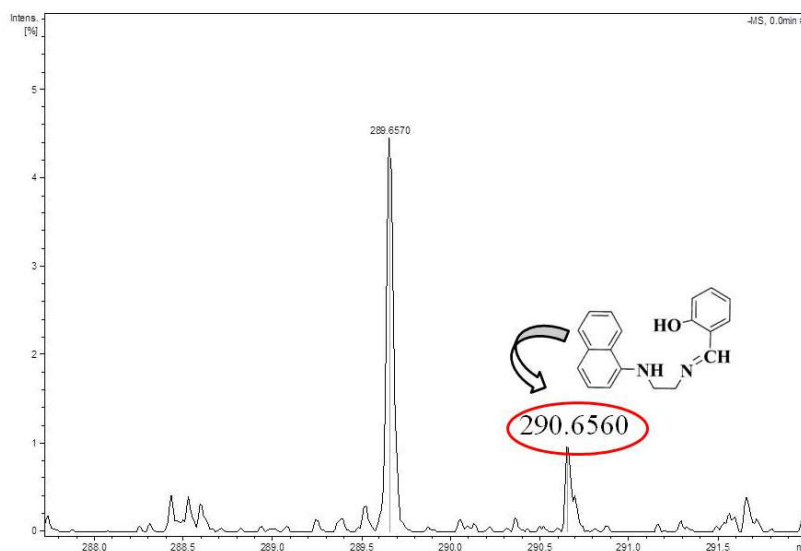
Fig. 7.26 ESI mass spectrum of NED2 in methanol−acetonitrile solution
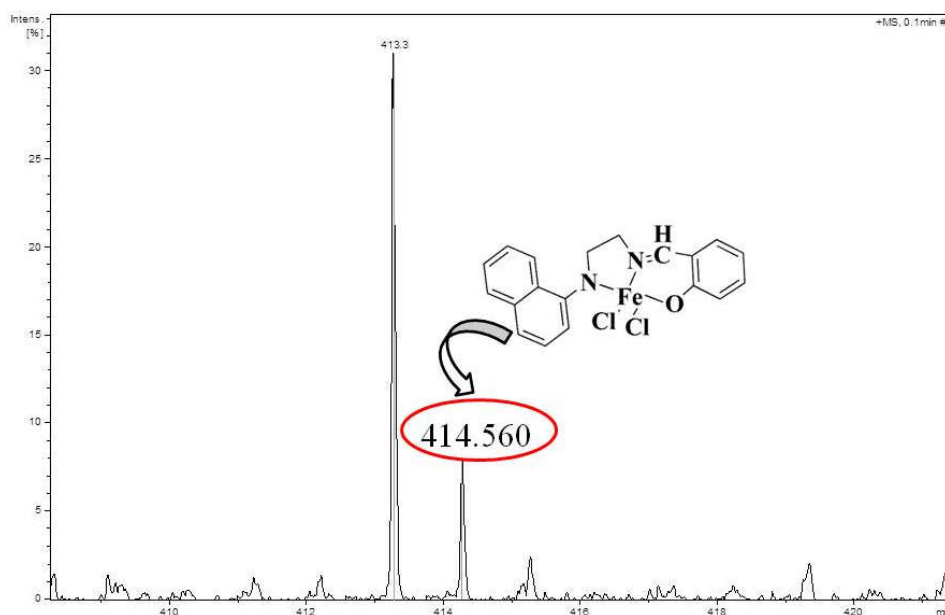
Fig. 7.27 ESI mass spectrum of NED2 and Fe (III) 10 eq in methanol−acetonitrile mixture

Further, limit of detection of Fe(III) was also calculated for a linear range of 10-60 μM and found to be 20.85 μM (Fig. 7.28).
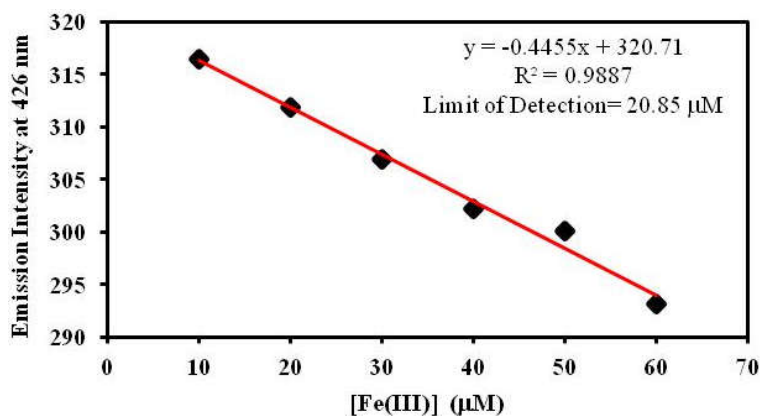
Fig. 7.28 Limit of detection calculated for a linear range of 10−60 μM (wavelength 426 nm)

7.3.10. Reversibility of fluorescence of probe NED2

For better insight into the mechanism of Fe(III) sensing, fluorescence titration were conducted in presence of EDTA. EDTA has a strong tendency to chelate with Fe(III) and formation of Fe−EDTA complex stops the electronic interaction of probe with Fe(III) ion.

Hence instead of the fluorescence quenching, enhancement of fluorescence was observed in presence of EDTA. Further addition of Fe(III) ion to the solution gave rise to fluorescence quenching. Hence titration of probe NED2 with EDTA showed binding of Fe(III) with probe is reversible to some extent. This experiment also supports the electron transfer pathway for quenching of the probe (Fig. 7.29). Hence probe NED2 can be considered as a reversible sensor for Fe(III) metal ion sensing.[338]
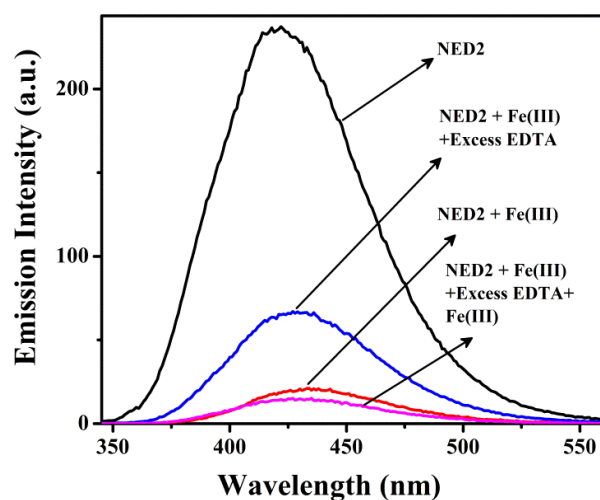
Fig. 7.29 Reversibility experiment from fluorescence spectra of probe NED2 in the presence of Fe(III) with excess of EDTA methanol

7.3.11. Density functional theory (DFT) calculations

To understand the mechanism of such processes, theoretical calculations were also performed. DFT calculations for NED2 and NED2−Fe(III) complex was performed at the B3LYP level using LANL2DZ basis set for Fe center and 6−31G(d) basis set for non metal atoms.[428] The highest occupied molecular orbital (HOMO) and the lowest unoccupied molecular orbital (LUMO) of NED2 and NED2−Fe(III) complexes has been shown in Fig. 7.30.
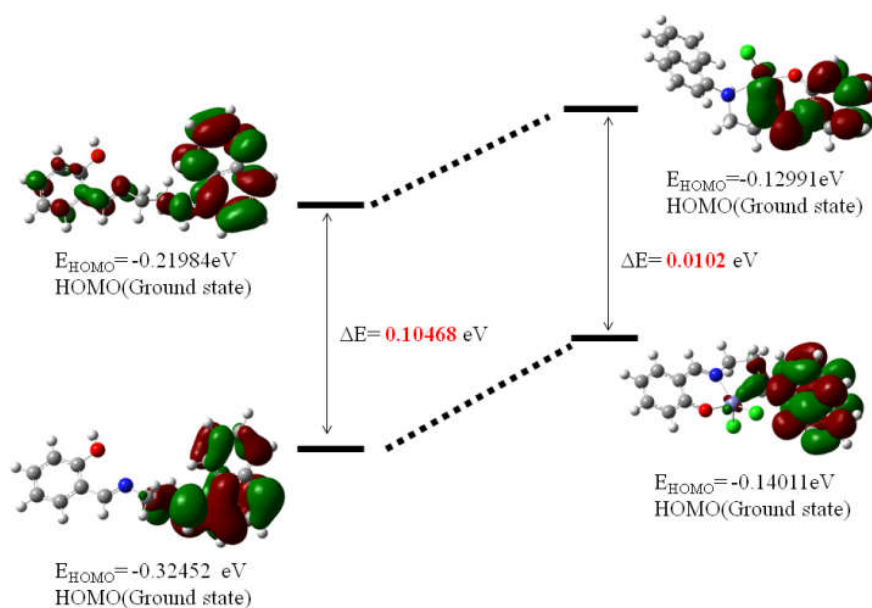
Fig. 7.30 Energy diagrams of HOMO and LUMO orbitals of probe NED2 and NED2–Fe(III) complex calculated at the DFT level using a B3LYP/6–31+G(d,p) basis set

The energy gaps between HOMO and LUMO was also calculated and the values for the probe NED2 and NED2–Fe(III) complex were 0.10468 eV and 0.0102 eV respectively. Energy gap between HOMO and LUMO in adduct decreases in NED2–Fe(III) favors to the complexation on addition of Fe(III) in probe NED1 as proposed. These findings suggest suitable binding of Fe(III) with tridentate probe having NNO donor.[620]

7.3.12. Logic gate application

Logic gates have been attracted the interest of researchers due to their growing application in molecular switches and molecular keypad devices.[621–626] We tried to utilize these results for the logic gate application. Here we have chosen Fe(III) and EDTA used for reversibility experiment as input.[627] Truth table and logic gate have been given in Fig. 7.31. Emission intensity at 100 has been taken as a threshold value at wavelength 420 nm. Emission intensity above threshold gives a state OUT= 0 and below OUT= 1.
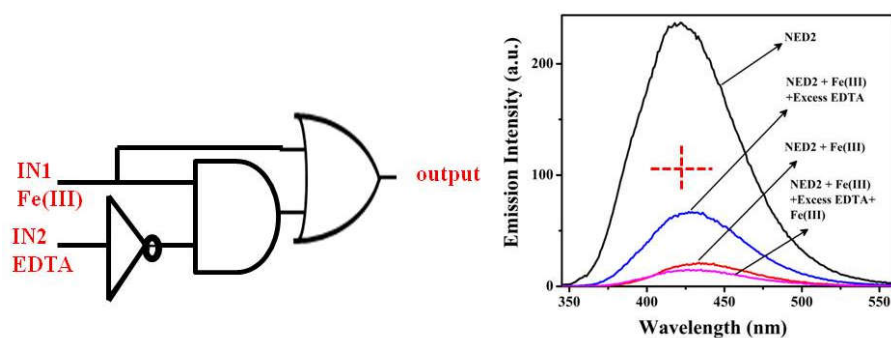
Truth Table

IN1(Fe⁺³)	IN2(EDTA)	OUT(Emission intensity at 420nm)
0	0	0
0	1	0
1	0	1
1	1	1

Fig. 7.31 Change in emission spectra NED2 upon chemical inputs of Fe(III) IN1, EDTA IN2. Truth table indicates and logic functions

7.4. Conclusions

In this present work a simple and novel probe NED2 has been synthesized *via* a simple one step synthetic procedure and resultant compound was characterized by various spectroscopic techniques such as IR, UV-visible, GC-MS and NMR spectral studies. Photo−physical properties of NED2 have been monitored for metal ion sensing in methanolic solution. Probe NED2 was found to be a naked eye sensor and selectively detect iron in both II and III oxidation states giving rise to yellow−brown and purple color respectively. There is a little interference of copper during absorption spectral studies. Probe NED2 was extremely sensitive and selective towards Fe(III) during fluorimetric studies. Fe(III) efficiently quenches fluorescence of the probe NED2 in presence of served metal ions. Static nature of quenching was supported by the data optimized *via* life time measurement, Stern−Volmer plot and UV−visible spectral studies. Probe NED2 and Fe(III) bind in 1:1 stoichiometry. Theoretical studies were also performed. DFT calculation provided that the decrease in the energy gap between HOMO and LUMO is probably

responsible for the quenching of fluorescence. Absorption spectral and fluorescence spectral studies in mixed (water and methanol) solvent were also performed. UV−visible experiments clearly showed the disappearance of bands near 500 nm which were responsible for the color. Hence presence of water decreases the sensitivity of iron among served metal ions.

7.5. Experimental section

7.5.1. Materials and synthetic methods

N−(1−naphthyl)−ethylenediaminedihydrochloride purchased from Thomas Baker, India. Salicylaldehyde was purchased from SRL, Mumbai, India. All metal salts used in the synthesis were purchased from commercial source and used directly (without any purification). ^{1}H−NMR and ^{13}C−NMR spectra of NED2 in CDCl$_3$ were recorded using Bruker AVANCE, 500.13 MHz spectrometer; GC−MS spectrometry was recorded with Perkin Elmer. The UV−visible spectra were obtained by using Evolution 600, Thermo Scientific UV−visible spectrophotometer. Emission spectra were obtained from RF−5301PC with a 3cm standard quartz cell.

7.5.2. Synthesis of 2-((2-(naphthalen-1-ylamino)ethylimino)methyl)phenol NED2

N-(1-naphthyl)-ethylenediaminedihydrochloride salt was dissolved in water and then neutralized using a saturated solution of KOH. Free amine was extracted with the help of dichloromethane and dried over Na$_2$SO$_4$. A solution of salicylaldehyde (122 mg, 1.00 mmol) in 5 mL of methanol was added to (186 mg, 1.00 mmol) of N−(1−naphthyl)−ethylenediamine in 10 mL methanol with continuous stirring. After refluxing of few hours, reaction was cooled to room temperature. An oily compound obtained after evaporation of solvent. GC−MS (MeOH, m/z): 290 M$^+$. Selected IR data (KBr, ν_{max}/cm^{-1}): 3428,ν_{N-H},1631,$\nu_{C=Nimine.}$ UV−visible [CH$_3$OH, λ_{max}/nm (ε/M^{-1}cm^{-1})]: 400 (1,190), 325 (9,730), 247 (24,700), 213 (65,560). ^{1}H−NMR (CDCl$_3$, δ/ppm, 500 MHz): 3.251 (t, 2H), 3.318 (dd, 2H), 4.586 (s, 1H), 6.702 (d, J= 7.5, 1H), 7.198 (d, J= 7.5, 1H),7.267 (d, J= 7.5 Hz, 1H), 7.270-7.451 (m, 5H), 7.742 (d, J= 8.5, 1H), 7.799 (d, J= 8, 1H), 8.005 (d, J= 8, 1H), 8.345 (s, 1H),13.260 (s, 1H). ^{13}C−NMR (CDCl$_3$, δ/ppm, 500 MHz):44.41, 58.12, 104.7,117, 117.8, 118.73, 118.78, 119.82, 123.58, 124.97, 125.89,

126.54, 128.73, 131.53, 132.53, 134.42, 142.69, 161.09, 166.7. Anal. Calcd for $C_{18}H_{17}N_3$: C, 78.52; H, 6.22; N, 15.26, Found: C, 76.88; H, 6.46; N, 14.45.

7.5.3. UV−visible and fluorescence measurements

Stock solution of NED2 (1 mM) and chloride salt (10 mM) of metals Zn(II), Sn(II), Ni(II), Mn(II), Mg(II), Hg(II), Fe(II), Fe(III), Cu(II), Co(II), Cd(II), Ca(II) and Ba(II) were prepared in methanol for metal sensing. All fluorescence spectra of NED2 were recorded with the slit width 3/3. Fluorescence quantum yield (QY) was calculated by comparative method using 2−aminophenol solution in 0.1N H_2SO_4 as the standard.[628]

7.5.4. Determination of fluorescence quantum yield

As described in chapter 6.

7.5.5. Life time measurements

As described in chapter 6.

7.5.6. Determination of the binding stoichiometry and constants and Stern Volmer constant

As described in chapter 6.

7.5.7. Calculation of detection limit

As described in chapter 6.

7.5.8. Density functional theory (DFT) calculations

As described in chapter 6.
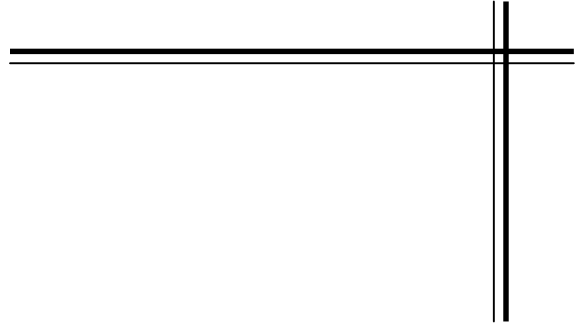
Summary
and
Conclusions

In the present study we have designed and synthesized novel ligands and characterized by various spectroscopic studies. Manganese and iron complexes derived from these novel ligands were synthesized and characterized. Electrochemical investigations were also performed on the designed metal complexes. Molecular structure of the representative complexes in the series were determined by X-ray crystallography. DFT and TD-DFT calculations were also performed to support the experimental data. Several activities were explored using synthesized ligands and complexes designed for the present work. Some of the ligands synthesized were utilized for the metal ion sensing due to their remarkable photophysical properties. These ligands were proved to be excellent sensor for iron sensing in aqueous as well as non☐aqueous media. Similarly designed metal complexes were also subjected for various studies such as interaction studies with the biomolecules, catalytic applications. Some manganese complexes exhibited superoxide scavenging activity (SOD activity) in xanthine/xanthine oxidase nitro blue tetrazolium (NBT) assay and these complexes found to be potent SOD mimic. Binding studies with the DNA showed good interaction with the manganese and iron complexes. These studies were further elaborated by monitoring nuclease activity for these complexes. Nuclease activity exhibited that complexes are capable to cleave in presence of oxidizing agent H_2O_2 and hence behaves as an artificial chemical nuclease. During the designing of the ligands we have designed some ligands with non☐innocent character. Therefore the complexes derived from these ligands were also utilized for catalytic as well as interaction studies with the biomolecules. Iron complexes derived from these ligands showed remarkable oxidation of o-aminophenol. Moreover representative complex from the series were subjected to the nuclease as well as protease activity in absence of any oxidizing or reducing agent and afforded these activities via self-activation. Similarly manganese complexes of these ligands were utilized to optimize the phenoxyl radical generation using UV-visible spectroscopy. The representative complex from the series also exhibited self-activated nuclease and protease.

Hence we synthesized and characterized ligands and several manganese as well as iron complexes and explored their application in several activity studies. We are trying to explore several other facets including in vivo biological activities, metal ion sensing and magnetic studies of the results obtained from the present study.
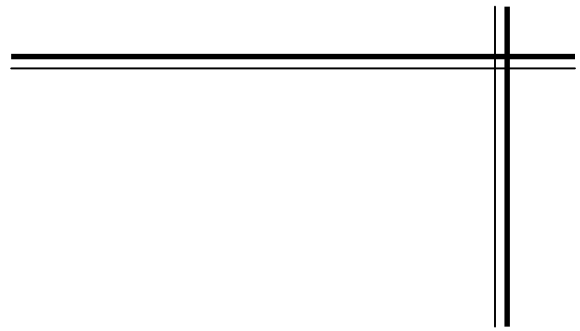
References

References

1. Cotton, F. A.; Wilkinson, G.; Murillo, C. A.; BochMann, M. "Advanced inorganic chemistry" 6th ed. Wiley, New York, **2003**.

2. Cowan, J. A.; "Inorganic biochemistry, an introduction" 6th ed. Wiley, New York, **1997**.

3. Bertini, I.; Gray, H. B.; Lippard, S. J.; Valentine, J. S. "Bioinorganic chemistry" South asia. ed. university science books, **1998**.

4. Da Silva, J. J. R. F.; Williams, R. J. P. "The inorganic chemistry of life" Oxford university press, **1993**.

5. Greenwood, N. N.; Earnshaw, A. "Chemistry of the elements" 2nd ed. Pergamon press, **1997**.

6. Huheey, J. E.; Keiter, E. A.; Keiter, R. L. "Inorganic chemistry,principles of structure and reactivity" 4th ed.; Harpercollins college publishers **1993**.

7. Malik, W. U.; Tuli, G. D.; Madan, R. D. "Selected topics in inorganic chemistry" S. chand and co. ltd, **2010**.

8. Sainna, M. A.; Sil, D.; Sahoo, D.; Martin, B.; Rath, S. P.; Comba, P.; de Visser, S. P. "Spin–state ordering in hydroxo–bridged diiron(III)bisporphyrin complexes" *Inorg. Chem.* **2015**, *54*, 1919.

9. Andreini, C.; Banci, L.; Bertini, I.; Rosato, A. "Zinc through the three domains of life" *J. Proteome Res.* **2006**, *5*, 3173.

10. Anastassopoulou, I.; Banci, L.; Bertini, I.; Cantini, F.; Katsari, E.; Rosato, A. "Solution structure of the apo and copper(I)–loaded human metallochaperone HAH1" *Biochemistry* **2004**, *43*, 13046.

11. Andreini, C.; Bertini, I.; Rosato, A. "Metalloproteomes: A bioinformatic approach"

Acc. Chem. Res. **2009**, *42*, 1471.

12. Faller, P. "Copper in alzheimer disease: Too much, too little, or misplaced?" *Free Radic. Biol. Med.* **2012**, *52*, 747.

13. Andreini, C.; Banci, L.; Bertini, I.; Rosato, A. "Counting the zinc–proteins encoded in the human genome" *J. Proteome Res.* **2006**, *5*, 196.

14. Miessler, G. L.; Tarr, D. A. "Inorganic chemistry" 3rd ed. prentice hall, **2000**.

15. Bal, W.; Sokołowska, M.; Kurowska, E.; Faller, P. "Binding of transition metal ions to albumin: Sites, affinities and rates" *Biochim. Biophys. Acta* **2013**, *1830*, 5444.

16. Mascharak, P. K. "Structural and functional models of nitrile hydratase" *Coord. Chem. Rev.* **2002**, *225*, 201.

17. Reedijk, J.; Bouwman, E. "Bioinorganic catalysis" 2nd ed. CRC Press, **1999**.

18. Shriver Atkins; T. Overton; Rourke, J.; Weller, M.; Armstrong, F.; .Hagerman, M. "Inorganic chemistry" 5th ed.; Oxford university press, **2009**.

19. Bertini, I.; Sigel, A.; Sigel, H. "Handbook on metalloproteins" Marcel Dekker Inc., **2001**.

20. Nelson, D. L.; Cox, M. M. "Principles of biochemistry" 4th ed., W.H. Freeman and company: New York, **2005**.

21. McCord, J. M.; Fridovich, I. "Superoxide dismutase: An enzymatic function for erythrocuprein" *J. Biol. Chem.* **1969**, *244*, 6049.

22. Khindaria, A.; Barr, D. P.; Aust, S. D. "Lignin peroxidases can also oxidize manganese" *Biochemistry* **1995**, *34*, 7773.

23. Que, L.; Widom, J.; Crawfordl, R. L. "3,4–dihydroxyphenylacetate 2,3–dioxygenase: A manganese(II) dioxygenase from *Bacillus brevis*" *J. Biol. Chem.* **1981**, *256*, 10941.

24. Wagner, T.; Shumilin, I. A; Bauerle, R.; Kretsinger, R. H "Structure of 3–deoxy–D–arabino–heptulosonate–7–phosphate synthase from *Escherichia coli*: Comparison of the Mn(II) 2–phosphoglycolate and the Pb(II) 2–phosphoenolpyruvate complexes and implications for catalysis" *J. Mol. Biol.* **2000**, *301*, 389.

25. Richard, S. B.; Ferrer, J. L.; Bowman, M. E.; Lillo, A. M.; Tetzlaff, C. N.; Cane, D. E.; Noel, J. P "Structure and mechanism of 2–c–methyl–d–erythritol 2,4–cyclodiphosphate synthase: An enzyme in the mevalonate–independent isoprenoid biosynthetic pathway" *J. Biol. Chem.* **2002**, *277*, 8667.

26. Harutyunyan, E. H.; Oganessyan, V. Y.; Oganessyan, N. N.; Avaeva, S. M.; Nazarova, T. I.; Vorobyeva, N. N.; Kurilova, S.A; Huber, R.; Mather, T "Crystal structure of holo inorganic pyrophosphatase from *Escherichia coli* at 1.9 A resolution. Mechanism of hydrolysis" *Biochemistry* **1997**, *36*, 7754.

27. Durbecq, V.; Sainz, G.; Oudjama, Y.; Clantin, B.; Bompard–Gilles, C.; Tricot, C.; Caillet, J.; Stalon, V.; Droogmans, L.; Villeret, V. "Crystal structure of isopentenyl diphosphate: Dimethylallyl diphosphate isomerase" *EMBO J.* **2001**, *20*, 1530.

28. Su, C.; Oliw, E. H. "Manganese lipoxygenase: Purification and characterization" *J. Biol. Chem.* **1998**, *273*, 13072.

29. Requena, L.; Bornemann, S "Barley (hordeum vulgare) oxalate oxidase is a manganese–containing enzyme" *Biochem. J.* **1999**, *343*, 185.

30. Woo, E. J.; Dunwell, J. M.; Goodenough, P. W.; Marvier, A. C.; Pickersgill, R. W "Germin is a manganese containing homohexamer with oxalate oxidase and superoxide dismutase activities" *Nat. Struct. Biol.* **2000**, *7*, 1036.

31. Tanner, A.; Bowater, L.; Fairhurst, S. A.; Bornemann, S "Oxalate decarboxylase

requires manganese and dioxygen for activity: Overexpression and characterization of *Bacillus* subtilis YvrK and YoaN" *J. Biol. Chem.* **2001**, *276*, 43627.

32. Dismukes, G. C "Manganese enzymes with binuclear active sites" *Chem. Rev.* **1996**, *96*, 2909.

33. Viator, R. J.; Rest, R. F.; Hildebrandt, E.; McGee, D. J "Characterization of *Bacillus anthracis* arginase: Effects of pH, temperature, and cell viability on metal preference" *BMC Biochem.* **2008**, *9*, 14.

34. Barynin, V. V.; Whittaker, M. M.; Antonyuk, S. V.; Lamzin, V. S.; Harrison, P. M.; Artymiuk, P. J.; Whittaker, J. W "Crystal structure of manganese catalase from *Lactobacillus plantarum*" *Structure* **2001**, *9*, 725.

35. Gonzales, T.; Robert–baudouy, J "Bacterial aminopeptidases: Properties and functions" *FEMS Microbiol. Rev.* **1996**, *18*, 319.

36. Seemann, J. E.; Schulz, G. E. "Structure and mechanism of l–fucose isomerase from *Escherichia coli*" *J. Mol. Biol.* **1997**, 256.

37. Focia, P. J.; Craig, S. P.; Eakin, A. E "Approaching the transition state in the crystal structure of a phosphoribosyltransferase" *Biochemistry* **1998**, *37*, 17120.

38. Gill, H. S.; Eisenberg, D. "The crystal structure of phosphinothricin in the active site of glutamine synthetase illuminates the mechanism of enzymatic inhibition" *Biochemistry* **2001**, *40*, 1903.

39. Jedrzejas, M. J.; Chander, M.; Setlow, P.; Krishnasamy, G "Mechanism of catalysis of the cofactor–independent phosphoglycerate mutase from *Bacillus stearothermophilus*: Crystal structure of the complex with 2–phosphoglycerate" *J. Biol. Chem.* **2000**, *275*, 23146.

References

40. Kok, B.; Forbush, B.; Mcgloin, M. "Cooperation of charges in photosynthetic oxygen evolution: A linear four step mechanism" *Photochem. Photobiol.* **1970**, *11*, 457.

41. Chowdhury, A. D.; Ray, R.; Lahiri, G. K "An iron catalyzed regioselective oxidation of terminal alkenes to aldehydes" *Chem. Commun.* **2012**, *48*, 5497.

42. Chowdhury, A. D; Lahiri, G.K "A generalized approach for iron catalyzed chemo– and regioselective formation of anti–markovnikov acetals from styrene derivatives" *Chem. Commun.* **2012**, *48*, 3448.

43. Jaafar, H.; Vileno, B.; Thibon, A.; Mandon, D "tuning the conversion of cyclohexane into cyclohexanol/one by molecular dioxygen, protons and reducing agents at a single non–porphyrinic iron centre and chemical versatility of the tris(2–pyridylmethyl)amine TPAFe(II)Cl$_2$ complex in mild oxidation chemist" *Dalton. Trans.* **2011**, *40*, 92.

44. Bousejra–ElGarah, F.; Bijani, C.; Coppel, Y.; Faller, P.; Hureau, C "Iron(II) binding to amyloid–β, the alzheimer's peptide" *Inorg. Chem.* **2011**, *50*, 9024.

45. Banci, L.; Bertini, I.; Gray, H. B.; Luchinat, C.; Reddig, T.; Rosato, A; Turano, P "Solution structure of oxidized horse heart cytochrome c" *Biochemistry* **1997**, *36*, 9867.

46. Arnesano, F.; Banci, L.; Bertini, I.; Faraone–Mennella, J.; Rosato, A.; Barker, P. D.; Fersht, A. R "The solution structure of oxidized *Escherichia coli* cytochrome b562" *Biochemistry* **1999**, *38*, 8657.

47. Sahoo, D.; Quesne, M. G.; de Visser, S. P.; Rath, S. P "Hydrogen–bonding interactions trigger a spin–flip in iron(III) porphyrin complexes" *Angew. Chem. Int. Ed.* **2015**, *54*, 4796.

48. Bertini, I.; Cavallaro, G.; Rosato, A. "Principles and patterns in the interaction between mono–heme cytochrome c and its partners in electron transfer processes" *Metallomics*

2011, *3*, 354.

49. Bertini, I.; Cavallaro, G.; Rosato, A "Cytochrome c: Occurrence and functions" *Chem. Rev.* **2006**, *106*, 90.

50. Sil, D.; Tuglak Khan, F. S.; Rath, S. P "Axial thiophenolate coordination on diiron(III) bisporphyrin: Influence of heme–heme interactions on structure, function and electrochemical properties of the individual heme center" *Inorg. Chem.* **2014**, *53*, 11936.

51. Paine, T. K.; Sheet, D.; Weyhermüller, T.; Chaudhuri, P "Iron(II)–mediated reductive cleavage of disulfide and diselenide bonds: Iron(III) complexes of mixed O,X,O and O,X (X = S, Se) donor ligands" *Eur. J. Inorg. Chem.* **2011**, *34*, 5250.

52. Bhowmik, S.; Ghosh, S. K.; Rath, S. P. "Control of spins by ring deformation in a diiron(III)bisporphyrin: Reversal of ClO_4^- and $CF_3SO_3^-$ ligand field strength in the magnetochemical series" *Chem. Commun.* **2011**, *47*, 4790.

53. Ghosh, S. K.; Rath, S. P "A remarkably bent diiron(III)–μ–hydroxo bisporphyrin: Unusual stabilization of two spin states of iron in a single molecular framework" *J. Am. Chem. Soc.* **2010**, *132*, 17983.

54. Hool, L. C "Reactive oxygen species in cardiac signalling: From mitochondria to plasma membrane ion channels" *Proc. Aust. Physiol. Soc.* **2005**, *36*, 55.

55. Chandran, K.; McCracken, J.; Peterson, F. C.; Antholine, W. E.; Volkman, B. F.; Kalyanaraman, B "Oxidation of histidine residues in copper–zinc superoxide dismutase by bicarbonate–stimulated peroxidase and thiol oxidase activities: Pulse EPR and NMR Studies" *Biochemistry* **2010**, *49*, 10616.

56. Mattson, M.; Mark, R.; Furukawa, K.; Bruce, A. J " Disruption of brain cell ion

homeostasis in alzheimer's disease by oxy radicals, and signaling pathways that protect therefrom" *Chem. Res. Toxicol.* **1997**, *10*, 507.

57. Parkin, G "The bioinorganic chemistry of zinc: Synthetic analogues of zinc enzymes that feature tripodal ligands" *Chem. Commun.* **2000**, 1971.

58. Sheng, Y.; Abreu, I. A.; Cabelli, D. E.; Maroney, M. J.; Miller, A. F.; Teixeira, M.; Valentine, J. S "Superoxide dismutases and superoxide reductases" *Chem. Rev.* **2014**, *114*, 3854.

59. McCord, J. M.; Fridovich, I "Superoxide dismutase: The first twenty years (1968–1988)" *Free Radic. Biol. Med.* **1988**, *5*, 363.

60. Amatore, C.; Arbault, S.; Guille, M.; Lemaître, F. "Electrochemical monitoring of single cell secretion: Vesicular exocytosis and oxidative stress" *Chem. Rev.* **2008**, *108*, 2585.

61. Barondeau, D. P.; Kassmann, C. J.; Bruns, C. K.; Tainer, J. A.; Getzoff, E. D "Nickel superoxide dismutase structure and mechanism" *Biochemistry* **2004**, *43*, 8038.

62. Pecoraro, V. L.; Baldwin, M. J.; Gelasco, A " Interaction of manganese with dioxygen and its reduced derivatives" *Chem. Rev.* **1994**, *94*, 807.

63. Dupont, C. L.; Neupane, K.; Shearer, J.; Palenik, B "Diversity, function and evolution of genes coding for putative Ni–containing superoxide dismutases" *Environ. Microbiol.* **2008**, *10*, 1831.

64. Wolfe–Simon, F.; Grzebyk, D.; Schofield, O.; Falkowski, P. G "The role and evolution of superoxide dismutases in algae" *J. Phycol.* **2005**, *41*, 453.

65. May, B. P.; Dennis, P. P "Superoxide dismutase from the extremely halophilic archaebacterium halobacterium cutirubrum" *J. Bacteriol.* **1987**, *169*, 1417.

66. Knapp, S.; Kardinahl, S.; Hellgren, N.; Tibbelin, G.; Schäfer, G.; Ladenstein, R "Refined crystal structure of a superoxide dismutase from the hyperthermophilic archaeon sulfolobus acidocaldarius at 2.2 Å resolution" *J. Mol. Biol.* **1999**, *285*, 689.

67. Fridovich, I. "Superoxide dismutases" *Annu. Rev. Biochem.* **1975**, *44*, 147.

68. Valentine, J. S.; Doucette, P. A.; Zittin Potter, S "Copper–zinc superoxide dismutase and amyotrophic lateral sclerosis" *Annu. Rev. Biochem.* **2005**, *74*, 563.

69. Lah, M. S.; Dixon, M. M.; Pattridge, K. a; Stallings, W. C.; Fee, J. a; Ludwig, M. L "Structure–function in *Escherichia coli* iron superoxide dismutase: Comparisons with the manganese enzyme from *Thermus thermophilus*" *Biochemistry* **1995**, *34*, 1646.

70. Holm, R. H.; Kennepohl, P.; Solomon, E. I. "Structural and functional aspects of metal sites in biology" *Chem. Rev.* **1996**, *96*, 2239.

71. Hunter, T.; Ikebukuro, K.; Bannister, W. H.; Bannister, J. V.; Hunter, G. J. "The conserved residue tyrosine 34 is essential for maximal activity of iron–superoxide dismutase from *Escherichia coli*" *Biochemistry* **1997**, *36*, 4925.

72. Ludwig, M. L.; Metzger, A. L.; Pattridge, K. A.; Stallings, W. C "Manganese superoxide dismutase from *Thermus thermophilus*: A structural model refined at 1.8 Å resolution" *J. Mol. Biol.* **1991**, *219*, 335.

73. Whittaker, M. M.; Whittaker, J. W. "Mutagenesis of a proton linkage pathway in *Escherichia coli* manganese superoxide dismutase" *Biochemistry* **1997**, *36*, 8923.

74. Klivenyi, P.; St Clair, D.; Wermer, M.; Yen, H. C.; Oberley, T.; Yang, L.; Flint Beal, M "Manganese superoxide dismutase overexpression attenuates MPTP toxicity" *Neurobiol. Dis.* **1998**, *5*, 253.

75. Dees, A.; Zahl, A.; Puchta, R.; Hommes, N. J. R. V. E.; Heinemann, F. W.; Ivanović–

Burmazović, I. "Water exchange on seven–coordinate Mn(II) complexes with macrocyclic pentadentate ligands: Insight in the mechanism of Mn(II) SOD mimetics" *Inorg. Chem.* **2007**, *46*, 2459.

76. Friedel, F. C.; Lieb, D.; Ivanović–Burmazović, I "Comparative studies on manganese–based SOD mimetics, including the phosphate effect, by using global spectral analysis" *J. Inorg. Biochem.* **2012**, *109*, 26.

77. Kose, M.; Goring, P.; Lucas, P.; Mckee, V "Mono–, di– and tri–nuclear manganese(II) complexes derived from a quinquedentate ligand: Superoxide dismutase and catalase mimetic studies" *Inorg. Chim. Acta* **2015**, *435*, 232.

78. Ledesma, G. N.; Eury, H.; Anxolabéhère–Mallart, E.; Hureau, C.; Signorella, S. R "A new mononuclear manganese(III) complex of an unsymmetrical hexadentate N_3O_3 ligand exhibiting superoxide dismutase and catalase–like activity: Synthesis, characterization, properties and kinetics studies" *J. Inorg. Biochem.* **2015**, *146*, 69.

79. Clares, M. P.; Serena, C.; Blasco, S.; Nebot, A.; Soriano, C.; Domènech, A.; Sánchez–sánchez, A. V.; Soler–calero, L.; Luis, J.; García–españa, A.; García–españa, E "Mn (II) complexes of scorpiand–like ligands . A model for the MnSOD active centre with high *in vitro* and *in vivo* activity" *J. Inorg. Biochem.* **2015**, *143*, 1.

80. Wu, H.; Shi, F.; Wang, X.; Zhang, Y.; Bai, Y.; Kong, J.; Wang, C "Synthesis, crystal structures, antioxidant activities and DNA–binding studies of two manganese(II) complexes with 1,3–bis(1–ethylbenzimidazol–2–yl)–2–oxopropane ligands" *Trans. Met. Chem.* **2014**, *39*, 261.

81. Kovala–Demertzi, D.; Staninska, M.; Garcia–Santos, I.; Castineiras, A.; Demertzis, M. A "Synthesis, crystal structures and spectroscopy of meclofenamic acid and its metal

complexes with manganese(II), copper(II), zinc(II) and cadmium(II). Antiproliferative and superoxide dismutase activity" *J. Inorg. Biochem.* **2011**, *105*, 1187.

82. Lupidi, G.; Marchetti, F.; Masciocchi, N.; Reger, D. L.; Tabassum, S.; Astolfi, P.; Damiani, E.; Pettinari, C "Synthesis, structural and spectroscopic characterization and biomimetic properties of new copper, manganese, zinc complexes: identification of possible superoxide–dismutase mimics bearing hydroxyl radical generating/scavenging abilities" *J. Inorg. Biochem.* **2010**, *104*, 820.

83. Lieb, D.; Friedel, F. C.; Yawer, M.; Zahl, A.; Khusniyarov, M. M.; Heinemann, F. W.; Ivanović–Burmazović, I "Dinuclear seven–coordinate Mn(II) complexes: Effect of manganese(II)–hydroxo species on water exchange and superoxide dismutase activity" *Inorg. Chem.* **2013**, *52*, 222.

84. Iranzo, O "Manganese complexes displaying superoxide dismutase activity: A balance between different factors" *Bioorg. Chem.* **2011**, *39*, 73.

85. Pursche, D.; Triller, M. .; Slinn, C.; Reddig, N.; Rompel, A.; Krebs, B "Mimicking the reduced, oxidized and azide inhibited form of manganese superoxide dismutase by mononuclear Mn compounds utilizing tridentate ligands" *Inorg. Chim. Acta* **2004**, *357*, 1695.

86. Lin, J.; Tu, C.; Lin, H.; Jiang, P.; Ding, J.; Guo, Z "Crystal structure and superoxide dismutase activity of a six–coordinate manganese (III) complex" *Inorg. Chem. Commun.* **2003**, *6*, 262.

87. Cisnetti, F.; Pelosi, G.; Policar, C "Synthesis and superoxide dismutase–like activity of new manganese(III) complexes based on tridentate N_2O ligands derived from histamine" *Inorg. Chim. Acta* **2007**, *360*, 557.

88. Durot, S.; Policar, C.; Cisnetti, F.; Lambert, F.; Renault, J. P.; Pelosi, G.; Blain, G.; Korri–Youssoufi, H.; Mahy, J. P "Series of Mn complexes based on N–centered ligands and superoxide–reactivity in an anhydrous medium and SOD–like Activity in an aqueous medium correlated to Mn^{II}/Mn^{III} redox potentials" *Eur. J. Inorg. Chem.* **2005**, 3513.

89. Policar, C.; Durot, S.; Lambert, F.; Cesario, M.; Ramiandrasoa, F.; Morgenstern–Badarau, I "New Mn^{II} complexes with an N/O coordination sphere from tripodal N – centered ligands: Characterization from solid state to solution and reaction with superoxide in non–aqueous and aqueous media" *Eur. J. Inorg. Chem.* **2001**, 1807.

90. Liao, Z. R.; Zheng, X. F.; Luo, B.S.; Shen, L.R.; Li, D.F.; Liu, H.L.; Zhao, W "Synthesis, characterization and SOD–like activities of manganese–containing complexes with N,N,N′,N′–tetrakis(2′–benzimidazolyl methyl)–1,2–ethanediamine (EDTB)" *Polyhedron* **2001**, *20*, 2813.

91. Doctrow, S. R.; Huffman, K.; Marcus, C. B.; Tocco, G.; Malfroy, E.; Adinolfi, C. A.; Kruk, H.; Baker, K.; Lazarowych, N.; Mascarenhas, J.; Malfroy, B "Salen–manganese complexes as catalytic scavengers of hydrogen peroxide and cytoprotective agents: Structure–activity relationship studies" *J. Med. Chem.* **2002**, *45*, 4549.

92. Bruce, A.; Malfroy, B.; Baudry, M "β–Amyloid toxicity in organotypic hippocampal cultures: Protection by EUK–8, a synthetic catalytic free radical scavenger" *Proc. Natl. Acad. Sci.* **1996**, *93*, 2312.

93. Riley, D. P.; Weiss, R. H "Manganese macrocyclic ligand complexes as mimics of superoxide dismutase" *J. Am. Chem. SOC* **1994**, *116*, 387.

94. Rong, Y.; Doctrow, S. R.; Tocco, G.; Baudry, M "EUK–134, a synthetic superoxide

dismutase and catalase mimetic, prevents oxidative stress and attenuates kainate–induced neuropathology" *Proc. Natl. Acad. Sci.* **1999**, *96*, 9897.

95. Pierre, G.; Alain, S.; Xavier, B.; Rene, P.; Dominique, M.; Saiji, H.; Bernad, M. "A synthetic superoxide dismutase and catalase mimetic, protects rat kidneys from ischemia-reperfusion-induced damage" *Transplantation* **1996**, *62*, 1664.

96. Riley, D. P "Functional mimics of superoxide dismutase enzymes as therapeutic agents" *Chem. Rev.* **1999**, *99*, 2573.

97. Hitomi, Y.; Iwamoto, Y.; Kashida, A.; Kodera, M "Mononuclear nonheme iron (III) complexes that show superoxide dismutase–like activity and antioxidant effects against menadione–mediated oxidative stress" *Chem. Commun.* **2015**, *51*, 8702.

98. Kripli, B.; Baráth, G.; Balogh–Hergovich, É.; Giorgi, M.; Simaan, A. J.; Párkányi, L.; Pap, J. S.; Kaizer, J.; Speier, G "Correlation between the SOD–like activity of hexacoordinate iron(II) complexes and their Fe(III) and Fe(II) redox potentials" *Inorg. Chem. Commun.* **2011**, *14*, 205.

99. Liu, G. F.; Filipović, M.; Heinemann, F. W.; Ivanović–Burmazović, I "Seven–coordinate iron and manganese complexes with acyclic and rigid pentadentate chelates and their superoxide dismutase activity" *Inorg. Chem.* **2007**, *46*, 8825.

100. Horn, A.; Parrilha, G. L.; Melo, K. V.; Fernandes, C.; Horner, M.; Visentin, L. D. C.; Santos, J. A. S.; Santos, M. S.; Eleutherio, E. C. A; Pereira, M. D "An iron–based cytosolic catalase and superoxide dismutase mimic complex" *Inorg. Chem.* **2010**, *49*, 1274.

101. Moon, D.; Kim, J.; Lah, M "Synthesis and characterization of mononuclear octahedral Fe(III) complex containing a biomimetic tripodal ligand, N–(benzimidazol–

2–ylmethyl) iminodiacetic acid" *Bull. Chem.* **2006**, *27*, 1597.

102. Tamura, M.; Urano, Y.; Kikuchi, K.; Higuchi, T.; Hirobe, M.; Nagano, T "Synthesis and superoxide dismutase activity of novel iron complexes" *J. Organomet. Chem.* **2000**, *611*, 586.

103. Irano, T. H.; Irobe, M. H.; Obayashi, K. K.; Dani, A. O.; Amauchi, O. Y.; Hsawa, M. O.; Atow, Y. S.; Agano, T. N "Mechanism of superoxide dismutase–like activity of Fe (II) and Fe(III) complexes of tetrakis– N,N,N´,N´(2–pyridylmethyl) ethylenediamine" *Chem. Pharm. Bull.* **2000**, *48*, 223.

104. Batinić–Haberle, I.; Spasojevic, I.; Hambright, P.; Benov, L.; Crumbliss, A. L.; Fridovich, I "Relationship among redox potentials, proton dissociation constants of pyrrolic nitrogens, and *in vivo* and *in vitro* superoxide dismutating activities of manganese(III) and iron(III) water–soluble porphyrins" *Inorg. Chem.* **1999**, *38*, 4011.

105. Asayama, S.; Kasugai, N.; Kubota, S.; Nagaoka, S.; Kawakami, H "Superoxide dismutase as a target enzyme for Fe–porphyrin–induced cell death" *J. Inorg. Biochem.* **2007**, *101*, 261.

106. Daier, V. A.; Palopoli, C. M.; Hureau, C.; De Candia, A.; Signorella, S. R "Properties and antioxidant activity of water–soluble iron catalysts with schiff base ligands. Comparison with their manganese counterparts" *Arkivoc* **2011**, 327.

107. Paria, S.; Que, L.; Paine, T. K "Oxidative decarboxylation of benzilic acid by a biomimetic iron(II) complex: Evidence for an iron(IV)–oxo–hydroxo oxidant from O_2" *Angew. Chem. Int. Ed.* **2011**, *50*, 11129.

108. Sheet, D.; Halder, P.; Paine, T. K "Enhanced reactivity of a biomimetic iron(II) α–keto acid complex through immobilization on functionalized gold nanoparticles.

Angew. Chem. Int. Ed. **2013**, *52*, 13314.

109. Sheet, D.; Bhattacharya, S.; Paine, T. K "Dioxygen activation and two consecutive oxidative decarboxylations of phenylpyruvate by nonheme iron(II) complexes: Functional models of hydroxymandelate synthase (HMS) and CloR" *Chem. Commun.* **2015**, *51*, 7681.

110. Simandi, T. M.; Simandi, L. I.; Gyor, M.; Rockenbauer, A.; Gomory, A "Kinetics and mechanism of the ferroxime(II)–catalysed biomimetic oxidation of 2–aminophenol by dioxygen. A functional phenoxazinone synthase model" *Dalton Trans.* **2004**, *7*, 1056.

111. Halder, P.; Paine, T. K "Rearrangement of the tris(2–pyridylthio)methanido ligand in an iron(II) complex containing an Fe–C bond" *Inorg. Chem.* **2011**, *50*, 708.

112. Das, O.; Chatterjee, S.; Paine, T. K "Functional models of α–keto acid dependent nonheme iron oxygenases: Synthesis and reactivity of biomimetic iron(II) benzoylformate complexes supported by a 2,9–dimethyl–1,10–phenanthroline ligand" *J. Biol. Inorg. Chem.* **2013**, *18*, 401.

113. Mandon, D.; Jaafar, H.; Thibon, A "Exploring the oxygen sensitivity of $FeCl_2$ complexes with tris(2–pyridylmethyl)amine–type ligands: O_2 coordination and a quest for superoxide" *New J. Chem.* **2011**, *35*, 1986.

114. Chatterjee, S.; Paine, T. K. "Olefin cis–dihydroxylation and aliphatic C–H bond oxygenation by a dioxygen–derived electrophilic iron–oxygen oxidant" *Angew. Chem. Int. Ed.* **2015**, 1.

115. Bugg, T. D. H " Dioxygenase enzymes: Catalytic mechanisms and chemical models" *Tetrahedron* **2003**, *59*, 7075.

References

116. Chatterjee, S.; Sheet, D.; Paine, T. K. "Catalytic and regiospecific extradiol cleavage of catechol by a biomimetic iron complex" *Chem. Commun.* **2013**, *49*, 10251.

117. Vetting, M. W.; Ohlendorf, D. H "The 1.8 Å crystal structure of catechol 1,2–dioxygenase reveals a novel hydrophobic helical zipper as a subunit linker" *Structure* **2000**, *8*, 429.

118. Han, S.; Eltis, L. D.; Timmis, K. N.; Muchmore, S. W.; Bolin, J. T "Crystal structure of the biphenyl–cleaving extradiol dioxygenase from a PCB–degrading pseudomona" *Science.* **1995**, *270*, 976.

119. Kita, A.; Kita, S. I.; Fujisawa, I.; Inaka, K.; Ishida, T.; Horiike, K.; Nozaki, M.; Miki, K "An archetypical extradiol–cleaving catecholic dioxygenase: The crystal structure of catechol 2,3–dioxygenase (metapyrocatechase) from *Pseudomonas putida* mt–2" *Structure* **1999**, *7*, 25.

120. Sugimoto, K.; Senda, T.; Aoshima, H.; Masai, E.; Fukuda, M.; Mitsui, Y "Crystal structure of an aromatic ring opening dioxygenase LigAB, a protocatechuate 4,5–dioxygenase, under aerobic conditions" *Structure* **1999**, *7*, 953.

121. Brivio, M.; Schlosrich, J.; Ahmad, M.; Tolond, C.; Bugg, T. D. H "Investigation of acid–base catalysis in the extradiol and intradiol catechol dioxygenase reactions using a broad specificity mutant enzyme and model chemistry" *Org. Biomol. Chem.* **2009**, *7*, 1368.

122. Bugg, T. D.; Ramaswamy, S "Non–heme iron–dependent dioxygenases: Unravelling catalytic mechanisms for complex enzymatic oxidations" *Curr. Opin. Chem. Biol.* **2008**, *12*, 134.

123. Whiting, A. K.; Boldt, Y. R.; Hendrich, M. P.; Wackett, L. P.; Que, L

"Manganese(II)– dependent extradiol–cleaving catechol dioxygenase from *Arthrobacter globiformis* CM–2" *Biochemistry* **1996**, *35*, 160.

124. Reddig, N.; Pursche, D.; Krebs, B.; Rompel, A "Mononuclear manganese(III) catechol compounds as substrate adduct complexes for manganese–substituted intradiol cleaving catechol dioxygenases" *Inorg. Chim. Acta* **2004**, *357*, 2703.

125. Lin, G.; Reid, G.; Bugg, T. D. H "Extradiol oxidative cleavage of catechols by ferrous and ferric complexes of 1,4,7–triazacyclononane: Insight into the mechanism of the extradiol catechol dioxygenases" *J. Am. Chem. Soc.* **2001**, *123*, 5030.

126. Eley, K. L.; Crowley, P. J.; Bugg, T. D "A solvolytic C–C cleavage reaction of 6–acetoxycyclohexa–2,4–dienones: Mechanistic implications for the intradiol catechol dioxygenases" *J. Org. Chem.* **2001**, *66*, 2091.

127. Xin, M.; Bugg, T. D. H "Evidence from mechanistic probes for distinct hydroperoxide rearrangement mechanisms in the intradiol and extradiol catechol dioxygenases" *J. Am. Chem. Soc.* **2008**, *130*, 10422.

128. Spence, E. L.; Langley, G. J.; Bugg, T. D. H "Cis–trans isomerization of a cyclopropyl radical trap catalyzed by extradiol catechol dioxygenases: Evidence for a semiquinone intermediate" *J. Am. Chem. Soc.* **1996**, *118*, 8336.

129. Sanvoisin, J.; Langley, G. J.; Bugg, T. D. H "Mechanism of extradiol catechol dioxygenases: Evidence for a lactone intermediate in the 2,3–dihydroxyphenylpropionate 1,2–dioxygenase reaction" *J. Am. Chem. Soc.* **1995**, *117*, 7836.

130. Cox, D. D.; Que Jr., L "Functional models for catechol 1, 2–dioxygenase. The role of the iron (III) center" *J. Am. Chem. Soc.* **1988**, *110*, 8085.

131.   Jang, H. G.; Cox, D. D.; Que, L "A highly reactive functional–model for the catechol dioxygenases–structure and properties of [Fe(TPA)DBC] BPh$_4$" *J. Am. Chem. Soc.* **1991**, *113*, 9200.

132.   Jo, D. H.; Chiou, Y. M.; Que, J "Models for extradiol cleaving catechol dioxygenases: Syntheses, structures, and reactivities of iron(II)–monoanionic catecholate complexes" *Inorg. Chem.* **2001**, *40*, 3181.

133.   Costas, M.; Mehn, M. P.; Jensen, M. P.; Que, L "Dioxygen activation at mononuclear nonheme iron active sites: Enzymes, models, and intermediates" *Chem. Rev.* **2004**, *104*, 939.

134.   Sundaravel, K.; Suresh, E.; Palaniandavar, M "Iron(III) complexes of tridentate N$_3$ ligands as models for catechol dioxygenases: Stereoelectronic effects of pyrazole coordination" *Inorg. Chim. Acta* **2010**, *363*, 2768.

135.   Visvaganesan, K.; Ramachitra, S.; Palaniandavar, M "Functional models for enzyme–substrate adducts of catechol dioxygenase enzymes: The lewis basicity of facially coordinating tridentate phenolate ligands tunes the rate of dioxygenation and product selectivity" *Inorg. Chim. Acta* **2011**, *378*, 87.

136.   Mayilmurugan, R.; Visvaganesan, K.; Suresh, E.; Palaniandavar, M "Iron(III) complexes of tripodal monophenolate ligands as models for non–heme catechol dioxygenase enzymes: Correlation of dioxygenase activity with ligand stereoelectronic properties" *Inorg. Chem.* **2009**, *48*, 8771.

137.   Mayilmurugan, R.; Suresh, E.; Palaniandavar, M "A new tripodal iron(III) monophenolate complex: Effects of ligand basicity, steric hindrance, and solvent on regioselective extradiol cleavage" *Inorg. Chem.* **2007**, *46*, 6038.

138. Velusamy, M.; Mayilmurugan, R.; Palaniandavar, M "Iron(III) complexes of sterically hindered tetradentate monophenolate ligands as functional models for catechol 1,2–dioxygenases: The role of ligand stereoelectronic properties" *Inorg. Chem.* **2004**, *43*, 6284.

139. Mayilmurugan, R.; Stoeckli Evans, H.; Palaniandavar, M "Novel iron(III) complexes of sterically hindered 4N ligands: Regioselectivity in biomimetic extradiol cleavage of catechols" *Inorg. Chem.* **2008**, *47*, 6645.

140. Visvaganesan, K.; Mayilmurugan, R.; Suresh, E.; Palaniandavar, M "Iron(III) complexes of tridentate 3N ligands as functional models for catechol dioxygenases: The role of ligand N–alkyl substitution and solvent on reaction rate and product selectivity" *Inorg. Chem.* **2007**, *46*, 10294.

141. Sundaravel, K.; Suresh, E.; Saminathan, K.; Palaniandavar, M "Iron(III) complexes of N_2O and N_3O donor ligands as functional models for catechol dioxygenase enzymes: Ether oxygen coordination tunes the regioselectivity and reactivity" *Dalton Trans.* **2011**, *40*, 8092.

142. Sankaralingam, M.; Saravanan, N.; Anitha, N.; Suresh, E.; Palaniandavar, M "Biomimetic iron(III) complexes of facially and meridionally coordinating tridentate 3N ligands: Tuning of regioselective extradiol dioxygenase activity in organized assemblies" *Dalton Trans.* **2014**, *43*, 6828.

143. Balamurugan, M.; Vadivelu, P.; Palaniandavar, M. "Iron(III) complexes of tripodal tetradentate 4N ligands as functional models for catechol dioxygenases: The electronic *vs.* steric effect on extradiol cleavage" *Dalton Trans.* **2014**, *43*, 14653.

144. Dhanalakshmi, T.; Bhuvaneshwari, M.; Palaniandavar, M "Iron(III) complexes of

certain meridionally coordinating tridentate ligands as models for non–heme iron enzymes: The role of carboxylate coordination" *J. Inorg. Biochem.* **2006**, *100*, 1527.

145. Palaniandavar, M.; Visvaganesan, K "Mononuclear non–heme iron(III) complexes of linear and tripodal tridentate ligands as functional models for catechol dioxygenases: Effect of N–alkyl substitution on regioselectivity and reaction rate" *J. Chem. Sci.* **2011**, *123*, 145.

146. Paria, S.; Halder, P.; Paine, T. K "A functional model of extradiol–cleaving catechol dioxygenases: Mimicking the 2–his–1–carboxylate facial triad" *Inorg. Chem.* **2010**, *49*, 4518.

147. Mitra, K.; Patil, S.; Kondaiah, P.; Chakravarty, A. R "2–(phenylazo)pyridineplatinum(II) catecholates showing photocytotoxicity, nuclear uptake, and glutathione–triggered ligand release" *Inorg. Chem.* **2015**, *54*, 253.

148. Das, O.; Chatterjee, S.; Paine, T. K "Iron and cobalt complexes of 4,4,9,9–tetramethyl–5,8–diazadodecane–2, 11–dione dioxime ligand : Synthesis , characterization and reactivity studies" *J. Chem. Sci.* **2011**, *123*, 839.

149. Lipscomb, J. D.; Orville, A. M. "Metal Ions in Biological Systems" Dekker, **1992**.

150. Lendenmann, U.; Spain, J. C "2–aminophenol 1, 6–dioxygenase: A novel aromatic ring cleavage enzyme purified from *Pseudomonas pseudoalcaligenes* JS45" *J. Bacteriol.* **1996**, 6227.

151. Nishino, S. F.; Spain, J. C "Degradation of nitrobenzene by a *Pseudomonas–pseudoalcaligenes*" *Appl. Environ. Microbiol.* **1993**, *59*, 2520.

152. Bittner, M. M.; Lindeman, S. V; Fiedler, A. T. A "synthetic model of the putative Fe(II)–iminobenzosemiquinonate intermediate in the catalytic cycle of *o*–aminophenol

dioxygenases" *J. Am. Chem. Soc.* **2012**, *134*, 5460.

153. Chakraborty, B.; Paine, T. K. "Aromatic ring cleavage of 2–amino–4–*tert*–butylphenol by a nonheme iron(II) complex: Functional model of 2–aminophenol dioxygenases" *Angew. Chem. Int. Ed.* **2013**, *52*, 920.

154. Chakraborty, B.; Bhunya, S.; Paul, A.; Paine, T. K "Reactivity of biomimetic iron(II)–2–aminophenolate complexes toward dioxygen: Mechanistic investigations on the oxidative C–C bond cleavage of substituted 2–aminophenols" *Inorg. Chem.* **2014**, *53*, 4899.

155. Banerjee, S.; Halder, P.; Paine, T. K "Probing the reactivity of redox–active 2–aminophenolates on iron complexes of a carbanionic N$_3$C donor ligand" *Z. Anorg. Allg. Chem.* **2014**, *640*, 1168.

156. Chatterjee, S.; Paine, T. K "Oxygenative aromatic ring cleavage of 2–aminophenol with dioxygen catalyzed by a nonheme iron complex: Catalytic functional model of 2–aminophenol dioxygenases" *Inorg. Chem.* **2015**, *54*, 1720.

157. Freeman, J. C.; Nayar, P. G.; Begley, T. P.; Villafranca, J. J "Stoichiometry and spectroscopic identity of copper centers in phenoxazinone synthase: A new addition to the blue copper oxidase family" *Biochemistry* **1993**, *32*, 4826.

158. Barry, C. E.; Nayar, P. G.; Begley, T. P. "Phenoxazinone synthase: Mechanism for the formation of the phenoxazinone chromophore of actinomycin"*Biochemistry* **1989**, *28*, 6323.

159. Simándi, L. I.; Barna, T.; Németh, S "Kinetics and mechanism of the cobaloxime(II)–catalysed oxidation of 2–aminophenol by dioxygen. A phenoxazinone synthase model involving free–radical intermediates" *Dalton Trans.* **1996**, 473.

160. Szigyártó, I. C.; Simándi, T. M.; Simándi, L. I.; Korecz, L.; Nagy, N "A functional phenoxazinone synthase model based on dioximatomanganese(II) kinetics and mechanism of the catalytic oxidation of 2–aminophenols by dioxygen" *J. Mol. Catal. A Chem.* **2006**, *251*, 270.

161. Kaizer, J.; Baráth, G.; Csonka, R.; Speier, G.; Korecz, L.; Rockenbauer, A.; Párkányi, L "Catechol oxidase and phenoxazinone synthase activity of a manganese(II) isoindoline complex" *J. Inorg. Biochem.* **2008**, *102*, 773.

162. Panja, A. "Metal ionic size directed complexation in manganese(II) coordination chemistry: Efficient candidates showing phenoxazinone synthase mimicking activity" *RSC Adv.* **2014**, *4*, 37085.

163. Bakshi, R.; Kumar, R.; Mathur, P "Bis–benzimidazole diamide iron (III) Complexes as mimics of phenoxazinone synthase" *Catal. Commun.* **2012**, *17*, 140.

164. Szávuly, M.; Csonka, R.; Speier, G.; Barabás, R.; Giorgi, M.; Kaizer, J "Oxidation of 2–aminophenol by iron(III) isoindoline complexes" *J. Mol. Catal. A: Chem.* **2014**, *392*, 120.

165. Panja, A "Mononuclear cobalt(III) and iron(II) complexes with diimine ligands: Synthesis, structure, DNA binding and cleavage activities, and oxidation of 2–aminophenol" *Polyhedron* **2012**, *43*, 22.

166. Tyagi, N.; Mathur, P "Iron(III) complexes of bis(benzimidazol–2–yl)methyl) thiophene–2,5–dicarboxamide: Synthesis, spectral and oxidation of *o*–phenylenediamine" *Spectrochim. Acta. Part A.* **2012**, *96*, 759.

167. Gale, E. M.; Narendrapurapu, B. S.; Simmonett, A. C.; Schaefer, H. F.; Harrop, T. C "Exploring the effects of H–bonding in synthetic analogues of nickel superoxide

dismutase (Ni–SOD): Experimental and theoretical implications for protection of the Ni–SCys Bond" *Inorg. Chem.* **2010**, *49*, 7080.

168. Banci, L.; Bertini, I.; Cramaro, F.; Del Conte, R.; Viezzoli, M. S "The Solution structure of reduced dimeric copper zinc superoxide dismutase: The structural effects of dimerization" *Eur. J. Biochem.* **2002**, *269*, 1905.

169. Chaudhuri, P.; Hess, M.; Müller, J.; Hildenbrand, K.; Bill, E.; Weyhermüller, T.; Wieghardt, K "Aerobic oxidation of primary alcohols (including methanol) by copper(II) and zinc(II) phenoxyl radical catalysts" *J. Am. Chem. Soc.* **1999**, *121*, 9599.

170. Ochiai, E.–I. "Bioinorganic chemistry: A survey" Academic press, **2008**.

171. Whittaker, J. W "Free radical catalysis by galactose oxidase" *Chem. Rev.* **2003**, *103*, 2347.

172. Whittaker, J. W.; Whittaker, M. M "Radical copper oxidases, one electron at a time" *Pure Appl. Chem.* **1998**, *70*, 903.

173. Whittaker, M. M.; Whittaker, J. W "The active site of galactose oxidase" *J. Biol. Chem.* **1988**, *263*, 6074.

174. Whittaker, M. M.; Kersten, P. J.; Nakamura, N.; Sanders–Loehr, J.; Schweizer, E. S.; Whittaker, J. W "Glyoxal oxidase from *Phanerochaete chrysosporium* is a new radical–copper oxidase" *J. Biol. Chem.* **1996**, *271*, 681.

175. Hammel, K. E.; Mozuch, M. D.; Kenneth A. jensen, J.; Kersten, P. J "H_2O_2 recycling during oxidation of the arylglycerol p–aryl ether lignin structure by lignin peroxidase and glyoxal oxidase" *Biochemistry* **1994**, *33*, 13349.

176. Rakshit, R.; Ghorai, S.; Biswas, S.; Mukherjee, C "Effect of ligand substituent coordination on the geometry and the electronic structure of Cu(II)–diradical

complexes" *Inorg. Chem.* **2014**, *53*, 3333.

177. Ye, L.; Spiteller, D.; Ullrich, R.; Boland, W.; Nüske, J.; Diekert, G. "Fluoride–dependent conversion of organic compounds mediated by manganese peroxidases in the absence of Mn(II) ions" *Biochemistry* **2010**, *49*, 7264.

178. Avigad, G.; Amaral, D.; Asensio, C.; Horecker, B. L "The D–galactose oxidase of polyporus circinatus" *J. Biol. Chem.* **1962**, *237*, 2736.

179. Whittaker, J. W. "Advances in protein chemistry" Academic Press, Inc, **2002**.

180. Whittaker, M. M.; Whittaker, J. W "Catalytic reaction profile for alcohol oxidation by galactose oxidase" *Biochemistry* **2001**, *40*, 7140.

181. Warren, J. J.; Tronic, T. A.; Mayer, J. M. "Thermochemistry of proton–coupled electron transfer reagents and its implications" *Chem. Rev.* **2010**, *110*, 6961.

182. Whittaker, J. W. "Metal Ions in Biological Systems*"* Marcel Dekker Inc. **1994**.

183. Firbank, S. J.; Rogers, M. S.; Wilmot, C. M.; Dooley, D. M.; Halcrow, M. A.; Knowles, P. F.; McPherson, M. J.; Phillips, S. E "Crystal structure of the precursor of galactose oxidase: An unusual self–processing enzyme" *Proc. Natl. Acad. Sci.* **2001**, *98*, 12932.

184. Clark, K.; Penner–Hahn, J. E.; Whittaker, M. M.; Whittaker, J. W "Oxidation–state assignments for galactose oxidase complexes from X–ray absorption spectroscopy. Evidence for Cu(II) in the active enzyme" *J. Am. Chem. Soc.* **1990**, *112*, 4499.

185. Markle, T. F.; Markle, T. F.; Rhile, I. J.; Rhile, I. J.; Dipasquale, A. G.; Dipasquale, A. G.; Mayer, J. M.; Mayer, J. M. "Probing concerted proton– electron transfer in phenol–imidazoles" *Sciences* **2009**, *105*, 8185.

186. Primus, J. L.; Grunenwald, S.; Hagedoorn, P. L.; Albrecht–Gary, A. M.; Mandon,

D.; Veeger, C "The nature of the intermediates in the reactions of Fe(III) and Mn(III) microperoxidase–8 with H_2O_2: A rapid kinetics study" *J. Am. Chem. Soc.* **2002**, *124*, 1214.

187. Filatov, M.; Reckien, W.; Peyerimhoff, S. D.; Shaik, S "What are the reasons for the kinetic stability of a mixture of H_2 and O_2" *J. Phys. Chem. A* **2000**, *104*, 12014.

188. Blanchard, S.; Derat, E.; Desage–El Murr, M.; Fensterbank, L.; Malacria, M.; Mouriès–Mansuy, V "Non–innocent ligands: New opportunities in iron catalysis" *Eur. J. Inorg. Chem.* **2012**, 376.

189. Kaim, W.; Schwederski, B "Non–innocent ligands in bioinorganic chemistry–an overview" *Coord. Chem. Rev.* **2010**, *254*, 1580.

190. Adam, B.; Bill, E.; Bothe, E.; Goerdt, B.; Haselhorst, G.; Hildenbrand, K.; Sokolowski, A.; Steenken, S.; Weyhermüller, T.; Wieghardt, K "Phenoxyl radical complexes of gallium, scandium, iron and manganese" *Chem. Eur. J.* **1997**, *3*, 308.

191. Mukherjee, C.; Weyhermu, T.; Bothe, E.; Chaudhuri, P "Targeted oxidase reactivity with a new redox–active ligand incorporating N_2O_2 donor atoms. Complexes of Cu(II), Ni(II), Pd(II), Fe(III), and V(V)" *Inorg. Chem.* **2008**, *47*, 11620.

192. Mu, J.; Kikuchi, A.; Bill, E.; Weyhermu, T.; Hildebrandt, P.; Ould–moussa, L.; Wieghardt, K. "Phenoxyl radical complexes of chromium(III), manganese(III), cobalt(III), and nickel(II)" *Inorg. Chim. Acta* **2000**, *297*, 265.

193. Kurahashi, T.; Fujii, H "One–electron oxidation of electronically diverse manganese(III) and nickel(II) salen complexes: Transition from localized to delocalized mixed–valence ligand radicals" *J. Am. Chem. Soc.* **2011**, *133*, 8307.

194. McGarrigle, E. M.; Gilheany, D. G. "Chromium and manganese salen promoted

epoxidation of alkenes" *Chem. Rev.* **2005**, *105*, 1563.

195. Mendes, L. L.; Fernandes, C.; Franco, R. W. A.; Lube, L. M.; Wei, S. H.; Reibenspies, J. H.; Darensbourg, D. J.; Jr., A. H "Iron complexes containing electrochemically active diazocycle–bis(di–tert–butyl–phenol) ligands" *J. Braz. Chem. Soc.* **2014**, *25*, 1050.

196. Saberikia, I.; Safaei, E.; Rafiee, M.; Cotič, P.; Bruno, G.; Rudbari, H. A "A biologically relevant iron(III) phenoxyl radical complex: A thermodynamic investigation on the structure–radical stability relationship" *J. Mol. Struct.* **2012**, *1022*, 109.

197. Lanznaster, M.; Hratchian, H. P.; Heeg, M. J.; Hryhorczuk, L. M.; McGarvey, B. R.; Schlegel, H. B.; Verani, C. N "Structural and electronic behavior of unprecedented five–coordinate iron(III) and gallium(III) complexes with a new phenol–rich electroactive ligand" *Inorg. Chem.* **2006**, *45*, 955.

198. Allard, M. M.; Sonk, J. A.; Heeg, M. J.; McGarvey, B. R.; Schlegel, H. B.; Verani, C. N "Bioinspired five–coordinate iron(III) complexes for stabilization of phenoxyl radicals" *Angew. Chem. Int. Ed.* **2012**, *51*, 3178.

199. Imbert, C.; Hratchian, H. P.; Lanznaster, M.; Heeg, M. J.; Hryhorczuk, L. M.; McGarvey, B. R.; Schlegel, H. B.; Verani, C. N. "Influence of ligand rigidity and ring substitution on the structural and electronic behavior of trivalent iron and gallium complexes with asymmetric tridentate ligands" *Inorg. Chem.* **2005**, *44*, 7414.

200. Kim, S. K.; Eriksson, S.; Kubista, M.; Nordbn, B "Interaction of 4',6–diamidino–2–phenylindole (DAPI) with poly[d(G–C)$_2$] and Poly[d(G–m5C)$_2$]: Evidence for major groove binding of a DNA probe" *J. Am. Chem. Soc.* **1993**, *115*, 3441.

References

201. Kumar, A.; Mitra, A.; Ajay, A. K.; Bhat, M. K.; Rao, C. P "Cu(II) complexes of glyco–imino–aromatic conjugates in DNA binding, plasmid cleavage and cell cytotoxicity" *J. Chem. Sci.* **2012**, *124*, 1217.

202. Kumar, A.; Chinta, J. P.; Ajay, A. K.; Bhat, M. K.; Rao, C. P "Synthesis, characterization, plasmid cleavage and cytotoxicity of cancer cells by a copper(II) complex of anthracenyl–terpyridine" *Dalton Trans.* **2011**, *40*, 10865.

203. Cejudo–Marín, R.; Alzuet, G.; Ferrer, S.; Borrás, J "Functional superoxide dismutase mimics. Structural characterization and magnetic exchange interactions of copper(II)–N–substituted sulfonamide dimer complexes" *Inorg. Chem.* **2004**, *43*, 6805.

204. Prakash, H.; Shodai, A.; Yasui, H.; Sakurai, H.; Hirota, S "Photocontrol of spatial orientation and DNA cleavage activity of copper(II)–bound dipeptides linked by an azobenzene derivative" *Inorg. Chem.* **2008**, *47*, 5045.

205. Humphreys, K. J.; Karlin, K. D.; Rokita, S. E " Efficient and specific strand scission of DNA by a dinuclear copper complex: Comparative reactivity of complexes with linked tris(2–pyridylmethyl)amine moieties" *J. Am. Chem. Soc.* **2002**, *124*, 6009.

206. Zeglis, B. M.; Pierre, V. C.; Barton, J. K "Metallo–intercalators and metallo–insertors" *Chem. Commun.* **2007**, 4565.

207. Langner, K. M.; Kedzierski, P.; Sokalski, W. A.; Leszczynski, J "Physical nature of ethidium and proflavine interactions with nucleic acid bases in the intercalation plane" *J. Phys. Chem. B* **2006**, *110*, 9720.

208. Richards, A. D.; Rodger, A "Synthetic metallomolecules as agents for the control of DNA structure" *Chem. Soc. Rev.* **2007**, *36*, 471.

209. Lippard, S. J; Hodgson, D. J. "Progress in Inorganic Chemistry" Wiley, **1977**.

210. Barton, J. K.; Lolis, E "Chiral discrimination in the covalent binding of bis(phenanthroline)dichlororuthenium(II) to B–DNA" *J. Am. Chem. soc* **1985**, *107*, 708.

211. Kagawa, T. F.; Geierstanger, B. H.; Wang, A. H. J.; Ho, P. S "Covalent modification of guanine bases in double–stranded DNA" *J. Biol. Chem.* **1991**, *266*, 20174.

212. Siddik, Z. H "Cisplatin: Mode of cytotoxic action and molecular basis of resistance" *Oncogene* **2003**, *22*, 7265.

213. Sherman, S. E.; Lippard, S. J "Structural aspects of platinum anticancer drug interactions with DNA" *Chem. Rev.* **1987**, *89*, 1153.

214. Jamieson, E. R.; Lippard, S. J "Structure, recognition, and processing of cisplatin–DNA adducts" *Chem. Rev.* **1999**, *99*, 2467.

215. Eichhorn, G. L.; Shin, Y. A "Interaction of metal ions with polynucleotides and related compounds. XII. Relative effect of various metal ions on DNA helicity" *J. Am. Chem. Soc.* **1968**, *90*, 7323.

216. Wang, B.; Cao, L.; Chiuman, W.; Li, Y.; Xi, Z "Probing the function of nucleotides in the catalytic cores of the 8–17 and 10–23 DNAzymes by abasic nucleotide and C3 spacer substitutions" *Biochemistry* **2010**, *49*, 7553.

217. Boyer, H. W "DNA restriction and modification mechanisms in bacteria" *Annu. Rev. Microbiol.* **1971**, *25*, 153.

218. Bickle, T. A; Krüger, D. H "Biology of DNA restriction" *Microbiol. Rev.* **1993**, *57*, 434.

219. Pogozelski, W. K.; Tullius, T. D. "Oxidative strand scission of nucleic acids: Routes initiated by hydrogen abstraction from the sugar moiety" *Chem. Rev.* **1998**, *98*, 1089.

220. Burrows, C. J.; Muller, J. G "Oxidative nucleobase modifications leading to strand scission" *Chem. Rev.* **1998**, *98*, 1109.

221. Gowda, K. R. S., Mathew, B. B.; Sudhamani, C. N.; Naik, H. S. B. "Mechanism of DNA binding and cleavage" *Biomedicine Biotechnol.* **2014**, *2*, 1.

222. Sawyer, D. T.; Valentine, J. S "How super is superoxide?" *Acc. Chem. Res* **1981**, *14*, 393.

223. Burger, R. M "Cleavage of nucleic acids by bleomycin" *Chem. Rev.* **1998**, *98*, 1153.

224. Rohde, J.U.; In, J.H.; Lim, M. H.; Brennessel, W. W.; Bukowski, M. R.; Stubna, A.; Münck, E.; Nam, W.; Que, L "Crystallographic and spectroscopic characterization of a nonheme Fe(IV)–O–Complex" *Science* **2003**, *299*, 1037.

225. Lim, M. H.; Rohde, J.–U.; Stubna, A.; Bukowski, M. R.; Costas, M.; Ho, R. Y. N.; Munck, E.; Nam, W.; Que, L "An Fe(IV)=O complex of a tetradentate tripodal nonheme ligand" *Proc. Natl. Acad. Sci.* **2003**, *100*, 3665.

226. Kaizer, J.; Klinker, E. J.; Oh, N. Y.; Rohde, J. U.; Song, W. J.; Stubna, A.; Kim, J.; Münck, E.; Nam, W.; Que, L "Nonheme Fe(IV)=O complexes that can oxidize the C–H bonds of cyclohexane at room temperature"*J. Am. Chem. Soc.* **2004**, *126*, 47.

227. Shan, X.; Que, L "High–valent nonheme iron–oxo species in biomimetic oxidations" *J. Inorg. Biochem.* **2006**, *100*, 421.

228. Wolfenden, R.; Ridgway, C.; Young, G "Spontaneous hydrolysis of ionized phosphate monoesters and diesters and the proficiencies of phosphatases and phosphodiesterases as catalysts" *J. Am. Chem. Soc.* **1998**, *120*, 833.

229. Williams, N. H.; Takasaki, B.; Wall, M.; Chin, J. "Structure and nuclease activity of simple dinuclear metal complexes: Quantitative dissection of the role of metal ions"

Acc. Chem. Res. **1999**, *32*, 485.

230. Chin, J "Developing artificial hydrolytic metalloenzymes by a unified mechanistic approach" *Acc. Chem. Res.* **1991**, *24*, 145.

231. Blaskó, A.; Bruice, T. C "Recent studies of nucleophilic, general–acid, and metal ion catalysis of phosphate diester hydrolysis" *Acc. Chem. Res.* **1999**, *32*, 475.

232. Sträter, N.; Lipscomb, W. N.; Klabunde, T.; Krebs, B "Two–metal ion catalysis in enzymatic acyl–and phosphoryl–transfer reactions" *Angew. Chem. Int. Ed.* **1996**, *35*, 2024.

233. Hegg, E. L.; Burstyn, J. N "Toward the development of metal–based synthetic nucleases and peptidases: A rationale and progress report in applying the principles of coordination chemistry" *Coord. Chem. Rev.* **1998**, *173*, 133.

234. Mancin, F.; Scrimin, P.; Tecilla, P.; Tonellato, U "Artificial metallonucleases" *Chem. Commun.* **2005**, 2540.

235. Saito, I.; Nakatani, K "Design of DNA–cleaving agents" *Bull. Chem. Soc. Jpn.* **1996**, *69*, 3007.

236. Armitage, B "Photocleavage of nucleic acids" *Chem. Rev.* **1998**, *98*, 1171.

237. Baghel, G. S.; Chinta, J. P.; Rao, C. P "Synthesis, characterization of the amido–conjugates of 1,1′–methylene–bis(2–naphthol) and recognition of Cu(II) in aqueous acetonitrile" *New J. Chem.* **2012**, *36*, 2397.

238. Thamilarasan, V.; Jayamani, A.; Sengottuvelan, N "Synthesis, molecular structure, biological properties and molecular docking studies on Mn(II), Co(II) and Zn(II) complexes containing bipyridine–azide ligands" *Eur. J. Med. Chem.* **2015**, *89*, 266.

239. Zhu, L. N.; Gao, H. R.; Wang, H. X.; Xu, M. Y.; Li, X. Z "Synthesis, crystal

structures, and DNA cleavage activities of manganese (II) complexes: A good example of the synergy between metal ions prompting DNA cleavage" *Eur. J. Inorg. Chem.* **2014**, 2396.

240. Tao, Z. W.; Wang, L. F.; Li, D. D "Comparison of nuclease activities of binuclear metal complexes with N_6O coordinating heptadentate ligands: $[M_2L(OAc)_2]$+ (M = Ni, Mn, L = 2,6–bis(((2–(dimethylamino)ethyl)(pyridin–2–ylmethyl)amino) methyl)–4–methoxyphenol)" *Trans. Met. Chem.* **2015**, *40*, 269.

241. Zampakou, M.; Akrivou, M.; Andreadou, E. G.; Raptopoulou, C. P.; Psycharis, V.; Pantazaki, A. A.; Psomas, G "Structure, antimicrobial activity, DNA– and albumin–binding of manganese(II) complexes with the quinolone antimicrobial agents oxolinic acid and enrofloxacin". *Inorg. Biochem.* **2013**, *121*, 88.

242. Macías, B.; Villa, M. V; Lapresa, R.; Alzuet, G.; Hernández–Gil, J.; Sanz, F "Mn(II) complexes with sulfonamides as ligands. DNA interaction studies and nuclease activity" *J. Inorg. Biochem.* **2012**, *115*, 64.

243. de Souza, B.; Xavier, F. R.; Peralta, R. a; Bortoluzzi, A. J.; Conte, G.; Gallardo, H.; Fischer, F. L.; Bussi, G.; Terenzi, H.; Neves, A "Oxygen–independent photonuclease activity of a new iron(II) complex" *Chem. Commun.* **2010**, *46*, 3375.

244. Bal–Demirci, T.; Congur, G.; Erdem, A.; Erdem–Kuruca, S.; Özdemir, N.; Akgün–Dar, K.; Varol, B.; Ülküseven, B "Iron(III) and nickel(II) complexes as potential anticancer agents: synthesis, physicochemical and structural properties, cytotoxic activity and DNA interactions" *New J. Chem.* **2015**, *39*, 5643.

245. Behnamfar, M. T.; Hadadzadeh, H.; Simpson, J.; Darabi, F.; Shahpiri, A.; Khayamian, T.; Ebrahimi, M.; Rudbari, H. A.; Salimi, M "Experimental and molecular

modeling studies of the interaction of the polypyridyl Fe(II) and Fe(III) complexes with DNA and BSA" *Spectrochim. Acta Part A* **2015**, *134*, 502.

246. Parveen, S.; Usman, M.; Tabassum, S.; Arjmand, F "Synthesis and characterization of Co(II) and Fe(II) peptide conjugates as hydrolytic cleaving agents and their preferential enantiomeric disposition for CT–DNA: Structural investigation of L–enantiomers by DFT and molecular docking studies" *RSC Adv.* **2015**, *5*, 72121.

247. Abdel Rahman, L. H.; El Khatib, R. M.; Nassr, L. a E.; Abu Dief, A. M "Synthesis, physicochemical studies, embryos toxicity and DNA interaction of some new iron(II) schiff base amino acid complexes" *J. Mol. Struct.* **2013**, *1040*, 9.

248. Joyner, J. C.; Reichfield, J.; Cowan, J. A "Factors influencing the DNA nuclease activity of iron, cobalt, nickel, and copper chelates" *J. Am. Chem. Soc.* **2011**, *133*, 15613.

249. Gu, Z.–G.; Na, J. J.; Bao, F. F.; Xu, X. X.; Zhou, W.; Pang, C. Y.; Li, Z "Synthesis, characterization, and DNA–binding of enantiomers of iron(II) schiff base complexes" *Polyhedron* **2013**, *51*, 186.

250. Saha, S.; Mallick, D.; Majumdar, R.; Roy, M.; Dighe, R. R.; Jemmis, E. D.; Chakravarty, A. R "Structure–activity relationship of photocytotoxic iron(III) complexes of modified dipyridophenazine ligands" *Inorg. Chem.* **2011**, *50*, 2975.

251. Benzeid, H.; Mothes, E.; Essassi, E. M.; Faller, P.; Pratviel, G. A "Thienoquinoxaline and a styryl–quinoxaline as new fluorescent probes for amyloid–β fibrils" *Comptes Rendus Chim.* **2012**, *15*, 79.

252. Chiti, F.; Dobson, C. M "Protein misfolding, functional amyloid, and human disease" *Annu. Rev. Biochem.* **2006**, *75*, 333.

253. Lindgren, M.; Hammarström, P "Amyloid oligomers: Spectroscopic characterization of amyloidogenic protein states" *FEBS J.* **2010**, *277*, 1380.

254. Roy, M.; Bhowmick, T.; Santhanagopal, R.; Ramakumar, S.; Chakravarty, A. R. "Photo–induced double–strand DNA and site–specific protein cleavage activity of L–histidine (μ–oxo)diiron(III) complexes of heterocyclic bases" *Dalton Trans.* **2009**, 4671.

255. Smith, S. J.; Peralta, R. A.; Jovito, R.; Horn, A.; Bortoluzzi, A. J.; Noble, C. J.; Hanson, G. R.; Stranger, R.; Jayaratne, V.; Cavigliasso, G.; Gahan, L. R.; Schenk, G.; Nascimento, O. R.; Cavalett, A.; Bortolotto, T.; Razzera, G.; Terenzi, H.; Neves, A.; Riley, M. J. "Spectroscopic and catalytic characterization of a functional (FeFeII)–Fe–III biomimetic for the active site of uteroferrin and protein cleavage" *Inorg. Chem.* **2012**, *51*, 2065.

256. Garai, A.; Basu, U.; Khan, I.; Pant, I.; Hussain, A.; Kondaiah, P.; Chakravarty, A. R. "Iron(III) benzhydroxamates of dipicolylamines for photocytotoxicity in red light and cellular imaging" *Polyhedron* **2014**, *73*, 124.

257. Basu, U.; Khan, I.; Koley, D.; Saha, S.; Kondaiah, P.; Chakravarty, A. R "Nuclear targeting terpyridine iron(II) complexes for cellular imaging and remarkable photocytotoxicity" *J. Inorg. Biochem.* **2012**, *116*, 77.

258. Basu, U.; Khan, I.; Hussain, A.; Gole, B.; Kondaiah, P.; Chakravarty, A. R. "Carbohydrate–appended tumor targeting iron(III) complexes showing photocytotoxicity in red light" *Inorg. Chem.* **2014**, *53*,2152.

259. Garai, A.; Basu, U.; Pant, I.; Kondaiah, P.; Chakravarty, A. R "Polypyridyl iron(II) complexes showing remarkable photocytotoxicity in visible light" *J. Chem. Sci.* **2015**,

127, 609.

260. Orvig, C.; Abrams, M. J "Medicinal inorganic chemistry: Introduction" *Chem. Rev.* **1999**, *99*, 2201.

261. Zhang, C. X.; Lippard, S. J "New Metal complexes as potential therapeutics" *Curr. Opin. Chem. Biol.* **2003**, *7*, 481.

262. Barnham, K. J.; Bush, A. I "Metals in alzheimer's and parkinson's diseases" *Curr. Opin. Chem. Biol.* **2008**, *12*, 222.

263. Sadler, P. J.; Guo, Z "Metal complexes in medicine: Design and mechanism of action" *Pure Appl. Chem.* **1998**, *70*, 863.

264. Thompson, K. H.; Orvig, C "Metal complexes in medicinal chemistry: New vistas and challenges in drug design" *Dalton Trans.* **2006**, 761.

265. Eroy–Reveles, A. A.; Hoffman–Luca, C. G.; Mascharak, P. K "Formation of a triply bridged μ–Oxo diiron(III) core stabilized by two deprotonated carboxamide groups upon photorelease of NO from a [Fe–NO]^6 iron nitrosyl" *Dalton Trans.* **2007**, *2*, 5268.

266. Rose, M. J.; Patra, A. K.; Olmstead, M. M.; Mascharak, P. K. "Structural and spectroscopic evidence for linkage isomerism of bound nitrite in a {Fe–NO}^{6} nitrosyl derived from a tetradentate dicarboxamide ligand: More parallels between heme and non–heme systems" *Inorg. Chim. Acta* **2010**, *363*, 2715.

267. Goswami, T. K.; Gadadhar, S.; Balaji, B.; Gole, B.; Karande, A. A; Chakravarty, A. R. "Ferrocenyl–L–amino acid copper(II) complexes showing remarkable photo–induced anticancer activity in visible light" *Dalton Trans.* **2014**, *43*, 11988.

268. Ghosh, K.; Kumar, P.; Mohan, V.; Singh, U. P.; Kasiri, S.; Mandal, S. S "Nuclease activity *via* self–activation and anticancer activity of a mononuclear copper(II)

complex: Novel role of the tertiary butyl group in the ligand frame" *Inorg. Chem.* **2012**, *51*, 3343.

269. David, S.; Perkins, R. S.; Fronczek, F. R.; Kasiri, S.; Mandal, S. S.; Srivastava, R. S. "Synthesis, characterization, and anticancer activity of ruthenium–pyrazole complexes" *J. Inorg. Biochem.* **2012**, *111*, 33.

270. Mandal, S. S "Metallo–salen complexes show promise towards treatment of leukemia" *Leuk. Res.* **2011**, *35*, 571.

271. Mjos, K. D.; Orvig, C "Metallodrugs in medicinal inorganic chemistry" *Chem. Rev.* **2014**, *114*, 4540.

272. Barry, N. P. E.; Sadler, P. J "Exploration of the medical periodic table: Towards new targets" *Chem. Commun.* **2013**, *49*, 5106.

273. Gaynor, D.; Griffith, D. M "The prevalence of metal–based drugs as therapeutic or diagnostic agents: Beyond platinum" *Dalton Trans.* **2012**, *41*, 13239.

274. Hartinger, C. G.; Dyson, P. J "Bioorganometallic chemistry from teaching paradigms to medicinal applications" *Chem. Soc. Rev.* **2009**, *38*, 391.

275. Ansari, K. I.; Kasiri, S.; Grant, J. D.; Mandal, S. S "Apoptosis and anti–tumour activities of manganese(III)–salen and –salphen complexes" *Dalton Trans.* **2009**, 40, 8525.

276. Gonzales, M. A.; Han, H.; Moyes, A.; Radinos, A.; Hobbs, A. J.; Coombs, N.; Oliver, S. R. J.; Mascharak, P. K "Light–triggered carbon monoxide delivery with Al–MCM–41–based nanoparticles bearing a designed manganese carbonyl complex" *J. Mater. Chem. B* **2014**, *2*, 2107.

277. Carrington, S. J.; Chakraborty, I.; Mascharak, P. K. "Rapid CO release from a Mn(I)

carbonyl complex derived from azopyridine upon exposure to visible light and its phototoxicity toward malignant cells" *Chem. Commun.* **2013**, *49*, 11254.

278.   Ansari, K. I.; Grant, J. D.; Woldemariam, G. A.; Kasiri, S.; Mandal, S. S "Iron(III)–salen complexes with less DNA cleavage activity exhibit more efficient apoptosis in MCF7 cells" *Org. Biomol. Chem.* **2009**, *7*, 926.

279.   Palmer, R. F.; Lasseter, K. C "Sodium Nitroprusside" *N. Engl. J. Med.* **1975**, *292*, 294.

280.   Tuzel, I. H "Sodium Nitroprusside : A review of its clinical effectiveness as a hypotensive agent" *J. Clin. Pharmacol.* **1974**, *14*, 494.

281.   Patra, A. K.; Afshar, R.; Olmstead, M. M.; Mascharak, P. K. "The first non–heme iron(III) complex with a ligated carboxamido group that exhibits photolability of a bound NO ligand" *Angew. Chem. Int. Ed.* **2002**, *114*, 2622.

282.   Patra, A. K.; Rose, M. J.; Olmstead, M. M.; Mascharak, P. K "Reactions of nitric oxide with a low–spin Fe(III) center ligated to a tetradentate dicarboxamide N4 ligand: Parallels between heme and non–heme systems" *J. Am. Chem. Soc.* **2004**, *126*, 4780.

283.   Afshar, R. K.; Patra, A. K.; Olmstead, M. M.; Mascharak, P. K "Syntheses, structures, and reactivities of (Fe–NO)^6 nitrosyls derived from polypyridine–carboxamide ligands: Photoactive NO–donors and reagents for S–nitrosylation of alkyl thiols" *Inorg. Chem.* **2004**, *43*, 5736.

284.   Phukan, B.; Patel, A. B.; Mukherjee, C. A "Water–soluble and water–coordinated Mn(II) complex: Synthesis, characterization and phantom MRI image study" *Dalton Trans.* **2015**, *44*, 12990.

285.   Caravan, P.; Ellison, J. J.; McMurry, T. J.; Lauffer, R. B. "Gadolinium(III) chelates

as MRI contrast agents: Structure, dynamics, and applications" *Chem. Rev.* **1999**, *99*, 2293.

286.   Lauffer, R. B "Paramagnetic metal complexes as water proton relaxation agents for NMR imaging: Theory and design" *Chem. Rev.* **1987**, *87*, 901.

287.   Caravan, P "Strategies for increasing the sensitivity of gadolinium based MRI contrast agents" *Chem. Soc. Rev.* **2006**, *35*, 512.

288.   Hermann, P.; Kotek, J.; Kubíček, V.; Lukeš, I. "Gadolinium(III) complexes as MRI contrast agents: Ligand design and properties of the complexes" *Dalton Trans.* **2008**, 3027.

289.   Laus, S.; Ruloff, R.; Tóth, É.; Merbach, A. E "Gd(III) complexes with fast water exchange and high thermodynamic stability: Potential building blocks for high–relaxivity MRI contrast agents" *Chem. Eur. J.* **2003**, *9*, 3555.

290.   Drahoš, B.; Lukeš, I.; Tóth, É " Manganese(II) complexes as potential contrast agents for MRI" *Eur. J. Inorg. Chem.* **2012**, 1975.

291.   Raymond, K. N.; Pierre, V. C "Next generation, high relaxivity gadolinium MRI agents" *Bioconjug. Chem.* **2005**, *16*, 3.

292.   Troughton, J. S.; Greenfield, M. T.; Greenwood, J. M.; Dumas, S.; Wiethoff, A. J.; Wang, J.; Spiller, M.; McMurry, T. J.; Caravan, P "Synthesis and evaluation of a high relaxivity manganese(II)–based MRI contrast agent" *Inorg. Chem.* **2004**, *43*, 6313.

293.   Rocklage, S. M.; Cacheris, W. P.; Quay, S. C.; Hahn, F. E.; Raymond, K. N "Manganese (II) N, N'–dipyridoxylethylenediamine–N, N'–diacetate 5, 5'–bis (phosphate). Synthesis and characterization of a paramagnetic chelate for magnetic resonance imaging enhancement" *Inorg. Chem.* **1989**, *28*, 477.

294. Wang, S.; Westmoreland, T. D "Correlation of relaxivity with coordination number in six–, seven–, and eight–coordinate Mn(II) complexes of pendant–arm cyclen derivatives" *Inorg. Chem.* **2009**, *48*, 719.

295. Caravan, P "Protein–targeted gadolinium–based magnetic resonance imaging (MRI) contrast agents: Design and mechanism of action" *Acc. Chem. Res* **2009**, *42*, 851.

296. Oakes, J.; Smith, E. G "Structure of Mn–EDTA^{2-} complex in aqueous solution by relaxation nuclear magnetic resonance" *J. Chem. Soc., Faraday Trans.* **1981**, *77*, 299.

297. Mastarone, D. J.; Harrison, V. S. R.; Eckermann, A. L.; Parigi, G.; Luchinat, C.; Meade, T. J "A modular system for the synthesis of multiplexed magnetic resonance probes" *J. Am. Chem. Soc.* **2011**, *133*, 5329.

298. Terreno, E.; Castelli, D. D.; Viale, A.; Aime, S "Challenges for molecular magnetic resonance imaging" *Chem. Rev.* **2010**, *110*, 3019.

299. Boros, E.; Polasek, M.; Zhang, Z.; Caravan, P "Gd(DOTAla): A single amino acid Gd–complex as a modular tool for high relaxivity MR contrast agent development" *J. Am. Chem. Soc.* **2012**, *134*, 19858.

300. Cersosimo, M. G.; Koller, W. C. "The diagnosis of manganese–induced parkinsonism" *Neurotoxicol.* **2006**, *27*, 340.

301.   Datta, A.; Raymond, K. N. "Gd–hydroxypyridinone (HOPO)–based high–relaxivity magnetic resonance Imaging (MRI) contrast agents" *Acc. Chem. Res.* **2009**, *42*, 938.

302. Aime, S.; Fasano, M.; Terreno, E. "Lanthanide(III) chelates for NMR biomedical applications" *Chem. Soc. Rev.* **1998**, *27*, 19.

303. Ghosh, P.; Mondal, P.; Ray, R.; Das, A.; Bag, S.; Mobin, S. M.; Lahiri, G. K. "Significant in fluence of coligands toward varying coordination modes of 2,2 ′ –

bipyridine–3,3 ′–diol in ruthenium complexes" *Inorg. Chem.* **2014**, *53*, 6094.

304.   Das, A.; Agarwala, H.; Kundu, T.; Ghosh, P.; Mondal, S.; Mobin, S. M.; Lahiri, G. K. "Electronic structures and selective fluoride sensing features of Os(bpy)$_2$(HL($^{2-}$)) and [{Os(bpy)$_2$}$_2$(µ–HL($^{2-}$))]($^{2+}$) (H$_3$L: 5–(1H–benzo[d]imidazol–2–yl)–1H–imidazole–4–carboxylic acid)" *Dalton Trans.* **2014**, *43*, 13932.

305.   Das, A.; Ghosh, P.; Plebst, S.; Schwederski, B.; Mobin, S. M.; Kaim, W.; Lahiri, G. K. "Ancillary ligand control of electronic structure in o–benzoquinonediimine–ruthenium complex redox series: Structures, electron paramagnetic resonance (EPR), and ultraviolet–visible–near–infrared (UV–Vis–NIR) Spectroelectrochemistry" *Inorg. Chem.* **2015**, *54*, 3376.

306.   Rakshit, R.; Ghorai, S.; Sarmah, A.; Tiwari, A.; Roy, R. K.; Mukherjee, C. "Inter–ligand azo (N=N) unit formation and Stabilization of a Co(II)–diradical complex *via* metal–to–ligand dπ–pπ* back donation: Synthesis, characterization, and theoretical study" *Dalton Trans.* **2015**, *44*, 3724.

307.   Mondal, P.; Ray, R.; Das, A.; Lahiri, G. K. "Revelation of varying bonding motif of alloxazine, a flavin analogue in selected ruthenium (II/III) frameworks" *Inorg. Chem.* **2015**, *54*, 3012.

308.   Romain, S.; Duboc, C.; Neese, F.; Riviere, E.; Hanton, L. R.; Blackman, A. G.; Philouze, C.; Lepretre, J.–C.; Deronzier, A.; Collomb, M.–N. "An unusual stable mononuclear Mn^{III} bis–terpyridine complex exhibiting Jahn–Teller compression: Electrochemical, synthesis, physical characterisation and theoretical study" *Chem. Eur. J.* **2009**, *15*, 980.

309.   Gomez–Coca, S.; Ruiz, E. "Exchange coupling and magnetic anisotropy of

exchanged–biased quantum tunnelling single–molecule magnet Ni_3Mn_2 complexes using theoretical methods based on density functional theory" *Dalton Trans.* **2012**, *41*, 2659.

310. Wang, M.; England, J.; Weyhermu, T.; Wieghardt, K. "Molecular and electronic structures of the members of the electron transfer series $[Mn(bpy)_3]$ (n = 2+, 1+, 0, 1–) and $[Mn(tpy)_2]^m$ (m= 4+, 3+, 2+, 1+, 0), an experimental and density functional theory study" *Inorg. Chem.* **2014**, *53*, 2276.

311. Merkle, A. C.; Fry, N. L.; Mascharak, P. K.; Lehnert, N. "Mechanism of NO photodissociation in photolabile manganese–NO complexes with pentadentate N_5 ligands" *Inorg. Chem.* **2011**, *50*, 12192.

312. Zheng, W.; Wu, S.; Zhao, S.; Geng, Y.; Jin, J.; Su, Z.; Fu, Q. "Carbonyl amine/schiff base ligands in manganese complexes: Theoretical study on the mechanism, capability of NO release" *Inorg. Chem.* **2012**, *51*, 3972.

313. Ivanova, A.; Romanova, J.; Tadjer, A.; Baumgarten, M. "Magnetostructural correlation for rational design of Mn(II) hybrid–spin complexes" *J. Phys. Chem. A* **2013**, *117*, 670.

314. Maiti, M.; Sadhukhan, D.; Thakurta, S.; Zangrando, E.; Pilet, G.; Bauza, A.; Frontera, A.; Dede, B.; Mitra, S. "Synthesis, structural characterization, theoretical calculations and catecholase mimetic activity of manganese–schiff base complexes" *Polyhedron* **2014**, *75*, 40.

315. Thamilarasan, V.; Sengottuvelan, N.; Sudha, A.; Srinivasan, P.; Siva, A. "Synthesis, molecular structure, theoretical calculation, DNA/protein interaction and cytotoxic activity of manganese(III) complex with 8–hydroxyquinoline" *J. Photochem.*

Photobiol. B. **2015**, *142*, 220.

316. Carrington, S. J.; Chakraborty, I.; Mascharak, P. K. "Exceptionally rapid CO release from a manganese(I) tricarbonyl complex derived from bis(4–chloro–phenylimino) acenaphthene upon exposure to visible light" *Dalton Trans.* **2015**, *44*, 13828.

317. Chen, J.; Cho, K.–B.; Lee, Y.–M.; Kwon, Y. H.; Nam, W. "Mononuclear nonheme iron(iv)–oxo and manganese(iv)–oxo complexes in oxidation reactions: Experimental results prove theoretical prediction" *Chem. Commun.* **2015**, *51*, 13094.

318. To, W.–P.; Wai–Shan Chow, T.; Tse, C.–W.; Guan, X.; Huang, J.–S.; Che, C.–M. "Water oxidation catalysed by iron complex of N,N′–dimethyl–2,11–diaza[3,3](2,6)pyridinophane. Spectroscopy of iron–oxo intermediates and density functional theory calculations" *Chem. Sci.* **2015**, *6*, 5891.

319. Pramanik, H. A. R.; Paul, P. C.; Mondal, P.; Bhattacharjee, C. R. "Mixed ligand complexes of cobalt(III) and iron(III) containing N_2O_2–chelating schiff base: Synthesis, characterisation, antimicrobial activity, antioxidant and DFT Study" *J. Mol. Struct.* **2015**, *1100*, 496.

320. Yang, X. "Bio–inspired computational design of iron catalysts for hydrogenation of carbon dioxide" *Chem. Commun.* **2015**, *51*, 13098.

321. Herchel, R.; Nemec, I.; Machata, M.; Travnicek, Z. "Experimental and theoretical investigations of magnetic exchange pathways in structurally diverse iron(III) schiff–base complexes" *Inorg. Chem.* **2015**, *54*, 8625.

322. Yamaguchi, M.; Ohira, A. "Density functional theory calculation of μ–oxo and μ–hydroxo bridged iron(III) aqua dimer complexes in perfluorinated sulfonic acid ionomer membranes" *Comput. Theor. Chem.* **2015**, *1071*, 61.

323. Kazaryan, A.; Baerends, E. J. "Ligand field effects and the high spin–high reactivity correlation in the H–abstraction by nonheme iron(IV)–oxo complexes: A DFT frontier orbital perspective" *ACS Catal.* **2015**, *5*, 1475.

324. Long, G. J.; Grandjean, F.; Harrop, T. C.; Petroccia, H. M.; Papaefthymiou, G. C. "Combined mössbauer spectral and density functional study of an eight–coordinate iron(II) complex" *Inorg. Chem.* **2015**, *54*, 8415.

325. Pathak, R. K.; Hinge, V. K.; Mondal, P.; Rao, C. P. "Ratiometric fluorescence off–on–off sensor for Cu^{2+} in aqueous buffer by a lower rim triazole linked benzimidazole conjugate of calix[4]arene" *Dalton Trans.* **2012**, *41*, 10652.

326. Prince, B. M.; Cundari, T. R.; Tymczak, C. J. "DFT study of the reaction of a two–coordinate iron(II) dialkyl complex with molecular oxygen" *J. Phys. Chem. A* **2014**, *118*, 11056.

327. Chen, X.; Pradhan, T.; Wang, F.; Kim, J. S.; Yoon, J. "Fluorescent chemosensors based on spiroring–opening of xanthenes and related derivatives" *Chem. Rev.* **2012**, *112*, 1910.

328. Boens, N.; Leen, V.; Dehaen, W. "Fluorescent indicators based on BODIPY" *Chem. Soc. Rev.* **2012**, *41*, 1130.

329. Kim, H. N.; Ren, W. X.; Kim, J. S.; Yoon, J. "Fluorescent and colorimetric sensors for detection of lead, cadmium, and mercury ions" *Chem. Soc. Rev.* **2012**, *41*, 3210.

330. Mummidivarapu, V. V. S.; Tabbasum, K.; Chinta, J. P.; Rao, C. P. "1,3–Di–amidoquinoline conjugate of calix[4]arene (L) as a ratiometric and colorimetric sensor for Zn^{2+}: Spectroscopy, microscopy and computational studies" *Dalton Trans.* **2012**, *41*, 1671.

References

331. Carter, K. P.; Young, A. M.; Palmer, A. E. "Fluorescent sensors for measuring metal ions in living systems" *Chem. Rev.* **2014**, *114*, 4564.

332. De Silva, A. P.; Gunaratne, H. Q. N.; Gunnlaugsson, T.; Huxley, A. J. M.; McCoy, C. P.; Rademacher, J. T.; Rice, T. E. "Signaling recognition events with fluorescent sensors and switches" *Chem. Rev.* **1997**, *97*, 1515.

333. Silva, J. J. R. F. da; Williams, R. J. P. "The Biological Chemistry of the Elements: The Inorganic Chemistry of Life" 2nd Ed.; Oxford University Press, **2001**.

334. Desai, N. K.; Kolekar, G. B.; Patil, S. R. "Off–on fluorescent polyanthracene for recognition of ferric and fluoride ions in aqueous acidic media: Application in pharmaceutical and environmental analysis" *New J. Chem.* **2014**, *38*, 4394.

335. Yang, Y. K.; Yook, K. J.; Tae, J. "A rhodamine–based fluorescent and colorimetric chemodosimeter for the rapid detection of Hg^{2+} ions in aqueous media" *J. Am. Chem. Soc.* **2005**, *127*, 16760.

336. Sen, S.; Sarkar, S.; Chattopadhyay, B.; Moirangthem, A.; Basu, A.; Dhara, K.; Chattopadhyay, P. "A ratiometric fluorescent chemosensor for iron: Discrimination of Fe^{2+} and Fe^{3+} and living cell application" *Analyst* **2012**, *137*, 3335.

337. Xiang, Y.; Tong, A. "A new rhodamine–based chemosensor exhibiting selective Fe(III)–amplified fluorescence" *Org. Lett.* **2006**, *8*, 1549.

338. Bhalla, V.; Sharma, N.; Kumar, N.; Kumar, M. "Rhodamine based fluorescence turn–on chemosensor for nanomolar detection of Fe^{3+} Ions" *Sens. Actuators, B* **2013**, *178*, 228.

339. Bae, S.; Tae, J. "Rhodamine–hydroxamate–based fluorescent chemosensor for Fe(III)" *Tetrahedron Lett.* **2007**, *48*, 5389.

340. Chereddy, N. R.; Suman, K.; Korrapati, P. S.; Thennarasu, S.; Mandal, A. B. "Design and synthesis of rhodamine based chemosensors for the detection of Fe^{3+} ions" *Dyes Pigments* **2012**, *95*, 606.

341. Liu, S. R.; Wu, S. P. "New water–soluble highly selective fluorescent chemosensor for Fe(III) ions and its application to living cell imaging" *Sens. Actuators, B* **2012**, *171–172*, 1110.

342. Liang, Z.–Q.; Wang, C.–X.; Yang, J.–X.; Gao, H.–W.; Tian, Y.–P.; Tao, X.–T.; Jiang, M.–H. "A highly selective colorimetric chemosensor for detecting the respective amounts of iron(II) and iron(III) ions in water" *New J. Chem.* **2007**, *31*, 906.

343. Silva, A. M. G.; Leite, A.; Andrade, M.; Gameiro, P.; Brandao, P.; Felix, V.; De Castro, B.; Rangel, M. "Microwave–assisted synthesis of 3–hydroxy–4–pyridinone/naphthalene conjugates. Structural characterization and selection of a fluorescent ion sensor" *Tetrahedron* **2010**, *66*, 8544.

344. Pathak, R. K.; Dessingou, J.; Hinge, V. K.; Thawari, A. G.; Basu, S. K.; Rao, C. P. "Quinoline driven fluorescence turn on 1,3–bis–calix[4]arene conjugate–based receptor to discriminate Fe^{3+} from Fe^{2+}" *Anal. Chem.* **2013**, *85*, 3707.

345. Komatsu, H.; Miki, T.; Citterio, D.; Kubota, T.; Shindo, Y.; Kitamura, Y.; Oka, K.; Suzuki, K. "Single molecular multianalyte (Ca^{2+}, Mg^{2+}) fluorescent probe and applications to bioimaging" *J. Am. Chem. Soc.* **2005**, *127*, 10798.

346. Zhang, X.; Xiao, Y.; Qian, X. "A ratiometric fluorescent probe based on FRET for Imaging Hg^{2+} ions in living cells" *Angew. Chem.* **2008**, *47*, 8025.

347. Peng, X.; Du, J.; Fan, J.; Wang, J.; Wu, Y.; Zhao, J.; Sun, S.; Xu, T. "A selective fluorescent sensor for imaging Cd^{2+} in living cells" *J. Am. Chem. Soc.* **2007**, *129*, 1500.

348. Kitajima, N.; Osawa, M.; Tamura, N.; Morooka, Y.; Hirano, T.; Hirob, M.; Nagano, T. "Monomeric (benzoato)manganese(II) complexes as manganese superoxide dismutase mimics" *Inorg. Chem.* **1993**, *32*, 1879.

349. Marmur, J. "A procedure for the isolation of deoxyribonucleic acid from micro–organisms" *J. Mol. Biol.* **1961**, *3*, 208.

350. Reichmann, M. E.; Rice, S. A; Thomas, C. A; Doty, P. "A further examination of the molecular weight and size of desoxypentose nucleic acid" *J. Am. Chem. Soc.* **1954**, *76*, 3047.

351. Shao, Y.; Sheng, X.; Li, Y.; Jia, Z.–L.; Zhang, J.–J.; Liu, F.; Lu, G.–Y. "DNA binding and cleaving activity of the new cleft molecule N,N'–bis(guanidinoethyl)–2,6–pyridinedicarboxamide in the absence or in the presence of copper(II)" *Bioconjug. Chem.* **2008**, *19*, 1840.

352. Liu, J.; Zhang, H.; Chen, C.; Deng, H.; Ji, L. "Interaction of macrocyclic copper (II) complexes with calf thymus DNA : Effects of the side chains of the ligands on the DNA–binding behaviors" *Dalton Trans.* **2003**, 114.

353. Armarego, W. L. F.; Chai, C. L. L. "Purification Of Laboratory Chemicals" 5th ed. Butter Heinemann, Elsevier Science: USA, **2002**.

354. Roy, M.; Santhanagopal, R.; Chakravarty, A. R. "DNA binding and oxidative DNA cleavage activity of (μ–Oxo)diiron(III) complexes in visible light" *Dalton Trans.* **2009**, 1024.

355. Rosenberg, B.; Vancamp, L.; Trosko, J. E.; Mansour, V. H. "Platinum compounds: A new class of potent antitumour agents" *Nature* **1969**, *222*, 385.

356. Galanski, M.; Jakupec M. A.; Keppler, B. K. "Update of the preclinical situation of

anticancer platinum complexes: novel design strategies and innovative analytical approaches" *Curr. Med. Chem.* **2005**, 2075.

357.   Wang, D.; Lippard, S. J. "Cellular processing of platinum anticancer drugs" *Nat Rev Drug Discov.* **2005**, *4*, 307.

358.   Umezawa, H. "Structure and action of bleomycin" *Prog. Biochem. Pharmacol.* **1976**, *11*, 18.

359.   Jung, Y.; Lippard, S. J. "Direct cellular responses to platinum–induced DNA damage direct cellular responses to platinum–induced DNA damage" *Chem. Rev.* **2007**, *107*, 1387.

360.   Loganathan, R.; Ramakrishnan, S.; Suresh, E.; Riyasdeen, A.; Akbarsha, M. A.; Palaniandavar, M. "Mixed ligand copper(II) complexes of N, N–bis(benzimidazol–2–yl–methyl)amine (BBA) with diimine Co–ligands: Efficient chemical nuclease and protease activities and cytotoxicity" *Inorg. Chem.* **2012**, *51*, 5512.

361.   Giaccone, G.; Herbst, R. S.; Manegold, C.; Scagliotti, G.; Rosell, R.; Miller, V.; Natale, R. B.; Schiller, J. H.; Pawel, J. von; Pluzanska, A.; Gatzemeier, U.; Grous, J.; Ochs, J. S.; Averbuch, S. D.; Wolf, M. K.; Rennie, P.; Fandi, A.; Johnson, D. H. "Gefitinib in combination with gemcitabine and cisplatin in advanced non–small–cell lung cancer: A phase III trial–INTACT1" *J. Clin. Oncol.* **2004**, *22*, 777.

362.   Tian, M.; Ihmels, H.; Brötz, E. "DNA cleavage by the Cu(II) complex of the DNA–intercalating 9–bis(pyridin–2–ylmethyl)aminobenzo[β]quinolizinium" *Dalton Trans.* **2010**, *39*, 8195.

363.   Jiang, Q.; Xiao, N.; Shi, P.; Zhu, Y.; Guo, Z. "Design of artificial metallonucleases with oxidative mechanism" *Coord. Chem. Rev.* **2007**, *251*, 1951.

364. Mitic, N.; Smith, S. J.; Neves, A.; Guddat, L. W.; Gahan, L. R.; Schenk, G. "The catalytic mechanisms of binuclear metallohydrolases" *Chem. Rev.* **2006**, *106*, 3338.

365. Bortolotto, T.; Silva, P. P.; Neves, A.; Pereira–Maia, E. C.; Terenzi, H. "Photoinduced DNA cleavage promoted by two copper(II) complexes of tetracyclines and 1,10–phenanthroline" *Inorg. Chem.* **2011**, *50*, 10519.

366. Goswami, T. K.; Chakravarthi, B. V. S. K.; Roy, M.; Karande, A. A.; Chakravarty, A. R. "Ferrocene–conjugated L–tryptophan copper(II) complexes of phenanthroline bases showing DNA photocleavage activity and cytotoxicity" *Inorg. Chem.* **2011**, *50*, 8452.

367. Tjioe, L.; Meininger, A.; Joshi, T.; Spiccia, L.; Graham, B.; Three, A. "Efficient plasmid DNA cleavage by Copper (II) complexes guanidinium groups" *Inorg. Chem.* **2010**, *50*, 4327.

368. Li, D.–D.; Huang, F.–P.; Chen, G.-J.; Gao, C.–Y.; Tian, J.–L.; Gu, W.; Liu, X.; Yan, S.–P. "Four new copper(II) complexes with 1,3–Tpbd ligand: Synthesis, crystal structures, magnetism, oxidative and hydrolytic cleavage of *pBR322* DNA" *J. Inorg. Biochem.* **2010**, *104*, 431.

369. Hadi, S. M.; Ullah, M. F.; Shamim, U.; Bhatt, S. H.; Azmi, A. S. "Catalytic therapy of cancer by ascorbic acid involves redox cycling of exogenous/endogenous copper ions and generation of reactive oxygen species" *Chemotherapy* **2010**, *56*, 280.

370. Gama, S.; Rodrigues, I.; Marques, F.; Palma, E.; Correia, I.; Carvalho, M. F. N. N.; Pessoa, J. C.; Cruz, A.; Mendo, S.; Santos, I. C.; Mendes, F.; Santos, I.; Paulo, A. "New ternary bipyridine–terpyridine copper(II) complexes as self–activating chemical nucleases" *RSC Adv.* **2014**, *4*, 61363.

371. Lia, K.; Zhoua, L.–H.; Zhanga, J.; Chena, S.–Y.; Zhangb, Z.–W.; Zhanga, J.–J.; Linb, H.–H.; Yu X.–Q. "Self–activating chemical nuclease: Ferrocenyl cyclen Cu(II) complexes act as efficient DNA cleavage reagents in the absence of reductant" *Eur. J. Med. Chem.* **2009**, *44*, 1768.

372. Borah, S.; Melvin, M. S.; Lindquist, N.; Manderville, R. A. "Copper–mediated nuclease activity of a tambjamine alkaloid" *J. Am. Chem. Soc.* **1998**, *120*, 4557.

373. Melvin, M. S.; Tomlinson, J. T.; Saluta, G. R.; Kucera, G. L.; Lindquist, N.; Manderville, R. A. "Double–strand DNA cleavage by copper–prodigiosin" *J. Am. Chem. Soc.* **2000**, *122*, 6333.

374. Roelfes, G.; Branum, M. E.; Wang, L.; Que Jr., L.; Feringa, B. L. "Efficient DNA cleavage with an iron complex without added reductant" *J. Am. Chem. Soc.* **2000**, *122*, 11517.

375. Sissi, C.; Mancin, F.; Gatos, M.; Palumbo, M.; Tecilla, P.; Tonellato, U. "Efficient plasmid DNA cleavage by a mononuclear copper(II) complex" *Inorg. Chem.* **2005**, *44*, 2310.

376. Lamour, E.; Routier, S.; Bernier, J. L.; Catteau, J. P.; Bailly, C.; Vezin, H. "Oxidation of Cu(II) to Cu(III), free radical production, and DNA cleavage by hydroxy–salen–copper complexes. Isomeric effects studied by ESR and electrochemistry" *J. Am. Chem. Soc.* **1999**, *121*, 1862.

377. Tonde, S. S.; Kumbhar, A. S.; Padhye, S. B.; Butcher, R. J. "Self–activating nuclease activity of copper(II) complexes of hydroxyl–rich ligands" *J. Inorg. Biochem.* **2006**, *100*, 51.

378. Maheswari, P. U.; Roy, S.; Den Dulk, H.; Barends, S.; Van Wezel, G.; Kozlevcar,

B.; Gamez, P.; Reedijk, J. "The square–planar cytotoxic [Cu^{II}(pyrimol)Cl] complex acts as an efficient DNA cleaver without reductant" *J. Am. Chem. Soc.* **2006**, *128*, 710.

379. Kellett, A.; O'Connor, M.; McCann, M.; McNamara, M.; Lynch, P.; Rosair, G.; McKee, V.; Creaven, B.; Walsh, M.; McClean, S.; Foltyn, A.; O'Shea, D.; Howe, O.; Devereux, M. "Bis–phenanthroline copper(II) phthalate complexes are potent *in vitro* antitumour agents with self–activating metallo–nuclease and DNA binding properties" *Dalton Trans.* **2011**, *40*, 1024.

380. Li, L.; Du, K.; Wang, Y.; Jia, H.; Hou, X.; Chao, H.; Ji, L. "Self–activating nuclease and anticancer activities of copper(II) complexes with aryl–modified 2,6–di(thiazol–2–yl)pyridine" *Dalton Trans.* **2013**, *42*, 11576.

381. Gallagher, J.; Zelenko, O.; Walts, A. D.; Sigman, D. S. "Protease activity of 1,10–phenanthroline–copper(I). targeted scission of the catalytic site of carbonic anhydrase" *Biochemistry* **1998**, *37*, 2096.

382. Ito, N.; Phillips, S. E. V; Stevens, C.; Ogel, Z. B.; McPherson, M. J.; Keen, J. N.; Yadav, K. D. S.; Knowles, P. F. "Novel thioether bond revealed by a 1.7 Å crystal structure of galactose oxidase" *Nature* **1991**, *350*, 87.

383. Thomson, A. J. "Radical copper in oxidases" *Nature* **1991**, *350*, 22.

384. Lam, K.–Y.; Gortier, D. G.; Sykes, A. G. "Redox reactivity of the tyrosine radical and Fe$^{III}_2$ of the B2 Subunit of *E. coli* ribonucleotide reductase" *Chem. Commun.* **1990**, 1019.

385. Simandi, L. I. "Catalytic activation of dioxygen by metal complexes" Kluwer Academic Publishers, Dordrecht, Boston, London, **1992**.

386. Derek, H. R.; Barton, A. E.; Martell, D. T.; Sawyer, E. "The activation of dioxygen

and homogeneous catalytic oxidation" Plenum Press, New York, **1993**.

387. Simándi, L. I. "Dioxygen activation and homogeneous catalytic oxidation" Elsevier Inc., New York, **1991**.

388. Begley, T. P. "Phenoxazinone synthase: Enzymatic catalysis of an aminophenol oxidative cascade" *J. Am. Chem. Soc.* **1988**, *110*, 3334.

389. Hollstein, U. "Actinomycin chemistry and mechanism of action" *Chem. Rev.* **1973**, *74*, 625.

390. Katz, E.; Weissbach, H. "Biosynthesis of the actinomycin chromophore; enzymatic conversion of 4–methyl–3–hydroxyanthranilic acid to actinocin" *J. Biol. Chem.* **1962**, *237*, 882.

391. Frei, E. "The Clinical use of actinomycin" *Cancer Chemother. Rep.* **1974**, *58*, 49.

392. Panja, A.; Shyamal, M.; Saha, A.; Mandal, T. K. "Methylene bridge regulated geometrical preferences of ligands in cobalt(III) coordination chemistry and phenoxazinone synthase" *Dalton Trans.* **2014**, *43*, 5443.

393. Panja, A. "Exclusive selectivity of multidentate ligands independent on the oxidation state of cobalt: influence of hindrance on dioxygen binding and phenoxazinone synthase activity" *Dalton Trans.* **2014**, *43*, 7760.

394. Panja, A.; Guionneau, P. "The first example of a centro–symmetrical bis(imido)–bridged dinuclear cobalt(III) complex: Synthesis *via* oxidative dehydrogenation and phenoxazinone synthase activity" *Dalton Trans.* **2013**, *42*, 5068.

395. Mukherjee, C.; Weyhermuller, T.; Bothe, E.; Rentschler, E.; Chaudhuri, P. A "Tetracopper(II)–tetraradical cuboidal core and its reactivity as a functional model of phenoxazinone Synthase" *Inorg. Chem.* **2007**, *46*, 9895.

396. Ghosh, K.; Tyagi, N.; Kumar, P.; Singh, U. P.; Goel, N. "Stabilization of Mn(II) and Mn(III) in mononuclear complexes derived from tridentate ligands with N_2O Donors: Synthesis, crystal structure, superoxide dismutase activity and DNA interaction studies" *J. Inorg. Biochem.* **2010**, *104*, 9.

397. Kotschy, A.; Farago, J.; Csámpai, A.; Smith, D. M. "The inverse electron–demand, Diels–Alder reaction in polymer synthesis, Part 5: Preparation and model reactions of some electron–rich bis–dienamines" *Tetrahedron* **2004**, *60*, 3421.

398. Ghosh, K.; Kumar, P.; Mohan, V.; Singh, U. P.; Kasiri, S.; Mandal, S. S. "Nuclease activity *via* self–activation and anticancer activity of a mononuclear copper(II) complex: Novel role of the tertiary butyl group in the ligand frame" *Inorg. Chem.* **2012**, *51*, 3343.

399. Gudasi, K. B.; Patil, S. a.; Vadavi, R. S.; Shenoy, R. V.; Nethaji, M.; Bligh, S. W. A. "Synthesis and spectral investigation of manganese(II), cadmium(II) and oxovanadium(IV) complexes with 2,6–diacetylpyridine bis(2–aminobenzoylhydrazone): Crystal structure of manganese(II) and cadmium(II) complexes" *Inorg. Chim. Acta* **2006**, *359*, 3229.

400. Bosnich, B. "An interpretation of the circular dichroism and electronic spectra of asalicylaldimine complexes of square–coplanar diamagnetic nickel(II)" *J. Am. Chem. Soc.* **1968**, *90*, 627.

401. Rosenthal, M. R. "The myth of the non–coordinating anion" *J. Chem. Educ.* **1973**, *50*, 331.

402. Bosnich, B. "An interpretation of the circular dichroism and electronic spectra of salicylaldimine complexes of square–coplanar diamagnetic nickel(II)" *J. Am. Chem.*

Soc. **1968**, *90*, 627.

403. Glaser, T.; Pawelke, R. H.; Heidemeier, M. Synthesis, "Structure, and spectroscopic properties of a dinuclear $Fe^{III}(\mu_2-O)Fe^{III}$ complex using a strongly electron–donating ligand: Implications for the generation of new high–valent species" *Z. Anorg. Allg. Chem.* **2003**, *629*, 2274.

404. Karpishin, T. B.; Gebhard, M. S.; Solomon, E. I.; Raymond, K. N. "Spectroscopic studies of the electronic structure of iron(III) tris(catecholates)" *J. Am. Chem. Soc.* **1991**, *113*, 2977.

405. Davis, M. I.; Orville, A. M.; Neese, F.; Zaleski, J. M.; Lipscomb, J. D.; Solomon, E. I. "Spectroscopic and electronic structure studies of protocatechuate 3,4–dioxygenase: Nature of tyrosinate–Fe(III) bonds and their contribution to reactivity" *J. Am. Chem. Soc.* **2002**, *124*, 602.

406. Geary, W. J. "The use of conductivity measurements in organic solvents for the characterisation of coordination compounds" *Coord. Chem. Rev.* **1971**, *7*, 81.

407. Costes, J. P.; Dahan, F.; Laurent, J. P. "Structural characterization and magnetic study (EPR and static susceptibility measurements) of a novel ferric spin–crossover complex: Bis(7–amino–4–methyl–5–aza–3–hepten–2–onato(1–))iron(III) tetraphenylborate" *Inorg. Chem.* **1990**, *29*, 2448.

408. Scheidt, W. R.; Geiger, D. K.; Haller, K. J. "Structural characterization of a variable–spin(porphinato)iron(III) complex. Molecular stereochemistry of bis(3–chloropyridine)(octaethylporphinato)iron(III) perchlorate at 98 K ($S = 1/2$) and 293 K ($S = 1/2$, $S = 5/2$)" *J. Am. Chem. Soc.* **1982**, *104*, 495.

409. Katz, B. A.; Strouse, C. E. "Molecular transformations in the solid state

crystallographic resolution of the spin isomers of tris(2–picolylamine)iron(II) dichloride and the structural relationship between the methanol and ethanol solvates" *J. Am. Chem. Soc.* **1979**, *101*, 6214.

410. Haddad, M. S.; Lynch, M. W.; Federer, W. D.; Hendrickson, D. N. "Spin–crossover ferric complexes: Curiosities observed for unperturbed solids" *Inorg. Chem.* **1981**, *20*, 123.

411. Timken, M. D.; Wilson, S. R.; Hendrickson, D. N. "Dynamics of spin–state interconversion and cooperativity for ferric spin–crossover complexes in the solid state. 2. Perturbations of the fast spin–flipping N_4O_2 complex [Fe(SalAPA)$_2$]ClO$_4$" *Inorg. Chem.* **1984**, *23*, 3870.

412. Timken, M. D.; Strouse, C. E.; Soltis, S. M.; Daverio, S. A; Hendrickson, D. N.; Abdel–Mawgoud, A. M.; Wilson, S. R. "Dynamics of spin–state interconversion and cooperativity for ferric spin–crossover complexes in the solid state. 5. Variable–temperature spectroscopic, magnetic, and single–crystal X–ray structural characterizations of the spin–state and order–disorder transformation of a schiff–base complex." *J. Am. Chem. Soc.* **1986**, *108*, 395.

413. Oshio, H.; Toriumi, K.; Maeda, Y.; Takashima, Y. "Temperature–dependent crystallographic studies on ferric spin–crossover complexes with different spin–interconversion rates" *Inorg. Chem.* **1991**, *30*, 4252.

414. Shongwe, M. S.; Al–Rashdi, B. A; Adams, H.; Morris, M. J.; Mikuriya, M.; Hearne, G. R. "Thermally induced two–step, two–site incomplete 6A1<—>2T2 crossover in a mononuclear iron(III) phenolate–pyridyl schiff–base complex: A rare crystallographic observation of the coexistence of pure S=5/2 and 1/2 metal centers in the asymmetric

unit" *Inorg. Chem.* **2007**, *46*, 9558.

415.   Conti, A. J.; Chadba, R. K.; Sena, K. M.; Rheingold, A. L.; J, D. N. H. "Dynamics and phase transitions in spin–crossover complexes: X–ray structures and basic crossover phenomena in the solvate series [Fe(3–OEt–SalAPA)$_2$](ClO$_4$).S" *Inorg. Chem.* **1993**, *32*, 2670.

416.   Hwang, J.; Govindaswamy, K.; Koch, S. A. "The coordination chemistry of amine triphenolate tripod ligands with iron (III) old organic compounds but new tripod ligands the coordination chemistry of new C$_3$ symmetric tripheno– late amine tripod ligands has been demonstrated with". *Chem. Commun.* **1998**, *859*, 1667.

417.   Beckmann, U.; Bill, E.; Weyhermuller, T.; Wieghardt, K. "Exchange interactions and covalency in dinuclear complexes of iron(III) and gallium(III) containing the redox–non innocent ligand 1,2–bis(3,5–di–tert–butyl–2–hydroxyphenyl)oxamide" *Eur. J. Inorg. Chem.* **2003**, 9, 1768.

418.   Desiraju, G. R. "The weak hydrogen bond in structural chemistry and biology" Oxford university press, New York, **1999**.

419.   Lanznaster, M.; Heeg, M. J.; Yee, G. T.; McGarvey, B. R.; Verani, C. N. "Design of molecular scaffolds based on unusual geometries for magnetic modulation of spin– diverse complexes with selective redox response" *Inorg. Chem.* **2007**, *46*, 72.

420.   Low, D. W.; Hill, M. G.; Sciences, G.; Suite, E. G. A. V; Francisco, S. S.; Angeles, L.; August, R. V. "Rational fine–tuning of the redox potentials in chemically synthesized rubredoxins" *J. Am. Chem. Soc.* **1998**, *120*, 11536.

421.   Roy, S.; Maheswari, P. U.; Lutz, M.; Spek, A. L.; Dulk, H. den; Barends, S.; Franti˘, V. P.; Hartlc, S.; Reedijk, J. "DNA cleavage and antitumour activity of platinum(II) and

copper(II) compounds derived from 4–methyl–2–N–(2–pyridylmethyl)aminophenol: Spectroscopic, electrochemical and biological investigation" *Dalton. Trans.* **2009**, 10846.

422. Kang, H. M.; Saltveit, M. E. "Antioxidant enzymes and DPPH–radical scavenging activity in chilled and heat–shocked rice (oryza sativa) seedlings radicles" *J. Agric. Food Chem.* **2002**, *50*, 513.

423. Foti, M. C.; Daquino, C.; Geraci, C. "Electron–transfer reaction of cinnamic acids and their methyl esters with the DPPH radical in alcoholic solutions" *J. Org. Chem.* **2004**, *69*, 2309.

424. Chandrasekara, A.; Shahidi, F. "Inhibitory activities of soluble and bound millet seed phenolics on free radicals and reactive oxygen species" *J. Agric. Food Chem.* **2011**, *59*, 428.

425. Ionita, P. "Is DPPH stable free radical a good scavenger for oxygen Active species ?" *Chem. Pap.* **2005**, *59*, 11.

426. Tyagi, N. "Studies on iron and manganese complexes of polydentate ligands" Thesis, IIT Roorkee, **2010**.

427. Hofslokken, N. U.; Skattebol, L. "Convenient method for the ortho formylation of phenol" *Acta Chem. Scand.* **1999**, *53*, 258.

428. Risch, M. J.; Trucks, G. W.; Schlegel, H. B.; Scuseria, G. E.; Robb, M. A.; Cheeseman, J. R.; Montgomery, J. A., Jr.; Vreven, T.; Kudin, K. N.; Burant, J. C.; Millam, J. M.; Iyengar, S. S.; Tomasi, J.; Barone, V.; Mennucci, B.; Cossi, M.; Scalmani, G.; Re, J. A. "Gaussian 03". Gaussian Inc. Pittsburgh, PA **2007**.

429. Becke, A. D. "Density–functional thermochemistry I. The role of exact exchange –

only gradient correction" *J. Chem. Phys.* **1992**, *96*, 2155.

430. Becke, A. D. "Density–functional thermochemistry III. The role of exact exchange" *J. Chem. Phys.* **1993**, *98*, 5648.

431. Wu, A. J.; Penner–Hahn, J. E.; Pecoraro, V. L. "Structural, spectroscopic, and reactivity models for the manganese catalases" *Chem. Rev.* **2004**, *104*, 903.

432. Kaizer, J.; Baráth, G.; Pap, J.; Speier, G.; Giorgi, M.; Réglier, M. "Manganese and iron flavonolates as flavonol 2,4–dioxygenase mimics" *Chem. Commun.* **2007**, *351*, 5235.

433. Watanabe, Y.; Namba, A.; Umezawa, N.; Kawahata, M.; Yamaguchi, K.; Higuchi, T. "Enhanced catalase–like activity of manganese salen complexes in water: Effect of a three–dimensionally fixed auxiliary" *Chem. Commun.* **2006**, 4958.

434. Levanon, H.; Norris, J. R. "Transition–metal–catalyzed epoxidations" *Chem. Rev.* **1989**, *89*, 419.

435. Gunter, M. J.; Turner, P. "Metalloporphyrins as models for the cytochromes P–450" *Coord. Chem. Rev.* **1991**, *108*, 8545.

436. Magnets, S.; Gatteschi, D.; Sessoli, R. "Quantum tunneling of magnetization and related phenomena in molecular materials" *Angew. Chem. Int. Ed.* **2003**, *42*, 268.

437. Kono, Y.; Fridovich, I. "Isolation and characterization of the pseudocatalase of *Lactobacillus plantarum*" *J. Biol. Chem.* **1983**, *258*, 6015.

438. Jr, W. F. B.; Fridovich, I. "Pseudocatalase from *Lactobacillus plantarum*: Evidence for a homopentameric structure containing two atoms of manganese per subunit" *Biochemistry* **1985**, *24*, 6460.

439. V. V. Barynin, A. A. Vagin, W. R.Melik–Adamyan, A. I. Grebenko, S. V.

References

Khangulov, A. N. Popov, M. E. Andrianova and B. K. Vainshtein, D. A. N. "The three–dimensional structure of the di–MN catalase and rile environment of the di–MN sites in different redox states" *J. Inorg. Biochem.* **1986**, *288*, 877.

440. Mukhopadhyay, S.; Mandal, S. K.; Bhaduri, S.; Armstrong, W. H. "Manganese clusters with relevance to photosystem II". *Chem. Rev.* **2004**, *104*, 3981.

441. Allgood, G. S.; Perry, J. J. "Characterization of a manganese–containing catalase from the obligate *Thermophile thermoleophilum* album" *J. Bacteriol.* **1986**, *168*, 563.

442. Tsutomu, K. "Catalytic asymmetric oxidations using optically active (salen)manganese(III) complexes as catalysts" *Coord. Chem. Rev.* **1995**, *140*, 189.

443. Moutet, J.–C.; Ourari, A. "Electrocatalytic epoxidation and oxidation with dioxygen using manganese(III) schiff–base complexes" *Electrochim. Acta* **1997**, *42*, 2525.

444. Moutet, J.; Ouennoughi, Y.; Ourari, A.; Hamar–Thibault, S. "Electrocatalytic hydrogenation on noble metal particles dispersed in polymer films. Enhanced catalytic activity induced by the incorporation of bimetallic catalytst" *Electrochim. Acta* **1995**, *40*, 1827.

445. Anjos, A.; Bortoluzzi, A. J.; Caro, M. S. B.; Peralta, R. A. "New phenoxyl radical complexes of manganese, gallium, indium and iron based on an H$_2$bbpen ligand derivative" *J. Braz. Chem. Soc.* **2006**, *17*, 1540.

446. Dehkordi, M. N.; Bordbar, A.–K.; Lincoln, P.; Mirkhani, V. "Spectroscopic study on the interaction of CT–DNA with manganese salen complex containing triphenyl phosphonium groups" *Spectrochim. Acta. Part A.* **2012**, *90*, 50.

447. Abdel Aziz, A. A. "Microwave–assisted synthesis of Mn(II), Co(II), Ni(II), Cu(II), and Zn(II) complexes of tridentate schiff base N–(2–hydroxyphenyl) 2–hydroxy–5–

bromobenzaldimine: Characterization, DNA interaction, antioxidant, and *in vitro* antimicrobial studies" *Synth. React. Inorg. Met. Org. Chem.* **2013**, *44*, 1137.

448. Peng, B.; Zhou, W.–H.; Yan, L.; Liu, H.–W.; Zhu, L. "DNA–binding and cleavage studies of chiral Mn(III) salen complexes" *Trans. Met. Chem.* **2009**, *34*, 231.

449. Ansari, K. I.; Grant, J. D.; Kasiri, S.; Woldemariam, G.; Shrestha, B.; Mandal, S. S. "Manganese(III)–salens induce tumor selective apoptosis in human cells" *J. Inorg. Biochem.* **2009**, *103*, 818.

450. Khan, N.–U. H.; Pandya, N.; Kumar, M.; Bera, P. K.; Kureshy, R. I.; Abdi, S. H. R.; Bajaj, H. C. "Influence of chirality using Mn(III) salen complexes on DNA binding and antioxidant activity" *Org. Biomol. Chem.* **2010**, *8*, 4297.

451. Kurahashi, T.; Fujii, H. "Chiral distortion in a Mn(IV)(salen)(N$_3$)$_2$ derived from Jacobsen's catalyst as a possible conformation model for its enantioselective reactions" *Inorg. Chem.* **2008**, *47*, 7556.

452. Guedes, D. F. C.; Leod, T. C. O. Mac; Gotardo, M. C. A. F.; Schiavon, M. A.; Yoshida, I. V. P.; Ciuffi, K. J.; Assis, M. D. "Investigation of a new oxidative catalytic system involving Jacobsen's catalyst in the absence of organic solvents" *Appl. Catal. A* **2005**, *296*, 120.

453. Canali, L.; Sherrington, D. C. "Utilisation of homogeneous and supported chiral metal(salen) complexes in asymmetric catalysis" *Chem. Soc. Rev.* **1999**, *28*, 85.

454. Bonadies, J. A.; Maroney, M. J.; Pecorar, V. L. "Structurally diverse manganese(III) schiff base complexes: Solution speciation via paramagnetic ^{1}H NMR spectroscopy and electrochemistry" *Inorg. Chem.* **1989**, *11*, 2044.

455. González–Riopedre, G.; Bermejo, M. R.; Fernández–García, M. I.; González–Noya,

A. M.; Pedrido, R.; Rodríguez–Doutón, M. J.; Maneiro, M. "Alkali–Metal–ion–directed self–assembly of redox–active manganese(III) supramolecular boxes" *Inorg. Chem.* **2015**, *54*, 2512.

456. Bedrtoncello, K.; Fallon, G. D.; Murray, K. S.; Tiekink, E. R. T. " Manganese(III) complexes of a binucleating schiff–base ligand based on 1,3–diaminopropan–2–ol backbone" *Inorg. Chem.* **1991**, *30*, 1.

457. Larson, E.; Lah, M. S.; Li, X.; Bonadies, J. A; Pecoraro, V. L. "Manganese manganese separations in oxide– and alkoxide–bridged complexes: Correlation of structure with ligand" *Inorg. Chem.* **1992**, *31*, 373.

458. Bhargavi, G.; Rajasekharan, M. V; Tuchagues, J. P. "Antiferromagnetic interactions through phenoxo bridges and lattice water: Synthesis, structure, and magnetic properties of new Mn(III) schiff base complexes in combination with thiocyanate ligand" *Inorg. Chim. Acta* **2009**, *362*, 3247.

459. Maneiroa, M.; Bermejoa, M. R.; Sousaa, A; Fondoa, M.; Gonzáleza, A. M.; Sousa–Pedraresa, A.; McAuliffe, C. A. "Synthesis and structural characterisation of new manganese (II) and (III) complexes. Study of their photolytic and catalase activity and X–ray crystal structure of [Mn(3–OMe,5–Br–Salpn)(EtOH)(H$_2$O)]ClO$_4$" *Polyhedron* **2000**, *19*, 47.

460. Bhargavi, G.; Rajasekharan, M. V.; Costes, J. P.; Tuchagues, J. P. "Synthesis, crystal structure and magnetic properties of dimeric mn^{III} schiff base complexes including pseudohalide ligands: Ferromagnetic interactions through phenoxo bridges and single molecule magnetism" *Polyhedron* **2009**, *28*, 1253.

461. Daier, V.; Moreno, D.; Duhayon, C.; Tuchagues, J.; Signorella, S. "Synthesis,

characterization and combined superoxide dismutase and catalase activities of manganese complexes of 1,4-bis(salicylidenamino)butan-2-ol" *Eur. J. Inorg. Chem.* **2010**, 965.

462. Itoh, S.; Taki, M.; Kumei, H.; Takayama, S.; Nagatomo, S.; Kitagawa, T.; Sakurada, N.; Arakawa, R.; Fukuzumi, S. "Model complexes for the active form of galactose oxidase. Physicochemical properties of Cu(II)– and Zn(II)–phenoxyl radical complexes" *Inorg. Chem.* **2000**, *39*, 3708.

463. Altwicker, E. R. "The chemistry of stable phenoxy radicals" *Chem. Rev.* **1967**, *67*, 475.

464. Kurahashi, T.; Kikuchi, A.; Tosha, T.; Shiro, Y.; Kitagawa, T.; Fujii, H. "Transient intermediates from Mn(salen) with sterically hindered mesityl groups: Interconversion between Mn^{IV}–phenolate and Mn^{III}–phenoxyl radicals as an origin for unique reactivity" *Inorg. Chem.* **2008**, *47*, 1674.

465. Kurahashi, T.; Kobayashi, Y.; Nagatomo, S.; Tosha, T.; Kitagawa, T.; Fujii, H. "Oxidizing intermediates from the sterically hindered iron salen complexes related to the oxygen activation by nonheme iron enzymes" *Inorg. Chem.* **2005**, *44*, 8156.

466. Chaudhuri, P.; Wieghardt, K. "Phenoxyl radical complexes" *Prog. Inorg. Chem.* John Wiley and sons, inc., **2002**.

467. Law, N.; Caudle, M. T.; Pecoraro, V. L. "Manganese Redox Enzymes and Model Systems: Properties, Structures, and Reactivity" Adv. Inorg. Chem. **1998**, *46*, 305.

468. Mullins, C. S.; Pecoraro, V. L. "Reflections on small molecule manganese models that seek to mimic photosynthetic water oxidation chemistry" *Coord. Chem. Rev.* **2008**, *252*, 416.

469. Pradeep, C. P.; Zacharias, P. S.; Das, S. K. "Synthesis, structural characterization and properties of an optically active mononuclear Mn(IV) complex" *Polyhedron* **2005**, *24*, 1410.

470. Umena, Y.; Kawakami, K.; Shen, J.–R.; Kamiya, N. "Crystal structure of oxygen–evolving photosystemII at a resolution of 1.9 Å" *Nature* **2011**, *473*, 55.

471. McEvoy, J. P.; Brudvig, G. W. "Water–splitting chemistry of photosystem II". *Chem. Rev.* **2006**, *106*, 4455.

472. Oliw, E. H.; Jernerén, F.; Hoffmann, I.; Sahlin, M.; Garscha, U. "Manganese lipoxygenase oxidizes bis–allylic hydroperoxides and octadecenoic acids by different mechanisms" *Biochim. Biophys. Acta.* **2011**, *1811*, 138.

473. Reaction, L.; Hamberg, M.; Su, C.; Oliw, E. "Manganese lipoxygenase, discovery of a bis–allylic hydroperoxide as product and intermediate in a lipoxygenase reaction" *Biochemistry* **1998**, *273*, 13080.

474. Su, C. "Kinetics of manganese lipoxygenase with a catalytic mononuclear redox center" *J. Biol. Chem.* **2000**, *275*, 18830.

475. Goldsmith, C. R.; Cole, A. P.; Stack, T. D. P. "C–H activation by a mononuclear manganese(III) hydroxide complex: Synthesis and characterization of a manganese–lipoxygenase mimic?" *J. Am. Chem. Soc.* **2005**, *127*, 9904.

476. Jackson, T. A; Brunold, T. C. "Combined spectroscopic/computational studies on Fe– and Mn–dependent superoxide dismutases: Insights into second–sphere tuning of active site properties" *Acc. Chem. Res.* **2004**, *37*, 461.

477. Miller, A.–F. "Redox tuning over almost 1 V in a structurally conserved active site: Lessons from Fe–containing superoxide dismutase" *Acc. Chem. Res.* **2008**, *41*, 501.

478. Vance, C. K.; Miller, A. F. "Novel insights into the basis for *Escherichia coli* superoxide dismutase's metal ion specificity from Mn–Substituted FeSOD and its very high Em" *Biochemistry* **2001**, *40*, 13079.

479. Bull, C.; Niederboffer, E. C.; Tatsuro Yoshida, L.; Fee, J. A. "Kinetic studies of superoxide dismutases: Properties of the manganese–containing protein from *Thermus thermophihs*" *J. Am. Chem. Soc.* **1991**, *113*, 4069.

480. Boal, A. K.; Jr., J. A. C.; Stubbe, J.; Rosenzweig, A. C. "Structural basis for activation of class Ib ribonucleotide reductase" *Science* **2010**, *329*, 1526.

481. Maneiro, M.; Bermejo, M. R.; Isabel Fernández, M.; Gómez–Fórneas, E.; González–Noya, A. M.; Tyryshkin, A. M. "A new type of manganese–schiff base complex, catalysts for the disproportionation of hydrogen peroxide as peroxidase mimics" *New J. Chem.* **2003**, *27*, 727.

482. Bermejo, M. R.; Fernández, M. I.; González–Noya, A. M.; Maneiro, M.; Pedrido, R.; Rodríguez, M. J.; García–Monteagudo, J. C.; Donnadieu, B. "Novel peroxidase mimics: μ–aqua manganese–schiff base dimers" *J. Inorg. Biochem.* **2006**, *100*, 1470.

483. Niu, S.; Zhao, M.; Hu, L.; Zhang, S. "Carbon nanotube–enhanced DNA biosensor for DNA hybridization detection using rutin–Mn as electrochemical indicator". *Sens. Actuators, B Chem.* **2008**, *135*, 200.

484. Ivanovicburmazovic, I. "Catalytic dismutation *vs.* reversible binding of superoxide" *Adv. Inorg. Chem.* **2008**, *60*, 59.

485. Rebouças, J. S.; Spasojević, I.; Batinić–Haberle, I. "Pure manganese(III) 5,10,15,20–tetrakis(4–benzoicacid)porphyrin (MnTBAP) is not a superoxide dismutase mimic in aqueous systems: A case of structure–activity relationship as a watchdog mechanism in

experimental therapeutics and biology" *J. Biol. Inorg. Chem.* **2008**, *13*, 289.

486. Groni, S.; Blain, G.; Policar, C.; Anxolabe, E. "Reactivity of Mn(II) with superoxide. Evidence for a [Mn^{III}OO]$^+$ unit by low–temperature spectroscopies. *Inorg. Chem.* **2007**, *46*, 1951.

487. Liu, G.–F.; Dürr, K.; Puchta, R.; Heinemann, F. W.; van Eldik, R.; Ivanović–Burmazović, I. "Chelate electronic properties control the redox behaviour and superoxide reactivity of seven–coordinate manganese(II) complexes" *Dalton Trans.* **2009**, 6292.

488. Sjödin, M.; Gätjens, J.; Tabares, L. C.; Thuéry, P.; Pecoraro, V. L.; Un, S. "Tuning the redox properties of manganese(II) and its implications to the electrochemistry of manganese and iron superoxide dismutases" *Inorg. Chem.* **2008**, *47*, 2897.

489. Eckshtain, M.; Zilbermann, I.; Mahammed, A.; Saltsman, I.; Okun, Z.; Maimon, E.; Cohen, H.; Meyerstein, D.; Gross, Z. "Superoxide dismutase activity of corrole metal complexes" *Dalton Trans.* **2009**, 7879.

490. Cisnetti, F.; Lefèvre, A.–S.; Guillot, R.; Lambert, F.; Blain, G.; Anxolabéhère–Mallart, E.; Policar, C. "A new pentadentate ligand forms both a di– and a mononuclear mnii complex: Electrochemical, spectroscopic and superoxide dismutase activity studies" *Eur. J. Inorg. Chem.* **2007**, *2007*, 4472.

491. Prousek, J. "Fenton chemistry in biology and medicine" *Pure Appl. Chem.* **2007**, *79*, 2325.

492. Daly, M. J.; Gaidamakova, E. K.; Matrosova, V. Y.; Vasilenko, A; Zhai, M.; Venkateswaran, A; Hess, M.; Omelchenko, M. V; Kostandarithes, H. M.; Makarova, K. S.; Wackett, L. P.; Fredrickson, J. K.; Ghosal, D. "Accumulation of Mn(II) in

deinococcus radiodurans facilitates gamma–radiation resistance" *Science* **2004**, *306*, 1025.

493. Jiang, W.; Han, Y.; Pan, Q.; Shen, T.; Liu, C. "Roles of exogenous divalent metals in the nucleolytic activity of Cu, Zn superoxide dismutase" *J. Inorg. Biochem.* **2007**, *101*, 667.

494. Devereux, M.; O Shea, D.; Kellett, A.; McCann, M.; Walsh, M.; Egan, D.; Deegan, C.; Kedziora, K.; Rosair, G.; Müller–Bunz, H. "Synthesis, x–ray crystal structures and biomimetic and anticancer activities of novel copper(II)benzoate complexes incorporating 2–(4′–thiazolyl)benzimidazole (thiabendazole), 2–(2–pyridyl)benzimidazole and 1,10–phenanthroline as chelating nitrogen donor" *J. Inorg. Biochem.* **2007**, *101*, 881.

495. Groni, S.; Hureau, C.; Guillot, R.; Blondin, G.; Blain, G.; Anxolabéhère–Mallart, E. "Characterizations of chloro and aqua Mn(II) mononuclear complexes with amino–pyridine ligands. Comparison of their electrochemical properties with those of Fe(II) counterparts" *Inorg. Chem.* **2008**, *47*, 11783.

496. Pap, J. S.; Kripli, B.; Váradi, T.; Giorgi, M.; Kaizer, J.; Speier, G. "Comparison of the SOD–like activity of hexacoordinate Mn(II), Fe(II) and Ni(II) complexes having isoindoline–based ligands" *J. Inorg. Biochem.* **2011**, *105*, 911.

497. Ghosh, K.; Tyagi, N.; Kumar, P. "Role of carboxamido nitrogen in mononuclear manganese complex: Superoxide scavenging activity and nuclease activity" *Inorg. Chem. Commun.* **2010**, *13*, 380.

498. Wu, H.; Yuan, J.; Bai, Y.; Wang, H.; Pan, G.; Kong, J. A. "Seven–coordinated manganese(II) complex with v–shaped ligand bis(N–benzylbenzimidazol–2–

ylmethyl)benzylamine: Synthesis, structure, DNA–binding properties and antioxidant activities" *J. Photochem. Photobiol. B.* **2012**, *116*, 13.

499. Bergamo, A.; Sava, G. "Ruthenium complexes can target determinants of tumour malignancy" *Dalton Trans.* **2007**,*13*, 1267.

500. Dyson, P. J.; Sava, G. "Metal–based antitumour drugs in the post genomic era" *Dalton Trans.* **2006**, *16*, 1929.

501. Liu, H. K.; Berners–Price, S. J.; Wang, F. Y.; Parkinson, J. A.; Xu, J. J.; Bella, J.; Sadler, P. J. "Diversity in guanine–selective DNA binding modes for an organometallic ruthenium arene complex" *Angew. Chem–Int. Ed.* **2006**, *45*, 8153.

502. Pacor, S.; Zorzet, S.; Cocchietto, M.; Bacac, M.; Vadori, M.; Turrin, C.; Gava, B.; Castellarin, A.; Sava, G. "Intratumoral NAMI–A treatment triggers metastasis reduction, which correlates to CD44 regulation and tumor infiltrating lymphocyte recruitment" *J. Pharmacol. Exp. Ther.* **2004**, *310*, 737.

503. Sava, G.; Capozzi, I.; Clerici, K.; Gagliardi, G.; Alessio, E.; Mestroni, G. "Pharmacological control of lung metastases of solid tumours by a novel ruthenium complex" *Clin. Exp. Metastasis* **1998**, *16*, 371.

504. Mohan V. "Studies on chemistry of some polydentate ligands and their metal complexes" Thesis IIT Roorkee **2014**.

505. Zhou, D.–F.; Chen, Q.–Y.; Qi, Y.; Fu, H.–J.; Li, Z.; Zhao, K.–D.; Gao, J. "Anticancer activity, attenuation on the absorption of calcium in mitochondria, and catalase activity for manganese complexes of N–substituted di(picolyl)amine" *Inorg. Chem.* **2011**, *50*, 6929.

506. Zampakou, M.; Rizeq, N.; Tangoulis, V.; Papadopoulos, A. N.; Perdih, F.; Turel, I.;

References

Psomas, G. "Manganese(II) complexes with the non–steroidal anti–inflammatory drug tolfenamic acid: Structure and biological perspectives" *Inorg. Chem.* **2014**, *53*, 2040.

507. Ghosh, K.; Tyagi, N.; Dhara, K. A.; Singh, U. P. "Spontaneous reduction of mononuclear high–spin iron(III) complexes to mononuclear low–spin iron(II) complexes in aqueous media and nuclease activity *via* self–activation" *Chem.Asian J.* **2015**, *10*, 350.

508. Tang, J.; Si, S.; Wang, L.; Liao, D.; Jiang, Z.; Yan, S.; Cheng, P.; Liu, X. "Binuclear complexes of macrocyclic oxamide M(II)–Cu(II) (M=Cu, Ni, Mn): Synthesis, crystal structure and magnetic properties" *Inorg. Chim. Acta* **2003**, *343*, 288.

509. Karastogianni, S.; Dendrinou–Samara, C.; Ioannou, E.; Raptopoulou, C. P.; Hadjipavlou–Litina, D.; Girousi, S. "Synthesis, characterization, DNA binding properties and antioxidant activity of a manganese(II) complex with NO_6 chromophore" *J. Inorg. Biochem.* **2013**, *118*, 48.

510. Guilherme, L. R.; Drechsel, S. M.; Tavares, F.; da Cunha, C. J.; Castaman, S. T.; Nakagaki, S.; Vencato, I.; Bortoluzzi, A. J. "Synthesis, structural characterization, catalase–like function and epoxidation activity of a mononuclear manganese(II) complex" *J. Mol. Catal. A: Chem.* **2007**, *269*, 22.

511. Kaizer, J.; Csay, T.; Kovári, P.; Speier, G.; Párkányi, L. "Catalase mimics of a manganese(II) complex: The effect of axial ligands and pH" *J. Mol. Catal. A Chem.* **2008**, *280*, 203.

512. Singh, A.; Bharty, M. K.; Kushawaha, S. K.; Butcher, R. J.; Singh, N. K. "A seven membered chelate ring complex of Mn(II) derived from bis(5–phenyl–2H–1,2,4–triazole)–3–yl–disulfane and cleavage of the S–S bond in a Co(II) complex: Synthesis,

spectral and structural characterization" *Polyhedron* **2011**, *30*, 1927.

513. Pouralimardan, O.; Chamayou, A.–C.; Janiak, C.; Hosseini–Monfared, H. "Hydrazone schiff base–manganese(II) complexes: Synthesis, crystal structure and catalytic reactivity" *Inorg. Chim. Acta* **2007**, *360*, 1599.

514. Roberts, M. N.; Nagle, J. K.; Finden, J. G.; Branda, N. R.; Wolf, M. O. "Linker–dependent metal–sensitized photoswitching of dithienylethenes" *Inorg. Chem.* **2009**, *48*, 19.

515. Li, Y.–P.; Yang, P. "Synthesis, crystal structure and nuclease activity of a new Mn(II) complex involving 2–(2–1H–imidazolyl)–1H–imdazolium ligand" *Inorg. Chem. Commun.* **2011**, *14*, 545.

516. Cramer, C. J. "Essentials of Computational Chemistry: Theories and Models" 2nd ed., Wiley, England, **2004**.

517. Koch, W.; Holthausen, M. C. "A Chemist's Guide to Density Functional Theory" 2nd ed.; Wiley, New York **2001**.

518. Tysoe, S.; Morgan, R. "Spectroscopic investigation of differential binding modes of. Δ–And. Δ –Ru (bpy) $_2$ (ppz)$^{2+}$ with calf thymus DNA" *J. Phys.Chem.* **1993**, *2*, 1707.

519. Wolfe, A; Shimer, G. H.; Meehan, T. "Polycyclic aromatic hydrocarbons physically intercalate into duplex regions of denatured DNA" *Biochemistry* **1987**, *26*, 6392.

520. Dimitrakopoulou, A.; Dendrinou–Samara, C.; Pantazaki, A. A.; Alexiou, M.; Nordlander, E.; Kessissoglou, D. P. "Synthesis, structure and interactions with DNA of novel tetranuclear, [Mn$_4$(II/II/II/IV)] mixed valence complexes" *J. Inorg. Biochem.* **2008**, *102*, 618.

521. Tarushi, A.; Psomas, G.; Raptopoulou, C. P.; Kessissoglou, D. P. "Zinc complexes

of the antibacterial drug oxolinic acid: Structure and DNA–binding properties" *J. Inorg. Biochem.* **2009**, *103*, 898.

522.   Kumar, P.; Gorai, S.; Santra, M. K.; Mondal, B.; Manna, D. "DNA binding, nuclease activity and cytotoxicity studies of Cu(II) complexes of tridentate ligands" *Dalton Trans.* **2012**, *41*, 7573.

523.   Picard–Jean, F.; Bougie, I.; Bisaillon, M. "Characterization of the DNA– and dNTP– binding activities of the human cytomegalovirus DNA polymerase catalytic subunit UL54" *Biochem. J.* **2007**, *407*, 331.

524.   Velusamy, M.; Mayilmurugan, R.; Palaniandavar, M. "Functional models for catechol dioxygenases: Iron(III) complexes of cis–facially coordinating linear 3N ligands" *J. Inorg. Biochem.* **2005**, *99*, 1032.

525.   Visvaganesan, K.; Mayilmurugan, R.; Suresh, E.; Palaniandavar, M. "Iron(III) complexes of tridentate 3N ligands as functional models for catechol dioxygenases: The role of ligand N–alkyl substitution and solvent on reaction rate and product selectivity" *Inorg. Chem.* **2007**, *46*, 10294.

526.   Kripli, B.; Baráth, G.; Balogh–Hergovich, É.; Giorgi, M.; Simaan, A. J.; Párkányi, L.; Pap, J. S.; Kaizer, J.; Speier, G. "Correlation between the SOD–like activity of hexacoordinate iron(II) complexes and their Fe^{3+}/Fe^{2+} redox potentials" *Inorg. Chem. Commun.* **2011**, *14*, 205.

527.   Benhamou, L.; Lachkar, M.; Mandon, D.; Welter, R. "The preparation and full characterization of dichloroferrous complexes of mono–, bis– and tris–alpha–methyl substituted tris(2–pyridylmethyl)amine (TPA) ligands. Structural bases of stability of the complexes in solution" *Dalton Trans.* **2008**, 6996.

528. Kumar, S.; Mandon, D. "Versatile coordination mode of a new pyridine–based ditopic ligand with transition metals: From regular pyridine to alkyne and alkenyl bindings and indolizinium formation" *Inorg. Chem.* **2015**, *54*, 7481.

529. Mandon, D.; Nopper, A.; Litrol, T.; Goetz, S.; Organome, L. D. "Tridentate coordination of monosubstituted derivatives of the tris(2–pyridylmethyl)amine ligand to FeCl$_3$: Structures and spectroscopic properties of ((2–bromopyridyl)methyl)bis– (2–pyridylmethyl)amine Fe^{III}Cl$_3$ and (((2–*p*– methoxyphenyl)pyridyl)methyl)bis(2–pyridyl– methyl)]amine Fe^{III}Cl$_3$ and comparison with the bis(2–pyridylmethyl)]amine Fe^{III}Cl$_3$ complex" *Inorg. Chem.* **2001**, *40*, 4803.

530. Kojima, T.; Leising, R. a; Yan, S.; Que, L. "Alkane functionalization at nonheme iron centers . Stoichiometric transfer of metal–bound ligands to alkane" *J. Am. Chem. Soc.* **1993**, *115*, 11328.

531. Hitomi, Y.; Arakawa, K.; Funabiki, T.; Kodera, M. "An iron(III)–monoamidate complex catalyst for selective hydroxylation of alkane C–H bonds with hydrogen peroxide" *Angew. Chem. Int. Ed.* **2012**, *51*, 3448.

532. Roelfes, G.; Lubben, M.; Hage, R.; Que, Lawrence, J.; Feringa, B. L. "Catalytic oxidation with a non–heme iron complex that generates a low–spin Fe^{III}OOH intermediate" *Chem. Eur. J.* **2000**, *6*, 2152.

533. Hoselton, M. A.; Wilson, L. J.; Drago, R. S. "Substituent effects on the spin equilibrium observed with hexadentate ligands on iron(II)" *J. Am. Chem. Soc.* **1975**, *97,* 1722.

534. Seredyuk, M.; Gaspar, A. B.; Ksenofontov, V.; Galyametdinov, Y.; Kusz, J.; Gütlich, P. "Iron(II) metallomesogens exhibiting coupled spin state and liquid crystal

phase transitions near room temperature" *Adv. Funct. Mater.* **2008**, *18*, 2089.

535.   Bowman, A. C.; Milsmann, C.; Bill, E.; Turner, R.; Lobkovsky, E.; Debeer, S.; Wieghardt, K.; Chirik, P. J. "Synthesis and electronic structure determination of N–alkyl–substituted bi(imino)pyridine iron imides exhibiting spin crossover behavior" **2011**, *88*, 17353.

536.   O'Reilly, R. K.; Gibson, V. C.; White, A. J. P.; Williams, D. J. "Five–coordinate iron(II) complexes bearing tridentate nitrogen donor ligands as catalysts for atom transfer radical polymerisation" *Polyhedron* **2004**, *23*, 2921.

537.   Hoyt, J. M.; Schmidt, V. A.; Tondreau, A. M.; Chirik, P. J. "Iron–catalyzed intermolecular [2+2] cycloadditions of unactivated alkenes" *Science.* **2013**, *349*, 960.

538.   Schmidt, V. A.; Hoyt, J. M.; Margulieux, G. W.; Chirik, P. J. "Cobalt–catalyzed [2π + 2π] cycloadditions of alkenes: Scope, mechanism, and elucidation of electronic structure of catalytic intermediates" *J. Am. Chem. Soc.* **2015**, *137*, 7903.

539.   Margulieux, G. W.; Turner, Z. R.; Chirik, P. J. "Synthesis and ligand modification chemistry of a molybdenum dinitrogen complex: Redox and chemical activity of a bis(imino)pyridine ligand" *Angew. Chem. Int. Ed.* **2014**, *53*, 14211.

540.   Atienza, C. C. H.; Diao, T.; Weller, K. J.; Nye, S. A.; Lewis, K. M.; Delis, J. G. P.; Boyer, J. L.; Roy, A. K.; Chirik, P. J. "Bis(imino)pyridine cobalt–catalyzed dehydrogenative silylation of alkenes: Scope, mechanism, and origins of selective allylsilane formation" *J. Am. Chem. Soc.* **2014**, *136*, 12108.

541.   Milsmann, C.; Semproni, S. P.; Chirik, P. J. "N–N bond cleavage of 1,2–diarylhydrazines and N–H bond formation *via* H–atom transfer in vanadium complexes supported by a redox–active ligand" *J. Am. Chem. Soc.* **2014**, *136*, 12099.

542. Ghosh, K.; Kumar, P.; Mohan, V.; Singh, U. P. "Self–activated DNA cleavage and nitric oxide reactivity studies on mononuclear copper complexes derived from tetradentate ligands" *Inorg. Chem. Commun.* **2012**, *15*, 56.

543. Ghosh, K.; Kumar, P.; Tyagi, N.; Singh, U. P. "Novel diphenoxo–bridged dinuclear zinc complexes: Generation of phenoxyl–radical species and nuclease activity" *Inorg. Chem.* **2010**, *49*, 7614.

544. Ghosh, K.; Kumar, P.; Tyagi, N.; Singh, U. P.; Aggarwal, V.; Baratto, M. C. "Synthesis and reactivity studies on new copper(II) complexes: DNA binding, generation of phenoxyl radical, SOD and nuclease activities" *Eur. J. Med. Chem.* **2010**, *45*, 3770.

545. Ghosh, K.; Kumar, P.; Tyagi, N.; Singh, U. P.; Goel, N.; Chakraborty, A.; Roy, P.; Baratto, M. C. "DNA interaction, superoxide scavenging and cytotoxicity studies on new copper(II) Complexes derived from a tridentate ligand" *Polyhedron* **2011**, *30*, 2667.

546. Ghosh, K.; Kumar, P.; Tyagi, N.; Singh, U. P.; Goel, N. "Synthesis, structural characterization and DNA interaction studies on a mononuclear copper complex: Nuclease activity *via* self–activation" *Inorg. Chem. Commun.* **2011**, *14*, 489.

547. Ghosh, K.; Kumar, P.; Tyagi, N. "Synthesis, crystal structure and DNA interaction studies on mononuclear zinc complexes" *Inorg. Chim. Acta* **2011**, *375*, 77.

548. Ghosh, K.; Mohan, V.; Kumar, P.; Singh, U. P. "DNA Binding, nuclease and superoxide scavenging activity studies on mononuclear cobalt complexes derived from tridentate ligands" *Polyhedron* **2013**, *49*, 167.

549. Ghosh, K.; Tyagi, N.; Kumar, P.; Singh, U. P. "Synthesis , structure , redox

properties and DNA interaction studies on mononuclear iron (III) complexes with amidate ligand" *Inorg. Chim. Acta* **2014**, *412*, 20.

550. Ghosh, K.; Tyagi, N.; Kumar, H.; Rathi, S. "DNA interaction, SOD, peroxidase and nuclease activity studies of iron complex having ligand with carboxamido nitrogen donors" *Spectrochim. Acta, Part A* **2015**, *146*, 292.

551. Tyagi, N.; Chakraborty, A.; Singh, U. P.; Roy, P.; Ghosh, K. "Mononuclear iron(III) complexes of tridentate ligands with efficient nuclease activity and Studies of their cytotoxicity" *Org. Biomol. Chem.* **2015**, *13*, 11445.

552. Patra, A. K.; Olmstead, M. M.; Mascharak, P. K. "Spontaneous reduction of a low–spin Fe(III) complex of a neutral pentadentate N_5 schiff base ligand to the corresponding Fe(II) species in acetonitrile" *Inorg. Chem.* **2002**, *41*, 5403.

553. Nakamoto, K. "In infrared and raman spectra of inorganic and coordination compounds" 6th ed. Wiley, NewYork **1978**.

554. Sreekanth, A.; Kurup, M. R. P. "Synthesis, EPR and mössbauer spectral studies of new iron(III) complexes with 2–benzoylpyridine–N(4), N(4)–(butane–1,4–diyl) thiosemicarbazone (HBpypTsc): X–ray structure of $[Fe(BpypTsc)_2]FeCl_4 \cdot 2H_2O$ and the free ligand" *Polyhedron* **2004**, *23*, 969.

555. Sarkar, T.; Banerjee, S.; Hussain, A. "Significant photocytotoxic effect of an iron(III) complex of a schiff base ligand derived from vitamin B_6 and thiosemicarbazide in visible light" *RSC Adv.* **2015**, *5*, 29276.

556. Geary, W. J. "The use of conductivity measurements in organic solvents" *Coord. Chem. Rev.* **1970**, *7*, 81.

557. Cotton, S. A. "Some aspects of the coordination chemistry of iron(III)" *Coord.*

Chem. Rev. **1972**, *8*, 185.

558. Tao, X.; Stephan, D. W.; Mascharak P. K. "Synthetic analogue approach to metallobleomycins. 2. Synthesis, structure, and properties of the low–spin iron(III) complex of N–(2–(4–imidazolyl)ethyl)pyridine–2–carboxamide" *Inorg. Chem.* **1987**, *26*, 754.

559. Koch, W.; Holthausen, M. C. Wolfram Koch , Max C . Holthausen "A chemist's guide to density functional theory" 2nd ed.Wiley, New York **2001**.

560. McLean, A. D.; Chandler, G. S. "Contracted gaussian basis sets for molecular calculations. I. second row atoms, Z=11–18" *J. Chem. Phys.* **1980**, *72*, 5639.

561. Krishnan, R.; Binkley, J. S.; Seeger, R.; Pople, J. A. "Self–consistent molecular orbital methods. XX. A basis set for correlated wave functions" *J. Chem. Phys.* **1980**, *72*, 650.

562. Le Pecq, J. B.; Paoletti, C. "A fluorescent complex between ethidium bromide and nucleic acids" *J. Mol. Biol.* **1967**, *27*, 87.

563. Cox, P. J.; Psomas, G.; Bolos, C. A. "Characterization and dna–interaction studies of 1,1–dicyano–2,2–ethylene dithiolate Ni(II) mixed–ligand complexes with 2–amino–5–methyl thiazole, 2–amino–2–thiazoline and imidazole. Crystal structure of [Ni(i–MNT)(2a–5mt)(2)]" *Bioorg. Med. Chem.* **2009**, *17*, 6054.

564. Wittwer, C. T.; City, S. L. "A study of the interactions of some polypyridylrutheniumn(I) complexes with DNA using fluorescence spectroscopy, topoisomerisation and thermal denaturation" *Nucleic Acids Res.* **1985**, *13*, 6017.

565. Pyle, A. M.; Rehmann, J. P.; Meshoyrer, R.; Kumar, C. V; Turro, N. J.; Barton, J. K. "Mixed–ligand complexes of ruthenium (II): Factors governing binding to DNA" *J.*

Am. Chem. Soc. **1989**, *111*, 3051.

566. Qian, J.; Tian, J.–L.; Feng, L.; Gu, W.; Zhao, X.–J.; Yan, S.–P. "Synthesis, crystal structure, magnetic property, and nuclease activity of a binuclear iron(III) complex" *J. Coord. Chem.* **2009**, *62*, 1260.

567. Shahabadi, N.; Mirzaei Kalar, Z.; Hosseinpour Moghadam, N. "DNA interaction studies of a platinum (II) complex containing an antiviral drug, ribavirin: The effect of metal on dna binding" *Spectrochim. Acta Part A* **2012**, *96*, 723.

568. Jiang, C.; Chao, H.; Li, H.; Ji, L. "Syntheses, characterization and DNA–binding studies of ruthenium (II) terpyridine complexes: [Ru(Tpy)(PHBI)]$^{2+}$ and [Ru(Tpy)(PHNI)] $^{2+}$". *J. Inorg. Biochem.* **2003**, *93*, 247.

569. Indumathy, R.; Weyhermüller, T.; Nair, B. U. "Biimidazole containing cobalt(III) mixed ligand complexes: Crystal structure and photonuclease activity" *Dalton Trans.* **2010**, *39*, 2087.

570. Zhang, G.; Hu, X.; Fu, P. "Spectroscopic studies on the interaction between carbaryl and calf thymus DNA with the use of ethidium bromide as a fluorescence probe" *J. Photochem. Photobiol. B* **2012**, *108*, 53.

571. Behnamfar, M. T.; Hadadzadeh, H.; Simpson, J.; Darabi, F.; Shahpiri, A.; Khayamian, T.; Ebrahimi, M.; Rudbari, H. A.; Salimi, M. "Experimental and molecular modeling studies of the interaction of the polypyridyl Fe(II) and Fe(III) complexes with DNA and BSA" *Spectrochim. Acta Part A* **2015**, *134*, 502.

572. Guo, X.; Qian, X.; Jia, L. "A highly selective and sensitive fluorescent chemosensor for Hg^{2+} in neutral buffer aqueous solution" *J. Am. Chem. Soc.* **2004**, *126*, 2272.

573. Nolan, E. M.; Lippard, S. J. "Turn–on and ratiometric mercury sensing in water with

a red–emitting probe" *J. Am. Chem. Soc.* **2007**, *129*, 5910.

574. Wang, J.; Qian, X.; Cui, J. "Detecting Hg^{2+} ions with an ICT fluorescent sensor molecule: Remarkable emission spectra shift and unique selectivity" *J. Org. Chem.* **2006**, *71*, 4308.

575. Ono, A.; Togashi, H. "Highly selective oligonucleotide–based sensor for mercury(II) in aqueous solutions" *Angew. Chem. Int. Ed.* **2004**, *43*, 4300.

576. Yang, H.; Zhou, Z.; Huang, K.; Yu, M.; Li, F.; Yi, T.; Huang, C. "Multisignaling optical–electrochemical sensor for Hg^{2+} based on a rhodamine derivative with a ferrocene unit" *Org. Lett.* **2007**, *9*, 4729.

577. Hyman, L. M.; Franz, K. J. "Probing oxidative stress: Small molecule fluorescent sensors of metal ions, reactive oxygen species, and thiols" *Coord. Chem. Rev.* **2012**, *256*, 2333.

578. Xue, L.; Liu, Q.; Jiang, H. "Ratiometric Zn^{2+} fluorescent sensor and new approach for sensing Cd^{2+} by ratiometric displacement" *Org. Lett.* **2009**, *11*, 3454.

579. Maity, D.; Govindaraju, T. A "Differentially selective sensor with fluorescence turn–on response to Zn^{2+} and dual–mode ratiometric response to Al^{3+} in aqueous media" *Chem. Commun.* **2012**, *48*, 1039.

580. Basa, P. N.; Sykes, A. G. "Differential sensing of Zn(II) and Cu(II) *via* two independent mechanisms" *J. Org. Chem.* **2012**, *77*, 8428.

581. Xu, Y.; Zhang, D.; Li, B.; Zhang, Y.; Sun, S.; Pang, Y. "A near infrared fluorescent dye for trivalent ions sensing and working as a molecular keypad lock" *RSC Adv.* **2014**, *4*, 11634.

582. Kumar, M.; Kumar, R.; Bhalla, V. "A reversible fluorescent Hg^{2+}/K^+ switch that

works as keypad lock in the presence of F$^-$ ion" *Chem. Commun.* **2009**, 7384.

583. Suresh, M.; Ghosh, A.; Das, A. "A simple chemosensor for Hg^{2+} and Cu^{2+} that works as a molecular keypad lock" *Chem. Commun.* **2008**, 33, 3906.

584. Pischel, U. "Chemical approaches to molecular logic elements for addition and subtraction" *Angew. Chem. Int. Ed.* **2007**, *46*, 4026.

585. Szaciłowski, K. "Digital information processing in molecular systems" *Chem. Rev.* **2008**, *108*, 3481.

586. Yuan, M.; Zhou, W.; Liu, X.; Zhu, M.; Li, J.; Yin, X.; Zheng, H.; Zuo, Z.; Ouyang, C.; Liu, H.; Li, Y.; Zhu, D. "A multianalyte chemosensor on a single molecule: Promising structure for an integrated logic gate" *J. Org. Chem.* **2008**, *73*, 5008.

587. Ghosh, K.; Rathi, S.; Kushwaha, R. "Sensing of Fe(III) ion via turn–on fluorescence by fluorescence probes derived from 1–naphthylamine" *Tetrahedron Lett.* **2013**, *54*, 6460.

588. Ghosh, K.; Rathi, S. "A novel probe for selective colorimetric sensing of Fe(II) and Fe(III) and specific fluorometric sensing of Fe(III): DFT calculation and logic gate application" *RSC Adv.* **2014**, *4*, 48516.

589. Mikata, Y.; Nakagaki, F.; Nakanishi, K. "Thioether–tethered bisquinoline derivatives as fluorescent probes for mercury(II) and iron(III) ions" *New J. Chem.* **2013**, *37*, 2236.

590. Koner, R. R.; Sinha, S.; Kumar, S.; Nandi, C. K.; Ghosh, S. "2–aminopyridine derivative as fluorescence "on–off" molecular switch for selective detection of Fe^{3+}/Hg^{2+}" *Tetrahedron Lett.* **2012**, *53*, 2302.

591. Kunkely, H.; Vogler, A. "Dichloroplatinum(II). fluorescence of the appended naphthyl substituent" *Z. Naturforsch.* **2002**, *4*, 709.

References

592. Chereddy, N. R.; Thennarasu, S.; Mandal, A. B. "Incorporation of triazole into a quinoline–rhodamine conjugate imparts iron(III) selective complexation permitting detection at nanomolar levels" *Dalton Trans.* **2012**, *41*, 11753.

593. Wallace, K. J.; Gray, M.; Zhong, Z.; Lynch, V. M.; Anslyn, E. V. "An artificial siderophore for the detection of iron(III)" *Dalton Trans.* **2005**, 2436.

594. Hou, H.; Li, G.; Song, Y.; Fan, Y.; Zhu, Y.; Zhu, L. "Synthesis, crystal structures and third–order nonlinear optical properties of two novel ferrocenyl schiff–base complexes [Ag(L)$_2$](NO$_3$) (MeOH)·(EtOH) and [HgI$_2$(L)] {L=1,2–bis[(ferrocen–L–ylmethylene)amino]ethane}" *Eur. J. Inorg. Chem.* **2003**, *2003*, 2325.

595. Tian, M.; Ihmels, H. "Selective ratiometric detection of mercury(II) ions in water with an acridizinium–based fluorescent probe" *Chem. Commun.* **2009**, 3175.

596. Yang, Y.; Gou, X.; Blecha, J.; Cao, H. "A highly selective pyrene based fluorescent sensor toward Hg^{2+} detection" *Tetrahedron Lett.* **2010**, *51*, 3422.

597. Singh, N.; Kaur, N.; Dunn, J.; MacKay, M.; Callan, J. F. "A new fluorescent chemosensor for iron(III) based on the β–aminobisulfonate receptor" *Tetrahedron Lett.* **2009**, *50*, 953.

598. Parker, C. A.; Rees, W. T. "Correction of fluorescence spectra and measurement of fluorescence quantum efficiency" *Analyst* **1960**, *85*, 587.

599. Suresh, M.; Das, A. "New coumarin–based sensor molecule for magnesium and calcium ions" *Tetrahedron Lett.* **2009**, *50*, 5808.

600. Das, P.; Ghosh, A.; Bhatt, H.; Das, A. "A highly selective and dual responsive test paper sensor of Hg^{2+}/Cr^{3+} for naked eye detection in neutral water" *RSC Adv.* **2012**, *2*, 3714.

601. Li, N.; Xu, Q.; Xia, X.; Wang, L.; Lu, J.; Wen, X. "A polymeric chemosensor for Fe^{3+} based on fluorescence quenching of polymer with quinoline derivative in the side chain" *Mater. Chem. Phys.* **2009**, *114*, 339.

602. Das, P.; Chandar, N. B.; Chourey, S.; Agarwalla, H.; Ganguly, B.; Das, A. "Role of metal ion in specific recognition of pyrophosphate ion under physiological conditions and hydrolysis of the phosphoester linkage by alkaline phosphatase" *Inorg. Chem.* **2013**, *52*, 11034.

603. Chereddy, N. R.; Suman, K.; Korrapati, P. S.; Thennarasu, S.; Mandal, A. B. "Design and synthesis of rhodamine based chemosensors for the detection of Fe^{3+} ions" *Dye. Pigment.* **2012**, *95*, 606.

604. Ghosh, S.; Dey, C. K.; Manna, R. "Epoxy–based polymer bearing 1–naphthylamine units: Highly selective fluorescent chemosensor for ferric ion" *Tetrahedron Lett.* **2010**, *51*, 3177.

605. Lohani, C. R.; Lee, K.–H. "The effect of absorbance of Fe^{3+} on the detection of fe^{3+} by fluorescent chemical sensors" *Sens. Actuators B* **2010**, *143*, 649.

606. Mao, J.; Wang, L.; Dou, W.; Tang, X.; Yan, Y.; Liu, W. "Tuning the selectivity of two chemosensors to Fe(III) and Cr(III)" *Org. Lett.* **2007**, 4567.

607. Xu, M.; Wu, S.; Zeng, F.; Yu, C. "Cyclodextrin supramolecular complex as a water–soluble ratiometric sensor for ferric ion sensing" *Langmuir* **2010**, *26*, 4529.

608. Sumner, J. P.; Kopelman, R. "Alexa fluor 488 as an iron sensing molecule and its application in PEBBLE nanosensors" *Analyst* **2005**, *130*, 528.

609. Zhang, X.; Shiraishi, Y.; Hirai, T. "A new rhodamine–based fluorescent chemosensor for transition metal cations synthesized by one–step facile condensation"

Tetrahedron Lett. **2007**, *48*, 5455.

610. Lim, N. C.; Pavlova, S. V.; Brückner, C. "Squaramide hydroxamate–based chemidosimeter responding to iron (III) with a fluorescence intensity increase" *Inorg. Chem.* **2009**, *48*, 1173.

611. Wolf, C.; Mei, X.; Rokadia, H. K. "Selective detection of Fe(III) ions in aqueous solution with a 1,8–diacridylnaphthalene–derived fluorosensor" *Tetrahedron Lett.* **2004**, *45*, 7867.

612. Ma, Y. M.; Luo, W.; Quinn, P. J.; Liu, Z. D.; Hider, R. C. "Design, synthesis, physicochemical properties, and evaluation of novel iron chelators with fluorescent sensors" *J. Med. Chem.* **2004**, *47*, 6349.

613. Wu, X.; Xu, B.; Tong, H.; Wang, L. "Phosphonate–functionalized polyfluorene film sensors for sensitive detection of iron(III) in both organic and aqueous media" *Macromolecules* **2010**, *43*, 8917.

614. Konetschny–Rapp, S.; Jung, G.; Raymond, K. N.; Meiwes, J.; Zahner, H. "Solution thermodynamics of the ferric complexes of new desferrioxamine siderophores obtained by directed fermentation. *J. Am. Chem. Soc.* **1992**, *114*, 2224.

615. Yang, M.; Sun, M.; Zhang, Z.; Wang, S. "A novel dansyl–based fluorescent probe for highly selective detection of ferric ions" *Talanta* **2013**, *105*, 34.

616. Lakowicz, J. R. "Principles of Fluorescence Spectroscopy" 3rd ed. Springer: New York, **2006**.

617. Senthilvelan, A.; Ho, I. T.; Chang, K. C.; Lee, G. H.; Liu, Y. H.; Chung, W. S. "Cooperative recognition of a copper cation and anion by a calix[4]arene substituted at the lower rim by a β–Amino–α,β–unsaturated ketone" *Chem.– Eur. J.* **2009**, *15*, 6152.

References

618. Benesi, H. A.; Hildebrand, J. H. "A spectrophotometric investigation of the interaction of iodine with aromatic hydrocarbons" *J. Am. Chem. Soc.* **1949**, *71*, 2703.

619. Wu, S.–P.; Wang, T.–H.; Liu, S.–R. "A highly selective turn–on fluorescent chemosensor for copper(II) ion" *Tetrahedron* **2010**, *66*, 9655.

620. Xu, H. .; Liu, Z. .; Sheng, L. .; Chen, M. .; Huang, D. .; Zhang, H. .; Song, C. .; Chen, S. "A novel "turn–on" fluorescent probe for Fe^{3+} in aqueous media based on C=N isomerization" *New J. Chem.* **2012**, *37*, 274.

621. Devi, M.; Dhir, A.; Pradeep, C. P. "Au microparticles mediated construction of a logic based dual channel molecular keypad lock" *Dalton Trans.* **2013**, *42*, 7514.

622. Kumar, M.; Dhir, A.; Bhalla, V. "A molecular keypad lock based on the thiacalix [4] arene of 1 , 3–alternate conformation" *Org. Lett.* **2009**, *11*, 2567.

623. Margulies, D.; Felder, C. E.; Melman, G.; Shanzer, A. "A molecular keypad lock: a photochemical device capable of authorizing password entries" *J. Am. Chem. Soc.* **2006**, *129*, 347.

624. Misra, A.; Srivastava, P.; Shahid, M. "fluorescent probe mimicking multiple logic gates and a molecular keypad lock upon interaction with Hg^{2+} and bovine serum albumin" *Analyst* **2012**, *137*, 3470.

625. Bhalla, V.; Roopa; Kumar, M. "Fluoride triggered fluorescence "turn on" sensor for Zn^{2+} ions based on pentaquinone scaffold that works as a molecular keypad lock" *Org. Lett.* **2012**, *14*, 2802.

626. Rout, B.; Milko, P.; Iron, M. A.; Motiei, L.; Margulies, D. "Authorizing multiple chemical passwords by a combinatorial molecular keypad lock" *J. Am. Chem. Soc.* **2013**, *135*, 15330.

627. Wang, S.; Men, G.; Zhao, L.; Hou, Q.; Jiang, S. "Binaphthyl–derived salicylidene schiff base for dual–channel sensing of Cu, Zn cations and integrated molecular logic gates" *Sens. Actuators, B* **2010**, *145*, 826.

628. Kagit, R.; Yildirim, M.; Ozay, O.; Yesilot, S.; Ozay, H. "Phosphazene based multicentered naked–eye fluorescent sensor with high selectivity for Fe^{3+} ions" *Inorg. Chem.* **2014**, *53*, 2144.